Effects of heavy fields on inflationary cosmology

Ortiz, P.

Effects of Heavy Fields on Inflationary Cosmology

Pablo Ortiz

On the front cover: illustration by *Pablo Ortiz*.

Effects of Heavy Fields on Inflationary Cosmology

PROEFSCHRIFT

TER VERKRIJGING VAN
DE GRAAD VAN DOCTOR AAN DE UNIVERSITEIT LEIDEN,
OP GEZAG VAN RECTOR MAGNIFICUS
PROF. MR. C.J.J.M. STOLKER,
VOLGENS BESLUIT VAN HET COLLEGE VOOR PROMOTIES
TE VERDEDIGEN OP DINSDAG 30 SEPTEMBER 2014
KLOKKE 11.15 UUR

DOOR

Pablo Ortiz

GEBOREN TE MADRID, SPANJE

IN 1985.

Promotiecommissie:

Promotor:	Prof. dr. A. Achúcarro (Leiden University)
Co-Promotor:	Prof. dr. J. -W. van Holten (Leiden University and Nikhef)
Overige leden:	Prof. dr. E. R. Eliel (Leiden University)
	Dr. G. A. Palma (University of Chile, Santiago, Chile)
	Dr. M. Postma (Nikhef)
	Dr. D. Roest (University of Groningen)

Casimir PhD Series, Delft-Leiden, 2014-24
ISBN 978-90-8593-197-3

This work was partially supported by the Foundation for Fundamental Research on Matter (FOM), which is part of the Netherlands Organization for Scientific Research (NWO). It was part of the research program "Theoretical Particle Physics in the Era of the LHC", program number FP 104.

To my parents,
my sister, and Helena.

Las matemáticas son como una corriente de agua.
Existen diversas teorías complicadas, es cierto,
pero la lógica básica es muy sencilla.
De igual modo que el agua fluye
desde un lugar elevado hacia otro más bajo
tomando la distancia más corta,
sólo hay una corriente matemática.
Al observar con atención,
el curso se hace visible por sí solo.
Basta con que mires fijamente.
No tienes que hacer nada más.
Si te concentras y aguzas la vista, todo se aclara.
En este mundo no hay nada, salvo las matemáticas,
que me trate con tanta amabilidad.

Math is like water.
It has a lot of difficult theories, of course,
but its basic logic is very simple.
Just as the water flows from high to low
over the shortest possible distance,
figures can only flow in one direction.
You just have to keep your eye on them
for the route to reveal itself. That's all it takes.
You don't have to do a thing.
Just concentrate your attention
and keep your eyes open,
and the figures make everything clear to you.
In this whole, wide world,
the only thing that treats me so kindly is math.

Haruki Murakami, *1Q84*

Contents

Preface

The very early universe is a tremendously exciting scenario which has always raised many fundamental and philosophical questions. Before the 1960's we have always assumed that the universe was very homogeneous and isotropic on large scales, which is a corollary of the Copernican principle, that roughly states that we are not located in any particular instant in time or point in space. This was an assumption about the universe called 'cosmological principle'. But in 1965, Penzias and Wilson measured the temperature of the cosmic microwave background (CMB) radiation and found out that it was extremely homogeneous and isotropic, which basically proved what had been assumed until then. The discovery of the CMB gave them the Nobel prize in Physics in 1978.

The physics of the CMB radiation is very well understood and is determined by the hydrodynamical behaviour of the cosmic fluids present before and after the time when the CMB was emitted, approximately 380000 years after the Big Bang. Before that time, the cosmic fluid formed by baryons, photons, and dark matter, was extremely hot and the hydrogen was ionised. Because of that, the electrons of the hydrogen atoms were free and continuously scattering with the photons, which did not let the photons travel freely through the cosmic fluid, and therefore the universe was opaque. It was not until the universe cooled down sufficiently and reached a temperature of about 0.3 eV that the hydrogen atoms were formed, binding the free electrons. This moment is called *recombination*. Right after this happens, the photons' mean free path rapidly increases and they become practically free to travel through the cosmic fluid, eventually reaching us today. This epoch is known as *decoupling* and the burst

of photons released at that time constitutes the CMB radiation. This explains why the CMB is so important for cosmologists: it provides the oldest 'picture' of the universe, or at least the oldest picture that our 'cameras' are able to capture.

The most important property of the CMB is its strikingly homogeneous distribution, with temperature anisotropies of the level of only one part in a hundred thousand, which later on grow to form the large scale structure observed nowadays. These observations gave rise to the Big Bang puzzles, since a universe where gravity was always attractive would undergo a decelerated expansion, unable to explain such a degree of homogeneity. In short, if the evolution was tracked down backwards in time, regions separated by more than two degrees in the CMB sky were *never* in causal contact, and the homogeneity puzzle becomes a problem of very unlikely initial conditions. It was then realised in the 1980's that an early epoch of accelerated expansion could explain how the whole CMB sky arose from one single causal patch of the universe, hence solving the homogeneity puzzle.

The stage of accelerated expansion of space is called inflation. The natural candidate to describe a perfect fluid with negative pressure that can lead to accelerated expansion is a scalar field whose kinetic energy is much smaller than its potential energy. This scalar field is called *the inflaton*. It turns out that the generic predictions of a single scalar field slowly rolling down on a scalar potential are in remarkable agreement with the observations, and therefore inflation driven by a scalar field had a tremendous success. More importantly, in the quantum mechanical picture of inflation, the quantum fluctuations of this scalar field will cause the universe to inflate slightly different in different parts, and these same quantum fluctuations can explain the temperature fluctuations observed in the CMB radiation. The dynamics of the inflaton fluctuations interplays with the energy density of photons, baryons, and dark matter, altogether originating the pattern observed when the CMB is emitted. Remarkably, the CMB contains primordial information about the inflaton fluctuations that we are able to decipher in order to access more detailed information about the inflationary era.

Nowadays, thanks to the overwhelming experimental effort, we cosmologists are extremely lucky to count on many data sets that allow us to penetrate into the finest details of the inflationary stage. In particular, precise measurements of the two- and three-point correlation functions allow us to perform model selection, since the three-point function is very sensitive to the dynamical details of the inflationary model in question. More specifically, the simplest standard inflationary models whose two-point function agrees with the observations, also predict a very suppressed three-point function. Thus, a detection of a large enough three-point function is a smoking gun for non-canonical models of inflation. Despite the success of these simplest models, it has been recently detected a series of hints of anomalies in both the two- and the three-point function, which make us think that there might be a mechanism during inflation

generating scale-dependent features in the correlation functions.

Over the last decades, many different extensions of the simplest inflationary models have been proposed, in particular the possibility of having more degrees of freedom present during inflation, which would interact with the inflaton producing a rich phenomenology. This is motivated not only from the observational point of view, but also from the theoretical point of view, since the high energies at which inflation occurs suggest a theoretical framework based on high energy theories such as supergravity or string theory, where the presence of additional fields is ubiquitous.

I was lucky enough to start my research in cosmology when the experiments have reached the level of accuracy where these additional degrees of freedom might be detected. In particular, the Planck mission was able to measure the three-point function of the CMB, although the data has not been made public yet. Therefore, I was motivated to study in which situations the theory is robust in the presence of additional fields, under which conditions inflation can succeed including these interactions, and which situations would yield detectable features in the observations of the CMB. In particular, in the papers (chapters 2 and 3)

- '*Localized correlated features in the CMB power spectrum and primordial bispectrum from a transient reduction in the speed of sound.*' Ana Achúcarro, Vicente Atal, Pablo Ortiz and Jesús Torrado. *Phys.Rev.* **D89** (2014) 103006, `arXiv:1311.2552[astro-ph.CO]`,

- '*Inflation with moderately sharp features in the speed of sound: GSR and in-in formalism for power spectrum and bispectrum.*' Ana Achúcarro, Vicente Atal, Bin Hu, Pablo Ortiz and Jesús Torrado. *Phys.Rev.* **D90** (2014) 023511, `arXiv:1404.7522[astro-ph.CO]`,

we studied the theoretical regime in which interactions of the inflaton with heavy fields can lead to detectable imprints in the two- and three-point correlation functions of the CMB. We then searched for signatures coming from these interactions in the CMB data and we found reasonable fits to the power spectrum. In addition, these features have a correlated signature in the bispectrum that is also in reasonable agreement with the analyses of the Planck collaboration. More importantly, we restrict ourselves to the regime where the fits to data can be consistently interpreted by a well motivated and consistent theoretical framework, and we provided new techniques that allow us to explore wider regions of the theoretical landscape in a simpler manner.

In this same spirit, I explored the restrictions imposed by additional sectors of fields in supergravity scenarios, where there might be hundreds of additional degrees of freedom. Therefore, it is of extreme importance to keep under theoretical control the interactions with the inflaton field, which also lead to restrictions on

the parent supergravity and on the different inflationary regimes that might be realised. In the paper (chapter4)

- '*Sgoldstino Inflation.*' Ana Achúcarro, Sander Mooij, Pablo Ortiz and Marieke Postma. *JCAP* **1208** (2012) 013, `arXiv:1203.1907[hep-th]`.

we propose a setup in which all the additional fields preserve supersymmetry and the type of couplings permit a consistent truncation and decoupling from the inflaton field. This allows us to give a consistent description of inflation in terms of two real scalar fields, in which the truncated sector of fields must satisfy certain conditions in order to not spoil inflation.

Last, we extended the work in supergravity by including more general couplings between the inflaton and the additional fields. Moreover, we used the tools of random matrix theory to account for the statistics of a large number of additional fields. Apart from inflation, we also explored the possibility of achieving stable vacua able to describe the stage of present expansion of the universe (or else a hypothetical vacuum before inflation). This imposes other restrictions on the sector of additional fields. Thus, with the paper (chapter 5)

- '*Perturbative stability along the supersymmetric directions of the landscape.*' Kepa Sousa and Pablo Ortiz. `arXiv:1408.6521[hep-th]`.

we are cornering the landscape of supergravity theories that can lead to successful inflation and/or description of the present vacuum, or alternatively, a hypothetical pre-inflationary vacuum state. In order to do this, we are characterising the truncated sector by its statistical and geometrical properties. We are also incorporating a new element, utilising not only the supersymmetry breaking direction to derive constraints, but also the supersymmetric directions in field space, which are to be described by their statistics.

All together, the research done with my collaborators has helped in analysing the possibility that additional fields are present during inflation, where we have studied many different aspects of it: from the theoretical consistency to the detectability. We have taken care of providing consistent descriptions and taking into account the (sometimes forgotten) presence of additional heavy degrees of freedom during inflation. We have provided novel methods to calculate their impact on the CMB observations, and we have studied the regimes in which supergravity theories can consistently describe inflation with multiple sectors.

1

Cosmological inflation: its realisations and observables

In this first chapter I give an overview of cosmological inflation, which will gradually become more concrete and focused on the topics that are treated in depth in the remaining chapters. Thus, I provide the basic ingredients necessary to follow the articles [1–4] presented in the main body of this thesis. Throughout this manuscript, unless specified, I will work in units of $\hbar = c = 1$ and will set the Planck mass to $M_p = (8\pi G)^{-1/2} = 1$.

1.1 Introduction: an expanding universe

Cosmological inflation is a paradigm that was invented over thirty years ago [5–10]. It is defined as an era of accelerated expansion of the very early universe. The key observation that led to this idea was that the universe is highly homogeneous and isotropic on large scales. This was an assumption that physicists called "cosmological principle" and that was later confirmed by the observation of the Cosmic Microwave Background (CMB) radiation by Penzias and Wilson [11] in 1965. This radiation is, roughly speaking, a picture of the photon temperature distribution in two dimensions corresponding to the time when the photons decoupled from the hot plasma (380000 years after the 'Big Bang'), as I will explain in detail in section 1.3. The spectrum of this radiation is that of a perfect black body with temperature 2.73K, and deviations from this average temperature are only of one part in 10^5.

An important question that comes when observing such a homogeneous radiation was that, patches of the universe that in principle were never causally connected have the same temperature, how is this possible? If gravity was always

attractive, then the initial size of the universe would be larger than the causally connected patch at that time. Given the observations, the initial state of the universe should be such that all the causally disconnected regions have roughly the same temperature. Either the initial conditions were inexplicably given just like that, or there is a mechanism underneath that explains them. Of course physicists pursued the second alternative.

In addition to the high degree of homogeneity and isotropy, the universe is extremely flat, which is also very unnatural for a decelerating universe, since it is an unstable stage. Having seen this, it seems rather natural to ask which initial conditions led to such a 'perfect' universe. The main motivation for inflation was to propose a mechanism such that these characteristics were *predicted*, rather than accepted as very unlikely initial conditions, and it turns out that inflation has succeeded tremendously in this respect. In this thesis I will not focus on the detailed description of the initial condition problems, and refer to those interested in them to the excellent reviews and textbooks [12–16]. The key feature of inflation that solves these problems of initial conditions is the accelerated expansion. Furthermore, we will see that inflation yields the generation of primordial density perturbations, which explain the tiny inhomogeneities of the CMB temperature, and that later on generated the large scale structure observed nowadays.

The plan of this chapter is the following: I will briefly review the geometry of an expanding universe and the conditions for an accelerated expansion. The natural candidate to drive such an expansion is a scalar field, whose quantum fluctuations originate the primordial density perturbations that seeded the growth of structure, as I will explain at the beginning of section 1.2. The correlation functions of the primordial curvature perturbation contain valuable information that remains frozen for a long time and whose evolution can be tracked down until the time when the CMB is emitted, which allows us to study the footprints of the quantum fluctuations during inflation. At the end of section 1.2 I provide the standard well-known predictions for the two- and three-point correlation functions. But one of the most important successes of inflationary cosmology is the predictive power and the stunning agreement with CMB measurements. Especially in the last decade cosmologists have been very fortunate to count on the WMAP, Planck and BICEP experiments, which have given us the opportunity to test our theories. In section 1.3 I briefly explain the physics of the CMB, I will review the (very exciting) current experimental status, and I will explain how the CMB data help us constraining the incredible amount of inflationary models. We will see that there is still much room for a rich variety of inflationary setups, and in particular I have explored in this thesis the effect of additional degrees of freedom, which naturally arise in UV completable theories. Therefore, it is natural to ask ourselves whether it is possible or not to detect, and under which circumstances, those additional particles that play inflation

along with the inflaton. In section 1.4 I focus on inflationary scenarios embedded in supergravity and the tools that enable us to give a simpler, yet consistent, theoretical description. Finally, in section 1.5 I explain how the inflaton field feels the presence of additional heavy fields and how this affects the observable predictions.

1.1.1 The Friedmann - Lemaître - Robertson - Walker universe

The series of works [17–22] gave name to what we know today as the Friedmann-Lemaître-Robertson-Walker (FLRW) universe. It is basically described by a space-time that is homogeneous and isotropic for each time slice, with distance between two comoving observers proportional to the scale factor $a(t)$. The line element in the FLRW metric can be written in spherical coordinates as follows:

$$ds^2 = g_{\mu\nu}dx^\mu dx^\nu = -dt^2 + a^2(t)\left[\frac{dr^2}{1-kr^2} + r^2\left(d\theta^2 + \sin^2\theta\, d\phi^2\right)\right] , \quad (1.1.1)$$

where k gives the spatial curvature, as can be read from the spatial Ricci scalar $R^{(3)} = 2k/a^2$. The constant k can take values $+1, -1$ and 0, that describe space-times with positive curvature, negative curvature, and flat, respectively. Since all the observations are in excellent agreement with a flat universe, in this thesis I will only describe flat FLRW space-times with $k = 0$, which in cartesian coordinates can be simply written as:

$$ds^2 = -dt^2 + a^2(t)\left(dx^2 + dy^2 + dz^2\right) . \quad (1.1.2)$$

An important quantity derived from the scale factor is the Hubble parameter

$$H(t) \equiv \frac{\dot{a}}{a} , \quad (1.1.3)$$

which measures the expansion rate of the universe. Along this manuscript, for convenience I will often measure time using the conformal time $\tau \equiv \int dt/a(t)$,[1] in terms of which the FLRW metric is conformally flat, which means that it can be expressed as a conformal transformation of the Minkowski metric. Then, using the conformal time the metric reads:

$$ds^2 = a^2(\tau)\left(-d\tau^2 + dx^2 + dy^2 + dz^2\right) . \quad (1.1.4)$$

This settles the description of the space-time in which inflation occurs. The other essential ingredient we need to describe the cosmology is the matter, which is

[1] The conformal time is usually written as η instead of τ, but I will reserve the former to denote the second order slow-roll parameter that will appear repeatedly in the text.

specified through the energy-momentum tensor $T_{\mu\nu}$. The energy (or matter) content and the geometry of the space-time satisfy the Einstein equations:[2]

$$G_{\mu\nu} \equiv R_{\mu\nu} - \tfrac{1}{2} g_{\mu\nu} R - \Lambda g_{\mu\nu} = T_{\mu\nu} \ , \tag{1.1.5}$$

where $R_{\mu\nu}$ is the Ricci tensor, R is the Ricci curvature scalar, and Λ is the cosmological constant term. The Λ-term represents the vacuum energy and can always be written as a constant contribution to the energy momentum tensor, thus from now on I will set $\Lambda = 0$, and later on the cosmological constant will be often given by the value of the scalar potential at the vacuum.

On large scales the cosmic fluid is well approximated by a perfect fluid, characterised by its energy density ρ, pressure p, and velocity u^μ, and for which the energy-momentum is

$$T^{\mu\nu} = (p + \rho) u^\mu u^\nu + p\, g^{\mu\nu} \ . \tag{1.1.6}$$

The conservation of the energy-momentum tensor follows from the Bianchi identities applied to the Einstein tensor $G_{\mu\nu}$, which in terms of energy and pressure gives the continuity equation:

$$\dot{\rho} = -3H(p + \rho) \ , \tag{1.1.7}$$

which is nothing else than the conservation of energy for a perfect fluid in a homogeneous and isotropic universe. In addition to the previous equation, the Einstein equations (1.1.5) for a FLRW universe filled with a perfect fluid characterised by eq. (1.1.6) are well known as the Friedmann equations, which read:

$$H^2 = \left(\frac{\dot{a}}{a}\right)^2 = \frac{\rho}{3} \quad , \qquad \dot{H} + H^2 = \frac{\ddot{a}}{a} = -\frac{1}{6}(\rho + 3p) \ . \tag{1.1.8}$$

One can combine the previous equations to obtain a very useful expression:

$$\dot{H} = -\frac{1}{2}(p + \rho) \ . \tag{1.1.9}$$

It is clear then that once the equation of state of the fluid $p(\rho)$ is given, the evolution of the scale factor $a(t)$ and of the fluid are determined. The most interesting situations in cosmology are characterised by $p = w\rho$. For instance, for radiation one has $w_{\rm rad} = 1/3 \Rightarrow \rho_{\rm rad} \sim a^{-4}$, for matter $w_{\rm mat} = 0 \Rightarrow \rho_{\rm mat} \sim a^{-3}$, and for vacuum energy or a cosmological constant $w_\Lambda = -1 \Rightarrow \rho_\Lambda \sim$ const. Notice that the universe is (positively) accelerated when

$$w < -\tfrac{1}{3} \quad \Rightarrow \quad \ddot{a} > 0 \quad \text{(inflation)} \ . \tag{1.1.10}$$

An accelerated expansion solves the homogeneity puzzle, as illustrated in figure

[2] See appendix A for conventions.

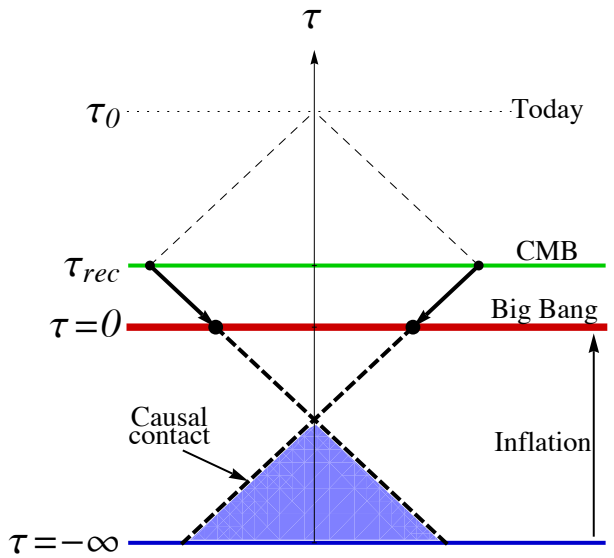

Figure 1.1 *– Diagram illustrating the solution to the horizon problem. If there exists a sufficiently long period of accelerated expansion before the Big Bang, two apparently disconnected regions were in reality connected before. This explains why the CMB radiation has an almost perfectly uniform temperature distribution.*

1.1, because it makes possible the creation of our universe from a causally connected domain, even if outside this domain the universe is initially very inhomogeneous. This is because the physical size of the perturbation grows faster than the curvature scale (H^{-1}). Due to the same reason, the flatness problem is also solved by a period of accelerated expansion. The evolution of the curvature dictates that positive acceleration drives the curvature to zero, and becomes an attractor of inflation.

By inspecting the Friedmann equations (1.1.8) one can see that $p < -\rho/3$ produces an accelerated expansion. One could first consider $H = \text{const}$ and therefore exponential expansion. However, perfect exponential expansion would never end, so we will need small deviations that will be parameterised by

$$\epsilon \equiv -\frac{\dot{H}}{H^2} \ , \tag{1.1.11}$$

such that the condition for an accelerated universe translates now into $\epsilon < 1$. Inflation must last sufficiently long to stretch a small domain to the size of the observable universe, and also to flatten the possible initial inhomogeneities to the level observed in the CMB. The duration or amount of inflation is usually measured as a function of the *number of e-folds*, N, which is roughly speaking

the amount of times that the universe expands by a factor e, and its definition is:

$$dN = H\,dt = \frac{da}{a}\ . \tag{1.1.12}$$

Typically the solution of the flatness and horizon problems demands an amount between 60 and 70 e-folds of inflation. This also implies that the value of ϵ at the beginning of inflation should be approximately one percent or less. In the next section we will see how we can achieve accelerated expansion long enough.

1.2 Inflating the universe with a scalar field

The natural candidate to drive inflation is a scalar field ϕ, which easily describes the energy density and pressure of a perfect fluid in terms of its kinetic energy and a scalar potential $V(\phi)$. In this case the field ϕ drives inflation and is therefore called the *inflaton*. If one takes the action for a scalar field in a FLRW metric and calculates the energy-momentum tensor, it is easy to see that the energy density and the pressure are given by:

$$\rho = \tfrac{1}{2}\dot{\phi}^2 + V(\phi) \quad , \qquad p = \tfrac{1}{2}\dot{\phi}^2 - V(\phi)\ . \tag{1.2.1}$$

Also, the equation of motion for a homogeneous scalar field in a FLRW background is

$$\ddot{\phi} + 3H\dot{\phi} + V_\phi = 0\ , \tag{1.2.2}$$

where the subindex in V_ϕ denotes derivative with respect to the scalar field.

Slow-roll conditions

Let us make a brief interlude to define the slow-parameters that must be small in order to achieve a sufficiently large amount of inflation. As can be seen from eq. (1.1.9), the universe undergoes quasi-exponential expansion if the equation of state of the fluid is $p \simeq -\rho$, which in view of (1.2.1) translates into

$$\tfrac{1}{2}\dot{\phi}^2 \ll V(\phi) \quad \text{(slow-roll)}\ . \tag{1.2.3}$$

Since the kinetic energy must be much smaller than the potential, the name slow-roll is obvious. Using the Friedmann equations (1.1.8) and substituting the energy density and pressure for our scalar field (1.2.1), one clearly sees that slow-roll requires $\epsilon \ll 1$ for a sufficiently large amount of time. The condition of small ϵ lasting long enough is usually expressed in terms of a second slow-roll parameter η, however in the literature there is no clear consensus on how to define this parameter[3]. Some of the alternatives that make sense are the following:

$$\eta_1 = -\frac{\dot{\epsilon}}{H\epsilon} \quad , \qquad \eta_2 = -\frac{\ddot{H}}{H\dot{H}} \quad , \qquad \eta_3 = -\frac{\ddot{\phi}}{H\dot{\phi}}\ . \tag{1.2.4}$$

[3]When dealing with multiple scalar fields, there are even more possible definitions, as I will explain in section 1.5.1.

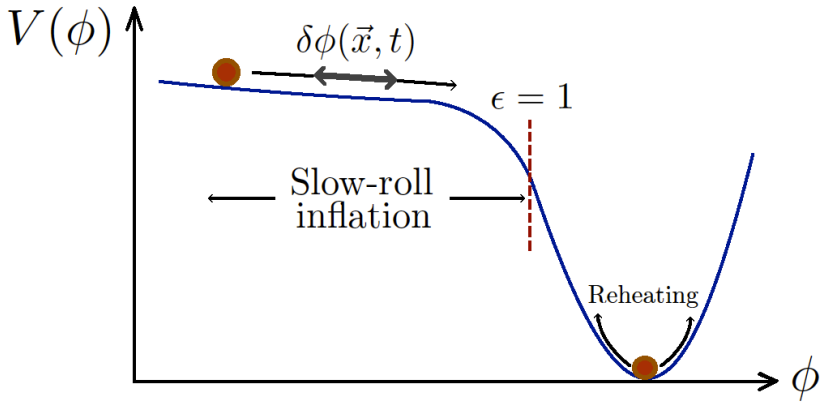

Figure 1.2 *– Typical scalar potential for slow-roll inflation. Accelerated expansion (inflation) ends when $\epsilon = 1$, and reheating starts when the inflaton oscillates around the minimum.*

The first two are related through the equality:

$$\eta_1 = \eta_2 - 2\epsilon \ . \tag{1.2.5}$$

There is still an alternative definition of the first slow-roll parameter ϵ in terms of the scalar potential. This definition is somewhat intuitive since it involves the slope of the potential, which must be very small compared to the height of the potential, and therefore one can define

$$\epsilon_V \equiv \frac{1}{2}\left(\frac{V_\phi}{V}\right)^2 = \epsilon\left(\frac{3-\eta_3}{3-\epsilon}\right)^2 \ . \tag{1.2.6}$$

Let me make an important point here. In the above expression, it is clear that the usual slow-roll limit $\epsilon, \eta_3 \ll 1$ implies $\epsilon_V \simeq \epsilon \ll 1$, but it is important to notice that the opposite is not true. In fact, one can have $\epsilon > 1$ and still get $\epsilon_V < 1$. In this thesis I will always be using the kinematical parameter ϵ instead of the potential parameter ϵ_V.

For completeness, I will define yet another potential slow-roll parameter which has to do with the curvature of the scalar potential. The same way that for slow-roll one needs a small slope, for it to last long enough one needs small curvature, and therefore it is convenient to define

$$\eta_V \equiv \frac{V_{\phi\phi}}{V} = \frac{3}{3-\epsilon}\left[\epsilon + \left(1 - \frac{\xi}{3}\right)\eta_3\right] \quad , \qquad \text{with} \quad \xi \equiv -\frac{\dddot{\phi}}{H\ddot{\phi}} \ , \tag{1.2.7}$$

which will actually be more relevant for the multiple-field case, where it is related to the eigenvalues of the mass matrix coming from the Hessian of the potential.

This discussion will be enough to go on, and I will go into more subtleties later in the multiple-field case. Let us establish the standard single-field slow-roll conditions as $\epsilon, \eta_3 \ll 1$.

In the following I will consider the quantum mechanical picture of inflation, which is an essential step to describe the origin of primordial inhomogeneities.

1.2.1 Quantisation and mode equations

The fluctuations of the inflaton field can be written as $\delta\phi(\mathbf{x}, t) = \phi(\mathbf{x}, t) - \phi_0(t)$, with $\phi_0(t)$ the homogeneous part satisfying the background equation of motion (1.2.2). The spatial dependence is just telling us that different regions of the universe will inflate by slightly different amount, which will produce fluctuations in the local densities and eventually originate the temperature fluctuations of the CMB. Let us write the action for the inflaton field:

$$S = \int d^4x\, a^3(t) \left[\frac{1}{2}R - \frac{1}{2}g^{\mu\nu}\partial_\mu\phi\partial_\nu\phi - V(\phi)\right] . \tag{1.2.8}$$

When perturbing the action above, we find 5 scalar modes, responsible for the gravitational instability and structure formation, 4 vector modes, which decay very quickly and therefore are not important, and 2 tensor modes, which are the gravitational waves, whose analysis are out of the scope of this thesis. If we focus on the scalar modes, invariance under the transformations $t \to t + c_0$, $x_i \to x_i + \partial_i c$ remove two scalar modes. The Einstein equations remove two more scalar modes, and we are finally left with only one scalar degree of freedom. There are many different gauge choices, but we will just content ourselves with studying the *comoving gauge* [23], in which $\delta\phi = 0$, and thus the perturbations are put in the metric:

$$\delta g_{ij} = a^2(1 - 2\zeta)\delta_{ij} + \text{grav. waves} , \tag{1.2.9}$$

where ζ is the so-called *curvature perturbation*, since the spatial curvature scalar is $R_{(3)} = 4\nabla^2\zeta/a^2$. The beauty of this gauge resides in the fact that it explicitly exposes the conservation of the curvature perturbation on large scales outside the Hubble horizon (superhorizon scales), that is:

$$\dot{\zeta}_{\mathbf{k}} = 0 \qquad \text{for} \quad k \ll aH . \tag{1.2.10}$$

A careful treatment of the perturbed Einstein equations is not relevant for this thesis, and the purpose of this subsection is just to show the quadratic action in terms of the canonical variables. Thus, I will assume that we have solved the perturbed Einstein equations, rewritten the quadratic action in conformal time, and changed variables to obtain canonical kinetic terms. This leads to the following quadratic action:

$$S_2 = \frac{1}{2}\int d\tau\, d^3\mathbf{x} \left[v'^2 - (\nabla v)^2 + \frac{z''}{z}v^2\right] , \tag{1.2.11}$$

where the prime denotes derivative with respect to conformal time, and $v = z\zeta = a\sqrt{2\epsilon}\,\zeta$. This action can be seen as that of a harmonic oscillator with a time-dependent mass. Expanding in creation and annihilation operators:

$$v(\tau,\mathbf{x}) = \int \frac{d^3\mathbf{k}}{(2\pi)^{3/2}} \left[a^-_{\mathbf{k}} v_k(\tau) \mathrm{e}^{i\mathbf{k}\cdot\mathbf{x}} + a^+_{\mathbf{k}} v^*_k(\tau)\mathrm{e}^{-i\mathbf{k}\cdot\mathbf{x}}\right] . \tag{1.2.12}$$

Now we can promote v, its canonical conjugated momentum π, and a^-, a^+ to operators, such that

$$[\hat{v}(\tau,\mathbf{x}),\hat{\pi}(\tau,\mathbf{y})] = i\delta(\mathbf{x}-\mathbf{y}) \quad , \qquad \left[\hat{a}^-_{\mathbf{k}},\hat{a}^+_{\mathbf{k}'}\right] = \delta(\mathbf{k}-\mathbf{k}') \tag{1.2.13}$$

are the canonical commutation relations. We will assume from now on that they are operators and drop the hats. Now that we have quantised the system, let us derive the equations of motion in Fourier space from the action (1.2.11):

$$v_k''(\tau) + \left(k^2 - \frac{z''}{z}\right) v_k(\tau) = 0 . \tag{1.2.14}$$

This is called the Mukhanov-Sasaki equation [24, 25]. For the simplest case of a quasi-de Sitter universe with $\epsilon \simeq \text{const} \ll 1$, we have $z''/z \simeq 2/\tau^2$, where we have used $\tau \simeq -(aH)^{-1}$. [4] Before displaying the solution, let us fix the initial conditions, and the standard choice is to impose that for $\tau \to -\infty$ (beginning of inflation) the mode function corresponds to a Minkowski state:

$$\lim_{\tau\to-\infty} v_k(\tau) = \frac{1}{\sqrt{2k}}\mathrm{e}^{-ik\tau} . \tag{1.2.15}$$

This is known as the Bunch-Davies vacuum [26], and although other choices are possible and are actually endowed with a rich phenomenology (for instance, see [27–30]), in this thesis I will always consider a Bunch-Davies vacuum state. Then, the solution to the mode equation is

$$v_k(\tau) = \frac{\mathrm{e}^{-ik\tau}}{\sqrt{2k}}\left(1 - \frac{i}{k\tau}\right) . \tag{1.2.16}$$

It can be easily checked that for subhorizon modes ($k \gg aH$) the curvature perturbation $\zeta = v/a\sqrt{2\epsilon}$ has oscillating solutions, while for superhorizon modes ($k \ll aH$) it is constant. The very important consequence of this is that the curvature perturbation remains frozen after crossing the Hubble horizon, which allows us to obtain information from the inflationary epoch by looking at the statistical properties of the CMB, as illustrated in figure 1.3. In what follows, I review the standard predictions of single-field slow-roll inflation for the two- and three-point functions of the curvature perturbation, also known as the primordial power spectrum and bispectrum.

[4] A much more general and detailed treatment will be given in chapter 3, where we consider non-canonical kinetic terms and deviations from the quasi-de Sitter stage. However, the zero order solutions displayed here are the pillar over which more general solutions are constructed.

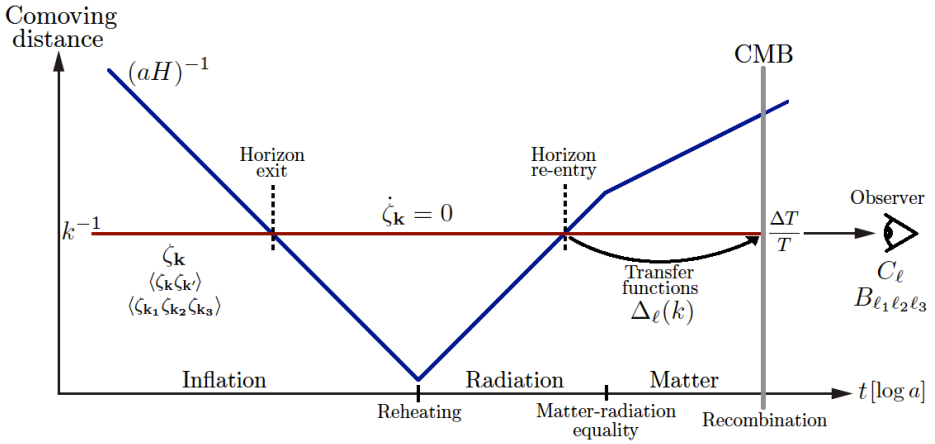

Figure 1.3 – *Scheme of the evolution of the comoving Hubble horizon (blue) in relation to perturbations of a given wavelength (red). During inflation the perturbations exit the horizon and remain frozen, and after reheating they re-enter the horizon, preserving the information of the inflationary epoch. Then they evolve together with the photon-baryon fluid, and the density perturbations leave their imprints on the photon temperature distribution, that is observed in the CMB when the photons are released. Figure adapted from [13].*

1.2.2 Standard predictions: correlation functions

Once we have the solution of our mode equations (1.2.14), it is possible to calculate the correlation functions of the adiabatic curvature perturbation $\zeta_{\mathbf{k}}$. Any distribution, and in particular that of the CMB temperature, is completely specified by its correlation functions. As it happens, the CMB temperature distribution is almost gaussian as far as we know [31, 32], and therefore the two-point function, i.e. the power spectrum, almost completely specifies the spectrum of perturbations. However, the three-point function (bispectrum) and higher order correlation functions play an important role in breaking degeneracies among different inflationary models, and therefore it is important to know as much as possible about them, even if they are small, because they represent departures from a perfect gaussian spectrum. The definitions of the primordial power spectrum and bispectrum are:

$$\langle\zeta_{\mathbf{k}}\zeta_{\mathbf{k}'}\rangle \equiv (2\pi)^3\delta(\mathbf{k}+\mathbf{k}')\,P_\zeta(k)\ , \tag{1.2.17}$$

$$\langle\zeta_{\mathbf{k_1}}\zeta_{\mathbf{k_2}}\zeta_{\mathbf{k_3}}\rangle \equiv (2\pi)^3\delta(\mathbf{k_1}+\mathbf{k_2}+\mathbf{k_3})\,B_\zeta(\mathbf{k_1},\mathbf{k_2},\mathbf{k_3})\ . \tag{1.2.18}$$

It is often convenient to define the dimensionless scalar power spectrum

$$\mathcal{P}_\mathcal{R}(k) \equiv \frac{k^3}{2\pi^2}P_\zeta(k)\ . \tag{1.2.19}$$

The power spectrum can be evaluated at horizon crossing, i.e. $k = aH$, since the curvature perturbation freezes then. Taking the solution to the mode equations (1.2.16) and performing the commutation operations in terms of creation and annihilation operators, one finally obtains [26]:

$$\mathcal{P}_{\mathcal{R}}(k) = \left.\frac{H^2}{8\pi^2\epsilon}\right|_{k=aH} , \tag{1.2.20}$$

which is scale-invariant except for the slight time dependence of H^2 and ϵ. To evaluate this scale dependence one can do the following computation [33]:

$$n_s - 1 \equiv \frac{d\ln\mathcal{P}_{\mathcal{R}}}{d\ln k} \simeq -2\epsilon + \eta_1 + \mathcal{O}(\epsilon^2) , \tag{1.2.21}$$

where I have neglected higher order slow-roll corrections. The scalar *spectral tilt* n_s measures the deviation of the scalar power spectrum from scale invariance. The deviation from scale invariance is a strong probe of inflation, since that is one of its most general predictions, and furthermore $n_s < 1$ also indicates that inflation comes to an end. It has been recently confirmed by the Planck collaboration [34] with more than 5σ c.l. that this is the case:

$$n_s = 0.9603 \pm 0.0073 \quad (1\sigma \text{ c.l.}) . \tag{1.2.22}$$

Later in section 1.3 I will go into the details of the experimental status regarding the power spectrum and bispectrum measurements. Since n_s is roughly speaking an 'average' of the tilt of the power spectrum, oscillations on top of the flat shape are allowed, and as we will see in chapters 2 and 3, these features may come together with some other interesting predictions for the bispectrum. The possibility of having non-trivial shapes fitting the data better than the standard result reviewed above is worth exploring in detail, since it may hint at additional degrees of freedom apart from the inflaton.

As for the primordial bispectrum, I will review the main results and leave further details for chapter 3, where I compute in full detail the complete bispectrum for a feature model. The first estimations of the bispectrum in slow-roll single-field models were given in [35–38], while the complete calculation was made in [39]. In these works it was stated that the bispectrum is of order of the slow-roll parameters and therefore very suppressed.

In order to calculate the bispectrum one has to expand the action in fluctuations of the inflaton field $\delta\phi$ around the homogeneous solution ϕ_0 to cubic order, where the non-linearities (interactions) arise. The expectation value we want to calculate can be computed using the *in-in formalism* [40, 41] and is given by:

$$\langle\zeta^3\rangle = \langle U_{\rm int}^{-1}\zeta^3 U_{\rm int}(t,t_0)\rangle \quad , \qquad U_{\rm int} = T\exp\left[-i\int_{t_0}^{t} dt'\, H_{\rm int}(t')\right] , \tag{1.2.23}$$

where $H_{\rm int}$ is the interaction Hamiltonian, which for the cubic terms equals $-L_{\rm int}$. Taking the first order approximation for the exponential above, the expectation value is then

$$\langle\zeta^3\rangle = -i\int_{t_0}^{t} dt' \left\langle\left[\zeta^3(t'), H_{\rm int}(t')\right]\right\rangle . \tag{1.2.24}$$

After a lengthy calculation[5], one obtains the following result [39]:

$$B(k_1,k_2,k_3) = \frac{(2\pi)^4 {\mathcal{P}_{\mathcal{R}}}^2 \epsilon}{8k_1^3k_2^3k_3^3}\mathcal{A} , \tag{1.2.25}$$

where

$$\mathcal{A} = (1-\frac{2\eta_3}{\epsilon})\sum_i k_i^3 + \sum_{i\neq j} k_i k_j^2 + \frac{8}{K}\sum_{i>j} k_i^2 k_j^2 , \tag{1.2.26}$$

and $K \equiv k_1+k_2+k_3$. This result implies that the bispectrum in the standard single-field slow-roll paradigm is suppressed by the slow-roll parameters. There are different scenarios that depart from these simplest models, for instance non-Bunch-Davies initial vacuum state, non-canonical kinetic terms, sharp steps in the scalar potential, or multiple fields during inflation can in principle enhance the non-gaussianity. As I will show in chapters 2 and 3, the influence of heavy fields during inflation may give rise to scale-dependent features in the power spectrum and bispectrum that are in reasonable agreement with the CMB data. In the next section I explain how from the CMB temperature anisotropies we can extract information about the quantum fluctuations of the inflaton field, and I will give an overview of the current experimental status.

1.3 The Cosmic Microwave Background Radiation

The CMB radiation is a tremendously exciting subject for early universe cosmologists, since it contains the footprints of inflation. In this section I give a qualitative explanation on how and why this is the case, and a more precise discussion on this issue can be found for instance in [42]. Although the details of the physical processes involved and the precise results are not essential for the rest of this thesis, I believe that is important to posses a qualitative understanding of the CMB physics in order to comprehend the relevance of the results presented in the following chapters. Throughout this section I will often refer to a sketch of the different eras involved in the transition from inflaton fluctuations to CMB temperature anisotropies, shown in figure 1.3. I will describe the events and physical phenomena that explain the shape of the temperature spectrum, and

[5] In chapter 3 I explain in detail the procedure that one must follow to calculate the bispectrum using the in-in formalism. Although the calculation is performed for a particular feature model, the same methodology applies to any case.

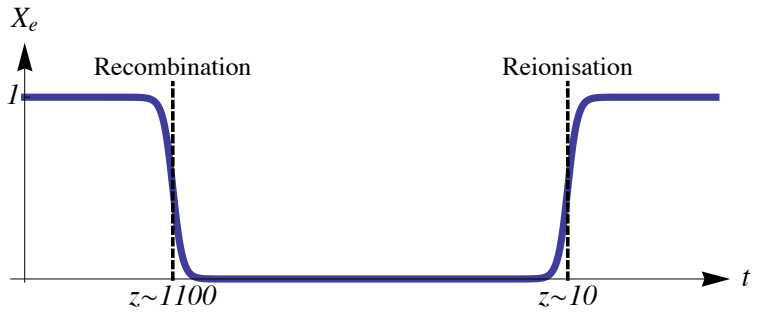

Figure 1.4 *– Fraction of ionised hydrogen atoms as a function of time. At recombination, hydrogen is neutralised and the photons can travel freely, then the CMB is emitted. When stars are formed, the UV photons emitted from them reionise the universe, but it has already diluted enough so that only about 10% of the CMB photons scatter, as parameterised by the optical depth.*

in the last part I will review the experimental status of power spectrum and bispectrum measurements.

Right after the Big Bang, the universe is at such a high temperature that hydrogen is ionised, which in particular means that electrons are freely floating around. That is the reason why we cannot see the photons of that time, because they were scattering off those electrons and their mean free path was of a few centimetres. Eventually, after approximately 380000 years, the universe drops its temperature to about 0.3 eV, which is sufficiently low for the hydrogen atoms to bind, and therefore *recombination* occurs. The figure 1.4 illustrates this process. Then the mean free path of the photons rapidly increases and quickly becomes larger than the Hubble horizon. At this point the photons can travel freely towards us, this moment is known as *decoupling*. These are the CMB photons.

The CMB radiation as measured by the Planck collaboration [32] can be seen in figure 1.5. As mentioned in the beginning of this chapter, the remarkable property of this radiation is that the temperature is basically uniform, fluctuations being only of order $\Delta T/T \sim 10^{-5}$. This outstanding homogeneity can be explained by having a period of inflation before the Big Bang, as shown in figure 1.1: since recombination happens very close in time to the Big Bang, regions separated by more than two degrees in the sky do not have time to be in causal contact. Roughly speaking, what inflation does is to extend this period further to the past, so that these regions were in causal contact.

Now, if we look back at figure 1.3, in order to understand how the inflaton fluctuations translate into the CMB temperature anisotropies, one has to follow the evolution of dark matter and the photon-baryon fluid in the presence

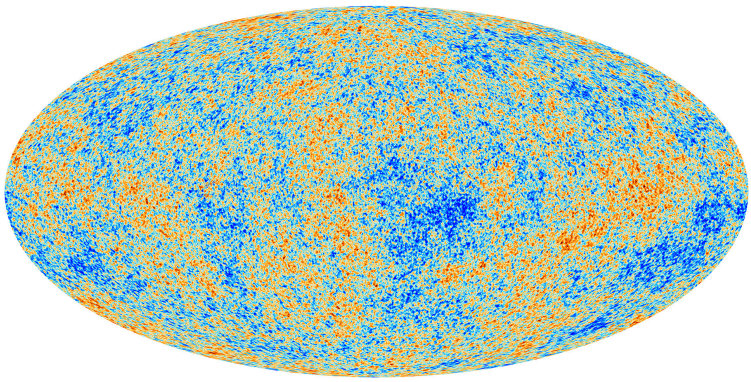

Figure 1.5 *– CMB temperature anisotropies as measured by the Planck collaboration, released on 21 March 2013 [32]. The temperature fluctuations are of one part in 100000, and the statistical properties of the distribution contain unique information about quantum fluctuations during inflation.*

of gravity throughout the radiation and matter eras. Basically, the inflaton fluctuations can be written in terms of metric perturbations, as we saw in eq. (1.2.9). Therefore, before recombination, the density and velocity of the baryon-radiation plasma will oscillate according to an equation for a harmonic oscillator in the presence of a gravitational potential. The beautiful physics involved is governed by the Boltzmann equation, the continuity equation and the Euler equation for our cosmic fluid. The CMB temperature distribution is then given as a function of the gravitational potential, the photon density fluctuations, and the velocity of the baryon-radiation plasma at recombination, which are at the same time determined by the inflationary perturbations, the Hubble constant, and the densities of baryons, cold dark matter, and dark energy.

All these effects can be effectively implemented by the *transfer functions*, which incorporate the evolution of the density perturbations between the times of horizon crossing and recombination. These are normally calculated with computer programs, as we did in the works presented in chapters 2 and 3, however in this section the aim is to provide an insight on the physics that determines the evolution from primordial to CMB anisotropies.

When observing the temperature fluctuations, we expand in spherical harmonics, which is the most natural way to decompose a two dimensional distribution:

$$\frac{\delta T}{T}(\Omega) = \sum_{\ell,m} a_{\ell m} Y_{\ell m}(\Omega) \quad \Rightarrow \quad a_{\ell m} = \int d\Omega \, Y^*_{\ell m}(\Omega) \frac{\delta T}{T}(\Omega) \ , \tag{1.3.1}$$

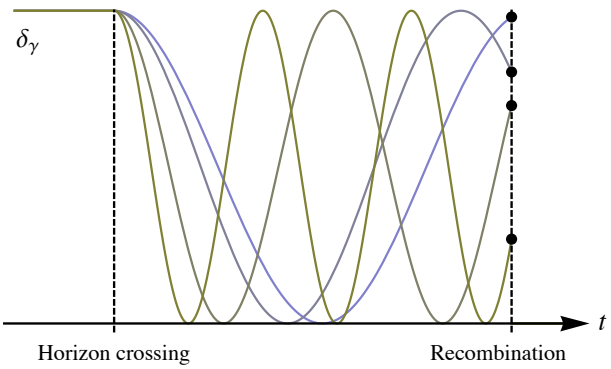

Figure 1.6 *– Photon density fluctuations since the metric perturbations re-enter the horizon until recombination. All the wavelengths start with the same phase because the photon density fluctuations are proportional to the curvature perturbation, which is frozen on superhorizon scales. The peak structure of the CMB power spectrum is partly due to this, otherwise the fluctuations of different wavelengths would be randomly distributed and they would average to zero, giving no peaks at all.*

and the CMB power spectrum is therefore determined by

$$C_\ell = \frac{1}{2\ell+1}\sum_m \langle a^*_{\ell m} a_{\ell m}\rangle \ . \tag{1.3.2}$$

The CMB power spectrum as measured by Planck [34] is showed in figure 1.7. One of the aims of this section is to explain the relationship between the primordial power spectrum (1.2.20) and the CMB power spectrum (1.3.2). In the following, I give a rough description of the physics that determines the several peculiarities of the CMB power spectrum (see figure 1.7), and a more detailed treatment of the subject can be found for instance in [15].

First of all, the peak structure is due to the fact that photon energy density fluctuations are proportional to the curvature perturbation. As argued above, the curvature perturbation remains frozen on superhorizon scales, and therefore when it re-enters the Hubble horizon, all photon wavelengths oscillate with the same phase. This behaviour is exemplified in figure 1.6. The same argument applies to the gravitational potential and photon velocities. If this were not the case, i.e. if the perturbations originated inside the horizon, the phases would be randomly distributed and they would average to zero, destroying then the peak pattern observed in the CMB temperature spectrum (see figure 1.7).

Second, there is an important transition happening in the first peak, that is the matter-radiation equality. As one can observe in figure 1.3, the first modes

exiting the Hubble horizon (low-k), will re-enter during the matter-dominated era. These modes contain more information about the inflationary era, since they do not have much time to evolve until recombination occurs, or no time at all. Unfortunately, the uncertainty for low ℓ measurements, known as *cosmic variance*, is large in this region. This uncertainty is due to the fact that we only have $2\ell + 1$ measurements for each ℓ, and therefore it is inevitable to have an error of $\Delta C_\ell / C_\ell \sim (2\ell + 1)^{-1/2}$. The maximum of the first peak corresponds to the matter-radiation equality, and subsequent modes of higher ℓ re-enter the horizon in the radiation-dominated era. Thus, these modes contain more information about the evolution of the cosmic fluid, and can be used to calibrate the *cosmological parameters* that characterise our cosmological model.

Another pattern we see in the peaks is that odd peaks are enhanced with respect to even peaks (before the exponential suppression, explained below), and moreover the valleys do not go down to zero. This is because the oscillating part of the CMB power spectrum contains two cosine functions[6], one having a period two times larger than the other, and therefore the odd peaks interfere constructively, while even peaks interfere destructively. However, since there is a relative phase shift between them, the interference is not perfect. In addition, the almost constant positive contribution represents the hydrostatic equilibrium inside the gravitational potential and enhances the whole spectrum.

Last, the peak structure is damped by two different phenomena: Silk damping and the finite thickness effect. The former is due to the fact that the photons can transfer energy from one region to another over distances determined by

[6] In order to see this, note that the temperature fluctuations observed at the present conformal time τ_0 coming from the direction $\mathbf{l}$ are given by [15]:

$$\frac{\delta T}{T}(\tau_0, \mathbf{x}_0, \mathbf{l}) = \int \frac{d^3k}{(2\pi)^{3/2}} \left[\left(\Phi + \frac{\delta}{4} \right)_{\mathbf{k}} - \frac{3\delta'_{\mathbf{k}}}{4k^2} \frac{\partial}{\partial \tau_0} \right]_{\tau_r} \mathrm{e}^{i\mathbf{k}[\mathbf{x}_0 + \mathbf{l}(\tau_r - \tau_0)]} \ ,$$

where τ_r is the conformal time at recombination, Φ the gravitational potential, and δ the radiation energy density fluctuation. When we calculate the average over all angular directions

$$C(\theta) = \left\langle \frac{\delta T}{T}(\mathbf{l}_1) \frac{\delta T}{T}(\mathbf{l}_2) \right\rangle = \frac{1}{4\pi} \sum_{\ell=2}^{\infty} (2\ell + 1) C_\ell P_\ell(\cos\theta)$$

and expand the sine function arising from the product of exponentials:

$$\frac{\sin\left[k|\mathbf{l}_1\tau_1 - \mathbf{l}_2\tau_2|\right]}{k|\mathbf{l}_1\tau_1 - \mathbf{l}_2\tau_2|} = \sum_{\ell=0}^{\infty} (2\ell + 1) j_\ell(k\tau_1) j_\ell(k\tau_2) P_\ell(\cos\theta) \ ,$$

we arrive at the following expression for the multipole moments:

$$C_\ell = \frac{2}{\pi} \int k^2 dk \left| \left[\Phi_k(\tau_r) + \frac{\delta_k(\tau_r)}{4} \right] j_\ell(k\tau_0) - \frac{3\delta'_k(\tau_r)}{4k} \frac{dj_\ell(k\tau_0)}{d(k\tau_0)} \right|^2 \ ,$$

which, when evaluated on small angular scales gives several non-oscillatory and oscillatory terms which result into the peak structure described in the text.

their mean free path. In other words, photons travel from hot to cold regions, mixing and scattering, with the final result of homogenising the temperature distribution and therefore this effect is seen as an exponential suppression[7]. As for the finite thickness effect, it refers to the finite duration of recombination. It is clear that due to this, there is an uncertainty as to the precise moment when a given photon last scatters. This affects inhomogeneities with scales smaller than the duration of recombination, which will be therefore strongly suppressed[8].

In summary, all these effects can be estimated analytically [42] in terms of cosmological parameters: the amplitude and spectral tilt of the primordial power spectrum, the Hubble constant today, the optical depth, the baryon and cold dark matter densities, the dark energy (or vacuum) density, and the curvature of the universe, which is rather assumed to be zero, in agreement with all experiments. In principle, the plateau for $\ell \ll 200$ and the first three acoustic peaks can determine most of the cosmological parameters. But including the damping scales introduces further dependence on the cosmological parameters and a precise determination of these requires the inclusion of higher peaks in the analysis. Moreover, there are several subdominant effects which I have not mentioned here, but that become relevant for very precise measurements of the CMB temperature spectrum and other observables. As mentioned before, the transfer functions that implement these effects are normally computed with Boltzmann solvers. Pioneering work on this subject was made in [43] and the two main codes used nowadays are CAMB [44] and CLASS [45, 46]. With all this rich phenomenology and tools at hand, one computes the CMB temperature fluctuations $\delta T/T$ given the initial conditions from inflation and the cosmological parameters. Then one compares the calculated CMB temperature spectrum in a given cosmological model to the observed one, and determines the cosmological parameters that reproduce the data best. In addition, one can test particular models of inflation where additional parameters are introduced, and find a fit for those parameters that reproduces well the data. In chapter 2 we present a well motivated model for which we performed this search.

Although there are another CMB observables, such as cross-correlated spectra and polarisation, I will focus on the power spectrum and bispectrum, which are the observables studied in this thesis. Regarding the bispectrum, the same physics determines its properties, as for the temperature spectrum. It is clear that the densities of baryons and cold dark matter, the optical depth, along with the expansion of the universe and the initial conditions coming from the inflationary era, are the ingredients that determine the evolution of the energy density of

[7] This suppression appears as a friction damping term in the equations of motion of the photon energy density fluctuations, that becomes important for scales of the order of the photon diffusion scale.

[8] The exponential suppression is the result of the infinite product of probabilities that a photon suffers Thomson scattering during the finite interval in which recombination occurs.

the photons and therefore the correlation functions of the CMB temperature distribution. In the next section I review the current status of power spectrum and bispectrum measurements, which will be relevant for chapters 2 and 3.

1.3.1 CMB power spectrum and bispectrum: experimental status

Let us now have a quick overview on the current status regarding the CMB power spectrum and bispectrum. First of all, the standard cosmological model ΛCDM is normally parameterised in terms of six cosmological parameters. On the one hand, the amplitude A_s and spectral index n_s of the primordial power spectrum. On the other hand, the primordial perturbations evolve in a flat FLRW universe parameterised by the densities of baryonic and cold dark matter, $\Omega_{\rm b}$ and $\Omega_{\rm cdm}$, and the current expansion rate H_0. The damping due to reionisation is parametrized by the optical depth $\tau_{\rm reio}$. For the analyses that we review here, the curvature is assumed to be zero, and the density of dark energy is then the critical density minus baryonic and cold dark matter densities. The latest data release by Planck [47] confirms once more that our universe is dominated by dark energy (68%), it has a substantial amount of cold dark matter (27%), and there is a small fraction of baryonic matter (5%). The precise results of these and the other cosmological parameters are given in [47].

So far, the data is in remarkable agreement with the baseline ΛCDM model, however the existence of certain anomalies in the power spectrum and bispectrum make us think that the baseline model might well be an effective description of a more complicated theory. More importantly, as I will show in chapters 2 and 3, an underlying theory able to predict not only features in the power spectrum and bispectrum, but also a direct correlation between them, would stand as a good candidate to describe the anomalies found in the data. Despite the existence of several data sets, I will focus on the latest results released by the Planck collaboration on the power spectrum [34] and the bispectrum [48], since they are the most precise at the time of writing this thesis.

The CMB power spectrum is shown in figure 1.7, which manifests the remarkable agreement between the data and the simple 6-parameter ΛCDM Planck baseline model [34]. Despite this, it also shows that there are many hints of anomalies between $50 < \ell < 1500$. The dip around $\ell = 1800$ has been questioned, since it seems to be only an effect coming from the 217×217 GHz map [49]. The uncertainties for $\ell < 50$ are not very significant due to the cosmic variance, as explained above. In chapter 2 we will see that models that produce localised oscillations can fit the data reasonably well [1], giving a prediction for the bispectrum that also seems to be in accordance with data.

Extracting primordial information from the CMB bispectrum is rather

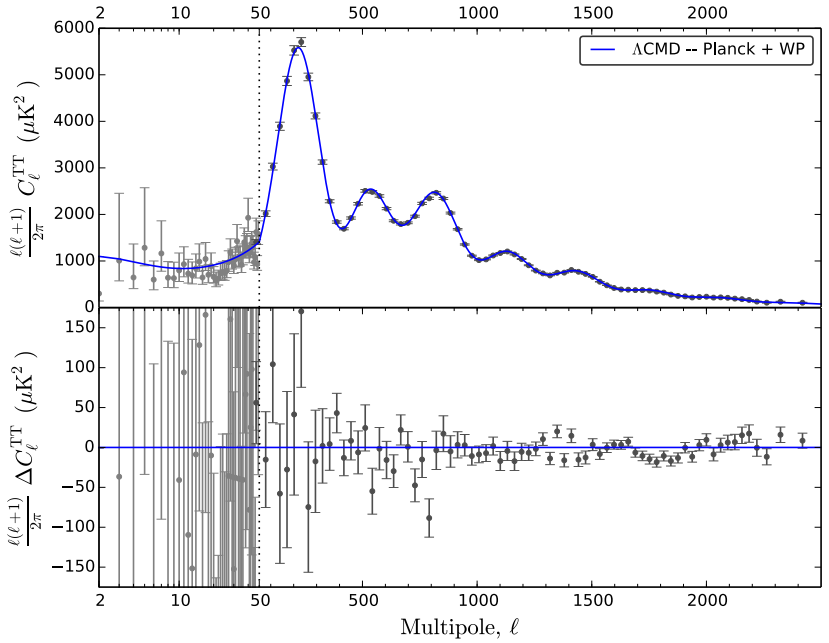

Figure 1.7 *– Planck data for the CMB power spectrum. The solid line represents the theoretical prediction of the Planck + WMAP polarisation baseline ΛCDM cosmological model. Note the series of hints of anomalies $> 1\sigma$ in the bottom plot, which measures the differences between the data points and the model.*

complicated, since there are three directions in ℓ-space. Thus, deconvolving the signal is computationally very challenging and the dependence on the parameters of the theory is much more intricate than for the power spectrum. Despite this, it is still possible to obtain some information on primordial non-gaussianity using the methods developed in [50–52]. The Planck collaboration performed several analyses on the bispectrum signal [48] that I shall briefly describe below.

It is worth noticing that a detection of non-gaussianity would be a smoking gun for models departing from the standard single-field slow-roll regime, since we saw in eq. (1.2.25) that for these models the bispectrum is strongly suppressed. One of the analysis of the Planck collaboration involves the search for primordial *scale-independent* non-gaussianity, parameterised by $f_{\rm NL}$. They looked for particular shapes of the triangle formed by the vectors $\{\mathbf{k_1}, \mathbf{k_2}, \mathbf{k_3}\}$, specifically for local, equilateral and orthogonal shapes, which form an almost orthogonal basis [53, 54], that is, they cover all the configuration space. They found that this type of

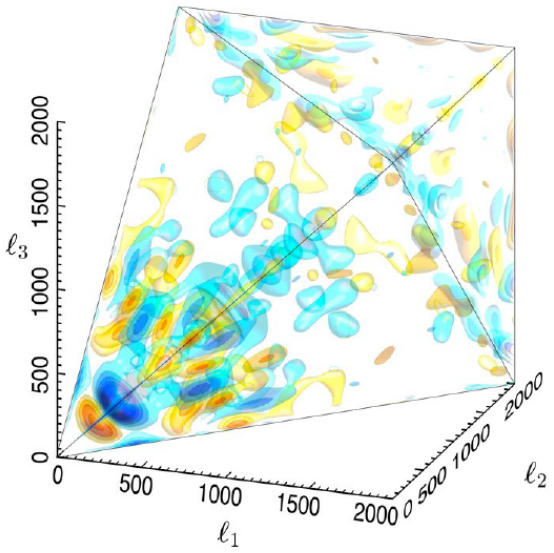

Figure 1.8 *– Reconstruction of CMB bispectrum from the Planck collaboration [48]. The red colour means positive values and blue colour negative values. This data reveals oscillations that are damped for* $\ell > 1500$.

non-gaussianity is small and consistent with zero:

$$f_{\rm NL}^{\rm loc} = 2.7 \pm 5.8 \quad , \quad f_{\rm NL}^{\rm eq} = -42 \pm 75 \quad , \quad f_{\rm NL}^{\rm orth} = -25 \pm 39 \qquad (1\sigma \text{ c.l.}) \, . \tag{1.3.3}$$

In addition, the Planck collaboration performed a search for *scale-dependent* bispectrum features [48], since the reconstruction of the CMB bispectrum data seems to indicate an oscillating signal, as shown in figure 1.8. Their search reveals anomalies of around 3σ with respect to a completely vanishing bispectrum. Although the search for scale-dependent features by Planck is analysed in detail in chapter 2, here I comment the main characteristics of their search. Essentially, they proposed primordial bispectrum templates with oscillations and computed the CMB bispectrum signal. Then they compare with the data and give the significance of their fits. Since this data is not public, the best attempt one can make to validate a bispectrum is to compare with their primordial templates. The Planck collaboration tested three types of primordial templates in the limit $k_1 = k_2 = k_3 = k$: linear oscillations in $\log k$, linear oscillations in k and linear localised oscillations with a gaussian envelope. As I will explain in detail in chapter 2, we proposed a feature model that predicts linear localised oscillations as well. As we will see, the underlying physical mechanism is consistent and well motivated, which justifies the introduction of additional parameters in the cosmological model. Interestingly enough, our functional form has a remarkable resemblance with theirs, and therefore we

were able to roughly test our templates using their analyses. The prospects are promising, since we found a reasonable agreement in our qualitative comparison [1].

Last, it is worth mentioning the recent striking results released by the BICEP2 collaboration [55], which claimed a detection of B-mode polarisation on degree scales that can be attributed to primordial gravitational waves. After this, the cosmology community has been (and still is) analysing all the possible consequences of this detection, but in my opinion these are not yet conclusive and the situation needs to settle down, therefore I prefer to keep a conservative approach. Among the most common arguments, one finds that if the BICEP2 results are confirmed, the inflaton field should have traversed transplanckian distances in order to produce a detectable tensor-to-scalar ratio [56], or in other words, primordial gravitational waves. However, the BICEP2 results have been questioned by several groups, see for instance [57, 58] for an analysis of the foregrounds. Therefore, in the absence of a robust confirmation, along this manuscript I take a cautious approach and consider these results as a possibility worth exploring and taking into account, but nevertheless the works presented in the following chapters do not aim to address the production of primordial gravitational waves.

Summarising, the present data confirms the most robust predictions of the standard inflationary paradigm with a single field and slow-roll regime. However, there is still room for more generic models as long as they predict observable features within the experimental bounds. If the hints of anomalies were confirmed by future data sets, it is important to provide a well-motivated underlying theory able to predict these features. Among these models, it is reasonable to propose inflationary setups which are embedded in UV completable theories, such as string theory of supergravity, since the energies at which inflation happens might be close to the Planck scale. In addition, the presence of additional fields (possibly representing the matter content) arises inevitably in these theories, fortunately or unfortunately. An alternative approach is to consider that new physics does not necessarily appear at high energies, and thus Higgs inflation models have been recycled from an old idea [59–62] by [63] and further studied, for instance, in [64–67]. Although this is a very well motivated scenario worth to explore, in this thesis we will discuss the possibility of having new physics.

In the next section I will review the characteristics of these UV embeddings and in particular the supergravity framework for inflation. Integrating out additional fields is subject to many subtleties that I will describe in the last section of this chapter, together with the possible observable features due to the presence of additional degrees of freedom.

1.4 UV completions of inflation

In this section we turn to more theoretical topics regarding the embedding of inflation in UV completable theories. It is natural to assume that given the energy scale at which inflation happens, a theoretical description that incorporates an UV completion is desirable. A great amount of work has been done in this direction, see for example the excellent reviews of inflation in string theory [68–71] (more recently [72]) and in supergravity [73–75].

From a theorist's perspective, embedding inflation in these theories might seem the natural thing to do. On the other hand, the great achievement of inflation lies on its predictive power, and therefore it is important to keep it as simple as possible, in line with Ockam's razor. Typically these theories introduce a large number of degrees of freedom and consequently a large number of parameters, losing their predictive power. In this situation one in principle has to face an inflationary setup with a large number of fields all coupled to each other, and still try to reduce the system to a simpler version which in the best case scenario can be studied analytically.

Let me stress that consistently integrating out or decoupling additional degrees of freedom is a far from trivial task. It is certainly not enough to argue that very heavy fields can be integrated out *à la Fermi* without consequences, because in a dynamical background there are plenty of effects which can excite these heavy degrees of freedom, invalidating the naive effective theory. In section 1.5 I will describe in detail the conditions for integrating out heavy fields consistently.

A complete review of the impressive amount of realisations of inflation in high-energy theories is out of range here, and therefore I will focus on the generic features of $\mathcal{N} = 1$ supergravity embeddings. In what follows I explain the peculiarities of the scalar potential in supergravity and what problems arise from the gravitational coupling. Details on the differential geometry concerning Kähler manifolds can be found in appendix A. A more self-contained and technical treatment of complex manifolds can be found for instance in [76]. I will focus on the phenomenological aspects of inflation in supergravity, for the formal aspects I refer to the reader to a pedagogical text on supergravity theories such as [77].

1.4.1 Inflation in $\mathcal{N} = 1$ supergravity

The bosonic part of the action for a set of N complex scalar fields Φ^a, $a = 1, \ldots, N$, is constructed with the Ricci scalar R, the kinetic terms of the scalar fields T and the scalar potential V:

$$S = \int d^4x\sqrt{-g}\left(\frac{1}{2}R + T - V\right) , \tag{1.4.1}$$

where g is the determinant of the space-time metric. In the absence of gauge fields, the couplings can be expressed entirely in terms of two functions of the scalars: the *Kähler potential* $K(\Phi, \bar{\Phi})$ and the holomorphic *superpotential* $W(\Phi)$. The fields Φ^a and their complex conjugates $\bar{\Phi}^{\bar{a}} = (\Phi^a)^*$ span a (complex) Kähler manifold whose metric is given by:

$$K_{a\bar{b}} = \frac{\partial^2 K}{\partial \Phi^a \partial \bar{\Phi}^{\bar{b}}} \ . \tag{1.4.2}$$

Unless specified, the partial derivatives with respect to Φ^a and $\bar{\Phi}^{\bar{a}}$ are denoted by subindices a and $\bar{a}$, and the metric $K_{a\bar{b}}$ and its inverse $K^{a\bar{b}}$ are used to raise and lower indices. The action (1.4.1) above can be expressed in terms of a single real scalar function combination of the Kähler potential and superpotential, the well known *Kähler function*, defined as:

$$G(\Phi, \bar{\Phi}) = K(\Phi, \bar{\Phi}) + \log |W(\Phi)|^2 \ , \tag{1.4.3}$$

which is well defined as long as $W \neq 0$. Throughout this manuscript, I will mostly use G instead of K and W, since the case $W = 0$ is not studied here. However, it is important to emphasise that the physical quantities, such as the scalar potential and its derivatives, are well defined for any value of the superpotential, and in some cases it will be interesting to take the limit $W \to 0$. In appendix A I provide a set of relations between quantities expressed in terms of G and in terms of K and W. The Kähler function is invariant under *Kähler transformations*:

$$K(\Phi, \bar{\Phi}) \to K(\Phi, \bar{\Phi}) + h(\Phi) + \bar{h}(\bar{\Phi}) \qquad \text{and} \qquad W(\Phi) \to W(\Phi) \mathrm{e}^{-h(\Phi)}, \tag{1.4.4}$$

with $h(\Phi)$ an arbitrary holomorphic function. In terms of the Kähler function, the kinetic terms and the scalar potential are given by:

$$T = G_{a\bar{b}}\, \partial_\mu \Phi^a \partial^\mu \Phi^{\bar{b}}, \qquad V = \mathrm{e}^G \left(G^a G_a - 3 \right) \ . \tag{1.4.5}$$

Supersymmetry is spontaneously broken when the expectation value of the supersymmetry transformations is non-zero, which for a bosonic configuration can only happen for the transformation of the chiral fermions χ^a:

$$\delta_\epsilon \chi^a = -\frac{1}{2}\, \mathrm{e}^{G/2} G^{a\bar{b}} G_{\bar{b}}\, \epsilon \ , \tag{1.4.6}$$

where ϵ is the parameter of supersymmetry transformations. Since the metric and the exponential are positive definite, the gradient of the Kähler function G_a defines a direction in field space known as the *sGoldstino* direction, which signals supersymmetry breaking. The sGoldstino corresponds to the supersymmetric partner of the would-be Goldstone fermion associated to broken supersymmetry.

In view of the above, when looking at the scalar potential in (1.4.5), one notices that in order to have inflation in supergravity we ought to break

supersymmetry, otherwise the scalar potential is negative and inflation cannot be realised. Therefore, there is always a sGoldstino direction in the field space. This will become relevant in chapter 4, where we identify the inflaton with the sGoldstino and study the possible regimes of inflation. Also, in both chapters 4 and 5 we use the projection of the mass matrix along the sGoldstino direction in order to get constraints on the stability of the fields.

Another characteristic feature of inflation in supergravity is the η-problem, which has to do with the second order slow-roll parameter given by the curvature of the potential, as in (1.2.7). Notice that the Kähler potential that gives canonical kinetic terms is of the following form[9]:

$$K = \Phi\bar{\Phi} \ . \tag{1.4.7}$$

The η-problem appears because of the exponential factor in the scalar potential. Due to this, the slow-roll parameter η_V reads:

$$\eta_V = 1 + \cdots \ , \tag{1.4.8}$$

hence the inflaton acquires an approximate mass of $\mathcal{O}(H)$ and slow-roll inflation does not last long enough. As will be described in more detail in chapter 4, there are possible ways out for this problem:

- For small field regimes one can always fine-tune the superpotential in such a way that the additional terms in $(\cdots)$ above conspire together to cancel the order unity contribution. This is not possible for large field regimes, since fine-tuning is not effective for a long trajectory.

- For large field regimes, one can invoke a symmetry, which is an elegant solution to provide flatness over a large trajectory. For instance, the Kähler potential in (1.4.7) has a flat direction for the phase, and therefore identifying the inflaton with the phase θ in $\Phi = |\Phi|e^{i\theta}$ would solve the η-problem. Several examples of different symmetries have been studied in [78–81]. The superpotential then introduces a soft breaking of the symmetry that produces the slope of the scalar potential.

Once the η-problem has been circumvented, we run into a more serious problem that in the literature is often assumed to be solved: the stabilisation of multiple fields. It is indeed a good first step to consider only one sector containing the inflaton, but what about considering the other sectors? Two potentially dangerous situations arise when considering additional fields: instabilities and isocurvature modes, both ruining the predictions of single-field inflation.

[9] Alternative forms related by a Kähler transformation are also possible, for instance one might have canonical kinetic terms for $K = \frac{1}{2}(\Phi + \bar{\Phi})^2$ or $K = -\frac{1}{2}(\Phi - \bar{\Phi})^2$.

1.4.2 Decoupling in supergravity

After taking care of the inflaton sector and making sure that the slow-roll conditions can be satisfied, one has to deal with the additional sectors. In order to solve the stability problems it is necessary to guarantee that the rest of fields remain *at least* heavy and stabilised during inflation. Even in that situation, it is still possible to see their influence in the CMB if they are coupled to the inflaton through turns in the scalar potential or non-canonical kinetic terms. The influence of additional fields during inflation will be discussed in detail in section 1.5. Ideally, for a perfect decoupling, the rest of fields must be stabilised on *geodesic trajectories*. Specifically, if we label the fields $\Phi^a = (X, \Phi^i)$, with X being the inflaton field and Φ^i being the additional fields, they satisfy the equation of motion:

$$\ddot{\Phi}^i + \Gamma^i_{ab}\dot{\Phi}^a\dot{\Phi}^b + 3H\dot{\Phi}^i + K^{i\bar{b}}V_{\bar{b}} = 0 \ , \tag{1.4.9}$$

where $\Gamma^i_{ab} = K^{i\bar{c}}K_{ab\bar{c}}$ (see appendix A) and geodesic trajectories, or straight lines on a manifold, must satisfy:

$$\ddot{\Phi}^i + \Gamma^i_{ab}\dot{\Phi}^a\dot{\Phi}^b \propto \dot{\Phi}^i \ . \tag{1.4.10}$$

Notice that the indices a, b contain the inflaton and thus satisfying both equations above is a very non-trivial task. A possible solution [3, 82–85] is to have a *separable Kähler function* such that:

$$G(X, \bar{X}, \Phi^i, \bar{\Phi}^{\bar{i}}) = G_{\rm inf}(X, \bar{X}) + G_{\rm other}(\Phi^i, \bar{\Phi}^{\bar{i}}) \ , \tag{1.4.11}$$

which in particular implies that the metric and the Christoffel symbols are block diagonal in the inflaton-others field space. In this case, if the other fields remain on a fixed position Φ^i_0 at a critical point of the potential $V_i(X, \Phi^i_0) = 0$, they are consistently truncated and we can study their dynamics separately. The only extra requirement we need is that the critical point is actually a minimum, and not a maximum. For this one has to check that the mass matrix of the truncated sector is positive definite. This imposes constraints on the inflationary dynamics and on the parent supergravity, as we will see in detail in chapters 4 and 5.

Satisfying the critical condition $V_i(X, \Phi^i_0) = 0$ is not straightforward, as can be seen from the expression of the derivative of the scalar potential:

$$V_i = G_i V + \mathrm{e}^G \left[G^j \nabla_j G_i + G_i\right] \ . \tag{1.4.12}$$

There is a simple way to achieve $V_i(X, \Phi^i_0) = 0$, and that is by having:

$$G_i(X, \Phi^i_0) = 0 \quad \Longrightarrow \quad V_i(X, \Phi^i_0) = 0 \ . \tag{1.4.13}$$

As explained above, this implies that the fields Φ^i preserve supersymmetry, and therefore the point Φ^i_0 satisfying $G_i(X, \Phi^i_0) = 0$ is called *supersymmetric*

critical point. This configuration yields a *consistent supersymmetric truncation* of the 'non-inflating' sector [83–85]. Notice that in view of the above, only the inflaton breaks supersymmetry and therefore the inflaton is the sGoldstino [3]. The constraints on the inflationary dynamics and on the truncated sector are explored in detail in chapter 4, as well as some working examples of different inflationary scenarios that are possible in this setup.

There is yet another possible approach to achieve a decoupling of sectors during inflation. Instead of having the inflaton and the sGoldstino directions to be parallel, they can be orthogonal, as in the model with vanishing superpotential during inflation proposed in [86], where they have:

$$D_X W(X, \Phi_0^i) = 0 \quad , \quad D_i W(X, \Phi_0^i) \neq 0 \ , \tag{1.4.14}$$

where $D_a W = K_a W + W_a \neq 0$ signals supersymmetry breaking, and is equivalent to $G_a \neq 0$ for non-vanishing superpotentials. This configuration leads to $V_i(X, \Phi_0^i) = 0$ for $W(X, \Phi_0^i) = W_X(X, \Phi_0^i) = 0$, and therefore in this case the supersymmetry breaking is sourced by $W_i(X, \Phi_0^i) \neq 0$, and successful inflation with consistent decoupling can be achieved as well. We will see in chapter 5 that this situation is also constrained, since we derived the conditions of stability along the supersymmetric directions as well.

Last, let me emphasise that even when one consistently truncates the theory to the level of one dynamical complex scalar field, there are two real scalar fields and we still must be aware of the subtleties of inflation with multiple fields: turns in the trajectory, non-canonical kinetic terms, and isocurvature modes. This is precisely the subject of the next section.

1.5 Effective field theories of inflation in the presence of heavy fields

In the previous sections of this chapter we have seen how single-field slow-roll inflation models work, and how the quantum fluctuations of the inflaton field translate into the CMB temperature anisotropies. Later on, we had an overview of the motivations and difficulties to embed inflation in UV completable theories such as supergravity, where, among others, the problem of field stabilisation arises. In this section I consider the presence of multiple dynamical degrees of freedom and I analyse the conditions under which a heavy field can be consistently integrated out. Then I review the construction of effective single-field theories and how we can see the effects of the additional heavy fields from the effective single field theory point of view. Finally, we will see that even very heavy fields can leave their imprint in the correlation functions, which will be followed by chapters 2 and 3, where we make a statistical study of the significance of this kind of imprints in the CMB.

1.5.1 Inflation with multiple fields

As stressed in the previous section, in high energy theories the presence of additional fields is common. In some of the literature these fields are, explicitly or implicitly, assumed to be stabilised, and the theory is *inconsistently* truncated to a single-field description. In addition, this assumption is sometimes incorrectly justified by calculating the potential slow-roll parameters defined in (1.2.6) and (1.2.7), which ignore the presence of additional fields, because they only account for the slope and curvature of the potential in the light field direction (supposedly the inflaton). This practise results into misleading results and completely ignores the rich phenomenology conferred by the dynamics of these heavy fields.

Inflationary scenarios with multiple fields have been extensively studied, an incomplete list of works where the multiple field dynamics has been studied is [87–95] (see [96] for an excellent review). Here we will focus on the main differences with respect to the single-field case reviewed in section 1.2.

Consider a set of N real scalar fields ϕ^a, $a = 1, \ldots, N$, spanning a real manifold of dimension N with metric γ_{ab}. Similarly to the complex case seen in the previous section, the kinetic terms are given by:

$$T = \frac{1}{2}\gamma_{ab}\,\partial_\mu\phi^a\partial^\mu\phi^b \ . \tag{1.5.1}$$

The background equations of motion for the set of homogeneous scalar fields $\phi^a(t)$ in a FLRW universe are:

$$\frac{D\dot{\phi}^a}{dt} + 3H\dot{\phi}^a + \gamma^{ab}V_b = 0 \ , \tag{1.5.2}$$

where $DX^a \equiv dX^a + \Gamma^a_{bc}X^b d\phi^c$, and Γ^a_{bc} is the Levi-Civita connection associated to the metric γ_{ab}. It is useful to define a unitary vector along the trajectory:

$$T^a = \frac{\dot{\phi}^a}{\dot{\phi}} \quad , \text{ with } \quad \dot{\phi}^2 = \dot{\phi}^a\dot{\phi}_a \ . \tag{1.5.3}$$

One can also define a normal vector perpendicular to the above one in $N-1$ directions, but for the sake of simplicity we will specialise to the case of two fields. The normal vector can be defined as:

$$N^a = \epsilon^{ab}T_b \ , \tag{1.5.4}$$

where ϵ_{ab} is the Levi-Civita totally antisymmetric symbol. The normal vector N^a then satisfies[10]:

$$N_aN^b + T_aT^b = \delta^b_a \quad , \quad N^aN^b + T^aT^b = \gamma^{ab} \ . \tag{1.5.5}$$

[10]For more than two fields, we need to define the projector along the orthogonal directions to the subspace spanned by the vectors T^a and N^a, given by $P^{ab} = \gamma^{ab} - (N^aN^b + T^aT^b)$.

Then one can define the directional derivatives of the potential $V_T \equiv V_a T^a$ and $V_N \equiv V_a N^a$. If we take now the projection of the equations of motion (1.5.2) along the parallel and normal directions, we obtain, respectively:

$$\ddot{\phi} + 3H\dot{\phi} + V_T = 0 \ , \tag{1.5.6}$$

$$\frac{DT^a}{dt} = -\frac{V_N}{\dot{\phi}} N^a \ . \tag{1.5.7}$$

Notice that the first equation is analogous to that of a single-field setup, while the second signals the departure from straight trajectories, which will become relevant very soon.

Slow-roll parameters

Let us now give some definitions of slow-roll parameters in the multiple field case. The first kinematic slow-roll parameter ϵ remains the same, since it is proportional to the total kinetic energy:

$$\epsilon = -\frac{\dot{H}}{H^2} = \frac{\dot{\phi}^2}{2H^2} \ , \tag{1.5.8}$$

but the second order kinematic slow-roll parameter η_3 can be decomposed in tangential and normal components as follows:

$$\eta^a \equiv -\frac{1}{H\dot{\phi}} \frac{D\dot{\phi}^a}{dt} = \eta_{\parallel} T^a + \eta_{\perp} N^a \ , \tag{1.5.9}$$

where

$$\eta_{\parallel} = -\frac{\ddot{\phi}}{H\dot{\phi}} = 3 + \frac{V_T}{H\dot{\phi}} \quad , \quad \eta_{\perp} = \frac{V_N}{H\dot{\phi}} = \frac{\dot{\theta}}{H} \ . \tag{1.5.10}$$

Note that the parallel component coincides with the single-field definition η_3 in (1.2.4). Let me stress that $\eta_{\perp} \neq 0$ signals a turn in the inflationary trajectory, with $\dot{\theta}$ being the turn rate, and that it does not necessarily have to be small, so in that sense $\eta_{\perp}$ is not a slow-roll parameter but a slow-turn parameter.

As for the potential slow-roll parameter ϵ_V, the definition for the multiple field case has to incorporate the slope of the potential in all the field directions, since the inflaton will always roll in the steepest direction, and therefore it reads:

$$\epsilon_V = \frac{1}{2V^2} \gamma^{ab} V_a V_b = \frac{1}{2} \left(\frac{V_T}{V} \right)^2 \left[1 + \left(\frac{V_N}{V_T} \right)^2 \right] \ , \tag{1.5.11}$$

which can be rewritten using the definitions in (1.5.10) as follows:

$$\epsilon_V = \frac{\epsilon}{(3-\epsilon)^2} \left[(3 - \eta_{\parallel})^2 + \eta_{\perp}^2 \right] \ . \tag{1.5.12}$$

Notice that for straight trajectories, $\eta_\perp = 0$, and the expression above reduces to the single-field parameter, as it should. Once we have these quantities at hand, let us turn to the phenomenological aspects.

Adiabatic and isocurvature (or entropy) perturbations

In this subsection our purpose is to explain that in the presence of multiple fields, isocurvature (or entropy) perturbations are not necessarily suppressed, and they might spoil the conservation of the adiabatic curvature perturbation on large scales, as opposed to the single field case. In the following I will review the main qualitative results of the analysis in [88].

For the purpose of this section, we will consider a set of scalar fields ϕ^a with canonical kinetic terms, i.e. the metric of the field manifold is the identity. I will denote field indices with the first letters of the alphabet $(a, b, \dots)$ and coordinate indices with the middle letters $(i, j, \dots)$. When considering linear perturbation of scalar fields, one must also consider metric perturbations, which can be parameterised as follows:

$$ds^2 = -(1+2A)\,dt^2 + 2a\partial_i B\,dx^i dt + a^2\left[(1-2\psi)\delta_{ij} + 2\partial_i\partial_j E\right]\,dx^i dx^j \ , \quad (1.5.13)$$

where the partial derivatives ∂_i denote derivatives with respect to the coordinates. Considering perturbations of the scalar fields of the form $\phi^a \to \phi^a(t) + \delta\phi^a(\mathbf{x}, t)$, the equations of motion in Fourier space read:

$$\begin{aligned}\delta\ddot{\phi}^a + 3H\delta\dot{\phi}^a + \frac{k^2}{a^2}\delta\phi^a + \delta^{ab}V_{bc}\delta\phi^c = -2A\delta^{ab}V_b \\ +\dot{\phi}^a\left[\dot{A} + 3\dot{\psi} + \frac{k^2}{a^2}\left(a^2\dot{E} - aB\right)\right] \ ,\end{aligned} \quad (1.5.14)$$

where the subindices denote derivatives with respect to the fields, and the background fields $\phi^a(t)$ satisfy the equations of motion (1.5.2) with a trivial field metric. Let us now define the comoving curvature perturbation (in the longitudinal gauge):

$$\mathcal{R} = \psi - \frac{H}{\dot{H}}\left(\dot{\psi} + HA\right) \ , \quad (1.5.15)$$

which is related to the curvature perturbation on uniform density hypersurfaces ζ as follows:

$$-\zeta = \mathcal{R} + \frac{2\rho}{3(p+\rho)}\left(\frac{k}{aH}\right)^2\psi \quad \xrightarrow{k\ll aH} \quad \mathcal{R} \ . \quad (1.5.16)$$

We will soon see that both $\mathcal{R}$ and ζ remain constant at large (superhorizon) scales for purely adiabatic perturbations. Since in this thesis we will focus on effectively single field inflation, and we will be mostly interested on the behaviour of correlation functions on superhorizon scales, I will often abuse the language

and refer to both of them as adiabatic curvature perturbation.

One can also define the (gauge-independent) total entropy perturbation by splitting the pressure perturbation in adiabatic and entropic parts:

$$\delta p = \frac{\dot{p}}{\dot{\rho}}\delta\rho + \frac{\dot{p}}{H}\mathcal{S} \quad , \quad \text{with} \quad \mathcal{S} = H\left(\frac{\delta p}{\dot{p}} - \frac{\delta\rho}{\dot{\rho}}\right) . \tag{1.5.17}$$

It can be shown [97] that on large scales, due to local energy conservation, the variation in the adiabatic curvature perturbation is

$$\dot{\mathcal{R}} = -3H\frac{\dot{p}}{\dot{\rho}}\mathcal{S} , \tag{1.5.18}$$

and therefore when the pressure perturbation is adiabatic ($\mathcal{S} = 0$), $\mathcal{R}$ is conserved on superhorizon scales. Let us evaluate the entropy perturbation for the cases of single-field and two-field inflation.

For **single-field**, since the scalar field φ is determined up to two integration constants, they describe adiabatic and entropic perturbations. It can be seen that in the longitudinal gauge the entropy perturbation can be written as:

$$\mathcal{S} = -\frac{V_\varphi}{6\pi G\dot{\varphi}^2\left(3H\dot{\varphi} + 2V_\varphi\right)}\left(\frac{k^2}{a^2}\psi\right) \quad \Longrightarrow \quad \dot{\mathcal{R}} = \frac{H}{\dot{H}}\frac{k^2}{a^2}\psi \quad \xrightarrow{k\ll aH} \quad 0 , \tag{1.5.19}$$

and therefore the curvature perturbation is conserved on large scales.

For **two-field** inflation, as explained above, one can choose a basis in field space such that one of the directions is parallel to the trajectory (adiabatic field) and the other direction perpendicular (entropy field). In order to facilitate the connection with [88], I will keep their notation unchanged, except for the quantities introduced in this text previously. The adiabatic and entropy fields can be defined as:

$$\dot{\phi} = T^a\dot{\phi}_a \quad , \quad \delta s = N^a\delta\phi_a , \tag{1.5.20}$$

where ϕ_a is the vector of two fields, and the tangential and normal unitary vectors (T^a, N^a) were defined in (1.5.3) and below. The entropy perturbation is then given by:

$$\mathcal{S} = -\frac{V_T}{6\pi G\dot{\phi}^2\left(3H\dot{\phi} + 2V_T\right)}\left(\frac{k^2}{a^2}\psi\right) - \frac{2V_N}{3\dot{\phi}^2}\delta s , \tag{1.5.21}$$

where an additional contribution coming from the entropy field proportional to the turn rate[11] $\dot{\theta} = V_N/\dot{\phi}$ appears at all scales. Due to this, the change in the

[11] Note the slight change of notation with respect to [88], where the turn rate is defined as $\dot{\theta} = -V_N/\dot{\phi}$.

adiabatic curvature perturbation receives an extra contribution of the form:

$$\dot{\mathcal{R}} = \frac{H}{\dot{H}}\frac{k^2}{a^2}\psi - \frac{2H}{\dot{\phi}}\dot{\theta}\delta s \ . \tag{1.5.22}$$

Here we clearly see how the presence of an additional field might produce superhorizon evolution of the adiabatic curvature perturbation, which is in disagreement with experiments. Despite of this, a large effective mass for the entropy field will suppress the entropy perturbation at superhorizon scales.

At the level of the equations of motion, both modes decouple for $\dot{\theta} = 0$, as one would expect. In fact, on large scales the entropy perturbation satisfies a homogeneous second order equation, however the adiabatic perturbation suffers from metric back-reaction and a source term coming from the entropy perturbation. This can be seen in the power spectrum, since the entropy perturbation enhances the adiabatic spectrum, but not vice versa.

To summarise, we have seen that when multiple fields participate on inflation, the only way to suppress isocurvature or entropy perturbations is to have straight trajectories and a heavy mass in the perpendicular direction, such that the entropy fluctuations do not survive at late times, unless there is a particular mechanism that avoids the generation of isocurvature perturbations. Note that non-canonical kinetic terms may cause the same turning effects on trajectories that would otherwise look straight. In the next subsection we will see some of these aspects in more detail, but formulated slightly different, in such a way that it permits us to establish direct connection with the effective field theory of inflation [98]. From now on we will focus on inflationary models that can be described by a single field after integrating out the heavy degrees of freedom. We will discuss the conditions under which this integration is valid and the fingerprints of the heavy physics on the low-energy effective theory.

1.5.2 Effective single-field inflation and the speed of sound

We will now focus on inflation with a light field and a heavy field and review the construction of an effective field theory for the light field. There has been extensive work in the last decade in this respect, for instance see [98–110] for work related to effective single-field theories and the integration of heavy fields.

Let us consider a set of N real scalar fields ϕ^a spanning a manifold with metric γ_{ab}. The kinetic energy of the fields is given by (1.5.1) and their equations of motion by (1.5.2). We parameterise the perturbations around the background solution $\phi_0^a(t)$ as indicated in figure 1.9: the field $\pi(t, \mathbf{x})$ represents displacements along the background trajectory, while $\mathcal{F}(t, \mathbf{x})$ parameterises deviations off the background trajectory along the perpendicular direction N^a at the time

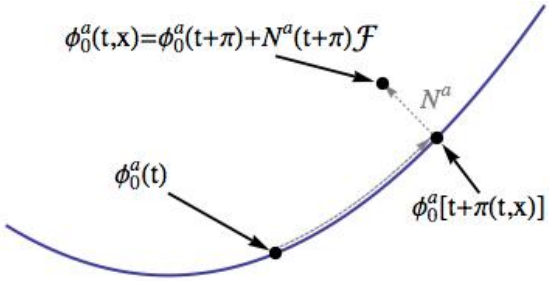

Figure 1.9 *– Parameterisation of perturbations along the background trajectory, using the displacement along the trajectory, π, and the unitary vector orthogonal to the background trajectory, N^a. The displacement in the orthogonal direction is proportional to the heavy mode $\mathcal{F}$. Figure adapted from [107].*

$t + \pi$. Intuitively, one would think that π is related to the adiabatic curvature perturbation $\mathcal{R}$ and $\mathcal{F}$ to the entropy perturbation $\mathcal{S}$, and indeed this is the case, because $\mathcal{R} = -\pi H$ [39] and $\mathcal{F} = \mathcal{S}\dot{\phi}_0/H$ (see, for instance [106]). We will work in terms of $\mathcal{R}$ and $\mathcal{F}$ to respect the notation of [106, 107].

In terms of $\mathcal{R}$ and $\mathcal{F}$, the quadratic action reads:

$$S_2 = \int d^4x \left[\frac{\dot{\phi}_0^2}{H^2}\dot{\mathcal{R}}^2 - \frac{\dot{\phi}_0^2}{H^2}\frac{1}{a^2}(\nabla\mathcal{R})^2 + \dot{\mathcal{F}}^2 - \frac{1}{a^2}(\nabla\mathcal{F})^2 + 4\dot{\phi}_0^2\eta_\perp\dot{\mathcal{R}}\mathcal{F} - M_{\rm eff}^2\mathcal{F}^2 \right] , \tag{1.5.23}$$

where $M_{\rm eff}^2 = V_{NN} + H^2\epsilon\mathbb{R} - \dot{\theta}^2 = m^2 - \dot{\theta}^2$ is interpreted as the mass of the heavy field $\mathcal{F}$, and $\mathbb{R}$ is the Ricci scalar of the field manifold. The equations of motion derived from the action above are:

$$\begin{aligned} \ddot{\mathcal{R}} + \left(3 + 2\epsilon - 2\eta_\parallel\right) H\dot{\mathcal{R}} - \frac{1}{a^2}\nabla^2\mathcal{R} &= -\frac{2H^2}{\dot{\phi}_0}\eta_\perp\left[\dot{\mathcal{F}} + \left(3 - \eta_\parallel - \xi_\perp\right) H\mathcal{F}\right] , \\ \ddot{\mathcal{F}} + 3H\dot{\mathcal{F}} - \frac{1}{a^2}\nabla^2\mathcal{F} + M_{\rm eff}^2\mathcal{F} &= 2\dot{\phi}_0\eta_\perp\dot{\mathcal{R}} , \end{aligned} \tag{1.5.24}$$

where $\xi_\perp = -\dot{\eta}_\perp/\eta_\perp H = -\ddot{\theta}/\dot{\theta}H - \epsilon$ is related to the turn acceleration. We can now clearly see that the equations of motion are coupled whenever $\eta_\perp \neq 0$, or in other words, when the inflationary trajectory traverses a turn.

Decoupling

The equations of motion (1.5.24) can be interpreted as two coupled harmonic oscillators with a derivative coupling, for which one can propose the ansatz:

$$\mathcal{F}(\mathbf{k}, t) = f(\mathbf{k})\mathrm{e}^{i\omega t} \quad , \quad \mathcal{R}(\mathbf{k}, t) = r(\mathbf{k})\mathrm{e}^{i\omega t} . \tag{1.5.25}$$

Let us take the slow-roll ($\epsilon, \eta_{\parallel} \ll 1$) and soft-turn ($\xi_{\perp} \ll 1$) limit, and disregard Hubble friction terms. Under those assumptions, the equations of motion in Fourier space can be approximated by:

$$\ddot{\mathcal{R}} + \frac{k^2}{a^2}\mathcal{R} = -\frac{2H}{\dot{\phi}_0}\dot{\theta}\dot{\mathcal{F}} \ ,$$

$$\ddot{\mathcal{F}} + \frac{k^2}{a^2}\mathcal{F} + M_{\rm eff}^2\mathcal{F} = 2\dot{\phi}_0\frac{\dot{\theta}}{H}\dot{\mathcal{R}} \ . \tag{1.5.26}$$

Plugging the ansatz (1.5.25) into the simplified equations of motion (1.5.26) we obtain the following equation for the frequencies:

$$\omega^4 - \omega^2\left(4\dot{\theta}^2 + \frac{2k^2}{a^2} + M_{\rm eff}^2\right) + \frac{k^2}{a^2}\left(\frac{k^2}{a^2} + M_{\rm eff}^2\right) = 0 \ , \tag{1.5.27}$$

whose solution is given by:

$$\omega_{\pm}^2 = \frac{1}{2}\left[\left(4\dot{\theta}^2 + \frac{2k^2}{a^2} + M_{\rm eff}^2\right) \pm \sqrt{\left(4\dot{\theta}^2 + M_{\rm eff}^2\right)^2 + 16\dot{\theta}^2\frac{k^2}{a^2}}\ \right] \ , \tag{1.5.28}$$

which is the result displayed in [102, 109]. Hence, the solutions for the curvature and isocurvature modes in (1.5.25) will be a linear combination of heavy modes of frequency ω_+ and light modes of frequency ω_-:

$$\mathcal{F}(\mathbf{k}, t) = f_+(\mathbf{k})\mathrm{e}^{i\omega_+ t} + f_-(\mathbf{k})\mathrm{e}^{i\omega_- t} \ ,$$

$$\mathcal{R}(\mathbf{k}, t) = r_+(\mathbf{k})\mathrm{e}^{i\omega_+ t} + r_-(\mathbf{k})\mathrm{e}^{i\omega_- t} \ , \tag{1.5.29}$$

where the relation between the amplitude of different modes can be found by substituting our ansatz in the equations of motion, and is given by:

$$\frac{r_{\pm}}{f_{\pm}} \simeq \frac{2iH\dot{\theta}\omega_{\pm}}{\dot{\phi}_0\left(\omega_{\pm}^2 - \frac{k^2}{a^2}\right)} \ , \tag{1.5.30}$$

or equivalently:

$$\frac{f_{\pm}}{r_{\pm}} \simeq -\frac{2i\dot{\phi}_0\dot{\theta}\omega_{\pm}}{H\left(\omega_{\pm}^2 - \frac{k^2}{a^2} - M_{\rm eff}^2\right)} \ . \tag{1.5.31}$$

At this point one can study all the different hierarchies between the parameters k/a, $M_{\rm eff}$ and $\dot{\theta}$, which will tell us in what limit the modes are decoupled, that is, when $f_+ \gg r_+$ and $f_- \ll r_-$ the mode $\mathcal{F}$ is mostly heavy with frequency $\omega_+ \gg \omega_-$, and the mode $\mathcal{R}$ is mostly light with frequency $\omega_- \ll \omega_+$. This happens in particular for $M_{\rm eff} \gg k/a, \dot{\theta}$, and surprisingly for $\dot{\theta} \gg H, k/a$.

As emphasised in [109], one would expect that for a large turn rate, the effective mass of the heavy field decreases and therefore the modes would not decouple. However, one observes that a large turn rate helps in mode decoupling, i.e. the gap between the frequencies $\omega_{\pm}$ increases. In the following I will describe the conditions under which the heavy field can be integrated out, so that one can write down an effective single field theory for the adiabatic curvature perturbation under the effects of the heavy mode.

Integrating out $\mathcal{F}$ and the sound speed

We focus now on the equation of motion for the heavy mode in (1.5.24). We will stick to the regime in which $M_{\rm eff} \gg H$ so that we can disregard isocurvature fluctuations, and also neglect the friction term in the equation of motion (1.5.24). Then, in the regime where $|\ddot{\mathcal{F}}| \ll M_{\rm eff}^2 |\mathcal{F}|$, in which the kinetic terms of $\mathcal{F}$ can be neglected, we can express the entropy (heavy) field in terms of the adiabatic (light) field as follows:

$$\mathcal{F}_{\mathcal{R}} = \frac{2\dot{\phi}_0 \eta_{\perp}}{k^2/a^2 + M_{\rm eff}^2} \dot{\mathcal{R}} \ . \tag{1.5.32}$$

Plugging this solution into the quadratic action (1.5.23) we find the following effective action for the adiabatic mode (see [107] for a elaborated treatment):

$$S_{\rm eff,2} = \int d^4x \, a^3 \epsilon \left[\frac{\dot{\mathcal{R}}^2}{c_s^2} - \frac{(\nabla \mathcal{R})^2}{a^2} \right] \ , \tag{1.5.33}$$

where we have defined the *speed of sound* of the adiabatic mode:

$$c_s^{-2} = 1 + \frac{4\dot{\theta}^2}{k^2/a^2 + M_{\rm eff}^2} \ . \tag{1.5.34}$$

Some important points are to be made here:

- Whenever the inflationary trajectory traverses a turn, from the effective field theory point of view it appears as a reduction in the speed of sound of the adiabatic mode. Isolated turns translate into transient reductions of the speed of sound.
- Reductions in the speed of sound are completely consistent with a slow-roll regime.
- Transient reductions in the speed of sound result into localised features in the power spectrum, which is evident from the presence of c_s^{-2} in the quadratic action. This happens as well for higher order correlation functions. In fact, in chapters 2 and 3 we will also show the effective cubic action and calculate the features both in the power spectrum and bispectrum. These can be calculated using the in-in formalism and considering the contribution

of the reduced speed of sound as a perturbation, as we will see in detail in chapter 3.

- Given that the speed of sound appears at all orders in the effective action, the features in the correlation functions are correlated [111, 112].

- The validity of the effective field theory is subject to the adiabatic condition $|\ddot{\mathcal{F}}| \ll M_{\rm eff}^2 |\mathcal{F}|$, which in terms of background quantities can be written as [106]:

$$\left| \frac{d}{dt} \ln(1 - c_s^{-2}) \right| \ll M_{\rm eff} \ , \tag{1.5.35}$$

  which essentially implies that turns cannot be too sudden (large angular acceleration), but they can still be strong (large angular turn rate).

To summarise the material presented in this section, we have seen that the presence of multiple fields during inflation produces a rich phenomenology. While the production of entropy fluctuations is dangerous, it is nevertheless possible to suppress them if the entropy field is sufficiently heavy. In that case, one can construct an effective single field theory for the adiabatic curvature perturbation, where the effect of the heavy physics is parameterised in terms of a reduced speed of sound for the adiabatic mode. The single-field description is valid as long as turns along the inflationary trajectory are not too sudden, and transient reductions of the speed of sound reveal themselves through localised features in the correlation functions. This has important consequences, since it opens a window to detect the presence of heavy fields during inflation. In fact, in chapter 2 I present the work in which we performed a search for this kind of features in the Planck CMB data, and in chapter 3 I present an elaborated treatment of the calculation of these features using different methods, and the consistency of the effective field theory.

2

Transient reductions of the inflaton speed of sound in the Planck data

As explained in the first chapter, the first year of observations by the Planck satellite mission shows that the CMB fluctuations are consistent with gaussian statistics in the primordial perturbations, a key prediction of the simplest models of inflation. However, there are hints of anomalies in the CMB power spectrum and bispectrum. In this chapter I present the work [1], where we check for the possibility that some of these anomalous features have a common physical origin in a transient reduction of the inflaton speed of sound. We do this by exploiting predicted correlations between the power spectrum and bispectrum. Our results strongly suggest that current data might already be sensitive enough to detect transient reductions in the speed of sound as mild as a few percent. Since this is a signature of interactions, it opens a new window for the detection of extra degrees of freedom during inflation.

2.1 Introduction

The paradigm of inflation [5–10] in its simplest realisations is consistent with the latest data releases from the Planck [32] and WMAP [31] satellites. However, hints of a primordial oscillatory signal in the CMB bispectrum [48] and of anomalies in the CMB power spectrum [31, 113] motivate a search for correlated features produced by inflationary scenarios beyond canonical single-field [1]. Such correlation is in general expected and will differ depending on its physical origin

[1] By canonical single-field we mean slow-roll regime, Bunch-Davies vacuum and canonical kinetic terms.

[98], so it can be used to discriminate among inflationary mechanisms.

On the theory side, several mechanisms that produce oscillatory features are being investigated. As first noted in [114], a step in the inflaton potential causes features in the spectra [115–124], and novel methodologies have been developed in [125–130] for more generic transient slow-roll violations. The effect of a variable speed of sound has also been analysed both in the power spectrum [103, 111, 131] (for sudden variations see [124, 129, 132–134]) and bispectrum [111, 130, 135] (see [124, 134] for sudden variations). Different initial vacuum states (see e.g. [27–30]) or multi-field dynamics [108, 136–138] may also cause oscillations in the primordial spectra.

On the observational side, searches in the CMB power spectrum data have been performed for a variety of scenarios, such as transient slow-roll violations [121, 129, 139–144], superimposed oscillations in the primordial power spectrum [145–151] and more general parametric forms (see [113] and references therein). In addition, the Planck collaboration searched for features in the CMB bispectrum for a number of theoretically motivated templates [48]. In none of these cases the statistical significance of the extended models has been found high enough to claim a detection. Still, it is becoming clear that hints of new physics (if any) are most likely to be detected in the correlation between different observables.

In this spirit, in this chapter I summarise the first paper [1] in which we search for transient reductions in the speed of sound of the adiabatic mode consistent with (effectively) single-field inflation and *uninterrupted* slow-roll. We do this by exploiting a very simple correlation between power spectrum and bispectrum noted in [111]. While more general situations are possible, and have been considered elsewhere [128, 130], there is a particularly interesting regime for which the *complete* primordial bispectrum is obtained to leading order in slow-roll [111]. The amplitude and the rate of change of the speed of sound must be large enough to dominate over slow-roll effects while being small enough to allow a perturbative calculation of the effect on the power spectrum and bispectrum.

Our test case consists of a gaussian reduction in the speed of sound occurring within the window of e-folds in which the scales corresponding to the angular scales probed by Planck exit the Hubble sound horizon. The functional form is inspired by soft turns along a multi-field inflationary trajectory with a large hierarchy of masses, a situation that is consistently described by an effective single-field theory [102, 103, 106, 107] (see also [108, 136]), as described in section 1.5. Nevertheless we stress that reductions in the speed of sound are a more general phenomenon within effective field theory (and hence may have diverse physical origins).

Our statistical analysis of the Planck CMB power spectrum reveals several

fits with a moderately improved likelihood compared to the best ΛCDM fit. For each of those fits we give the associated full primordial bispectrum. The Planck bispectrum data have not yet been released but, due to a lucky coincidence, templates very similar to our predictions have already been tested by Planck [48] (inspired by a step in the potential). We find that the predicted bispectra for some of our fits are reasonably consistent with the best fits of Planck. In addition, some of our best fits lie on a region of the parameter space not yet analysed by Planck. If confirmed, these correlations would constitute evidence for transient reductions in the speed of sound. It is interesting that rather mild reductions of the order of a few percent may already be observable in the data.

2.2 Correlated features in the primordial spectra from a transient reduction in the speed of sound

The quadratic action of a general single-field theory for the adiabatic curvature perturbation $\mathcal{R}$ is

$$S_2 = M_{\rm P}^2 \int \mathrm{d}^4x\, a^3 \epsilon \left[\dot{\mathcal{R}}^2 - \frac{(\nabla \mathcal{R})^2}{a^2} \right] + M_{\rm P}^2 \int \mathrm{d}^4x\, a^3 \epsilon \left(\frac{1}{c_s^2} - 1 \right) \dot{\mathcal{R}}^2 \ . \tag{2.2.1}$$

where c_s is the sound speed. The mode functions are easily found for the free ($c_s = 1$) action in the first line. Using the in-in formalism [40, 41], the change in the power spectrum due to a small transient reduction in the speed of sound, to first order in $u \equiv 1 - c_s^{-2}$, is found to be [111][2]

$$\frac{\Delta \mathcal{P}_{\mathcal{R}}}{\mathcal{P}_{\mathcal{R}}}(k) = k \int_{-\infty}^{0} \mathrm{d}\tau\ u(\tau) \sin(2k\tau) \ , \tag{2.2.2}$$

where $k \equiv |\boldsymbol{k}|$, $\mathcal{P}_{\mathcal{R}} = H^2/(8\pi^2 \epsilon M_{\rm P}^2)$ is the featureless power spectrum with $c_s = 1$, and τ is the conformal time. Here we see how changes in the speed of sound, independently of their physical origin, seed features in the power spectrum. However, different inflationary scenarios will give different coefficients for the cubic operators in the action, and therefore will in general be distinguishable at the level of the bispectrum [98, 107].

This method provides a clear advantage with respect to those in which the mode functions are calculated from the complete equations of motion

[2] The details of this calculation are presented in chapter 3, where the change in the bispectrum for a transient variation in c_s is calculated in detail using the in-in formalism. The same procedure applies to the power spectrum.

[121, 124, 125, 131, 132], where higher derivatives of c_s appear and extra hierarchies must be usually imposed. We have checked that both methods agree for sudden variations of the speed of sound [2], as I will present in detail in chapter 3. It is however important to note that (2.2.2) assumes $c_s = 1$ in the far past ($\tau = -\infty$) and at the end of inflation ($\tau = 0$).

One can also calculate the bispectrum disregarding slow-roll contributions $\mathcal{O}(\epsilon, \eta)$ with respect to u and $s \equiv \dot{c_s}/Hc_s$, which ensures that the standard slow-roll result [39] for $c_s = 1$ is subdominant with respect to this leading contribution, given by (see [111] for details):

$$\Delta B_{\mathcal{R}}(\boldsymbol{k}_i) = \left[c_0^{\triangle}(\boldsymbol{k}_i) \frac{\Delta \mathcal{P}_{\mathcal{R}}}{\mathcal{P}_{\mathcal{R}}} + c_1^{\triangle}(\boldsymbol{k}_i) \frac{\mathrm{d}}{\mathrm{d}k} \left(\frac{\Delta \mathcal{P}_{\mathcal{R}}}{\mathcal{P}_{\mathcal{R}}} \right) + c_2^{\triangle}(\boldsymbol{k}_i) \frac{\mathrm{d}^2}{\mathrm{d}k^2} \left(\frac{\Delta \mathcal{P}_{\mathcal{R}}}{\mathcal{P}_{\mathcal{R}}} \right) \right] \Bigg|_k , \tag{2.2.3}$$

where $k = \sum \frac{|\boldsymbol{k}_i|}{2}$. In this work, we choose to parameterise the reduction in the speed of sound as a gaussian in e-folds N as follows:

$$u = 1 - c_s^{-2} = B\, e^{-\beta (N - N_0)^2} = B\, e^{-\beta \left(\ln \frac{\tau}{\tau_0} \right)^2} , \tag{2.2.4}$$

where $\beta > 0$, $B < 0$ and N_0 (or τ_0) is the instant of maximal reduction. Assuming slow-roll, $\ln(-\tau) = (N_{\rm in} - N) - \ln(a_{\rm in} H_0)$, where $a_{\rm in} = a(N_{\rm in})$ and $N_{\rm in}$ is the time when the last ~ 60 e-folds of inflation start.

The angular scales probed by Planck ($\ell = 2 - 2500$) correspond to certain scales in momentum space crossing the Hubble horizon during the first $N_{\rm CMB} \simeq 7$ e-folds of the last ~ 60 e-folds of inflation. The range of N_0 and the lower bound on β are chosen to give a reduction of the speed of sound well contained within this CMB window. The range of B and the upper bound β must be such that the perturbative calculations are valid and the rate of change of the speed of sound is small. We take $|u|, |s| \ll 1$. Altogether, the allowed region of our parameter space is taken to be [2] (see chapter 3 for further details):

$$\mathcal{O}(\epsilon, \eta) \ll |B| \ll 1 , \tag{2.2.5a}$$

$$\frac{50}{N_{\rm CMB}^2} < \beta \ll \frac{2e}{B^2} , \tag{2.2.5b}$$

$$\frac{5}{\sqrt{2\beta}} < N_0 - N_{\rm in} < N_{\rm CMB} - \frac{5}{\sqrt{2\beta}} . \tag{2.2.5c}$$

This is a very conservative choice. First, (2.2.5c) and the lower bound in (2.2.5b) are more restrictive than the condition that the feature be observable. For example, we expect observable effects when the reduction occurs before the CMB window, since it would effectively modify the initial conditions of the modes subsequently leaving the sound horizon. We are also trying to avoid very broad

features that could be degenerate with cosmological parameters as the spectral index n_s and the optical depth $\tau_{\rm reio}$, as well as highly oscillating features (for large values of $|\tau_0|$) that make computational control difficult.

Secondly, this range is well within the region of the parameter space where the cubic Lagrangian is much smaller than the quadratic Lagrangian, and hence is perturbatively under control. An extension to other regions of the parameter space, such as larger β, might compromise the consistency of the effective single-field theory [2], and therefore we prefer to restrict our search to the region where we have good theoretical control and the physical interpretation is valid.

2.3 Methodology of the search

We consider features from a transient reduction in the speed of sound described by the ansatz (2.2.4). For its three parameters, we take uniform priors on B, $\ln\beta$ and $\ln(-\tau_0)$. Their ranges are given by eqs. (2.2.5) and a stronger restriction than (2.2.5c)

$$4.4 < \ln(-\tau_0) < 6 \ , \tag{2.3.1}$$

which is motivated by a search for bispectrum features by the Planck collaboration [48, sec. 7.3.3]. The model-dependent bound $|B| \gg \mathcal{O}(\epsilon, \eta)$ is ignored a priori.

The primordial power spectrum feature at eq. (2.2.2) is computed using a Fast Fourier Transform, and added to the primordial spectrum of the ΛCDM Planck baseline model described in ref. [47, sec. 2]. The resulting CMB power spectrum, calculated using the CLASS Boltzmann code [45, 46], is fitted to the Planck CMB temperature data [34] and the WMAP CMB low-ℓ polarisation data [31], using MONTE PYTHON [152] as a Markov-chain Monte Carlo (MCMC) sampler. We varied all cosmological, nuisance and feature parameters. For those last ones, the likelihood probability distribution is found to be multi-modal. Despite the multi-modal character of the likelihood in the feature parameter space, we were able to localise the different modes and split the parameter space into multiple uni-modal distributions, that were sampled separately varying both the feature and the Planck baseline model parameters (and the likelihood's nuisance parameters), in order to obtain definitive posterior probability distributions for the different modes.

2.4 Summary of results

The result of our search, having discarded small signals with $\Delta\chi^2 > -2$ (defined in [3]) over ΛCDM, is a series of five well-isolated bands of almost constant $\ln(-\tau_0)$,

[3] Hereafter, χ^2 refers to the *effective* quantity defined as $\chi^2_{\rm eff} = -2\ln\mathcal{L}$, see [153, p. 10]; in turn, Δ stands for the difference with the corresponding best fit value of Planck baseline model.

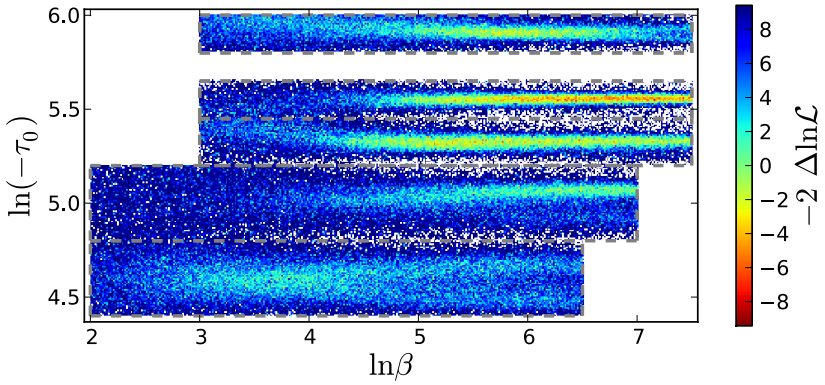

Figure 2.1 – *Profile of* $\Delta\chi^2_{\rm eff} = -2\Delta\ln\mathcal{L}$ *for the features in the CMB power spectrum in the* $(\ln\beta, \ln(-\tau_0))$ *plane.*

Mode	$-B\times10^2$	$\ln\beta$	$\ln(-\tau_0)$	$\Delta\chi^2_{\rm eff}$	$s_{\rm max}$
$\mathcal{A}$	$(4.5)\,3.7^{+1.6}_{-3.0}$	$(5.7)\,5.7^{+0.9}_{-1.0}$	$(5.895)\,5.910^{+0.027}_{-0.035}$	-4.3	0.33
$\mathcal{B}$	$(4.2)\,4.3\,\pm2.0$	$(6.3)\,6.3^{+1.2}_{-0.4}$	$(5.547)\,5.550^{+0.016}_{-0.015}$	-8.3	0.42
$\mathcal{C}$	$(3.6)\,3.1^{+1.6}_{-1.9}$	$(6.5)\,5.6^{+1.9}_{-0.7}$	$(5.331)\,5.327^{+0.026}_{-0.034}$	-6.2	0.40
$\mathcal{D}$	(4.4)	(6.5)	(5.06)	-3.3	0.48
$\mathcal{E}$ *	(1.5)	(4.0)	(4.61)	-2.2	0.05

Table 2.1 – *CMB power spectrum best fits (in parentheses), 68% c.l. intervals and effective* $\Delta\chi^2$ *at the best fit value for each of the different modes. The prediction for the bispectrum for* $\mathcal{E}$ *is not reliable (see text).*

with variable significance, see table 2.1 and figure 2.1. The fact that we obtain bands of almost constant τ_0 can be understood since τ_0 determines the oscillatory frequency of the feature in the CMB, and different frequencies can 'catch' the same data points and gain similar significance.

The amplitude B of the fits is rather small, $\mathcal{O}(10^{-2})$, and therefore comparable with neglected slow-roll terms. This means the bispectrum is dominated by terms of order $s = \dot{c_s}/(Hc_s)$. The maximum values of s at the best fits for the modes $\mathcal{A}$ to $\mathcal{E}$ in table 2.1 are respectively 0.33, 0.42, 0.40, 0.48, 0.05. Notice that the value of s for $\mathcal{E}$ is also comparable to neglected terms, so the prediction for the bispectrum based on eq. (2.2.3) cannot be trusted in this case. We therefore disregard this mode in the comparison with the bispectrum.

For the modes $\mathcal{A}$, $\mathcal{B}$ and $\mathcal{C}$ the table shows the 68% c.l. ranges. For bands $\mathcal{B}$ and $\mathcal{C}$ we were unable to put an upper bound on $\ln\beta$ due to a degeneracy

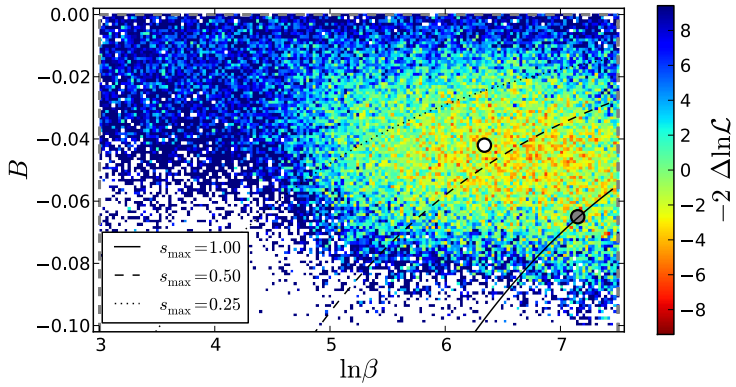

Figure 2.2 – *Profile of* $\Delta\chi^2_{eff} = -2\Delta \ln \mathcal{L}$ *for the mode* $\mathcal{B}$ *in the* $(\ln\beta, B)$ *plane, showing the* $\rho = -0.34$ *degeneracy between those two parameters. Some lines of* $s_{max} = const$ *are shown. Notice how the mode extends beyond the* $s = 1$ *prior limit.*

between that parameter and the amplitude $|B|$, which can be understood as follows: along the direction of simultaneous increase of $\ln\beta$ and $|B|$, the feature in the primordial power spectrum broadens towards smaller scales, while the amplitude of the tail on the larger scales remains almost constant. Since the signal at smaller scales will be suppressed in the CMB by diffusion damping, no significance is gained along the degeneracy direction, and this results in a plateau for $\Delta\chi^2$ (see figure 2.2). Along this plateau, the prior limit $s < 1$ in eq. (2.2.5b) gets saturated at $\ln\beta \simeq 7.5$. The best fit for $\mathcal{B}$ lies at $s \simeq 1$, so we present in table 2.1 the second best.

The lower bands $\mathcal{D}$ (and $\mathcal{E}$) are less significant and their likelihoods much less gaussian, so we only show their best fits (for parameter constraints see [2]). Despite their low significance, they are worthy of mention because they fall in the region overlapping with Planck's search for features in the bispectrum (see section 2.5).

As for the degeneracies between the feature parameters and cosmological parameters, those are explicitly given in the next chapter, where we will see that we only found two mild degeneracies of $\ln(-\tau_0)$ with $\omega_{\rm CDM}$ and H_0 [2]. It is reasonable that there are no further degeneracies, since localised oscillations with the frequencies and location that we found (see, for example, figures 2.3 and 2.4) are not easily mimicked by the cosmological parameters.

Considering that we are adding three extra parameters to the baseline ΛCDM model, a gain of $|\Delta\chi^2| \lesssim 10$ is expected and actually common in similar searches, which suggests that CMB power spectrum data alone cannot justify the intro-

duction of these features. Nevertheless, the aim of this work is to show that low-significance fits can still predict correlated features in the bispectrum which are possibly observable with the current data. Model selection should be done taking into account both observables (or naturally, any other combination).

2.5 Comparison with the search for features in Planck's bispectrum

A search for linearly oscillatory features was performed on Planck's bispectrum (cf. [48, sec. 7.3.3]), using as a template [154]

$$B(k_1,k_2,k_3)=\frac{6A^2 f_{\rm NL}^{\rm feat}}{(k_1k_2k_3)^2}\sin\left(2\pi\frac{\sum_{i=1}^3 k_i}{3k_c}+\phi\right)\,, \tag{2.5.1}$$

where $A=A_s k_*^{1-n_s}$, A_s and n_s being the amplitude and spectral index of the primordial power spectrum, and $k_*=0.05\,\mathrm{Mpc}^{-1}$ a pivot scale. They sampled the amplitude $f_{\rm NL}^{\rm feat}$ over a coarse grid of wavelengths k_c and phases ϕ.

Our features also present a linearly oscillatory pattern, which comes from the Fourier transform in (2.2.2). These oscillations enter the bispectrum approximately as $\exp(i\sum_i k_i\tau_0)$, cf. eq. (2.2.3), which compares to Planck's search as $\tau_0\approx 2\pi/(3k_c)$. Thus, Planck's search falls inside $\ln(-\tau_0)\in[4.43,5.34]$, while ours spans up to $\ln(-\tau_0)=6$ $\left(k_c=0.00519\,\mathrm{Mpc}^{-1}\right)$. The overlap includes our modes $\mathcal{C}$ and $\mathcal{D}$ (and also the discarded $\mathcal{E}$).

The search in [48] is later supplemented with a gaussian envelope centred at scales corresponding to the first acoustic peak, which dampens the signal in subsequent peaks for decreasing values of a falloff Δk. The envelope generally improves the significance, except for the 2σ signal at $k_c=0.01375\,,0.01500\,\mathrm{Mpc}^{-1}$. This suggests that this band's significance comes mostly from the second and third peaks (the signal from the fourth on would be most likely damped out).

In comparison, our best fits to the power spectrum predict bispectrum features which are mild at the first peak and more intense from the second peak onwards. The higher the value of $\ln\beta$, the smaller the scale at which the feature peaks. In the range of $\ln(-\tau_0)$ probed here, we were not able to reproduce the improvement Planck appears to see for features at the first peak. On the other hand, we find good matching around the second and third peak scales between the best fit of $\mathcal{D}$ with $k_c=0.01327\,\mathrm{Mpc}^{-1}$ and the 2.3σ signal of Planck at $k_c=0.01375\,\mathrm{Mpc}^{-1}$ with $f_{\rm NL}^{\rm feat}=345$ and $\phi=\pi/2$ (see fig. 2.3). A milder matching also occurs at the same scales between the best fit of $\mathcal{C}$ with $k_c=0.01014\,\mathrm{Mpc}^{-1}$ and Planck's 2.6σ signal with $k_c=0.01125\,\mathrm{Mpc}^{-1}$.

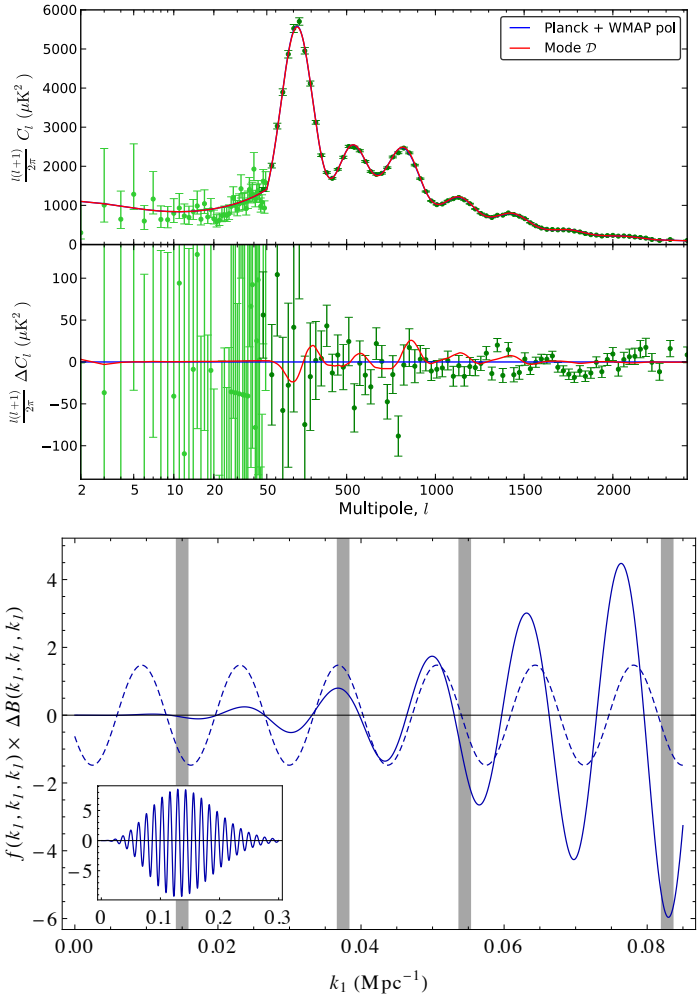

Figure 2.3 – *Features corresponding to the best fit of the mode $\mathcal{D}$ (see table 2.1), for which the comparison with Planck analysis for the bispectrum is possible.* ***Top:*** *Comparison of Planck's CMB power spectrum (blue) and the corresponding best fit of the mode $\mathcal{D}$ (red).* ***Bottom:*** *Comparison along the equilateral direction of Planck's* 2.3σ primordial *bispectrum fit with* $k_c = 0.01375\,\mathrm{Mpc}^{-1}$ *(dashed), and the expected signal in the* primordial *bispectrum for the best fit of $\mathcal{D}$ (solid). Both bispectra are normalised by* $f(k_1,k_2,k_3) = (10/3)\left((2\pi)^2 A_s k_*^{1-n_s}\right)^{-2} \prod_i k_i^3 \,/\, \sum_i k_i^3$. *The gray stripes show the approximate scales corresponding to the first four acoustic peaks in the CMB power spectrum. Although our signal extends beyond those scales (see zoom-out at the lower-left corner), from the third peak on, the primordial signal is highly suppressed by diffusion damping when transferred to the CMB.*

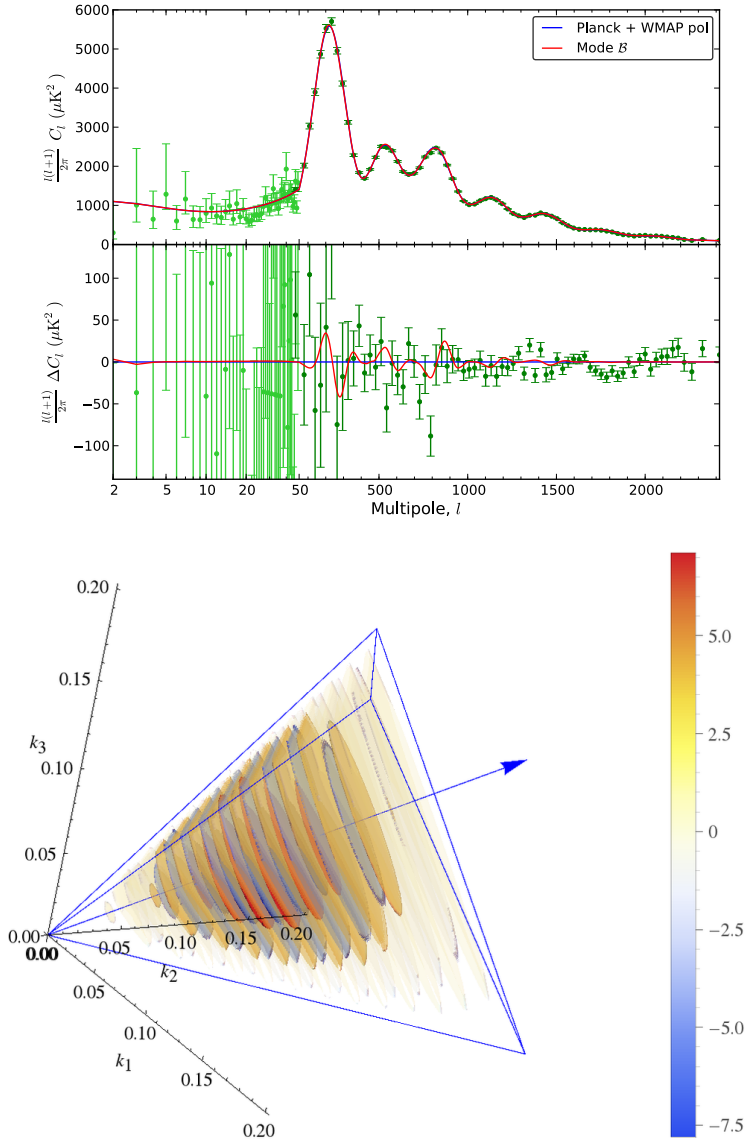

Figure 2.4 – ***Top:*** *Comparison between the CMB temperature power spectrum of Planck (blue) and the corresponding one of the second-best fit of mode $\mathcal{B}$ (red), see table 2.1.* ***Bottom:*** *full primordial bispectrum.*

Although this matching is not easy to quantify, it suggests enlarging the search in [48] to cover the frequencies corresponding to modes $\mathcal{A}$ and $\mathcal{B}$, and to test envelopes centred at smaller scales. For instance, in figure 2.4 we show the second-best fit of mode $\mathcal{B}$ to the CMB power spectrum and its corresponding prediction for the full primordial bispectrum. We expect the signal to be observable in the CMB at scales around the second and third acoustic peaks, since thereafter it will be suppressed by diffusion damping. In relation to Planck's search in [48, sec. 7.3.3], this feature would be localised at 68% c.l. within the interval $k_c \in [0.00801,\, 0.00826]\,\mathrm{Mpc}^{-1}$. Thus, testing for it in the current data would require enlarging their search to higher frequencies, i.e. smaller values of k_c in eq. (2.5.1). Additionally, the significance should be highest when an envelope is placed around the scales corresponding to the second and third peak of the CMB power spectrum.

2.6 Comparison with other searches for features in the CMB power spectrum

Due to the Fourier transform in eq. (2.2.2), our features oscillate as $\exp(i2k\tau_0)$. Thus it is natural to compare to other searches for linearly oscillating features in the Planck CMB power spectrum.

Ref. [151] searches for non-localised features with frequencies that compare to ours as $\omega_2 = 2|\tau_0|$. In the overlapping region, $\omega_2 \in [160,\, 810]$, they find peaks at roughly $\ln(-\tau_0) \sim \{5.0, 5.1, 5.3, 5.6, 5.7\}$ ($|\Delta\chi^2_{\mathrm{bf}}| \simeq 8$). We find three peaks in this region with similar significance; it could be that the discrepancies come from signals at scales at which our (localised) features are negligible.

Also, the Planck collaboration [113, sec. 8] searches for features motivated by step-inflation, using the parameterisation proposed in [141] with a frequency $\eta_f = |\tau_0|$. The profile likelihood in [113, fig. 19, middle] reveals peaks at $\ln\eta_f \in [4.5,\, 4.8]$ ($|\Delta\chi^2_{\mathrm{bf}}| \simeq 2$) and $\ln\eta_f \in [5.3,\, 5.7]$ ($|\Delta\chi^2_{\mathrm{bf}}| \simeq 8$), which is consistent with our results.

It is worth noting that in both searches above the overall best fit occurs at $\ln(-\tau_0) \simeq 8.2$ ($|\Delta\chi^2_{\mathrm{bf}}| \sim 14$), too high a frequency for the scope of this work.

2.7 Conclusions

We carried out a statistical search for localised oscillatory features in the CMB power spectrum produced by a transient reduction in the speed of sound. We have found a number of fits and calculated the associated primordial bispectra. Because of the small amplitude at the best fits, the bispectrum prediction closely

resembles that of step inflation, tested by the Planck collaboration, since a transient slow-roll violation switches on the same operator in the cubic action. It is then straightforward to compare our prediction with the templates used in that search, and the agreement is surprisingly good. This is remarkable, considering that these bispectrum features are *predicted from a search in the CMB power spectrum* with a very simple ansatz for c_s.

The functional form chosen for the reduction in the speed of sound is inspired by soft turns in a multi-field inflationary trajectory with a large hierarchy of masses, a situation that is consistent with an effectively single-field description with uninterrupted slow-roll. Other functional forms and parameter ranges are under investigation. We stress that our analysis is independent of the physical mechanism behind the reduction.

We emphasise that the CMB power spectrum data alone can hardly justify the introduction of features on top of the ΛCDM model; a gain of $|\Delta\chi^2| \lesssim 10$ is not uncommon. However, as we have shown, low-significance fits in the power spectrum can still predict correlated features that may be observable in the CMB bispectrum. Therefore, model selection should take into account both observables simultaneously.

Our results strongly suggest that, by exploiting correlations between different observables, current data might already be sensitive enough to detect transient reductions in the speed of sound as mild as a few percent, opening a new window for the presence of extra degrees of freedom during inflation.

In the next chapter we elaborate on the theoretical consistency of the methods used here and compare to other methods, showing that for the regime in which we are working, both methods produce very similar results and therefore there is no need for more complicated methods. We also argue that within this regime, the validity of the effective single-field theory is guaranteed. This is a very important point, since it distinguishes this work from others where a blind search with additional parameters is performed. In the works presented in this chapter and the next one, we provide a well-motivated physical scenario and we show that the fits to data can be consistently interpreted within that physical framework. Furthermore, we test our findings with an alternative Boltzmann code and give some more explicit details regarding the statistical search.

3

Inflation with moderately sharp features in the speed of sound: GSR and in-in formalism for power spectrum and bispectrum

In this chapter we continue the study of mild transient reductions in the speed of sound of the adiabatic mode during inflation, of their effect on the primordial power spectrum and bispectrum, and of their detectability in the CMB. We focus on the regime of *moderately sharp* mild reductions in the speed of sound during uninterrupted slow-roll inflation, a theoretically well motivated and self-consistent regime that admits an effective single-field description. The signatures on the power spectrum and bispectrum were previously computed using a slow-roll Fourier transform (SRFT) approximation, based on the in-in formalism, as reviewed in the previous chapter. Here we compare it with more complete generalised slow-roll (GSR) and in-in methods, for which we derive new formulas that account for moderately sharp features. The agreement between them is excellent, and also with the power spectrum obtained from the numerical solution to the equation of motion. We show that, in this regime, the SRFT approximation correctly captures with simplicity the effect of higher derivatives of the speed of sound in the mode equation, and makes manifest the correlations between power spectrum and bispectrum features. In the previous chapter, based on [1], we reported hints of these correlations in the Planck data and here we perform several consistency checks and further analyses of the best fits, such as polarisation and local significance at different angular scales. For the data analysis, we show the excellent agreement between the CLASS and CAMB Boltzmann codes. Our

results confirm that the theoretical framework is consistent, and they suggest that the predicted correlations are robust enough to be searched for in CMB.

3.1 Introduction

The paradigm of inflation as the explanation for the origin of cosmic structures has entered a decisive new phase. The latest data releases by the Planck [32] and WMAP [31] collaborations point towards models of inflation that produce a slightly red-tilted primordial power spectrum and a negligible amount of *scale-independent* bispectra, as predicted [33, 38, 39] by the simplest models of cosmological inflation[1], but with a mild deficit of power on large scales. There are also mild hints of *scale-dependent* features in the CMB power spectrum [31, 113] and in the primordial bispectrum [48]. Besides this, the discovery of B-mode polarization by BICEP2 [55], if it is confirmed to be result of primordial tensor modes, would have striking implications and put inflation on a much firmer footing. A large tensor-to-scalar ratio of $r \sim \mathcal{O}(0.1)$ suggests – again, in the context of canonical models – a high scale of inflation around $10^{16}\,\mathrm{GeV}$, a Hubble parameter $H \sim 10^{14}\,\mathrm{GeV}$ during inflation and a large, transplanckian excursion in field space for the inflaton [56].

According to [155], there is currently a "very significant tension" (around 0.1% unlikely) between the Planck temperature ($r < 0.11$ 95%c.l.) and BICEP2 polarization ($r = 0.2^{+0.05}_{-0.07}$) results. Recently, several fundamental/phenomenological models with features in the primordial spectra, such as sharp transition in the slow-roll parameters [156], false vacuum decay [157], initial fast roll [158], a non-Bunch-Davies initial state [159], or a bounce before inflation [160], among others, were proposed to explain the observed power deficit on large angular scales by Planck experiments. Alternatively, the tension could be resolved with new data releases.

Another consequence of the BICEP2 results is that a large tensor-to-scalar ratio seems to indicate a high energy scale of inflation around the grand unification theory (GUT) scale. If confirmed, one would need to find a successful UV embedding of the theory, and also deal with the problem of mass hierarchies in the presence of multiple degrees of freedom. This is challenging, but not impossible, and it seems that the energy range available could in principle host the inflaton and the possible additional UV degrees of freedom, while preserving a manageable mass hierarchy for which an effective single field theory is still possible. The BICEP2 results also suggest that the inflaton field underwent a super-Planckian excursion, which makes the theory very sensitive to higher dimensional operators. While we expect a (mildly broken) symmetry protecting

[1] These are slow-roll inflation models involving a single neutral scalar field with a canonical kinetic term and in the Bunch-Davies vacuum.

the overall flatness of the potential, this also leaves room for the presence of transient phenomena happening along the inflationary trajectory.

Among other phenomena, transient variations in the speed sound of the adiabatic mode may occur in the presence of additional degrees of freedom during inflation. For instance, when an additional heavy field can be consistently integrated out [104, 106, 107, 109, 110, 161], inflation is described by an effective single-field theory [98–100, 104, 107, 109] with a variable speed of sound. In particular, changes in the speed of sound result from derivative couplings[2] [101, 103, 106–109, 162–164]. Transient variations in the speed of sound will produce *correlated* features in the correlation functions of the adiabatic curvature perturbation [98, 111, 112, 124, 132, 133, 137, 165]. They are worth taking into account since we expect them to be very good model selectors.

The detection of transients poses some interesting challenges. The effects of a feature in the potential or a localised change in the speed of sound depend on its *location* (in time or e-folds), its *amplitude* and the *sharpness* (or inverse duration). If transients are too sharp, they can excite higher frequency modes that make the single-field interpretation inconsistent (see, for example, [104, 106, 166]). Notably, the best fit found so far in the data for a step feature in the potential [113, 142, 167] falls outside the weakly coupled regime that is implicitly required for its interpretation as a step in the single field potential [168, 169]. On the other hand, if the features are too broad, their signature usually becomes degenerate with cosmological parameters, making their presence difficult to discern. There is an interesting intermediate regime where the features are mild (small amplitude) and moderately sharp, which makes them potentially detectable in the CMB/LSS data, and also they remain under good theoretical control. This regime is particularly important if the inflaton field excursion is large and can reveal features in the inflationary potential and the presence of other degrees of freedom. At the same time, if slow-roll is the result of a (mildly broken) symmetry that protects the background in the UV completion, the same symmetry might presumably preclude very sharp transients.

In this chapter, based on [2], we study *mild and moderately sharp* features in the speed of sound of the adiabatic mode, that we define to be those for which the effects coming from a varying speed of sound are small enough to be treated at linear order, but large enough to dominate over the slow-roll corrections. This carries an implicit assumption of uninterrupted slow-roll[3]. We will show that this regime ensures the validity of the effective single-field theory, even though our analysis is blind to the underlying inflationary model.

[2] Or equivalently, turns in field space.

[3] In the particular case of reductions in the speed of sound coming from turns along the inflationary trajectory, this has been shown to be a consistent scenario.

In order to compare any model with data, it is important to develop fast and accurate techniques to compute the relevant observables of the theory, in this case, correlations functions of the adiabatic curvature perturbation. The calculation of correlation functions is often rather complicated and the use of approximate methods is needed. The study of transients often involves deviations from slow-roll and may be analysed in the generalised slow-roll (GSR) formalism [112, 124–130, 170]. This approach is based on solving the equations of motion iteratively using Green's functions. Although this formalism can cope with more general situations with both slow-roll and speed of sound features, one usually needs to impose extra hierarchies between the different parameters to obtain simple analytic solutions.

A notable exception that is theoretically well understood is a transient, mild, and moderately sharp reduction in the speed of sound such as would be found in effectively single-field models with uninterrupted slow-roll inflation, obtained by integrating out much heavier fields with derivative couplings that become transiently relevant. In this regime, an alternative approach is possible, that makes the correlation between power spectrum and bispectrum manifest [111]. The change in the power spectrum is simply given by the Fourier transform of the reduction in the speed of sound, and the *complete* bispectrum can be calculated to leading order in slow-roll as a function of the power spectrum. Hence we name this approximation slow-roll Fourier transform (SRFT). One of the aims of our work is to compare the GSR and SRFT approaches. In order to do this, we develop simple expressions within the GSR approach and the in-in formalism for computing the changes in the power spectrum and bispectrum due to moderately sharp features in the speed of sound. These are new and extend the usual GSR expressions for very sharp features.

The other aim of this work is to further scrutinise and validate the results of our previous work [1], presented in chapter 2, where we searched for moderately sharp features in the Planck CMB data. We reported several fits to the CMB power spectrum and gave the predicted, correlated, oscillatory signals for the primordial bispectrum. The functional form of the speed of sound was inspired by soft turns along a multi-field inflationary trajectory with a large hierarchy of masses, a situation that is consistently described by an effective single-field theory [102, 103, 106–108, 136].

In the first part of this chapter we study the intermediate regime of moderately sharp features in the speed of sound during uninterrupted slow-roll, in which both the SRFT and GSR approaches can give accurate results. More precisely:

- In section 3.2.1 we review the SRFT results for the power spectrum and bispectrum, and in section 3.2.2 we develop a simple formula within the GSR formalism that reduces to the SRFT result for nearly all scales and is

valid for arbitrary functional forms of the speed of sound within the regime we study.

- In section 3.2.3, by comparing both results with a numerical solution for the power spectrum, we show that the SRFT method correctly captures the effect of *all* the terms in the equation of motion in a very simple way, while the GSR method requires the inclusion of higher derivatives of the speed of sound to match the numerical result. Nevertheless, there is excellent agreement between both results with the numerical solution.

- Then we turn to the bispectrum. In section 3.2.4 we compute the features in the bispectrum using the in-in formalism, and we take into account the effect of additional operators with respect to previous results [124]. We show that, for transient reductions of the speed of sound, the contributions arising from the operators proportional to the amount of reduction and to the rate of change are of the same order, *independently of the sharpness* of the feature. In addition, because we study the not-so-sharp regime, we compute the linear correction to the approximation that other quantities do not vary during the time when the feature happens.

- In section 3.2.5 we compare the bispectra obtained with the SRFT approach and with the moderately sharp approximation, finding remarkable agreement for several functional forms of the speed of sound.

In the second part of this paper we perform a number of additional consistency checks regarding the theoretical framework and the statistical analysis described in the previous chapter. In particular:

- In section 3.3.1 we explain the choice of parameter space used for our statistical search of transient reductions of the speed of sound in the Planck data, which was designed to be theoretically consistent. In section 3.3.2 we check that adiabatic and unitary regimes are respected, and therefore the fits found in the data can be consistently interpreted as transient reductions in the speed of sound.

- In section 3.3.3 we analyse the implications of the BICEP2 results for the consistency of an effective single-field description of inflation. We conclude that, even with a inflationary scale at the level of the GUT scale, a single-field description may be possible, and we argue that moderately sharp reductions of the speed of sound are completely consistent with an adiabatic evolution, i.e. an effective single-field regime.

- In section 3.3.4 we review the main results of our previous work [1] and make an independent consistency check using two different Boltzmann codes and MCMC samplers, namely CLASS+MONTE PYTHON versus CAMB+COSMOMC, finding great agreement. We explicitly give the (small)

degeneracy of the cosmological parameters with the parameters of our model. Last, we also show the polarisation spectra and the local improvement of our fits to the CMB power spectrum as a function of the angular scale.

Finally, we leave section 3.4 for conclusions and outlook.

3.2 Moderately sharp variations in the speed of sound: primordial power spectrum and bispectrum

In the framework of the effective field theory (EFT) of inflation [98] one can write the effective action for the Goldstone boson of time diffeomorphisms $\pi(t, \mathbf{x})$, directly related to the adiabatic curvature perturbation $\mathcal{R}(t, \mathbf{x})$ via the linear relation[4] $\mathcal{R} = -H\pi$. Let us focus on a slow-roll regime and write the quadratic and cubic actions for π:

$$S_2 = \int d^4x\, a^3 M_{\rm Pl}^2 \epsilon H^2 \left\{ \frac{\dot\pi^2}{c_s^2} - \frac{1}{a^2} (\nabla\pi)^2 \right\} , \tag{3.2.1}$$

$$S_3 = \int d^4x\, a^3 M_{\rm Pl}^2 \epsilon H^2 \Bigg\{ - 2H s c_s^{-2} \pi \dot\pi^2 - \left(1 - c_s^{-2}\right) \dot\pi \left[\dot\pi^2 - \frac{1}{a^2} (\nabla\pi)^2 \right] \Bigg\} , \tag{3.2.2}$$

where $\epsilon = -\dot H / H^2$ and we are neglecting higher order slow-roll corrections, as well as higher order terms in u and s, defined as:

$$u \equiv 1 - c_s^{-2} \quad , \quad s \equiv \frac{\dot c_s}{c_s H} . \tag{3.2.3}$$

In this section we compare the different approaches to evaluating the power spectrum and bispectrum of the adiabatic curvature perturbation from (3.2.1) and (3.2.2) with a variable speed of sound, and show the excellent agreement between them.

The Slow-Roll Fourier Transform (SRFT) approach, developed in [111], is briefly reviewed in section 3.2.1. The advantage of this method is that one obtains very simple analytic formulas for both the power spectrum and bispectrum computed from (3.2.1) and (3.2.2). More importantly, correlations between features in the power spectrum and bispectrum show up explicitly. In section 3.2.2 we review the generalised slow roll (GSR) formalism [112, 121, 124, 125, 130–132, 170] and compute the power spectrum from the quadratic action (3.2.1)

[4] In this work, we do not need to consider non-linear correction terms, since we are in a slow-roll regime. For further details on this, see [39].

in the moderately sharp approximation. This method applies to more general situations where slow-roll is not necessarily preserved, but it requires solving iteratively the equations of motion, which include higher derivatives of the speed of sound. The GSR formalism gives very simple expressions in the case of very sharp features and has been used to calculate the effect of steps in the potential and in the speed of sound (see, for example, [124, 129]).

In section 3.2.3 we compare both methods with the power spectrum obtained from the numerical solution to the mode equations. We show that the SRFT method correctly captures the effect of higher derivative terms of the speed of sound in a very simple way, while the GSR method requires the inclusion of all terms in the equations of motion to match the numerical result at all scales (especially at the largest scales).

Then we turn to the bispectrum. In section 3.2.4 we compute the bispectrum from the cubic action (3.2.2) using an approximation for sharp features as in [124], but including the next order correction and additional operators. Last, in section 3.2.5 we check that the agreement with the SRFT result [111] is excellent. An important point we show is that the contributions to the bispectrum arising from the terms proportional to $(1-c_s^{-2})$ and s in (3.2.2) are of the same order, *independently of the sharpness of the feature*. We also eliminate the small discrepancy found in [124] between their bispectrum and the one obtained with GSR [121] for step features in the scalar potential, due to a missing term in the bispectrum.

3.2.1 Power spectrum and bispectrum with the SRFT method

In this formalism [111] we assume an uninterrupted slow-roll regime, which is perfectly consistent with turns along the inflationary trajectory. In order to calculate the power spectrum, we separate the quadratic action (3.2.1) in a free part and a small perturbation:

$$S_2 = \int d^4x\, a^3 M_{\rm Pl}^2 \epsilon H^2 \left\{ \dot\pi^2 - \frac{1}{a^2}\left(\nabla\pi\right)^2 \right\} - \int d^4x\, a^3 M_{\rm Pl}^2 \epsilon H^2 \left\{ \dot\pi^2 \left(1-c_s^{-2}\right) \right\} , \tag{3.2.4}$$

Then, using the in-in formalism [40, 41], the change in the power spectrum due to a small transient reduction in the speed of sound can be calculated to first order in $u \equiv 1-c_s^{-2}$, and it is found to be [111]

$$\frac{\Delta\mathcal{P}_\mathcal{R}}{\mathcal{P}_{\mathcal{R},0}}(k) = k\int_{-\infty}^{0} d\tau\; u(\tau)\sin\left(2k\tau\right) , \tag{3.2.5}$$

where $k \equiv |\mathbf{k}|$, $\mathcal{P}_{\mathcal{R},0} = H^2/(8\pi^2\epsilon M_{\rm Pl}^2)$ is the featureless power spectrum with $c_s = 1$, and τ is the conformal time. We made the implicit assumption that

the speed of sound approaches to one asymptotically, since we are perturbing around that value[5]. Here we see that the change in the power spectrum is simply given by the Fourier transform of the reduction in the speed of sound. Notice that the result above is independent of the physical origin of such reduction.

For the three-point function, we take the cubic action (3.2.2), written to first order in u and s, which implies that we must have $|u|_{\max}, |s|_{\max} \ll 1$. We also disregard the typical slow-roll contributions that one expects for a canonical featureless single-field regime [39]. Therefore, for the terms proportional to u and s to give the dominant contribution to the bispectrum, one must require that u and/or s are much larger than the slow-roll parameters, i.e. $\max(u, s) \gg \mathcal{O}(\epsilon, \eta)$, as we will recall in section 3.3.1. Using the in-in formalism, one finds [111]:

$$\Delta B_{\mathcal{R}}(\mathbf{k}_1, \mathbf{k}_2, \mathbf{k}_3) = \frac{(2\pi)^4 \mathcal{P}^2_{\mathcal{R},0}}{(k_1 k_2 k_3)^2} \times \tag{3.2.6}$$

$$\left\{ -\frac{3}{2}\frac{k_1 k_2}{k_3}\left[\frac{1}{2k}\left(1+\frac{k_3}{2k}\right)\frac{\Delta\mathcal{P}_{\mathcal{R}}}{\mathcal{P}_{\mathcal{R},0}} - \frac{k_3}{4k^2}\frac{d}{d\log k}\left(\frac{\Delta\mathcal{P}_{\mathcal{R}}}{\mathcal{P}_{\mathcal{R},0}}\right)\right] + 2 \text{ perm} \right.$$

$$+\frac{1}{4}\frac{k_1^2+k_2^2+k_3^2}{k_1 k_2 k_3}\left[\frac{1}{2k}\left(4k^2 - k_1k_2 - k_2k_3 - k_3k_1 - \frac{k_1k_2k_3}{2k}\right)\frac{\Delta\mathcal{P}_{\mathcal{R}}}{\mathcal{P}_{\mathcal{R},0}}\right.$$

$$\left.\left. -\frac{k_1k_2 + k_2k_3 + k_3k_1}{2k}\frac{d}{d\log k}\left(\frac{\Delta\mathcal{P}_{\mathcal{R}}}{\mathcal{P}_{\mathcal{R},0}}\right) + \frac{k_1k_2k_3}{4k^2}\frac{d^2}{d\log k^2}\left(\frac{\Delta\mathcal{P}_{\mathcal{R}}}{\mathcal{P}_{\mathcal{R},0}}\right)\right]\right\}\Bigg|_k ,$$

where $k_i \equiv |\mathbf{k}_i|$, $k \equiv (k_1 + k_2 + k_3)/2$, and $\Delta\mathcal{P}_{\mathcal{R}}/\mathcal{P}_{\mathcal{R},0}$ and its derivatives are evaluated at k. From the result above it is clear how features in the power spectrum seed correlated features in the bispectrum. Note that in the squeezed limit ($k_1 \to 0, k_2 = k_3 = k$) one recovers the single-field consistency relation [39, 171].

In the following sections, we compute the power spectrum and bispectrum using alternative methods and compare the results.

3.2.2 Power spectrum in the GSR formalism

One can calculate the power spectrum by solving iteratively the full equations of motion (first in [125, 170] and further developed in [112, 121, 126, 127, 130, 131]). The idea is to consider the Mukhanov-Sasaki equation of motion with a time-dependent speed of sound, namely:

$$\frac{d^2 v_{\mathbf{k}}(\tau)}{d\tau^2} + \left(c_s^2 k^2 - \frac{1}{z}\frac{d^2 z}{d\tau^2}\right) v_{\mathbf{k}}(\tau) = 0 \ , \tag{3.2.7}$$

[5] At the level of the power spectrum, the generalisation to arbitrary initial and final values of the speed of sound $c_{s,0}$ is straightforward, provided they are sufficiently close to each other.

with $v = z\mathcal{R}$, $z^2 = 2a^2 M_{\rm Pl}^2 \epsilon c_s^{-2}$ and

$$\frac{1}{z}\frac{d^2 z}{d\tau^2} = a^2 H^2 \Big[2 + 2\epsilon - 3\tilde{\eta} - 3s + 2\epsilon(\epsilon - 2\tilde{\eta} - s) + s(2\tilde{\eta} + 2s - t) + \tilde{\eta}\tilde{\xi} \Big] \ , \quad (3.2.8)$$

where we have used the following relations[6]:

$$\epsilon = -\frac{\dot{H}}{H^2} \quad , \quad \tilde{\eta} = \epsilon - \frac{\dot{\epsilon}}{2H\epsilon} \quad , \quad s = \frac{\dot{c}_s}{Hc_s} \quad , \quad t = \frac{\ddot{c}_s}{H\dot{c}_s} \quad , \quad \tilde{\xi} = \epsilon + \tilde{\eta} - \frac{\dot{\tilde{\eta}}}{H\tilde{\eta}} \ , \quad (3.2.9)$$

and here the dot denotes the derivative with respect to cosmic time. Defining a new time variable $d\tau_c = c_s d\tau$ and a rescaled field $y = \sqrt{2kc_s}v$, the above equation can be written in the form:

$$\frac{d^2 y}{d\tau_c^2} + \left(k^2 - \frac{2}{\tau_c^2} \right) y = \frac{g\,(\ln \tau_c)}{\tau_c^2} y \ , \quad (3.2.10)$$

where

$$g \equiv \frac{f'' - 3f'}{f} \qquad , \quad f = 2\pi z c_s^{1/2} \tau_c \ , \quad (3.2.11)$$

and $'$ denotes derivatives with respect to $\ln \tau_c$. Throughout this section (and only in this section), unless explicitly indicated, we will adopt the convention of positive conformal time ($\tau, \tau_c \geq 0$) in order to facilitate comparison with [127, 131]. Note that g encodes all the information with respect to features in the background. In this sense, setting g to zero represents solving the equation of motion for a perfect de Sitter universe, where the solution to the mode function is well known. Considering the r.h.s. of equation (3.2.10) as an external source, a solution to the mode function can be written in terms of the homogeneous solution. In doing so, we need to expand the mode function in the r.h.s. as the homogeneous solution plus deviations and then solve iteratively. To first order, the contribution to the power spectrum is of the form [127]:

$$\ln \mathcal{P}_{\mathcal{R}} = \ln \mathcal{P}_{\mathcal{R},0} + \int_{-\infty}^{\infty} d \ln \tau_c \, W\,(k\tau_c)\, G'\,(\tau_c) \, , \quad (3.2.12)$$

where the logarithmic derivative of the source function G reads:

$$G' = -2(\ln f)' + \frac{2}{3}(\ln f)'' \ , \quad (3.2.13)$$

and the window function W and its logarithmic derivative (used below) are given by

$$W\,(x) \quad = \quad \frac{3\sin\,(2x)}{2x^3} - \frac{3\cos\,(2x)}{x^2} - \frac{3\sin\,(2x)}{2x} \ , \quad (3.2.14)$$

$$W'(x) \quad \equiv \quad \frac{dW(x)}{d\ln x} = \left(-3 + \frac{9}{x^2} \right) \cos(2x) + \left(\frac{15}{2x} - \frac{9}{2x^3} \right) \sin(2x) \ . \quad (3.2.15)$$

[6] Note that $\tilde{\eta}$ corresponds to $\eta_2/2$ as defined in (1.2.4).

If we consider moderately sharp features in the speed of sound, such that $\epsilon, \tilde{\eta} \ll s, t$, the leading contribution to the function G' is the following:

$$G' = -\frac{2}{3}s + \frac{2}{3}\left(\frac{aH\tau_c}{c_s} - 1\right)^2 + \frac{2}{3}\left(\frac{aH\tau_c}{c_s} - 1\right)(4 - s) + \frac{1}{3}\left(\frac{aH\tau_c}{c_s}\right)^2 s\,(-3 + 2s - t)\ , \tag{3.2.16}$$

where t is defined in (3.2.9). Moreover, when $|s| \ll 1$ but $t \gtrsim \mathcal{O}(1)$, the logarithmic derivative of G is approximately given by:

$$G' \simeq s - \frac{\dot{s}}{3H}\ , \tag{3.2.17}$$

where we have used that $aH\tau_c/c_s \simeq 1 + s$. This result agrees with the results of [131] in the mentioned limits. In this approximation, the leading contribution to the power spectrum is:

$$\ln \mathcal{P}_{\mathcal{R}} \simeq \ln \mathcal{P}_{\mathcal{R},0} + \int_{-\infty}^{\infty} d\ln\tau_c \left[W(k\tau_c)s\,(\tau_c) - \frac{1}{3}W\,(k\tau_c)\,\frac{ds}{d\ln\tau_c}\right]\ . \tag{3.2.18}$$

Integrating by parts the term proportional to the derivative of s we obtain:

$$\begin{aligned}\ln \mathcal{P}_{\mathcal{R}} &\simeq \ln \mathcal{P}_{\mathcal{R},0} + \int_{-\infty}^{\infty} d\,\ln\tau_c \left[W\,(k\tau_c) + \frac{1}{3}W'\,(k\tau_c)\right] s\,(\tau_c) \\ &= \ln \mathcal{P}_{\mathcal{R},0} + \int_{-\infty}^{\infty} d\,\ln\tau_c \left[\frac{\sin(2k\tau_c)}{k\tau_c} - \cos(2k\tau_c)\right] s\,(\tau_c)\ .\end{aligned} \tag{3.2.19}$$

This is the result that we will compare in section 3.2.3 with the SRFT result (3.2.5). Let us recall that the regime in which this expression has been derived is for moderately sharp reductions such that $\mathcal{O}(\epsilon, \eta) \ll s \ll 1$ and $t \gtrsim \mathcal{O}(1)$. We would like to point out that the s term in the source function (3.2.17) provides the dominant contribution to the power spectrum on large scales. This can be seen by comparing W and W' in (3.2.19), which carry the contribution of s and $\dot{s}$, respectively. We will show in section 3.2.3 that when including this term, the power spectrum at large scales matches the numerical solution considerably better (see figure 3.3).

In the following, we will: **(i)** derive an analytic expression for the power spectrum (3.2.19) solely in terms of c_s in order to connect with the SRFT approach. **(ii)** Find an analytic approximation for arbitrary functional forms of the speed of sound in the moderately sharp regime specified above.

(i) For the first point, one can integrate by parts (3.2.19) in order to get a formula than only involves the speed of sound. Doing so, we obtain:

$$\ln \mathcal{P}_{\mathcal{R}} = \ln \mathcal{P}_{\mathcal{R},0} - \int_{-\infty}^{\infty} d\,\ln\tau_c \left[2\cos(2k\tau_c) - \frac{\sin(2k\tau_c)}{k\tau_c} + 2k\tau_c \sin(2k\tau_c)\right] \ln c_s\,(\tau_c)\ , \tag{3.2.20}$$

where we have used that $s \simeq d\ln c_s/d\ln\tau_c$ and that the asymptotic value of the speed of sound is one, otherwise the boundary term would not vanish. Therefore, the expression above is only valid for functional forms of the speed of sound that satisfy $c_s(\tau=0)=c_s(\tau=\infty)=1$. Let us restrict our attention to mild reductions of the speed of sound $|u|=|1-c_s^{-2}|\ll 1$, in which the SRFT approach is operative. In that case, for mild and moderately sharp reductions, the time τ_c is very well approximated by $\tau_c\simeq\tau$. Furthermore, the logarithmic term of the speed of sound can be expanded as follows:

$$\ln c_s(\tau)\simeq\frac{1}{2}\left(1-c_s^{-2}(\tau)\right)+\mathcal{O}(u^2)\ . \tag{3.2.21}$$

Using the expansion above and the fact that $\ln(\mathcal{P}_\mathcal{R}/\mathcal{P}_{\mathcal{R},0})=\ln(1+\Delta\mathcal{P}_\mathcal{R}/\mathcal{P}_{\mathcal{R},0})\simeq\Delta\mathcal{P}_\mathcal{R}/\mathcal{P}_{\mathcal{R},0}$, we can write:

$$\begin{aligned}\frac{\Delta\mathcal{P}_\mathcal{R}}{\mathcal{P}_{\mathcal{R},0}}&\simeq k\int_{-\infty}^{0}d\tau\ \left(1-c_s^{-2}\right)\left[\sin(2k\tau)+\frac{1}{k\tau}\cos(2k\tau)-\frac{1}{2k^2\tau^2}\sin(2k\tau)\right]\\&\simeq\begin{cases}\left.\frac{\Delta\mathcal{P}_\mathcal{R}}{\mathcal{P}_{\mathcal{R},0}}\right|_{\rm SRFT}+\mathcal{O}\left[(k\tau)^2\right]\ ,\ k\tau\ll 1\\ \left.\frac{\Delta\mathcal{P}_\mathcal{R}}{\mathcal{P}_{\mathcal{R},0}}\right|_{\rm SRFT}+\mathcal{O}\left[(k\tau)^{-1}\right]\ ,\ k\tau\gg 1\end{cases}\end{aligned} \tag{3.2.22}$$

where we have already returned to negative conformal time. Notice that when $k\tau\ll 1$ we retrieve the SRFT expression (3.2.5) with a subleading correction $\mathcal{O}(k\tau)$ inside the integral, and that for $k\tau\gg 1$ we also retrieve the SRFT result. The regime $k\tau\sim 1$ will generally involve large scales, where the change in the power spectrum is small, as can be seen in figure 3.3.

(ii) In what follows we derive an analytic approximation to the power spectrum (3.2.19) for *generic* forms of the speed of sound, provided they are moderately sharp, i.e. $\mathcal{O}(\epsilon,\eta)\ll s\ll 1$ and $t\gtrsim\mathcal{O}(1)$. As in **(i)**, in this regime we can safely consider $\tau_c\simeq c_{s,0}\tau$. Let us drop the rest of assumptions made in point **(i)**, which were only made to establish connection with the SRFT approach. We define the function $X(k\tau_c)\equiv -W'(k\tau_c)-3W(k\tau_c)$, which in general can be decomposed as follows:

$$X(kc_{s,0}\tau)=p_c(kc_{s,0}\tau)\cos(2kc_{s,0}\tau)+p_s(kc_{s,0}\tau)\sin(2kc_{s,0}\tau)\ , \tag{3.2.23}$$

where p_c and p_s denote the polynomials multiplying the cosine and sine, respectively. Following [124], we will parameterise c_s^2 in terms of the height σ_* and the sharpness β_s of the feature, and a function F describing the shape of the variation of the speed of sound:

$$c_s^2(\tau)=c_{s,0}^2\left[1-\sigma_* F\left(-\beta_s\ln\tfrac{\tau}{\tau_f}\right)\right]\ , \tag{3.2.24}$$

where τ_f is the characteristic time of the feature and we take $\sigma_* \ll 1$ to focus on small variations. The rate of change in the speed of sound can be written at first order in σ_* as follows:

$$s(\tau) = -\frac{1}{2}\sigma_* \beta_s F'\left(-\beta_s \ln \tfrac{\tau}{\tau_f}\right) + \mathcal{O}\left(\sigma_*^2\right) \ , \tag{3.2.25}$$

where $'$ denotes the derivative with respect to the argument. Since we are considering sharp features happening around the time τ_f, the functions involved in the integral (3.2.19) will only contribute for values in the neighbourhood of τ_f. Note that for polynomials with negative powers of $k\tau$, the approximation of evaluating them at $k\tau_f$ fails for small values of $k\tau$, since in that region they vary very rapidly. This may cause infrared divergences in the spectrum which, as we will see, can be cured by approximating the polynomials to first order around $k\tau_f$.

First, we define the variable $y \equiv -\beta_s \ln(\tau/\tau_f)$, and we expand the functions around $\tau = \tau_f$, which is equivalent to $y/\beta_s \ll 1$. Then, at first order, the expansion of X in (3.2.23) reads:

$$\begin{aligned} X(kc_{s,0}\tau) \simeq & \left[p_c\left(kc_{s,0}\tau_f\right) - y\frac{k\tau_f}{\beta_s}\frac{dp_c}{d(k\tau)}\bigg|_{\tau_f}\right]\cos\left[2kc_{s,0}\tau_f\left(1-\tfrac{y}{\beta_s}\right)\right] \\ & + \left[p_s\left(kc_{s,0}\tau_f\right) - y\frac{k\tau_f}{\beta_s}\frac{dp_s}{d(k\tau)}\bigg|_{\tau_f}\right]\sin\left[2kc_{s,0}\tau_f\left(1-\tfrac{y}{\beta_s}\right)\right] \ . \end{aligned} \tag{3.2.26}$$

Substituting in (3.2.19) the above expansion and the definition of s (3.2.25), the change in the power spectrum is given by:

$$\begin{aligned} \frac{\Delta\mathcal{P}_\mathcal{R}}{\mathcal{P}_{\mathcal{R},0}} = \frac{\sigma_*}{6}\Bigg\{ & \left[p_c\cos\theta_k + p_s\sin\theta_k\right]\int_{-\infty}^{\infty} dy\,\cos\left(\frac{\theta_k}{\beta_s}y\right)F'(y) \\ & + \left[p_c\sin\theta_k - p_s\cos\theta_k\right]\int_{-\infty}^{\infty} dy\,\sin\left(\frac{\theta_k}{\beta_s}y\right)F'(y) \\ & - \frac{k\tau_f}{\beta_s}\left[\frac{dp_s}{d(k\tau)}\bigg|_{\tau_f}\sin\theta_k + \frac{dp_c}{d(k\tau)}\bigg|_{\tau_f}\cos\theta_k\right]\int_{-\infty}^{\infty} dy\,\cos\left(\frac{\theta_k}{\beta_s}y\right)y\,F'(y) \\ & + \frac{k\tau_f}{\beta_s}\left[\frac{dp_s}{d(k\tau)}\bigg|_{\tau_f}\cos\theta_k - \frac{dp_c}{d(k\tau)}\bigg|_{\tau_f}\sin\theta_k\right]\int_{-\infty}^{\infty} dy\,\sin\left(\frac{\theta_k}{\beta_s}y\right)y\,F'(y)\Bigg\} \ , \end{aligned}$$

where $\theta_k \equiv 2kc_{s,0}\tau_f$. Note that the integrals above are the Fourier transforms of the symmetric and antisymmetric parts of the derivative of the shape function F.

We define the envelope functions resulting from these integrals as follows:

$$\int_{-\infty}^{\infty} dy\, \cos\left(\frac{\theta_k}{\beta_s}y\right) F'(y) \equiv \frac{1}{2}\mathcal{D}_A \ , \ \int_{-\infty}^{\infty} dy\, \sin\left(\frac{\theta_k}{\beta_s}y\right) F'(y) \equiv \frac{1}{2}\mathcal{D}_S \ , \quad (3.2.27)$$

$$\int_{-\infty}^{\infty} dy\, y\, F'(y) \cos\left(\frac{\theta_k}{\beta_s}y\right) = \frac{\beta_s k}{2\theta_k}\frac{d\mathcal{D}_S}{dk} \quad , \quad (3.2.28)$$

$$\int_{-\infty}^{\infty} dy\, y\, F'(y) \sin\left(\frac{\theta_k}{\beta_s}y\right) = -\frac{\beta_s k}{2\theta_k}\frac{d\mathcal{D}_A}{dk} \quad , \quad (3.2.29)$$

where $\mathcal{D}_S$ and $\mathcal{D}_A$ are the envelope functions corresponding to the symmetric and antisymmetric parts of F, respectively. Finally, the change in the power spectrum can be written as:

$$\begin{aligned}\frac{\Delta\mathcal{P}_{\mathcal{R}}}{\mathcal{P}_{\mathcal{R},0}} = \frac{\sigma_*}{12}\Bigg\{ &\Big[p_c\cos\theta_k + p_s\sin\theta_k\Big]\mathcal{D}_A + \Big[p_c\sin\theta_k - p_s\cos\theta_k\Big]\mathcal{D}_S\Bigg\} \\ &-\frac{\sigma_*}{24c_{s,0}}\Bigg\{\left[\left.\frac{dp_s}{d(k\tau)}\right|_{\tau_f}\sin\theta_k + \left.\frac{dp_c}{d(k\tau)}\right|_{\tau_f}\cos\theta_k\right] k\frac{d}{dk}\mathcal{D}_S \\ &\qquad + \left[\left.\frac{dp_s}{d(k\tau)}\right|_{\tau_f}\cos\theta_k - \left.\frac{dp_c}{d(k\tau)}\right|_{\tau_f}\sin\theta_k\right] k\frac{d}{dk}\mathcal{D}_A\Bigg\} \quad (3.2.30)\end{aligned}$$

Let us stress that the contributions from the second and third lines are comparable to the ones in the first line. The infrared limit of the symmetric part is finite and tends to zero, which would not have been the case if we had only considered the zeroth order terms (first line). We will now substitute the values of the polynomials for the particular regime we are analysing, $p_c = 1/3$ and $p_s = -1/(3kc_{s,0}\tau)$. In this case, the change in the power spectrum reads:

$$\begin{aligned}\frac{\Delta\mathcal{P}_{\mathcal{R}}}{\mathcal{P}_{\mathcal{R},0}} = \frac{\sigma_*}{36}\Bigg\{ &\Big[\cos\theta_k - \frac{2}{\theta_k}\sin\theta_k\Big]\mathcal{D}_A + \Big[\sin\theta_k + \frac{2}{\theta_k}\cos\theta_k\Big]\mathcal{D}_S\Bigg\} \\ &-\frac{\sigma_*}{72}\Bigg\{\left[\frac{4}{\theta_k^2}\sin\theta_k\right] k\frac{d}{dk}\mathcal{D}_S + \left[\frac{4}{\theta_k^2}\cos\theta_k\right] k\frac{d}{dk}\mathcal{D}_A\Bigg\} \ . \quad (3.2.31)\end{aligned}$$

Test for generic variations in the speed of sound

In this section we will test the approximation (3.2.30) in comparison with the full integral (3.2.19). For the following particular example, we will explicitly

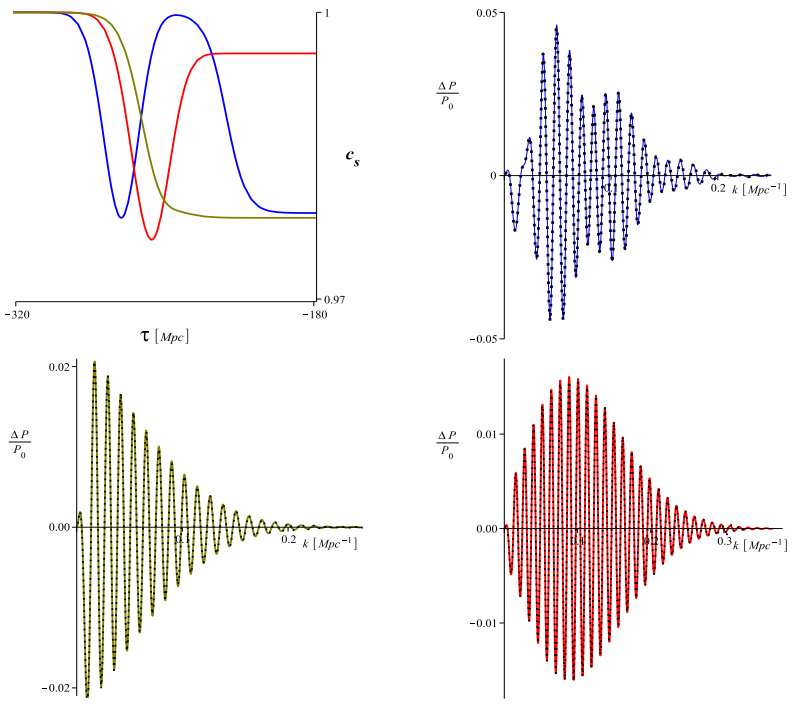

Figure 3.1 – *Speed of sound as defined in (3.2.32) for three different values of the parameters. We show the power spectra calculated with the full integral (3.2.19) (dotted line) and with the approximation (3.2.30) (solid line). The parameters, for the blue, olive and red figures, are respectively given by:* $A = [-0.021, -0.0215, -0.0043]$, $B = [-0.043, -0.0086, -0.043]$, $\alpha^2 = [\exp(6.3), \exp(6.3), \exp(7)]$, $\beta_s^2 = [\exp(6.3), \exp(6.3), \exp(7)]$, $\tau_{0_g} = [-\exp(5.6), -\exp(5.55), -\exp(5.55)]$, $\tau_{0_t} = [-\exp(5.4), -\exp(5.55), -\exp(5.55)]$. *For the first set of parameters the symmetric and antisymmetric parts have comparable magnitude, while for the second (third) set of parameters the antisymmetric (symmetric) part dominates. As can be seen by the very good agreement between the full integral and the approximation, the chosen parameters are all of them in the sharp feature regime.*

decompose c_s^2 into its symmetric and antisymmetric parts:

$$c_s^2 = 1 + A\left[1 - \tanh\left(\alpha \ln \frac{\tau}{\tau_{0_t}}\right)\right] + B\exp\left[-\beta_s^2\left(\ln\frac{\tau}{\tau_{0_g}}\right)^2\right]$$

$$= \left\{1 + A + B\exp\left[-\beta_s^2\left(\ln\frac{\tau}{\tau_{0_g}}\right)^2\right]\right\}_S + \left\{-A\tanh\left(\alpha\ln\frac{\tau}{\tau_{0_t}}\right)\right\}_A . \quad (3.2.32)$$

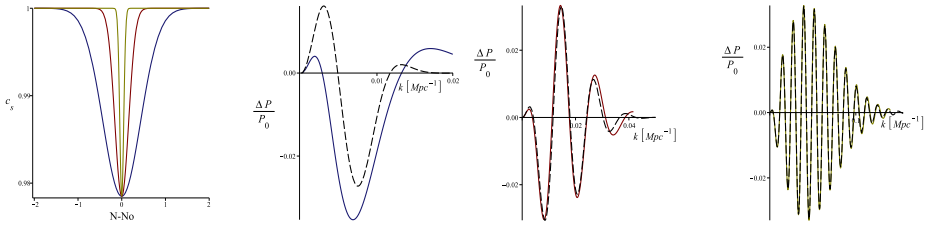

Figure 3.2 *– Here we test when the approximation (3.2.30) starts to break down. The full integral (3.2.19) is represented by dashed lines while the approximation (3.2.30) is given by solid lines. We take* $A = 0$, $B = -0.043$, $\tau_{0_g} = -\exp(5.55)$ *for the three profiles of the speed of sound, and* $\beta_g = [\exp(1), \exp(3), \exp(11/2)]$ *for the blue, red and olive figures respectively. We see that the approximation starts to fail for features with* $\Delta N \gtrsim 1$.

From the definitions (3.2.24) and (3.2.27) , the envelope functions are given by :

$$\mathcal{D}_A = -\frac{4\pi A}{\sigma_*}\frac{k\tau_{0_t}}{\alpha}\frac{1}{\sinh(\pi k\tau_{0_t}/\alpha)} \quad , \quad \mathcal{D}_S = \frac{4\sqrt{\pi}B}{\sigma_*}\frac{k\tau_{0_g}}{\beta_s}\exp\left(-\frac{k^2\tau_{0_g}^2}{\beta_s^2}\right) . \tag{3.2.33}$$

Since the symmetric and antisymmetric parts do not necessarily peak at the same time, the integrands involved in each part take values around τ_{0_g} and τ_{0_t}, respectively. We test our approximation for different values of the parameters above, and show our results in figure 3.1. We can see that the approximation is indeed very good, and that it allows to reproduce highly non-trivial power spectra. By allowing β_s and/or α to be small, we can see where the approximation starts to fail. We show these results in figure 3.2, where one can see that for features with $\Delta N \gtrsim 1$ the approximation breaks down.

3.2.3 Comparison of power spectra

In this section we apply both SRFT and GSR methods for moderately sharp reductions to calculate the change in the power spectrum, and compare them with the power spectrum calculated from the numerical solution to the mode equation (3.2.7). We will test a reduction in the speed of sound purely symmetric in the variable $y = -\beta_s \ln(\tau/\tau_f)$:

$$u = 1 - c_s^{-2} = B\, e^{-\beta_s^2 (N-N_f)^2} = B\, e^{-\beta_s^2 \left(\ln \frac{\tau}{\tau_f}\right)^2} . \tag{3.2.34}$$

In figure 3.3 we show the comparison between the power spectrum coming from the GSR result (3.2.30) with the one coming form the SRFT method (3.2.5), and with a numerical solution. In general terms, both methods are in good agreement with the numerical solution. We also note that at large scales the SRFT method reproduces the numerical results better than the GSR method. This is partly due

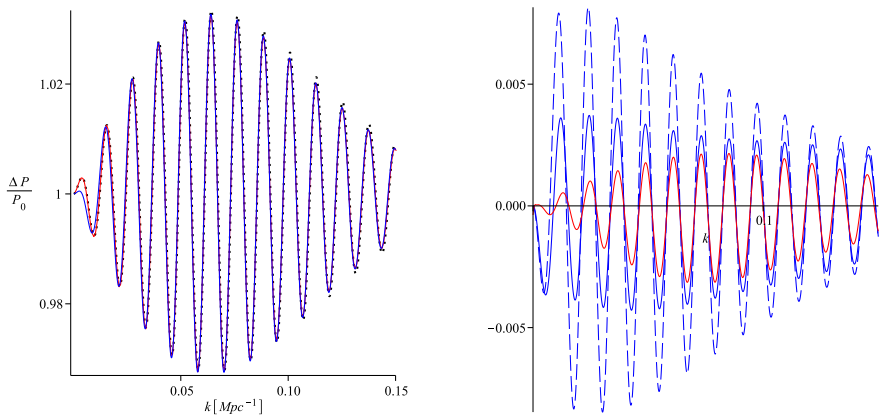

Figure 3.3 *– Change in the power spectrum due to a reduced speed of sound given by* (3.2.34)*, with the following choice of parameters:* $B = -0.043$*,* $\beta_s = 23.34$*,* $\ln(\tau_f) = 5.55$*, corresponding to one of our best fits to the Planck CMB power spectrum [1]. LEFT: different methods to compute the primordial power spectrum: GSR in the sharp feature approach (blue), SRFT (red), and a solution obtained from the numerical solution to the mode equation* (3.2.7) *(black dotted). RIGHT: differences of the GSR sharp feature method (solid blue) and SRFT (red) against the numerical solution. The dashed blue line is the GSR sharp feature approach if we had not taken into account the term proportional to* s *in the source function* (3.2.17)*. The numerical solution is calculated choosing* $\epsilon \simeq 1.25 \times 10^{-4}$ *and* $\tilde{\eta} \simeq -0.02$*. Higher values of* ϵ *need a proper accounting for the slow-roll corrections.*

to the fact that in the GSR approximation we have only taken a subset of the terms in the source function. The agreement would have been much worse if we had not taken into account the term proportional to s, as the dashed line in the right plot of figure 3.3 indicates. Note that $k\tau_f \sim 1$ corresponds to the first peak in the left plot of fig. 3.3 above, precisely the regime where we expect a discrepancy, as anticipated in eq. (3.2.22).

This shows that, in the regime of moderately sharp variations of the speed of sound, the simple SRFT formula (3.2.5) is capable of reproducing the effect of *all* the terms in the equation of motion, and that there is no need to impose any further hierarchy between the different terms of the equation of motion in order to have a simple expression, as long as slow-roll is uninterrupted.

3.2.4 Bispectrum for moderately sharp reductions

In this section we will compute the change in the bispectrum due to moderately sharp reductions in the speed of sound using the in-in formalism. Instead of the SRFT method reviewed in section 3.2.1, we will use an approximation based on

sharp features [124], as for the power spectrum. Our starting point is the cubic action in the effective field theory of inflation, where we will only take into account the contribution from variations in the speed of sound at first order:

$$S_3 = \int d^4x\, a^3 M_{\rm Pl}^2 \frac{\epsilon}{H}\left\{2Hsc_s^{-2}\mathcal{R}\dot{\mathcal{R}}^2 + \left(1-c_s^{-2}\right)\dot{\mathcal{R}}\left[\dot{\mathcal{R}}^2 - \frac{1}{a^2}\left(\nabla\mathcal{R}\right)^2\right]\right\}\,, \tag{3.2.35}$$

with $\mathcal{R} = -\pi H$. For sharp features ($\beta_s \gg 1$) and given the parameterisation in (3.2.24) and (3.2.25), one is tempted to think that the contribution of s will dominate over the contribution of $(1-c_s^{-2})$. However, we will show that the contributions arising from both terms are of the same order, *independently of the sharpness* β_s. As dictated by the in-in formalism, the three-point correlation function reads:

$$\begin{aligned}\langle \mathcal{R}_{\mathbf{k}_1}\mathcal{R}_{\mathbf{k}_2}\mathcal{R}_{\mathbf{k}_3}\rangle = \Bigg\langle \mathrm{Re}\Bigg\{2i\,\mathcal{R}_{\mathbf{k}_1}(0)\mathcal{R}_{\mathbf{k}_2}(0)\mathcal{R}_{\mathbf{k}_3}(0)\times \\ \int_{-\infty}^{0} d\tau \int d^3x\, a^4 M_{\rm Pl}^2\frac{\epsilon}{H}\Big[2Hsc_s^{-2}\mathcal{R}\dot{\mathcal{R}}^2 \\ + \left(1-c_s^{-2}\right)\dot{\mathcal{R}}^3 - H^2\tau^2\left(1-c_s^{-2}\right)\dot{\mathcal{R}}\left(\nabla\mathcal{R}\right)^2\Big]\Bigg\}\Bigg\rangle\,,\end{aligned} \tag{3.2.36}$$

where we have used that[7] $a = -1/(H\tau)$. After expressing the functions $\mathcal{R}(\tau,\mathbf{x})$ in Fourier space and using the Wick theorem, we obtain

$$\begin{aligned}\langle \mathcal{R}_{\mathbf{k}_1}\mathcal{R}_{\mathbf{k}_2}\mathcal{R}_{\mathbf{k}_3}\rangle = \mathrm{Re}\Bigg\{2i\,u_{\mathbf{k}_1}(0)u_{\mathbf{k}_2}(0)u_{\mathbf{k}_3}(0) \\ \times\int_{-\infty}^{0}\frac{d\tau}{\tau^2}\frac{\epsilon M_{\rm Pl}^2}{H^2}(2\pi)^3\int d^3q_1\int d^3q_2\int d^3q_3\,\delta(\mathbf{q}_1+\mathbf{q}_2+\mathbf{q}_3) \\ \times\Big[4sc_s^{-2}u^*_{\mathbf{q}_1}(\tau)u^{*\prime}_{\mathbf{q}_2}(\tau)u^{*\prime}_{\mathbf{q}_3}(\tau)\Big(\delta(\mathbf{k}_1-\mathbf{q}_1)\delta(\mathbf{k}_2-\mathbf{q}_2)\delta(\mathbf{k}_3-\mathbf{q}_3) \\ +\{\mathbf{k}_1\leftrightarrow\mathbf{k}_2\}+\{\mathbf{k}_1\leftrightarrow\mathbf{k}_3\}\Big) \\ -6\tau\left(1-c_s^{-2}\right)u^{*\prime}_{\mathbf{q}_1}(\tau)u^{*\prime}_{\mathbf{q}_2}(\tau)u^{*\prime}_{\mathbf{q}_3}(\tau)\delta(\mathbf{k}_1-\mathbf{q}_1)\delta(\mathbf{k}_2-\mathbf{q}_2)\delta(\mathbf{k}_3-\mathbf{q}_3) \\ -2\tau\left(1-c_s^{-2}\right)\left(\mathbf{q}_2\cdot\mathbf{q}_3\right)u^{*\prime}_{\mathbf{q}_1}(\tau)u^{*}_{\mathbf{q}_2}(\tau)u^{*}_{\mathbf{q}_3}(\tau)\Big(\delta(\mathbf{k}_1-\mathbf{q}_1)\delta(\mathbf{k}_2-\mathbf{q}_2)\delta(\mathbf{k}_3-\mathbf{q}_3) \\ +\{\mathbf{k}_1\leftrightarrow\mathbf{k}_2\}+\{\mathbf{k}_1\leftrightarrow\mathbf{k}_3\}\Big)\Big]\Bigg\}\,,\end{aligned} \tag{3.2.37}$$

where[8] $u_{\mathbf{k}}(\tau) = v_{\mathbf{k}}(\tau)/z$ (see eq. (1.2.16)) and we have used that

$$\langle \mathcal{R}_{\mathbf{k}}(\tau)\mathcal{R}_{\mathbf{q}}(\tau)\rangle = (2\pi)^3 u_{\mathbf{k}}(\tau)u^*_{\mathbf{q}}(\tau)\delta\left(\mathbf{k}-\mathbf{q}\right)\,. \tag{3.2.38}$$

[7] Note that the expression $a = -1/(H\tau)$ is only valid for uninterrupted slow-roll. In the case of slow-roll violations, especially for sharp steps in the potential, the corrections may give additional contributions to the correlation functions.

[8] The mode function $u_{\mathbf{k}}(\tau)$ should never be confused with the reduction in the speed of sound $u(\tau) = 1-c_s^{-2}$.

For the leading order contribution, it suffices to use the zeroth-order mode function

$$u_{\mathbf{k}}(\tau) = \frac{iH}{\sqrt{4\epsilon c_{s,0} k^3}} \left(1 + ikc_{s,0}\tau\right) e^{-ikc_{s,0}\tau} \ , \tag{3.2.39}$$

and the three-point correlation function is then:

$$\begin{aligned}
\langle \mathcal{R}_{\mathbf{k}_1} \mathcal{R}_{\mathbf{k}_2} \mathcal{R}_{\mathbf{k}_3} \rangle = {} & \frac{\mathcal{P}_{\mathcal{R},0}^2 (2\pi)^7 M_{\rm Pl}^6}{8 k_1^3 k_2^3 k_3^3} \delta(\mathbf{k}_1 + \mathbf{k}_2 + \mathbf{k}_3) \\
\times \int_{-\infty}^{0} d\tau \Big\{ & \cos\left(Kc_{s,0}\tau\right) \Big[4sc_s^{-2} c_{s,0}^3 \tau k_1 k_2 k_3 (k_1 k_2 + 2 \text{ perm}) \\
& - 2\tau c_{s,0} \left(1 - c_s^{-2}\right) \left[k_1^2 (k_2 + k_3)(\mathbf{k}_2 \cdot \mathbf{k}_3) + 2 \text{ perm} \right] \Big] \\
& - \sin\left(Kc_{s,0}\tau\right) \Big[4sc_s^{-2} c_{s,0}^2 (k_1^2 k_2^2 + 2 \text{ perm}) - 2\left(1 - c_s^{-2}\right) \left[k_1^2 (\mathbf{k}_2 \cdot \mathbf{k}_3) + 2 \text{ perm} \right] \\
& - 6\tau^2 c_{s,0}^4 \left(1 - c_s^{-2}\right) k_1^2 k_2^2 k_3^2 + 2\tau^2 c_{s,0}^2 \left(1 - c_s^{-2}\right) k_1 k_2 k_3 \left[k_1 (\mathbf{k}_2 \cdot \mathbf{k}_3) + 2 \text{ perm} \right] \Big] \Big\} \ ,
\end{aligned} \tag{3.2.40}$$

where $K \equiv k_1 + k_2 + k_3$ and[9] $\mathcal{P}_{\mathcal{R},0} = H^2/(8\pi^2 \epsilon M_{\rm Pl}^2 c_{s,0})$. Before we proceed, some comments are in order:

- For steps in the potential, one also has to calculate the contribution to the three-point function coming from similar cubic operators. It is easy to track the polynomials in k_i arising from the different operators if one pays attention to the form of the mode functions (3.2.39). This way, we noticed that the result for steps in the potential in [124, eq. 3.32] is missing a term, so it should display as follows:

$$\begin{aligned}
\frac{\mathcal{G}}{k_1 k_2 k_3} = \frac{1}{4} \epsilon_{\rm step} \mathcal{D}\left(\frac{K\tau_f}{2\beta}\right) \Bigg[& \left(\frac{k_1^2 + k_2^2 + k_3^2}{k_1 k_2 k_3 \tau_f} - K\tau_f \right) K\tau_f \cos(K\tau_f) \\
& - \left(\frac{k_1^2 + k_2^2 + k_3^2}{k_1 k_2 k_3 \tau_f} - \frac{\sum_{i \neq j} k_i^2 k_j}{k_1 k_2 k_3} K\tau_f + K\tau_f \right) \sin(K\tau_f) \Bigg]
\end{aligned} \tag{3.2.41}$$

  This is indeed good news, since the missing term $(+K\tau_f)$ above was the source of a small discrepancy found by the authors of [124] with respect to previous results [121], of order $10 - 15\%$ on large scales. We have checked that this discrepancy vanishes when the extra term is introduced.

- We consider sharp features ($\beta_s \gg 1$) peaking in τ_f and define the new variable y through $\tau = \tau_f \, e^{-y/\beta_s}$, as we did for the power spectrum. There are two kinds of functions appearing in (3.2.40): polynomials and oscillating

[9] Notice that the definition of $\mathcal{P}_{\mathcal{R},0}$ in section 3.2.1 did not include $c_{s,0}$, since in the SRFT approach it is taken to be one.

functions. For the latter, we substitute $\tau \simeq \tau_f(1 - y/\beta_s)$ and do not expand further, in order to keep the Fourier transforms. For the former, the zeroth order approximation $\tau \simeq \tau_f$ (as in [124]) provides excellent results[10], although we take the next order and evaluate them at $\tau \simeq \tau_f(1 - y/\beta_s)$ to test for not-so-sharp features. We will therefore calculate the first order correction to previous results. Furthermore we consider, apart from the operator $\mathcal{R}\dot{\mathcal{R}}^2$ (proportional to s), two extra contributions $\dot{\mathcal{R}}^3$ and $\dot{\mathcal{R}}(\nabla\mathcal{R})^2$ (proportional to u) and show that they all contribute at the same order, independently of the sharpness β_s. This is because, although s is proportional to the sharpness β_s, it is also proportional to the derivative of the shape function, F', defined in eq. (3.2.25). On the other hand, u is proportional to the shape function, but the Fourier transform of F introduces an additional factor β_s relative to the Fourier transform of F', cf. eqs. (3.2.27)–(3.2.29) and (3.2.42)–(3.2.45).

- The integrals in (3.2.40) contain Fourier transforms of the shape function F and its derivative, given the definitions in (3.2.24) and (3.2.25). The symmetric and antisymmetric envelope functions arising from the Fourier transform of F' were already defined in (3.2.27)–(3.2.29). For completeness, we will give the complementary definitions obtained when integrating by parts:

$$\int_{-\infty}^{\infty} dy\, F(y) \cos\left(\frac{\theta_k}{\beta_s} y\right) = -\frac{\beta_s}{2\theta_k} \mathcal{D}_S \ , \tag{3.2.42}$$

$$\int_{-\infty}^{\infty} dy\, F(y) \sin\left(\frac{\theta_k}{\beta_s} y\right) = \frac{\beta_s}{2\theta_k} \mathcal{D}_A \ , \tag{3.2.43}$$

$$\int_{-\infty}^{\infty} dy\, y\, F(y) \cos\left(\frac{\theta_k}{\beta_s} y\right) = \frac{1}{2}\left(\frac{\beta_s}{\theta_k}\right)^2 \left(K\frac{d\mathcal{D}_A}{dK} - \mathcal{D}_A\right) \ , \tag{3.2.44}$$

$$\int_{-\infty}^{\infty} dy\, y\, F(y) \sin\left(\frac{\theta_k}{\beta_s} y\right) = \frac{1}{2}\left(\frac{\beta_s}{\theta_k}\right)^2 \left(K\frac{d\mathcal{D}_S}{dK} - \mathcal{D}_S\right) \ , \tag{3.2.45}$$

where again $\theta_k = K c_{s,0} \tau_f$ and the slight change of notation between these definitions and those in (3.2.27)–(3.2.29) is given by $K \leftrightarrow 2k$. We also imposed that F asymptotically vanishes when integrating by parts, which will be the case in this calculation; that is, c_s asymptotically approaches $c_{s,0}$.

Taking into account the comments above, we calculate the bispectrum to leading order (3.2.40) for the particular case in which $c_{s,0} = 1$, so that we can compare to the SRFT method described in section 3.2.1. We will express the

[10] As opposed to the power spectrum, in this case we only have polynomials with positive powers of $k\tau$, and therefore evaluating them at $k\tau_f$ is already a good approximation for sufficiently sharp features.

bispectrum in terms of the normalised scale-dependent function $f_{\rm NL}(\mathbf{k}_1,\mathbf{k}_2,\mathbf{k}_3)$ defined by:

$$\begin{aligned}\langle\mathcal{R}_{\mathbf{k}_1}\mathcal{R}_{\mathbf{k}_2}\mathcal{R}_{\mathbf{k}_3}\rangle &= (2\pi)^3\delta(\mathbf{k}_1+\mathbf{k}_2+\mathbf{k}_3)\Delta B_{\mathcal{R}}\\ &= (2\pi)^7\delta(\mathbf{k}_1+\mathbf{k}_2+\mathbf{k}_3)\frac{3}{10}f_{\rm NL}(\mathbf{k}_1,\mathbf{k}_2,\mathbf{k}_3)\mathcal{P}^2_{\mathcal{R},0}M_{\rm Pl}^6\frac{k_1^3+k_2^3+k_3^3}{k_1^3k_2^3k_3^3}\ , \end{aligned}\quad (3.2.46)$$

and we will use the following identities for a triangle of vectors $\{\mathbf{k}_1,\mathbf{k}_2,\mathbf{k}_3\}$:

$$\begin{aligned}k_1(\mathbf{k}_2\cdot\mathbf{k}_3)+2\text{ perm} &= \frac{1}{2}\left[k_1^3+k_2^3+k_3^3-K(k_1k_2+2\text{ perm})+3k_1k_2k_3\right]\ ,\\ k_1^2(\mathbf{k}_2\cdot\mathbf{k}_3)+2\text{ perm} &= \frac{1}{2}\left[k_1^4+k_2^4+k_3^4-2(k_1^2k_2^2+2\text{ perm})\right]\ ,\\ k_1^2(k_2+k_3)(\mathbf{k}_2\cdot\mathbf{k}_3)+2\text{ perm} &= \frac{1}{2}\left[K(k_1^4+k_2^4+k_3^4)-(k_1^5+k_2^5+k_3^5)\right.\\ &\quad\left.-K(k_1^2k_2^2+2\text{ perm})-k_1k_2k_3(k_1k_2+2\text{ perm})\right]\ .\end{aligned}$$

Finally, the bispectrum contribution due to variations in the speed of sound as considered in the cubic action (3.2.35), to first order in the size of the feature σ_*, and to first order in the polynomial expansion $\tau\simeq\tau_f(1-y/\beta_s)$ reads:

$$\begin{aligned}f_{\rm NL}(\mathbf{k}_1,\mathbf{k}_2,\mathbf{k}_3) &= \frac{5}{24}\frac{\sigma_*}{k_1^3+k_2^3+k_3^3} \qquad (3.2.47)\\ &\times\left\{\cos(K\tau_f)\left\{\tau_f^2\frac{k_1k_2k_3}{K}\Big[(k_1^3+k_2^3+k_3^3)+K(k_1k_2+2\text{ perm})-3k_1k_2k_3\Big]\mathcal{D}_A\right.\right.\\ &\quad+\frac{\tau_f}{K}\Big[K(k_1^4+k_2^4+k_3^4)-(k_1^5+k_2^5+k_3^5)+K(k_1^2k_2^2+2\text{ perm})\\ &\qquad-4k_1k_2k_3(k_1k_2+2\text{ perm})+3\frac{k_1k_2k_3}{K}(k_1^3+k_2^3+k_3^3)-9\frac{k_1^2k_2^2k_3^2}{K}\Big]\mathcal{D}_S\\ &\quad-3\tau_f\frac{k_1k_2k_3}{K}\Big[(k_1^3+k_2^3+k_3^3)+\frac{1}{3}K(k_1k_2+2\text{ perm})-3k_1k_2k_3\Big]\frac{d\mathcal{D}_S}{dK}\\ &\quad-\frac{1}{K^2}\Big[3K(k_1^4+k_2^4+k_3^4)-2(k_1^5+k_2^5+k_3^5)-4K(k_1^2k_2^2+2\text{ perm})\\ &\qquad-2k_1k_2k_3(k_1k_2+2\text{perm})\Big]\mathcal{D}_A\\ &\quad+\frac{1}{K}\Big[2K(k_1^4+k_2^4+k_3^4)-2(k_1^5+k_2^5+k_3^5)-2k_1k_2k_3(k_1k_2+2\text{perm})\Big]\frac{d\mathcal{D}_A}{dK}\\ &\quad\left.-\frac{1}{\tau_fK^2}\Big[(k_1^4+k_2^4+k_3^4)-2(k_1^2k_2^2+2\text{ perm})\Big]\left(\mathcal{D}_S-K\frac{d\mathcal{D}_S}{dK}\right)\right\}\\ &\quad+\sin(K\tau_f)\Big\{\{\mathcal{D}_S\leftrightarrow\mathcal{D}_A\ ,\ \tau_f\leftrightarrow-\tau_f\}\Big\}\Big\}\ ,\end{aligned}$$

where the $\sin(K\tau_f)$ in the last line contains the same terms as the $\cos(K\tau_f)$, but changing $\mathcal{D}_S\leftrightarrow\mathcal{D}_A$ and $\tau_f\leftrightarrow-\tau_f$, as indicated. This is the formula we want to

compare with (3.2.6), after proper normalisation. Below, we show the comparison for different functional forms of the speed of sound.

3.2.5 Comparison of bispectra

In this section we compare the bispectrum obtained using the SRFT method (3.2.6) with that using the first order approximation for sharp features (3.2.47). As a first example, one can reproduce our test case of gaussian reductions in the speed of sound, cf. (3.3.1), by taking:

$$F = \mathrm{e}^{-\beta_s^2\left(\ln\frac{\tau}{\tau_f}\right)^2} \quad \Rightarrow \quad 1 - c_s^{-2} = -\sigma_* \, \mathrm{e}^{-\beta_s^2\left(\ln\frac{\tau}{\tau_f}\right)^2} + \mathcal{O}\left(\sigma_*\right)^2 \ , \qquad (3.2.48)$$

where the correspondence between this set of parameters and the one used in [1] is $\sigma_* \leftrightarrow -B$, $\tau_f \leftrightarrow \tau_0$, and $\beta_s \leftrightarrow \sqrt{\beta}$. Thus, we will corroborate that the predictions for the bispectrum presented in the previous chapter are solid and consistent with similar methods. In this case F is symmetric in the variable $y = -\beta_s \ln\frac{\tau}{\tau_f}$ and therefore only the symmetric envelope function $\mathcal{D}_S$ contributes, which is given by

$$\mathcal{D}_S = -\frac{2K\tau_f}{\beta_s}\sqrt{\pi}\exp\left(-\frac{K^2\tau_f^2}{4\beta_s^2}\right) \quad , \quad \mathcal{D}_A = 0 \ . \qquad (3.2.49)$$

In figure 3.4 we show the excellent agreement between the results obtained with (3.2.6) and (3.2.47) for the equilateral limit $k_1 = k_2 = k_3$. We have checked that for other configurations in momentum space, such as the folded or the squeezed shapes, the agreement is very similar. Note that in figure 3.4 we are plotting the absolute difference in $f_{\rm NL}$ and comparing with the total envelope of the signal[11]. At small scales one can see that the relative difference compared to the total signal is high, due to the fact that the approximation for sharp features starts to fail for large values of $K\tau$. However, the absolute signal is insignificant at such small scales.

As a second example, we propose a shape function with an antisymmetric part:

$$F = \mathrm{e}^{-\beta_s^2\left(\ln\frac{\tau}{\tau_f}\right)^2+\beta_s\ln\frac{\tau}{\tau_f}} \quad \Rightarrow \quad 1-c_s^{-2} = -\sigma_*\left(\frac{\tau}{\tau_f}\right)^{\beta_s} \mathrm{e}^{-\beta_s^2\left(\ln\frac{\tau}{\tau_f}\right)^2} + \mathcal{O}\left(\sigma_*\right)^2 \ , \qquad (3.2.50)$$

[11] We point out that the total envelope of the signal is not given by $\mathcal{D}_S$ or $\mathcal{D}_A$ alone. The total envelope is a combination of both functions, their derivatives, and the polynomials of k_i that appear in (3.2.47).

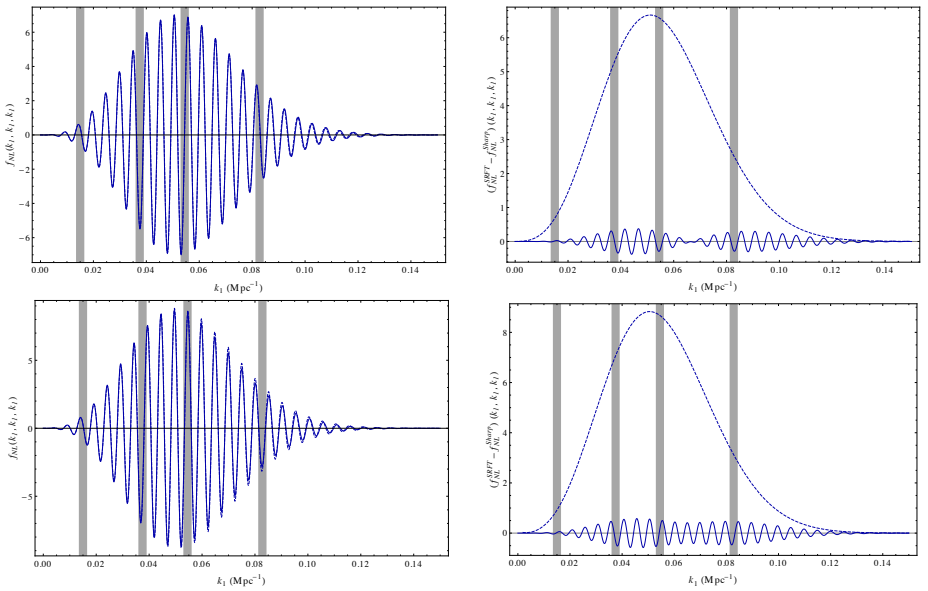

Figure 3.4 *– LEFT: bispectrum f_{NL} signal in the equilateral limit with the normalisation indicated in* (3.2.46)*, given by a symmetric reduction in the speed of sound as in* (3.2.48) *(TOP) and an asymmetric reduction as in* (3.2.50) *(BOTTOM), calculated with the SRFT formula* (3.2.6) *(solid) and with the sharp approximation* (3.2.47) *(dashed). RIGHT: absolute difference between the signals showed in the left plot (solid), together with the envelope of the signal (dashed). The gray strips represent the approximate scales of the first four acoustic peaks of the CMB temperature spectrum. The parameters are $\sigma_* = 0.04$, $\beta_s = 25.5$, $\ln(-\tau_f) = 6$. This gives $|s|_{max} \simeq 0.42$ for the symmetric case and $|s|_{max} \simeq 0.55$ for the asymmetric case. Note that in both cases the relative difference with respect to the envelope is large only at very small scales, which in any case will be indistinguishable at the observational level. We are also within the limit $|s|_{max} < 1$, where these signatures are reliable but sharp enough so that the sharp approximation works.*

for which the symmetric and antisymmetric envelope functions read:

$$\mathcal{D}_S = -\frac{2K\tau_f}{\beta_s}\sqrt{\pi}\exp\left(\frac{\beta_s^2 - K^2\tau_f^2}{4\beta_s^2}\right)\cos\left(\frac{K\tau_f}{2\beta_s}\right) \ , \tag{3.2.51}$$

$$\mathcal{D}_A = -\frac{2K\tau_f}{\beta_s}\sqrt{\pi}\exp\left(\frac{\beta_s^2 - K^2\tau_f^2}{4\beta_s^2}\right)\sin\left(\frac{K\tau_f}{2\beta_s}\right) \ . \tag{3.2.52}$$

We show in figure 3.4 the equilateral bispectrum signal produced by the asymmetric shape (3.2.50), again derived using (3.2.6) and (3.2.47). As one can see in figure 3.4, the agreement is also remarkable for functions with an antisymmetric part.

3.3 Parameter space and details of the search

In the previous chapter we studied a test case consisting of a gaussian reduction in the speed of sound [1]. The functional form is inspired by soft turns along a multi-field inflationary trajectory with a large hierarchy of masses, a situation that is consistently described by an effective single-field theory and uninterrupted slow roll [102, 103, 106–108, 136]. We parameterised the reduction in the speed of sound as a gaussian in e-folds N of inflation:

$$u = 1 - c_s^{-2} = B\, e^{-\beta(N-N_0)^2} = B\, e^{-\beta\left(\ln\frac{\tau}{\tau_0}\right)^2} \,, \tag{3.3.1}$$

where $\beta > 0$ is the sharpness, $B < 0$ is the amplitude, and N_0 (or τ_0) is the instant of maximal reduction. Assuming slow-roll, the conformal time τ is related to the e-folds of inflation through $\ln(-\tau) = (N_{\rm in} - N) - \ln(a_{\rm in}H_0)$, where $a_{\rm in} = a(N_{\rm in})$ and $N_{\rm in}$ is the time when the last ~ 60 e-folds of inflation start. Notice that the quantity $N_{\rm in}$ is irrelevant, since all the quantities in e-folds are defined with respect to $N_{\rm in}$.

3.3.1 Choice of parameter space

In the previous chapter we already gave a brief description of the constraints on our parameter space (see eqs. (2.2.5)), and now let us elaborate on this matter, which will serve as to connect with the adiabatic condition (1.5.35). There are two main criteria that we followed in order to determine the parameter regions that we explored:

(a) The angular scales probed by Planck ($\ell = 2 - 2500$) roughly correspond to certain momentum scales crossing the Hubble sound horizon during the first $N_{\rm CMB} \simeq 7$ e-folds of the last ~ 60 e-folds of inflation. If the data resembles features due to a reduced speed of sound, they are most likely to be found in this "CMB window", so we choose to 'look under the lamppost'. This means that the sharpness β and the position N_0 are chosen so that the reduction happens well within this window. As a by-product, we avoid degeneracies with the spectral index n_s and the optical depth $\tau_{\rm reio}$ due to very wide reductions.[12]

(b) The SRFT calculation of the power spectrum and the bispectrum is valid for mild and moderately sharp reductions of the speed of sound. Also, the slow-roll contributions to the bispectrum are disregarded with respect to the terms arising from the reduced speed of sound [111]. This means that the amplitude $|u|$ and the rate of change $s \equiv \frac{\dot{c}_s}{c_s H}$ must be much smaller than one,

[12] Note that the *lamppost* is actually bigger, since any feature happening in a particular window propagates in the primordial power spectra to a bigger region. E.g. modes that leave the horizon after the reduction in c_s has finished are also affected by it. Thus, it would be interesting to extend our search to larger values of $|\tau_0|$.

while being (at least one of them) much larger than the slow-roll parameters. As a bonus, later in the text we will argue that $|s| \ll 1$ is tightly related to an adiabatic evolution [106].

We took a very conservative definition for the total width of the reduction (in e-folds): ten standard deviations, $\Delta N = 10/\sqrt{2\beta}$. Then, from **(a)**, the position N_0 and the sharpness β should satisfy $5\sqrt{2\beta} < N_0 < N_{\rm CMB} - 5\sqrt{2\beta}$ and $10\sqrt{2\beta} < N_{\rm CMB}$. As to the perturbative regime, the rate of change s of the speed of sound (3.3.1) reads:

$$s(N) = \frac{dc_s}{c_s dN} = -\frac{B\beta(N-N_0)\, e^{-\beta(N-N_0)^2}}{1 - B\, e^{-\beta(N-N_0)^2}} \ . \tag{3.3.2}$$

Since we have to impose $|s| \ll 1$ for all values of N, it suffices to impose this condition at the point where $|s|$ takes its maximum value $|s(N_*)| = |s|_{\rm max}$, determined by:

$$N_* = N_0 \pm \frac{1}{\sqrt{2\beta}}\sqrt{1+\mathcal{O}(B)} \ \simeq \ N_0 \pm \frac{1}{\sqrt{2\beta}} \ , \tag{3.3.3}$$

which approximately corresponds to one standard deviation of our gaussian, and we have used that $|B| \ll 1$. Then the condition $|s|_{\rm max} \ll 1$ translates into $\beta \ll \frac{2e}{B^2} + \mathcal{O}(B^{-1})$. Altogether, the allowed region of our parameter space is taken to be the one indicated in chapter 2 by eqs. (2.2.5).

Notice that, as explained above in **(b)**, the bound $|B| \gg \mathcal{O}(\epsilon, \eta)$ can be avoided if $|s|_{\rm max} \gg \mathcal{O}(\epsilon, \eta)$. For computational purposes, we use the parameter $\ln(-\tau_0)$ instead of N_0 for the data analysis. The range for this parameter is taken to be more strongly restricted than by (2.2.5c):

$$4.4 \leq \ln(-\tau_0) \leq 6 \ , \tag{3.3.4}$$

The features in the power spectrum and bispectrum are linearly oscillating, as well as those tested in one of the searches for bispectrum features by the Planck collaboration [48, sec. 7.3.3]. The oscillatory frequency is determined by τ_0, and the range of frequencies covered in Planck's bispectrum analysis is equivalent to the interval $\ln(-\tau_0) \in [4.43, 5.34]$, which motivated us to search in the interval given above. Hence, our search is slightly larger than theirs in this respect, as explained in detail in section 2.5.

3.3.2 Perturbative unitarity and adiabatic evolution

In the works [168, 169], consistency conditions regarding inflationary models that produce features were studied. In particular they derive several bounds from the requirement that the theory describing the features is in the weak coupling regime. In this section we clarify what these bounds mean in the context

of soft transient reductions in the speed of sound, in particular for our test case [1].

In [169], they establish a hard upper bound on the sharpness of the feature, based on the loss of unitarity when the loop contribution to a correlation function becomes of the same order as the tree level correlator:[13] $\beta_{\rm CBM} \lesssim 160$, where $\beta_{\rm CBM}$ (labelled by the initials of the authors of [169]) defines the sharpness of the feature: $\beta_{\rm CBM} \equiv 1/(H\Delta t)$.

Our sharpness parameter β is related to that of [169] by $\beta = 50\beta^2_{\rm CBM}$, where we took the conservative definition of the width to be ten standard deviations, as explained in section 3.3.1. This imposes the following bound on our sharpness parameter:

$$\ln\beta \lesssim 14 \ . \tag{3.3.5}$$

Since we restricted our search to $2 < \ln\beta < 7.5$, the fits we found in that region [1] are perfectly consistent with the bound given above. Even if we take the crude definition for the width of only one standard deviation, the correspondence would be $\beta = \beta^2_{\rm CBM}$, and the bound would translate to $\ln\beta \lesssim 10$, which still leaves us in a safe region. The analysis of [168] goes along the same lines as that of [169], and similar results are obtained. They also identify additional scales above which the theory breaks down. Given that we *a priori* constrained our search to a region of the parameter space where the perturbative and adiabatic regimes are respected, it remains by far within the bounds derived in [168, 169], and therefore the predictions obtained are consistently interpreted by the underlying theory.

It was also found [168, 169] that the best fit so far for steps in the potential in the CMB [113, 142, 167] does not lie within the allowed theoretical bounds. This calls into question the consistency of the framework in which these predictions are derived. More interestingly, this motivates a new theoretical framework able to consistently describe those predictions, since the data is blind to whether a theory is internally consistent or not.

An important and evident conclusion of these analyses is that very sharp features are problematic from the theoretical point of view. In addition, one could speculate that if the data finally points to inflationary scenarios with large field excursions, a (slightly broken) symmetry should protect the background, and then we would not expect to find sharp features in the potential. This further motivates the study of moderately sharp features, which are still safely described by an underlying theory.

The previous results were obtained in the framework of the effective field theory of inflation [98] taking into account only the time dependence of the

[13] This calculation is possible thanks to the fact that for the case of a feature in the Hubble parameter the n-order Lagrangian acquires a particularly simple form [105].

Hubble parameter, and neglecting the variation of the rest of coefficients M_n^4, which accompany the quadratic and cubic operators. First of all, it is not clear whether similar conclusions would hold considering changes in the M_n^4 coefficients. It is possible to construct the n^{th}-order Lagrangian for the case of changes in the Hubble parameter and group all the terms together in a single vertex (for example π^n) by successive integration by parts. However, this is in general very difficult for changes in the M_n^4 coefficients, since the number of degrees of freedom is larger. In the absence of a UV theory that gives us a recipe for consistently calculating M_n^4, any estimate on how they determine the perturbative regime must be made with extreme caution.

Last but not least, the intuition in terms of scattering amplitudes is borrowed from the standard quantum field theory techniques which assume time-independent vertex coefficients. Intuitively, this will be applicable to time-dependent coefficients if they obey an adiabatic condition of the form $|\dot{\lambda}/\lambda T| \ll 1$, where T is the time scale of the scattering process. Within this regime, higher order interactions should be suppressed. Although this might relax the strong coupling bound coming from the scattering amplitudes, it is not clear how time dependence would affect the other strong coupling scales, as treated in detail in [168].

3.3.3 Validity of the effective single-field theory in the light of BICEP2

In this section we study the relationship between the rate of change of the speed of sound and an adiabatic evolution, or in other words, how strong a turn can be without invalidating the single-field description. Particle production due to sudden turns has been previously studied (see e.g. [166] and references therein), and it constitutes an important consistency check for a valid single-field description. However, the situation has become much more exciting in the light of the new results of BICEP2 [55], which pose an interesting challenge for effective single-field theories, as we will explain below. Let us first review the adiabatic condition in the context of integration of a heavy mode, as in section 1.5.2. The validity of the effective single-field theory is subject to the adiabatic condition [106]:

$$|\ddot{\mathcal{F}}_{\mathcal{R}}| \ll M_{\text{eff}}^2 |\mathcal{F}_{\mathcal{R}}| \,, \tag{3.3.6}$$

where $\mathcal{F}_{\mathcal{R}}$ is the isocurvature fluctuation, associated to the heavy mode, which we integrate out to get an effective single-field description for the adiabatic curvature perturbation. M_{eff} is the effective mass of the heavy field, determined by the turning rate in field space, the curvature of the scalar potential in the heavy direction, and the curvature of the field manifold (see e.g. [107]). The above

condition can be recast in terms of background quantities as follows[14] [106]:

$$\left|\frac{d}{dt}\ln\left(c_s^{-2}-1\right)\right| \ll M_{\rm eff}\ . \tag{3.3.7}$$

In a slow-roll regime, the conformal time is $\tau \simeq -1/(aH_0)$, and therefore $H_0\,dt = -d\tau/\tau$. Using this relation, we can rewrite the adiabatic condition (3.3.7) as follows:

$$|s| \ \ll\ \frac{1}{2}\left(1-c_s^2\right)\frac{M_{\rm eff}}{H_0}\ . \tag{3.3.8}$$

Since in this paper we are focusing on the regime $|s| < 1$, it is worth evaluating when the adiabatic condition (3.3.8) is automatically satisfied given the requirement of not-so-sharp turns $|s| < 1$. One can see that

$$\text{if}\quad c_s^2 < 1-\frac{2H_0}{M_{\rm eff}}\quad,\ \text{then}\quad |s|<1 \implies \text{Adiabatic}\ . \tag{3.3.9}$$

Given that in a valid EFT one should have $M_{\rm eff} \gg H_0$, it is clear that the condition $|s| < 1$ will ensure an adiabatic evolution. In terms of the effective mass, from (3.3.9) one can see that when the effective mass satisfies the lower bound

$$M_{\rm eff} \gtrsim \frac{2H_0}{|u|}\ , \tag{3.3.10}$$

the regime $|s| < 1$ automatically implies that we are in an effective single-field regime[15]. Note that these considerations apply to any effectively single-field inflationary scenario in which a large hierarchy of masses and slow-roll are respected.

Now let us turn the discussion to the possibilities one has to achieve an effective single-field regime in the light of the new BICEP2 results. In this context, the main concern raised by their results is that a large tensor-to-scalar ratio sets the inflationary scale to a value close to the GUT scale, and therefore the energy gap in which the inflaton and the possible additional UV degrees of freedom must cohabit is not very large. Given this, having a large hierarchy of masses does not seem so easy.

Putting in some numbers, a naive interpretation of $r = \mathcal{O}(0.1)$ would support $H_0 \sim 10^{14}$ GeV [172], leaving four orders of magnitude to the Planck scale. If there is new physics at the GUT scale (or above), then $|s| < 1$ and $10^{-2} \lesssim |u| < 1$ should be safely in the effectively single-field

[14] We are disregarding a short transient at the start and end of the turn, where a different condition is satisfied.

[15] We stress that (3.3.10) is not an adiabatic condition, it is the condition under which smooth turns ($|s| < 1$) imply an adiabatic regime. Even if the lower bound (3.3.10) is violated, the condition (3.3.7) will still ensure adiabaticity.

regime. Then, one could conclude that reductions in the speed of sound of a few percent are well motivated, and that the bound $|s| < 1$ implies an adiabatic regime.

Summarising, the new results by BICEP2, if confirmed, leave about five orders of magnitude in which the UV degrees of freedom and the inflaton must live together. Although the energy gap is not gigantic, one would expect the heavy physics energy scale to be at least a hundred times larger than the Hubble scale, and therefore the adiabatic condition is satisfied.

3.3.4 Review of our search and further analyses

In our previous work [1], summarised in chapter 2, we looked for correlated signatures in the primordial power spectrum and bispectrum due to a gaussian reduction in the speed of sound. Here we review the main results and provide some more details regarding the search. Further details can be found in the original paper [2].

We found several fits to the Planck CMB power spectrum data with an improvement[16] $2 < -\Delta\chi^2_{\text{eff}} < 10$, and calculated the predicted correlated signals in the primordial bispectrum, whose shape turned out to be surprisingly similar to a set of primordial bispectrum templates tested against CMB bispectrum data by the Planck collaboration [48, sec. 7.3.3].

Thanks to this similarity, we were able to qualitatively compare some of our predictions to some of their fits, finding a reasonable agreement [1] (see section 2.5). But we also found interesting differences: (1) the analysis of *localised* oscillations in the bispectrum performed by Planck only covers the region around the first acoustic peak, while our features are more significant around the second and third; (2) some of our best fits occur at values of $|\tau_0|$ corresponding to oscillatory frequencies which are slightly higher than those covered in Planck's analysis. Thus, an extended search for oscillatory features in the bispectrum data towards higher frequencies and smaller scales would help in confirming or falsifying our predictions. Although our fits are not very significant at the level of the CMB power spectrum, the mild agreement in the primordial bispectrum is more than encouraging, given that this prediction is solely based on a fit to the CMB power spectrum data, and that it comes from a well motivated and consistent theoretical framework.

Review of main results and numerical consistency check

The power spectrum features caused by a transient reduction in the speed of sound described by eq. (3.3.1), parametrized by B, β and τ_0, are combined with the primordial spectrum of the ΛCDM Planck baseline model described in [47,

[16] A similar result is obtained in the Standard Clock model [173].

sec. 2], parametrized by an amplitude A_s and a spectral index n_s. The primordial perturbations evolve in a flat FLRW universe parametrized by the densities of baryonic and cold dark matter, $\Omega_{\rm b}$ and $\Omega_{\rm cdm}$, and the current expansion rate H_0. The damping due to reionisation is parameterised by the optical depth $\tau_{\rm reio}$. Those six standard plus three feature parameters describe our cosmological model.

The features given by eq. (3.2.5) are calculated using a Fast Fourier Transform. The resulting CMB, calculated with the Boltzmann code CLASS [45, 46], is fitted to the ESA Planck mission temperature data of March 2013, using the likelihood provided by the experiment [34], and the low-ℓ CMB polarisation data of the WMAP experiment [31]. In that fit, we use flat priors on the six cosmological parameters and on B, $\ln\beta$ and $\ln(-\tau_0)$. The bounds on the priors are those defined in (2.2.5) and (2.3.1), ignoring a priori the bound $|B| \gg \mathcal{O}(\epsilon, \eta)$. The posterior probability is then maximised over the prior bounds using Markov-chain Monte Carlo (MCMC) methods, making use of the MCMC sampler MONTE PYTHON [152].

The resulting profile likelihood can be seen in figure 2.1. There, one can identify five *modes*, or defined regions of the parameter space where the likelihood is improved. The modes are well-isolated narrow bands of $\ln(-\tau_0)$, i.e. frequency of oscillation of the primordial spectrum feature. For each of the modes showed in the figure, the relevant parameter data is given in table 2.1: the numbers in parentheses are the best fit values, and the parameter ranges, when given, are 68% c.l. regions. The upper limit for $\ln\beta$ in the modes $\mathcal{B}$ and $\mathcal{C}$ is imposed by the prior, as we explained in the previous chapter (see figure 2.2 for an explanation of the plateau in $\Delta\chi^2$). For the modes $\mathcal{D}$ and $\mathcal{E}$, no parameter ranges are given, due to their low significance and non-gaussian character; only the respective best fits are shown.

As expected, we find only small degeneracies between the feature parameters and the ΛCDM parameters for modes $\mathcal{A}$, $\mathcal{B}$ and $\mathcal{C}$. Consequently, the best fits and 68%c.l. intervals of the ΛCDM parameters reproduce quite accurately those of Planck, cf. table 3.1. For the less significant modes $\mathcal{D}$ and $\mathcal{E}$, some of the correlations are slightly larger, since for lower $\ln(-\tau_0)$ the frequency of the fits drops, getting closer to the frequency of the acoustic oscillations. Further details on the degeneracies can be found in [2].

In order to make our results from CLASS+MONTE PYTHON more reliable, we cross-checked them with an independent Einstein-Boltzmann solver and a different MCMC sampler, namely CAMB [44] and COSMOMC [174]. As an example, in tab. 3.1 we explicitly show this comparison for the most significant mode $\mathcal{B}$ by varying both the primary ΛCDM parameters and the additional sound speed reduction parameters. We find excellent agreement between these two results.

Planck + WMAP Polarisation			
Parameter	CAMB	CLASS	Baseline [47]
$100\Omega_b h^2$	2.208 ± 0.027	2.214 ± 0.029	2.205 ± 0.028
$\Omega_c h^2$	0.1204 ± 0.0026	0.1203 ± 0.0027	0.1199 ± 0.0027
$\tau_{\rm reio}$	0.089 ± 0.013	0.090 ± 0.013	$0.089^{+0.012}_{-0.014}$
H_0	67.16 ± 1.14	67.29 ± 1.21	67.3 ± 1.2
n_s	0.9600 ± 0.0070	0.9598 ± 0.0074	0.9603 ± 0.0073
$\ln(10^{10} A_s)$	3.090 ± 0.023	3.088 ± 0.024	$3.089^{+0.024}_{-0.027}$
B	$-0.045^{+0.045}_{-0.034}$ (95%c.l.)	$-0.041^{+0.041}_{-0.031}$ (95%c.l.)	—
$\ln \beta$	$6.00^{+1.50}_{-3.00}$ (95%c.l.)	$6.06^{+1.44}_{-2.18}$ (95%c.l.)	—
$\ln(-\tau_0)$	5.55 ± 0.06 (95%c.l.)	5.55 ± 0.05 (95%c.l.)	—
$\chi^2_{\rm bf}$	9797.25	9797.58	9805.90

Table 3.1 – CAMB+CosmoMC *vs.* CLASS+Monte Python *consistency check: mean values and* 68% *(or* 95% *where indicated) confidence intervals for the primary* Λ*CDM parameters and the additional sound speed reduction parameters for the mode* $\mathcal{B}$*. We also show the parameter ranges found by the Planck collaboration [47] for a featureless model.*

Degeneracies in the modes and polarisation

The CMB temperature data is not able to restrict the maximum value of $\ln \beta$, as one can see in figure 2.1. After some value of it, the likelihood reaches a plateau with constant $\ln(-\tau_0)$ and increasing $\ln \beta$. The reason for the data not being able to restrict $\ln \beta$ and for this degeneracy is quite well explained by figure 2.2 and figure 3.5. In the last one, we have plotted the CMB temperature and E-mode polarisation spectra of the best fit of the mode $\mathcal{B}$ (white circle in figure 2.2), together with a similar fit (grey circle in figure 2.2) that improves $\Delta\chi^2_{\rm eff}$ marginally and saturates the $s = 1$ bound. Along the direction of simultaneous increase of $\ln \beta$ and $|B|$, the feature in the primordial spectrum broadens towards smaller scales, while the amplitude of the tail on the larger scales remains almost constant. Since at smaller scales much of the primordial signal is suppressed by diffusion damping in the CMB, no significance is gained along the degeneracy direction, causing a plateau in $\Delta\chi^2_{\rm eff}$.

Photon diffusion at the last scattering surface has the effect of polarising the CMB signal through Thomson scattering, so at smaller scales the polarisation spectrum will contain information about the primordial spectrum, complementary to that of the temperature spectrum. Therefore, the difference at small scales between two fits in the same plateau (for example the red and the green spectra in figure 3.5) is larger in the polarisation spectra (TE and EE). This suggests that the Planck polarisation data, expected to be released along 2014, may be able to set stronger bounds on the maximum value of $\ln \beta$.

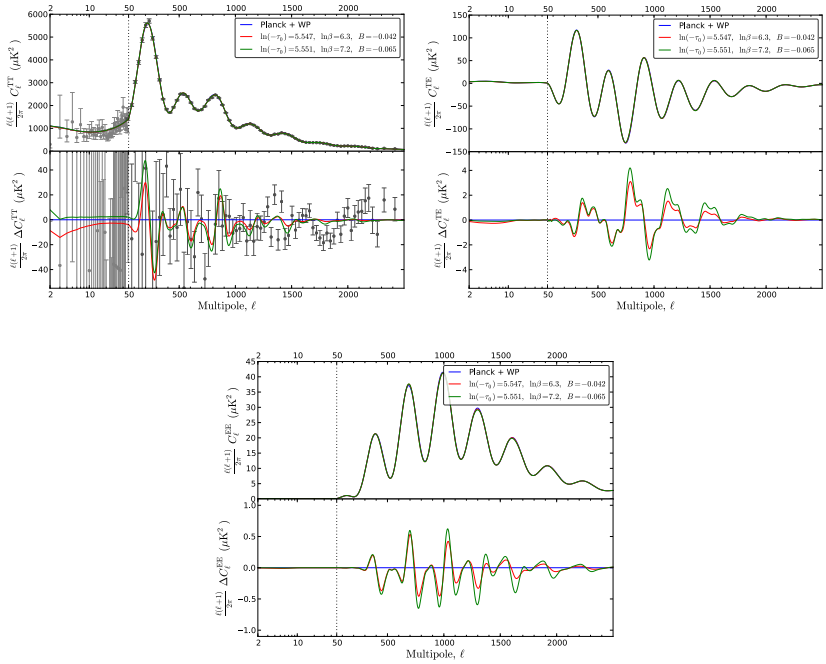

Figure 3.5 – *Comparison of the two fits indicated in figure 2.2 with a white circle (red, dashed line) and a gray circle (green, dotted line), in the TT, TE and EE CMB power spectra.*

Local improvement at different angular scales: $\Delta\chi^2(\ell)$

Given a fit to the CMB power spectrum of some feature model, it is interesting to know in which ranges of multipoles the feature describes the data better than the baseline ΛCDM model. This kind of *local improvement* can only be calculated approximately, since the temperature data points at different multipoles are in general correlated. Nevertheless, even a qualitative analysis can shed some light on where the feature fits better the data than the baseline model.

We have studied the local improvements along the multipoles of the four relevant fits, modes $\mathcal{A}$ to $\mathcal{D}$ (we show the result for mode $\mathcal{B}$ in figure 3.6). To do that, we have binned the multipoles with $\Delta\ell = 20$ and substituted pieces of the best fit for each mode into the best fit of the ΛCDM baseline model. For the sake of simplicity, we use for this analysis the preliminary fits found by keeping the cosmological and nuisance parameters fixed to their best fit values (hence the small difference in the total $\Delta\chi^2_{\text{eff}}$ between fig. 3.6 and tab. 2.1).

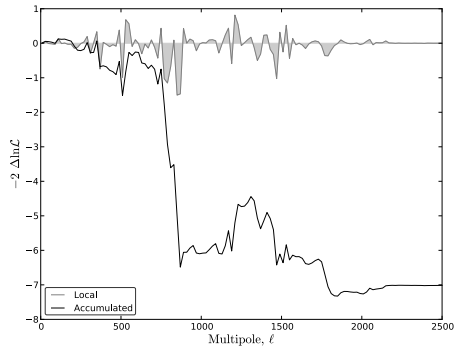

Figure 3.6 – *Gain in the likelihood of the best fit of mode $\mathcal{B}$ along the multipoles. The grey area shows the local difference in each bin, and the black line shows the accumulated difference for increasing multipoles.*

The results show that mode $\mathcal{A}$ gains its significance mostly in the first and third peak and loses some of it in the second; mode $\mathcal{B}$ (see fig. 3.6) and $\mathcal{C}$ gain most of their significance in the third peak, lose some of it in the fourth peak and improve a little again in the fifth and sixth. The mode $\mathcal{D}$ does not fit well the first and second peaks, gains most of its significance in the third peak, and some more in the fifth and sixth peaks.

3.4 Conclusions

In this chapter we have deepened our understanding about the regimes of validity of different methods to calculate the two- and three-point correlation functions of the adiabatic curvature perturbation. Moreover, we have shown that the fits we found to the data are consistently described by a well motivated and robust theoretical framework. In the following, let me summarise in more detail the relevance of the results presented in this chapter:

A detailed understanding of the origin and detectability of transient features in the primordial (and observed) correlation functions is now more important than it was before the BICEP2 results [55]. A large trans-Planckian field excursion should detect any features present in the scalar potential as well as changes in the dispersion relation of the adiabatic mode, if they are there, and arguably there were hints of both in the Planck data [48, 113]. At the same time, a high inflationary scale leaves less room for mass hierarchies in the UV completion, that would be needed to justify the single-field effective low energy description. This is a problem for very sharp features, as they tend to excite any higher frequency modes coupled to the inflaton. We have argued that the regime of moderately sharp features is particularly interesting. Most likely these cannot be detected in any partic-

ular dataset and have to be searched for in *correlations* between different data sets.

In this regime, the effect of a transient reduction in the speed of sound can be calculated with the simple SRFT approximation [111], in which the correlations between power spectrum and bispectrum are manifest. We emphasise that the simple expressions (3.2.5) and (3.2.6) hold provided $\mathcal{O}(\epsilon,\eta) \ll \max\left(|1-c_s^{-2}|, |\dot{c}_s/(Hc_s)|\right) \ll 1$ and $c_s = 1$ before and after the feature.

In this work we have presented an alternative way to calculate both the power spectrum and bispectrum, by consistently applying an approximation for moderately sharp features, both to the GSR power spectrum (eq. (3.2.30)) and to the in-in calculation of the bispectrum (eq. (3.2.47)). Within this regime, we have extended existing GSR calculations of the power spectrum to less sharp and arbitrary shapes of the speed of sound, and found excellent agreement with the SRFT approximation in the regime where both methods apply.

Given that the regimes of validity of the two methods are not entirely coincident, we are now equipped with a robust machinery that will allow us to describe features in the speed of sound for a broader region of the parameter space. Broad features can be calculated with the SRFT approach, while sharp features can be calculated using GSR for the power spectrum (eq. (3.2.30)) and the in-in approach for the bispectrum (eq. (3.2.47)).

In a previous paper [1] we performed a search for such correlated features assuming moderately sharp, mild reductions in the speed of sound of the adiabatic mode during uninterrupted slow-roll inflation. We reported several fits to the Planck CMB temperature spectrum data and predicted the correlated signatures in the complete primordial bispectrum. We qualitatively compared with the bispectrum search by Planck when possible and found reasonable agreement. We have performed additional tests to the results of our search in [1]. Namely, we have repeated it using independent codes and found practically equal results; we have studied more explicitly the small degeneracies among the cosmological and feature parameters, and proposed the CMB TE and EE polarisation spectra as a way to break degeneracies among the latter; and finally we have investigated at which multipoles each of our fits describe the CMB temperature data better than the baseline ΛCDM model.

The ability to make predictions in a wider region of the parameter space of features is of particular relevance, since new data sets may allow us to explore it. Besides, since different experiments generally have different foregrounds and systematics, a joint analysis could reduce the contamination of the primordial signal on the overlapping scales. In particular, we plan to extend our search to large scale structure surveys [175].

4

Sgoldstino inflation

In this chapter we continue the discussion on the effect of additional fields during inflation, but in the context of supergravity theories. Also, we will not discuss the explicit integration of heavy fields and their effect from an EFT point of view, but rather the decoupling between different sectors of the theory. In particular, we will discuss the decoupling between supersymmetric and non-supersymmetric sectors for a special type of couplings during the inflationary stage. We will see that even when a heavy sector is decoupled and stable, its influence on the dynamical sector can be translated into constraints. In chapter 5 we will discuss more general couplings and also the possibility of finding stable vacua. Meanwhile, in this chapter we discuss the possibility that inflation is driven by the sgoldstino, the superpartner of the goldstino. Unlike in generic supergravity scenarios, the sgoldstino decouples from all other fields in the theory, which allows for a simple and robust inflationary model. We argue that the two-field model given by this single complex scalar correctly captures the full multi-field inflationary phenomenology, that is, the non-inflationary sector is consistently truncated. On the other hand, the assumption of stability, along the entire inflationary trajectory, of the supersymmetry–preserving sector that is integrated out leads to supplementary constraints on the parent supergravity. We investigate small field, large field and hybrid sgoldstino inflation scenarios and provide some working examples. They are subject to the usual fine-tuning issues that are common to all supergravity models of inflation. We comment on some other proposed sgoldstino inflation models.

4.1 Introduction

Scalar fields are abundant in supersymmetric theories. They all couple to each other with at least gravitational strength interactions. Planck-suppressed

couplings are generically unimportant when describing processes at low energies, but such a decoupling does not work for inflation. This can be most easily inferred from the slow roll parameters, which get contributions from dimension five and six operators that are unsuppressed. Describing inflation in a generic supergravity model is thus a challenging task, as generically the scalar field dynamics pose a complicated multi-field problem, as already explained in sections 1.4 and 1.5.

There are good reasons why a single-field description is desirable. In line with Ockham's razor, it is the simplest model that fits the data. Multi-field slow-roll inflation with several (real) light fields has been studied for over a decade [88–91] (see [92, 96] and references therein), and is very constrained by the observations, in particular through the tight limits on isocurvature modes and non-gaussianity that we have reviewed in section 1.3. However, it is technically challenging to obtain single-field behavior in a full multi-field set-up.

As we have extensively described in the previous chapters, if there are turns in the inflationary trajectory, derivative interactions between the inflaton and the heavy fields can become transiently strongly coupled. These lead to features and non-gaussianity in the spectrum of primordial perturbations that would not be inferred from the naive EFT. Careful integration of the heavy fields recovers the general low energy effective field theory of inflation including a variable speed of sound for the adiabatic perturbations [98–101, 107, 176]. These interactions are unavoidable whenever the potential "valley" provided by the multi-field potential deviates from a geodesic of the multi-field sigma model metric. A corollary from the point of view of inflationary model building is that, when it comes to precision cosmology, the field space geometry of the "spectator" heavy fields (that are supposed to sit at their adiabatic minima during slow-roll inflation) is as important as their masses and couplings inferred from the potential alone.

Among the many scalars in a supersymmetric theory, the sgoldstino field stands out. The sgoldstino is the scalar partner of the goldstino, and belongs to the chiral superfield whose non-zero F-term breaks supersymmetry. It has the special property [82, 102, 177] that it decouples from all other fields in the theory. More precisely, setting all other superfields at the minimum of their potential is a consistent truncation from the $\mathcal{N} = 1$ supergravity multi-field parent theory to an effective $\mathcal{N} = 1$ supergravity with a single chiral superfield, the sgoldstino. In particular, the (real, two-dimensional) sgoldstino plane is a geodesically generated surface of the Kähler metric in the parent theory, so there are no derivative interactions with the truncated heavy fields: all turns in the inflationary trajectory are entirely confined to the sgoldstino plane. The effects of the fluctuations of the heavy fields are suppressed by their mass squared exactly as one would expect from an EFT expansion. This makes the sgoldstino an ideal inflaton candidate, for it allows for a description of inflation in terms of

a single complex field. From the point of view of inflationary modeling this is still multi-field inflation (with two real fields), but this two-field model is not a toy model, it really is the correct effective description for the full multi-field system.

If inflation is effectively driven by a single real scalar field, the inflaton, this can be identified with a suitable linear combination of the real and imaginary parts of the sgoldstino field. Meanwhile, the orthogonal combination is to remain stabilized at a local minimum of the potential during inflation. The effect of turns in the trajectory on the spectrum of primordial perturbations have to be taken into account when comparing to observations, but at least they can be calculated from the two-field model (see [93–95, 103, 178] and references therein).

Needless to say, this does not mean that all other scalars in the theory (from the supersymmetry-preserving superfields) can be completely neglected, as they have to be stabilised in a minimum of the potential during inflation. Even though the sgoldstino decouples from these fields, vice versa this is not true: the masses and couplings of all other fields generically depend on the field value of the sgoldstino field. As during inflation the sgoldstino evolves along its inflationary trajectory, the masses of the scalars change. If the inflaton is the sgoldstino, they will remain at the critical points, but they may become light or even tachyonic, triggering a waterfall-type exit from inflation that is not seen in the two-field model, and that most likely would ruin inflation. Although it is still a complicated task to determine the minimum of the multi-field potential along the inflationary trajectory, it is much simpler than the full multi-field *dynamics* needed for a generic inflationary model in supergravity.

The potential energy density driving inflation breaks supersymmetry spontaneously [179, 180]. This source of supersymmetry breaking in the inflaton sector is always present during inflation, and is in principle independent of the source of vacuum supersymmetry breaking. For sgoldstino inflation there are two possibilities. First, the same superfield that drives inflation is also responsible for low energy supersymmetry breaking[1]. This would be the ideal situation. Not only does inflation decouple from all other fields in the theory, it also links the scale of inflation to the scale of supersymmetry breaking. The second possibility is that the two sources of supersymmetry breaking are due to different fields. Both sources may be operative during inflation, or alternatively, it may be that only after inflation has ended, a phase transition takes place generating our present-day supersymmetry breaking. In both cases the present day sgoldstino field is not the sgoldstino during inflation.

The decoupling of the sgoldstino from the other fields fits in with recent

[1] This possibility has been discussed in [181–183] but as we will show it is difficult to implement in practice.

work on how to incorporate different fields, or sets of fields, in a supergravity set-up minimizing the coupling between them [82–85, 184–191]. Quite commonly different sectors – e.g. the fields and couplings responsible for supersymmetry breaking, for inflation, for moduli stabilisation, or making up the standard model – are combined by simply adding their respective Kähler- and superpotentials. However, following this procedure one cannot completely decouple these sectors. Even if the Kähler and superpotential do not contain direct interaction terms between fields in different sectors, the resulting scalar potential does. There are always at least Planck-suppressed interactions between the fields, and generically the mass matrix is not block diagonal in the different sectors. This complicates the analysis of the full model enormously. Sectors are affected by the presence of others, and although they work in isolation, they may no longer do so in the full set-up. Moreover, heavy fields generically cannot be integrated out in a consistent supersymmetric way.

The cross-couplings between sectors can be minimised if instead of adding Kähler and superpotentials, one adds the Kähler invariant functions $G = K + \ln|W|^2$ for the two sectors [83, 192]. This approach allows to integrate out fields in a supersymmetry preserving way [82]. In Ref. [83] the addition of Kähler functions was used to couple a supersymmetry breaking moduli sector (fields X^i) to a supersymmetry preserving sector, for example the standard model (fields z_i):

$$G^{\rm tot}(X^i, \bar{X}^{\bar{i}}, z_i, \bar{z}_{\bar{i}}) = g(X^i, \bar{X}^{\bar{i}}) + G^{\rm other}(z_i, \bar{z}_{\bar{i}}). \tag{4.1.1}$$

In this work we use the same idea to couple a supersymmetry breaking inflationary sector (fields X^i) to a supersymmetry preserving sector (z_k)[2]. For simplicity we restrict to effectively single field inflation, and models with a single inflaton field X. As supersymmetry is broken during inflation, the inflaton is then the sgoldstino. As it turns out, the ansatz (4.1.1) is actually too strict. We can allow for explicit couplings between the inflaton and the other fields, of the form

$$G(X, \bar{X}, z_k, \bar{z}_{\bar{k}}) = g(X, \bar{X}) + \frac{1}{2}\sum_{i\geq j}\Big[(z_i - (z_i)_0)(z_j - (z_j)_0) f^{(ij)}(X, \bar{X}, z_k, \bar{z}_{\bar{k}}) \\ + (z_i - (z_i)_0)(\bar{z}_{\bar{j}} - (\bar{z}_{\bar{j}})_0) h^{(ij)}(X, \bar{X}, z_k, \bar{z}_{\bar{k}}) + \text{h.c.}\Big] \tag{4.1.2}$$

with f, h arbitrary functions of their arguments. This is the most general ansatz consistent with X being the sgoldstino. The explicit X-dependence in the second term does not spoil the decoupling of the inflaton field, because the mass matrix remains block diagonal in the two sectors as long as the fields z_i sit at the supersymmetric critical point $(z_i)_0$ during inflation (recall section 1.4.2). As we will show, during sgoldstino inflation the Kähler function G is well defined,

[2] In [193] the separable form (4.1.1) was used to combine hybrid inflation with a supersymmetry breaking moduli sector in a successful way. In this set-up the inflaton is not the sgoldstino.

i.e. the superpotential is non-zero, maybe except from isolated points in field space.

Single field inflation can be divided into three main classes: large field, small field and hybrid inflation. We discuss whether and how sgoldstino inflation might work in these three regimes. Any supergravity model of inflation has to address the η-problem, as explained in section 1.4.1; this puts bounds on the Kähler geometry [194–196], since the spectator sector must remain stabilised in order to keep inflation going. As a summary of our findings, we find for these three different regimes the following:

- Large field sgoldstino inflation does not work, at least not for potentials that grow at most polynomial.
- Hybrid inflation provides the most natural embedding for sgoldstino inflation. Indeed, usual F-term hybrid inflation is an example of having a sgoldstino inflaton. In this set-up supersymmetry is restored in the vacuum, and there is no relation with low energy supersymmetry breaking. More complicated waterfall regimes may be devised, such that supersymmetry is broken in the minimum after inflation. However, such an analysis is multi-field, and complicated multi-field dynamics enters via the back door again.
- Small field inflation offers the best possibility to link inflation to supersymmetry breaking. Naively all that is needed is finding and tuning a saddle or maximum in a single field potential with a supersymmetry breaking Minkowski minimum. We only find inflection points suitable for inflation rather than a maximum or saddle point. Inflection point inflation yields [197, 198] a low spectral index $n_s \leq 0.92 - 0.93$ (for $N = 50 - 60$ efolds), which is ruled out by the CMB data, cf. eq. (1.2.22). However, in principle one may add non-canonical kinetic terms to alter this prediction, at the cost of tuning more coefficients. Interestingly enough, models in which supersymmetry is broken after inflation are much easier to embed in a multi-field set-up than models with a supersymmetry preserving vacuum. Finally, we comment on some claims in the literature for small field sgoldstino inflation [182, 183, 199] with no or very little fine-tuning. We will explain why these models cannot work.

Summarising, in this work we provide a systematic approach in which the additional sector of fields is consistently truncated in a supersymmetric way, and we provide working examples which illustrate the fact that fine-tuning is necessary in generic supergravity models in order to achieve successful inflation. As emphasised along this manuscript, it is of great importance to provide mechanisms that explain the consistent truncation of additional non-inflating degrees of freedom, especially in high-energy theories where their presence is inevitable. Additionally, the requirement of stabilisation imposes further constraints in the parent supergravity, which will be generalised in the next chapter.

4.2 Decoupling of the sgoldstino

In this section we show the decoupling of the sgoldstino field explicitly. In the first subsection we derive the mass matrix, which is block diagonal along the sgoldstino inflation trajectory. We will argue in subsection 4.2.2 that the Kähler function for a dynamical sgoldstino field can always be put in the form (4.1.2). In subsection 4.2.3 we show that this sgoldstino trajectory is independent of the field values of all the other fields. Vice versa that is not the case: the dynamics of the supersymmetry-preserving fields does depend on the sgoldstino field. Care must be taken so that these fields remain stabilised along the full inflationary trajectory. Finally, in subsection 4.2.4 we discuss the special limit of separable Kähler functions (4.1.1), which is a non-generic type of coupling, where the results of [83] are retrieved. In the next chapter we will discuss physical frameworks for which quasi-separable Kähler functions naturally arise.

4.2.1 Mass matrix

We start with the general formula for the mass matrix, then specialise to sgoldstino inflation. For the sake of clarity, we will repeat some of the formulas and statements established in section 1.4, where the basic notation is outlined, and refer to the reader to that section for conventions, and to appendix A for a translation of quantities in terms of G to quantities in terms of K and W. The scalar potential can be expressed solely in terms of the Kähler function[3] $G = K + \ln|W|^2$:

$$V_F = e^G[G_I G^{I\bar{J}} G_{\bar{J}} - 3], \tag{4.2.1}$$

with I, J running over all fields Φ_I. The mass matrix is given by

$$\mathcal{M} = \begin{pmatrix} M^I_J & M^I_{\bar{J}} \\ M^{\bar{I}}_J & M^{\bar{I}}_{\bar{J}} \end{pmatrix}, \qquad M^I_J = G^{I\bar{K}}\nabla_{\bar{K}}\nabla_J V, \quad M^I_{\bar{J}} = G^{I\bar{K}}\nabla_{\bar{K}}\nabla_{\bar{J}} V, \tag{4.2.2}$$

where $\nabla_K v_L = \partial_K v_L - \Gamma^M_{KL} v_M$ is the covariant derivative of some vector v_L. The eigenvalues and eigenvectors of the mass matrix correspond to the m^2–values and mass eigenstates respectively. The first derivative of the potential is

$$V_K = G_K V + \mathrm{e}^G[G^I \nabla_K G_I + G_K] \tag{4.2.3}$$

where we used metric compatibility $\nabla_K G_{I\bar{J}} = 0$, $\nabla_K G^I = \delta^I_K$ and introduced the notation $V_K = \partial_K V$, $G^I = G^{I\bar{J}} G_{\bar{J}}$. Stationarity is not assumed, as the inflaton field is displaced from its minimum during inflation. The second derivatives of

[3] This procedure is ill defined for $W = 0$. To cure this, one can use the variable $\phi \equiv \mathrm{e}^G$ instead, which remains well defined [200]. However, in the next section we show that $W = 0$ at most in isolated points in field space.

the potential are

$$\begin{aligned}\nabla_{\bar{L}}\nabla_K V &= (G_{K\bar{L}} - G_K G_{\bar{L}})V + 2G_{(K}V_{\bar{L})} \\ &\quad + \mathrm{e}^G[G^{I\bar{J}}(\nabla_{\bar{L}}G_{\bar{J}})(\nabla_K G_I) - R_{I\bar{J}K\bar{L}}G^I G^{\bar{J}} + G_{K\bar{L}}] \ , \\ \nabla_L\nabla_K V &= (\nabla_{(L}G_{K)} - G_{(K}G_{L)})V + 2G_{(K}V_{L)} + \mathrm{e}^G[2\nabla_{(K}G_{L)} + G^I\nabla_{(L}\nabla_{K)}G_I] \ ,\end{aligned} \tag{4.2.4}$$

where round brackets denote symmetrisation. We used that $[\nabla_{\bar{L}}, \nabla_K]G_I = \nabla_{\bar{L}}\nabla_K G_I = -R_{K\bar{L}I\bar{J}}G^{\bar{J}}$.

Now consider F-term breaking of supersymmetry, signalled by a non-zero $G_X \neq 0$. Here X is the scalar component of the chiral superfield which also contains the goldstino. Note that one can always make a field redefinition such that only one linear combination of fields breaks supersymmetry. All other fields in the theory, denoted by z_i (indexed by lower case latin letters), do not break supersymmetry. Hence, we split the fields in $\Phi_I = \{X, z_i\}$, with

$$G_X|_{z_0} \neq 0, \qquad G_i|_{z_0} = 0 \tag{4.2.5}$$

at some point in field space $z_0 = \{(z_1)_0, (z_2)_0, ...\}$, the so-called supersymmetric critical point.

We are interested in a cosmological situation, in which $X(t)$ is the inflaton rolling along some trajectory with $V_X \neq 0$. While the inflaton rolls in the X-direction, we want all orthogonal fields z_i to remain extremised at z_0. To that end we demand that

$$(\partial_X)^m (\partial_{\bar{X}})^n G_i|_{z_0} = 0, \qquad \forall m, n \in \mathbb{N}. \tag{4.2.6}$$

Indeed, from (4.2.3), we then have that

$$V_i|_{z_0} = G_i V + \mathrm{e}^G[G^P\nabla_i G_P + G_i] = \mathrm{e}^G G^X \nabla_i G_X = 0. \tag{4.2.7}$$

For notational convenience we dropped the $|_{z_0}$ on the right hand side, but the reader should keep in mind that all expressions should be evaluated at $z = z_0$.

Thus $z_i = (z_i)_0$ is an extremum of the potential. To see whether this is a maximum, minimum or saddle point, we must calculate the eigenvalues of the mass matrix, which need to be positive definite for a stable minimum. This analysis is simplified because (4.2.5) assures the mass matrix is in block diagonal form, i.e. $M_i^X|_{z_0} = M_i^{\bar{X}}|_{z_0} = 0$. To prove this last statement, it is enough to show the block diagonal form of the second covariant derivatives, as it follows from (4.2.6) that the field metric $G_{I\bar{J}}|_{z_0}$ is block diagonal as well. The first equation in (4.2.4) gives for mixed indices

$$\begin{aligned}\nabla_{\bar{i}}\nabla_X V|_{z_0} &= (G_{X\bar{i}} - G_X G_{\bar{i}})V + 2G_{(X}V_{\bar{i})} \\ &\quad + \mathrm{e}^G[G^{K\bar{L}}(\nabla_{\bar{i}}G_{\bar{L}})(\nabla_X G_K) - R_{K\bar{L}X\bar{i}}G^K G^{\bar{L}} + G_{X\bar{i}}] \\ &= -\mathrm{e}^G G^X G^{\bar{X}} R_{X\bar{X}X\bar{i}} = 0 \ .\end{aligned} \tag{4.2.8}$$

In the first step we used (4.2.5, 4.2.6) and that $\nabla_i G_X|_{z_0} = \nabla_X G_i|_{z_0} = 0$; in the second step that $R_{X\bar{X}X\bar{i}}|_{z_0} = G_{j\bar{i}}\partial_{\bar{X}}\Gamma^j_{XX} = 0$ as well, which also follows from (4.2.6). The second equation in (4.2.4) likewise vanishes for mixed indices:

$$\nabla_i\nabla_X V|_{z_0} = (\nabla_{(i}G_{X)} - G_{(X}G_{i)})V + 2G_{(X}V_{i)} + \mathrm{e}^G[2\nabla_{(X}G_{i)} + G^K\nabla_{(i}\nabla_{X)}G_K] = 0. \tag{4.2.9}$$

4.2.2 Kähler invariant function for sgoldstino inflation

Let us quickly comment on our use of the Kähler function $G = K + \ln|W|^2$, rather than expressing results in terms of the Kähler potential and superpotential. The potential danger in using G is that it becomes undefined when $W = 0$. However, it is easy to show that for sgoldstino inflation we nowhere have $W = 0$, except maybe for isolated points in field space. Therefore the Kähler function G is well defined. To illustrate this, consider a theory with two chiral fields – the extension to many fields is straightforward – with a superpotential $W = W(X, Z)$. For sgoldstino inflation, with X the goldstino superfield, we have

$$D_X W|_{\{X(t),Z_0\}} \neq 0, \qquad D_Z W|_{\{X(t),Z_0\}} = 0, \tag{4.2.10}$$

with $D_X W = K_X W + W_X$ the Kähler covariant derivative. Setting $W = 0$ along the *whole* trajectory implies

$$W|_{\{X(t),Z_0\}} = 0 \quad \Rightarrow \quad W_X|_{\{X(t),Z_0\}} = 0 \quad \Rightarrow \quad D_X W|_{\{X(t),Z_0\}} = 0 \tag{4.2.11}$$

in contradiction with (4.2.10). Therefore the superpotential can only vanish for sgoldstino inflation at accidental zeroes at isolated points in field space (possibly on the trajectory, but this does not change our conclusions).

As a side remark, note that when the inflaton is identified with the Z field rather than the sgoldstino field X, as for example in the models of Ref. [86], it is possible to have $W = 0$, $D_X W|_{\{X_0,Z(t)\}} \neq 0$ and $D_Z W|_{\{X_0,Z(t)\}} = 0$ along the whole trajectory $\{X_0, Z(t)\}$, as already mentioned in section 1.4. In this case the Kähler invariant function is not well defined, and a description in terms of K and W is needed. Despite this, let us stress that the physical quantities, such as the scalar potential and its derivatives, are well defined in any case.

Expanding the Kähler function around the supersymmetry critical point $z^i = z^i_0$, the most general form for sgoldstino inflation – satisfying (4.2.5) and (4.2.6) – can be written as in eq. (4.1.2).

4.2.3 Inflationary trajectory

We have seen in subsection 4.2.1 that along the inflationary trajectory all supersymmetry preserving fields are extremised at $z^i = z^i_0$. Since the mass matrix

is block diagonal, we can determine the stability of the z_i extremum from the sub-block of $\mathcal{M}$ with z_i indices. It can easily be shown that the inflaton trajectory itself is independent of the field values of the other fields. Indeed, the potential along the inflationary trajectory only depends on the function $g(X, \bar{X})$ in (4.1.2), and is thus independent of the field values of all other fields. The height $V_0 \equiv V|_{z_0}$, slope and second derivatives of the inflaton potential are given by (4.2.1, 4.2.3, 4.2.4) with I, J only running over X and $G \to g$. For example we have

$$V_0 = \mathrm{e}^g \left[g_X g^{X\bar{X}} g_{\bar{X}} - 3 \right], \tag{4.2.12}$$

$$V_X|_{z_0} = g_X V_0 + \mathrm{e}^g \left[g^X \nabla_X g_X + g_X \right]. \tag{4.2.13}$$

In contrast, the mass matrix along the orthogonal directions does depend on the inflaton field value. We find

$$\begin{aligned} M^i_j|_{z_0} &= G^{i\bar{k}} \nabla_{\bar{k}} \nabla_j V \\ &= G^{i\bar{k}} \left[G_{j\bar{k}} V_0 + \mathrm{e}^G [G^{l\bar{m}} (\nabla_{\bar{k}} G_{\bar{m}})(\nabla_j G_l) - R_{X\bar{X}j\bar{k}} G^X G^{\bar{X}} + G_{j\bar{k}}] \right] \\ &= \mathrm{e}^g \left[\delta^i_j (b+1) + x^i_{\bar{m}} x^{\bar{m}}_j + w^i_j \right] \end{aligned} \tag{4.2.14}$$

and

$$\begin{aligned} M^{\bar{i}}_j|_{z_0} &= G^{\bar{i}k} \nabla_k \nabla_j V \\ &= G^{\bar{i}k} \left[\nabla_{(k} G_{j)} V_0 + \mathrm{e}^G [2 \nabla_{(j} G_{k)} + G^X \nabla_{(k} \nabla_{j)} G_X] \right] \\ &= \mathrm{e}^g \left[x^{\bar{i}}_j (b+2) + y^{\bar{i}}_j \right] . \end{aligned} \tag{4.2.15}$$

Here we introduced the notation

$$b = V_0 \mathrm{e}^{-g} = g_X g^X - 3 \tag{4.2.16}$$

$$x^{\bar{i}}_j = G^{\bar{i}k} \nabla_k G_j = G^{\bar{i}k} \nabla_j G_k \tag{4.2.17}$$

$$w^i_j = -G^{i\bar{k}} G^X G^{\bar{X}} R_{X\bar{X}j\bar{k}} \tag{4.2.18}$$

$$y^{\bar{i}}_j = G^{\bar{i}k} G^X \nabla_{(k} \nabla_{j)} G_X . \tag{4.2.19}$$

Note that $b = V_0/m^2_{3/2}$ gives the height of the potential in units of the gravitino mass. During slow-roll this is approximately $b \simeq 3H^2/m^2_{3/2}$.

The functions b, x, y, w can be expressed in terms of the functions f, g, h appearing in the Kähler function (4.1.2). In general, the constraint that the squared masses should be positive is complicated, but there is a situation in which it simplifies considerably. As discussed in the next section, if the Kähler function is separable [83, 84], the matrices y and w vanish and the constraint only involves the eigenvalues of the x matrix. The diagonalisation for separable and quasi-separable Kähler functions is performed in detail in appendix B.

4.2.4 Separable Kähler function

Let us consider a set-up with separable Kähler functions [83–85]:

$$G(X,\bar{X},z_i,\bar{z}_i) = g(X,\bar{X}) + \tilde{g}(z_i,\bar{z}_i), \tag{4.2.20}$$

For the separable Kähler function above (4.2.20) all mixed derivatives of G, such as G_{zzX}, cancel. With this simplification

$$b = g_X g^X - 3, \qquad x^{\bar{i}}_m = \tilde{g}^{\bar{i}k}\tilde{g}_{km}, \qquad y^{\bar{i}}_j = w^i_j = 0. \tag{4.2.21}$$

We now consider the case with only one z field, which turns $x^{\bar{i}}_j$ into a scalar. As one can always diagonalise the matrix x, this simplification precisely gives the result along one of the eigenvectors, and thus can be straightforwardly generalised to several z fields. We recover the system studied in [83][4]:

$$M^z_z|_{z_0} = \mathrm{e}^g[(b+1)+|x|^2], \qquad M^{\bar{z}}_z|_{z_0} = \mathrm{e}^g(b+2)x, \tag{4.2.22}$$

which has eigenvalues[5]

$$m^2_\pm|_{z_0} = \mathrm{e}^g\left[1+b+|x|^2 \pm |(2+b)x|\right] = \mathrm{e}^g\left[\left(|x| \pm \frac{1}{2}|b+2|\right)^2 - \frac{b^2}{4}\right]. \tag{4.2.23}$$

The function b is bigger, equal or smaller than zero for a dS, Minkowksi or AdS universe, respectively. Take $b \geq 0$; in the opposite limit the masses m^2_- and m^2_+ are exchanged. The smallest mass eigenstate is positive $m^2_- > 0$, i.e., the z-field is stabilized along the inflationary trajectory, for $|x| < 1$ or $|x| > (1+b)$. We will put this analysis in practice for sgoldstino inflation in subsection 4.3.2 (hybrid inflation) and 4.3.3 (small field inflation).

Close to the instability bounds $|x| \lessapprox 1$ or $|x| \gtrapprox (1+b)$ the spectator field z is lighter than the Hubble scale, and cannot be integrated out. In a Minkowski vacuum after inflation either $b = 0$ or $b \to \infty$; the latter case may occur in a supersymmetric vacuum with $W \to 0$. For $b = 0$, the masses reduce to $m^2_\pm = m^2_{3/2}\left(1 \pm |x|\right)^2$, with $m_{3/2}$ the gravitino mass. For $|x| > 1$, the lightest scalars from the supersymmetric sector are heavier than the gravitino. However, for $|x| < 1$ the lightest of the two eigenstates is lighter than the gravitino and cannot be neglected from a low–energy description. This will play an important role later. In the supersymmetric vacuum with $b \to \infty$ we find $m^2_\pm \approx V_0(1 \pm |x|) \to 0$, and the spectators are massless. To avoid a plethora of massless fields in the theory, one has to either break the supersymmetry, or else go beyond the simple separable form of the Kähler function (4.2.20).

[4] The definition of b is different from [83], which has $b \leftrightarrow b-3$.

[5] See appendix B for further details.

4.3 Single field sgoldstino inflation

In this work we focus on effectively single field inflation models, for simplicity. The inflaton, a real scalar, is identified with a suitable linear combination of the real and imaginary parts of the sgoldstino field; the orthogonal combination is to remain stabilised at a local minimum of the potential during inflation. For the purpose of this chapter, we will not take into account the dynamics of the stabilised field, since the aim of this chapter is to show the restrictions on the parent supergravity, but for a complete and consistent description one should also take into account the dynamics of the stabilized field, as stressed along this thesis.

Single field inflation can be divided into three classes: small field, large field and hybrid inflation. In the first two cases, if the model only contains a single chiral superfield, the inflaton is automatically the sgoldstino. If several fields are present, as is the case for hybrid inflation, one has to be more careful, as the sgoldstino does not have to coincide with the inflaton direction.

As is well known any supergravity model of inflation has to address the η-problem [179, 201, 202], which has been explained in section 1.4.1, together with its possible solutions. In the remainder of this section we will discuss large field, small field and hybrid sgoldstino inflation, and how the η-problem may or may not be addressed in each case.

4.3.1 Large field inflation

In models of large field inflation [203], the inflaton field traverses super-Planckian distances in field space during inflation. For a potential dominated by a single monomial during inflation, $V \sim \lambda\phi^n$, the slow roll parameters

$$\epsilon = \frac{1}{2}\left(\frac{V_\phi}{V}\right)^2, \qquad \eta = \frac{V_{\phi\phi}}{V}, \tag{4.3.1}$$

both scale as $\eta, \epsilon \sim 1/\phi^2$, and are automatically suppressed for super-planckian field values. At first sight, no tuning of the potential is needed. However, the problem is that for such large field values *all* non-renormalisable operators are unsuppressed. Therefore, an explicit UV completion of the model is needed to determine whether inflation is possible.

Embedding large field inflation in supergravity provides a better control over the UV behavior of the theory. Because of the η-problem such an embedding is far from straightforward, as the potential grows exponentially rather than polynomial. Fine-tuning η is not an option, as η has to be small along the whole inflationary trajectory, which spans super-Planckian distances in field space $\Delta\phi > 1$ (in

Planck units). This is in contrast with small field inflation, discussed in subsection 4.3.3, where the η-problem can be solved by tuning η at a single point in field space.

Instead of fine-tuning, we can try to solve the η-problem by invoking a shift symmetry [80]. Consider a Kähler function $G = \mathcal{K}(X - \bar{X})$, which is symmetric under a shift $X \to X + c$ with c a real constant. Since G does not depend explicitly on $\phi \propto \mathrm{Re}(X)$, the exponent in the scalar potential is independent of ϕ and there is no η-problem. However, since we need a slope for the potential in order to obtain inflation, the shift symmetry needs to be weakly broken. To assure the breaking does not reintroduce exponential terms that ruin inflation, we add a logarithmic term $G = \mathcal{K}(X - \bar{X}) + \ln |W(X)|^2$ with W not growing faster than power law. Let us, for instance, consider a canonical Kähler potential[6] with a shift symmetry and a polynomial superpotential:

$$K = \frac{1}{2}\left(\phi + \bar{\phi}\right)^2 \ , \ W = \sum_n \lambda_n \phi^n \tag{4.3.2}$$

Let us assume that the real part of the field $\alpha = (\phi + \bar{\phi})/2$ is stabilised at the critical point $\alpha = 0$. The scalar potential and the potential slow-roll parameters for the imaginary part $\beta = (\phi - \bar{\phi})/2i$ are the following:

$$V(\beta) = \sum_n |\lambda_n|^2 \beta^{2n} \left(\frac{n^2}{\beta^2} - 3\right) \ , \tag{4.3.3}$$

$$\epsilon_V = \frac{2}{\beta^2} \frac{\sum_{n,m} n\, m |\lambda_n|^2 |\lambda_m|^2 \beta^{2(n+m)} \left[\frac{n(n-1)}{\beta^2} - 3\right] \left[\frac{m(m-1)}{\beta^2} - 3\right]}{\sum_{n,m} |\lambda_n|^2 |\lambda_m|^2 \beta^{2(n+m)} \left(\frac{n^2}{\beta^2} - 3\right) \left(\frac{m^2}{\beta^2} - 3\right)} \ , \tag{4.3.4}$$

$$\eta_V = \frac{2}{\beta^2} \frac{\sum_n n |\lambda_n|^2 \beta^{2n} \left[\frac{n(2n-3)(n-1)}{\beta^2} - 3(2n-1)\right]}{\sum_n |\lambda_n|^2 \beta^{2n} \left(\frac{n^2}{\beta^2} - 3\right)} \ . \tag{4.3.5}$$

We now distinguish two situations:

- If all the coefficients λ_n are of the same order, the highest monomial will dominate for values of the field $\beta > M_{\mathrm{P}}$. Given this, we must require that $n^2 > 3\beta^2$ along the whole trajectory in view of eq. (4.3.3), so $n \gg 1$ in any case. The slow-roll parameters are approximately given by:

$$\epsilon_V \approx \frac{2n^2}{\beta^2} > 6 \ , \ \eta_V \approx \frac{4n^2}{\beta^2} > 12 \tag{4.3.6}$$

  Clearly we cannot achieve inflation in this situation.

[6] Generalising to non-canonical terms is straightforward, since along the inflaton trajectory these become constant and can therefore be absorbed in a redefinition of the fields.

- If we tune the coefficients such that all the terms are equally important in the large field regime, we need:

$$|\lambda_0| \gg |\lambda_1| \gg \cdots \gg |\lambda_n| \tag{4.3.7}$$

At the same time, the highest monomials must cancel the negative contributions to the scalar potential coming from the lowest monomials, that is:

$$|\lambda_{n-p}|^2 \geq \frac{|\lambda_p|^2}{\beta^{2(n-2p)}} \left| \frac{p^2 - 3\beta^2}{(n-p)^2 - 3\beta^2} \right| \ , \ p < n/2 \tag{4.3.8}$$

As argued before, fine-tuning along the whole (large field) trajectory is not a viable option.

Although we did the analysis for a single field, this straightforwardly generalises to the multi-field case. If the inflaton is the sgoldstino, it decouples from the other fields, and its potential can be analysed independently and will always be of the form (4.3.3). We conclude that large field sgoldstino inflation in a supergravity model does not work as it is plagued by an instability in the scalar potential.

We note that it is certainly not impossible to have large field inflation in supergravity, only that it does not work with a single chiral superfield. Two-field models have been constructed that avoid the instability [80, 86], employing a shift symmetry to address the η-problem. However, in these models the inflaton is *not* the sgoldstino (rather the sgoldstino is the orthogonal field).

4.3.2 Hybrid inflation

Hybrid inflation is a multi-field model of inflation which in addition to the inflaton contains one or more so-called waterfall fields, which serve to end inflation [204]. During inflation the waterfall fields are stabilised in a local minimum, and inflation is effectively single field. If the inflaton field drops below a critical value, one of the waterfall fields becomes tachyonic, and inflation ends with a phase transition.

Standard F-term hybrid inflation [205, 206] is an example of sgoldstino inflation. The Kähler function is of the separable form (4.2.20) discussed in section 4.2.4.

$$G = g(X, \bar{X}) + \tilde{g}(\chi_1, \bar{\chi}_1, \chi_2, \bar{\chi}_2), \tag{4.3.9}$$

with[7]

$$g = X\bar{X} + k_s(X\bar{X})^2 + \ln|\kappa X|^2 + ..., \qquad \tilde{g} = \chi_1\bar{\chi}_1 + \chi_2\bar{\chi}_2 + \ln|\chi_1\chi_2 - \mu^2|^2 + ...$$

[7] To see that this setup is indeed of the general form (4.1.2), one can move a factor of $\ln|\mu^2|^2$ from $\tilde{g}$ to g and Taylor expand the remaining $\ln|\frac{\chi_1\chi_2}{\mu^2} - 1|^2$.

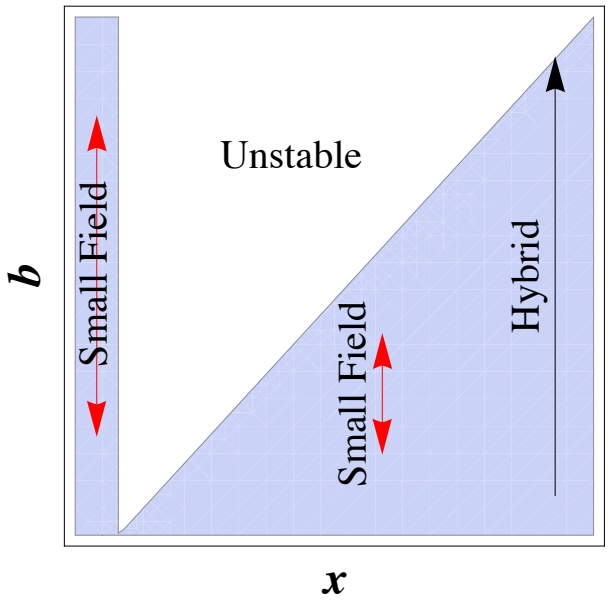

Figure 4.1 *– (Figure adapted from [83, 85].) Stability diagram for the separable case $G = g(X, \bar{X}) + \tilde{g}(z, \bar{z})$. The variables on the axes b, x are defined in (4.2.21), with x one of the eigenvalues of the $x^{\bar{i}}_{j}$ matrix. The masses of the spectator fields are positive in the shaded region, while the unstable region signals a tachyonic mode. The black arrow represents the inflationary trajectory for the proposed hybrid set-up, which ends when one of the spectator fields (the waterfall fields) becomes tachyonic. Also shown are possible inflationary trajectories for small field inflation (red arrows).*

The inflaton ϕ is identified with the real direction via the decomposition $X = (\phi + i\theta)/\sqrt{2}$. Inflation takes place for large $\phi > \phi_c = \sqrt{2}\mu$, and all other fields stabilised at zero field value. The potential along the inflationary trajectory is

$$V = \kappa^2 \mu^4 \left(1 - 2k_s \phi^2 + ...\right) \tag{4.3.10}$$

The η-problem is solved via a moderate fine-tuning of $k_s \lesssim 10^{-2}$. During inflation $G_X = \frac{\sqrt{2}}{\phi} + \frac{\phi}{\sqrt{2}} + \frac{k_s \phi^3}{\sqrt{2}}$ and $G_{\chi_1} = G_{\chi_2} = 0$. Hence ϕ is indeed the (real part of the) sgoldstino field. The Minkowski minimum after inflation is at $X = 0$, and $|\chi_1| = |\chi_2| = \mu$. In the minimum $G_X = G_{\chi_\pm} = 0$ and supersymmetry is restored, and therefore there is no relation between inflation and low energy supersymmetry breaking.

The masses of waterfall fields along the inflationary trajectory can be found using the results of section 4.2.4. The mass eigenstates are the linear combinations $\chi_\pm = (\chi_1 \pm \chi_2)/\sqrt{2}$. Using these as a basis the matrix $x^{\tilde{i}}_{m}$ becomes

diagonal during inflation. This shows that we can restrict our attention to only one of the complex fields $\chi_\pm$, the other field will give the same masses for its two real degrees of freedom. Now we can directly compute the masses from (4.2.23). The stability region as a function of b and $|x|$ is plotted in Fig 4.1. The inflationary trajectory corresponds to a vertical trajectory in the plot, going upwards as the field rolls down. When it irrevocably hits the instability region (i.e. when the lower mass eigenvalue becomes negative), inflation ends.

We note that a similar stability analysis can be done for all models of sgoldstino inflation. Whereas hybrid inflation critically makes use of the instability regions, for any non-hybrid scenario — being it small or large field inflation — the inflationary trajectory would have to stop before reaching the instability region. This is automatic for $|x| < 1$, otherwise the stability conditions place an upper bound on b during inflation. We will return to this point shortly when discussing small field inflation.

4.3.3 Small field inflation

Inflation in small field models [9, 10] takes place for sub-Planckian values of the inflaton field. This allows for a Taylor expansion of the inflaton potential around its Minkowski minimum. If one term in the polynomial expansion dominates during inflation, the slow roll parameters blow up: $\epsilon, \eta \sim 1/\phi^2$ in the small field limit, prohibiting inflation. The only way to get around this conclusion is that several terms in the expansion conspire together to nearly cancel, thus obtaining small slow-roll parameters.

This motivates to consider inflation near an extremum – a maximum, saddle point or inflection point – of the potential. This assures that the first slow roll parameter ϵ vanishes. The η-parameter can be made small by tuning the parameters in the potential. Since the inflaton field traverses only small, sub-Planckian distances in field space, tuning the curvature of the potential at a single point (the extremum) suffices, in contrast with large field inflation.

We were able to construct a fine-tuned small field inflation model in supergravity containing only a single chiral field. In such a set-up the inflaton is automatically the sgoldstino, and our example is proof of principle for small field sgoldstino inflation. Consider a model with[8]

$$K = \sum_n \alpha_n (X\bar{X})^n, \qquad W = \sum_n \lambda_n X^n. \tag{4.3.11}$$

We decompose the complex scalar $X = (\phi + i\theta)/\sqrt{2}$ with ϕ the inflaton field. The model parameters λ_n, α_n can be tuned in such a way that the potential

[8] This ansatz (4.3.11) is equivalent to $G = \sum_{n=1} \alpha_n (X\bar{X})^n + \log|\sum_{n=0} \lambda_n X^n|^2$.

allows for inflation near an inflection point which, without loss of generality, is located at the origin $(\phi, \theta) = (0, 0)$, and a Minkowski minimum at finite field value $(\phi, \theta) = (\phi_0, 0)$. In particular, we demand

- Vanishing slope and curvature of the potential at the origin 1) $V_\phi|_{(0,0)} = 0$ and 2) $V_{\phi\phi}|_{(0,0)} = 0$.
- The height 3) $V|_{(0,0)} \equiv V_0$ of the potential at the origin is fixed by the normalisation of the power spectrum given by the data.
- After inflation the inflaton settles in a local Minkowski minimum with 4) $V|_{(\phi_0,0)} = 0$ and 5) $V_\phi|_{(\phi_0,0)} = 0$. Moreover, the masses are positive definite 6) $m_i^2|_{(\phi_0,0)} > 0$.
- Along the whole trajectory, from the extremum to the minimum, the orthogonal field is stabilized 7) $V_\theta = V_{\phi\theta} = 0$ and 8) $m_\theta^2 \gtrsim H^2$.

We consider solutions with canonical kinetic terms, i.e. we set $\alpha_1 = 1$ and $\alpha_i = 0$ for $i \neq 1$. To satisfy conditions 1-5 we need at least five parameters and choose them accordingly. We take all λ_i real, and consider the first five in the expansion. Tuning is required to satisfy conditions (2) and (4) — the smallness of η parameter and of the cosmological constant — in the usual sense that large contributions should nearly cancel. Conditions 6-8 are then checked for consistency, but do not require any new input. Setting the minimum at $\phi_0 = 1$ we find two inflationary inflection point solutions[9]

$$\{\lambda_0, \lambda_1, \lambda_2, \lambda_3, \lambda_4\} = \sqrt{\frac{V_0}{23}} \times \{3, -5\sqrt{2}, 3, 0, 2\}, \tag{4.3.12}$$

and

$$\begin{aligned}\{\lambda_0, \lambda_1, \lambda_2, \lambda_3, \lambda_4\} = \frac{\sqrt{V_0}}{19\sqrt{73}} \times \\ \left\{3\sqrt{39287 - 1464\sqrt{6}}, \sqrt{2\left(543551 - 19764\sqrt{6}\right)}, \right. \\ \left. 3\sqrt{39287 - 1464\sqrt{6}}, 0, -2\sqrt{4943 - 1152\sqrt{6}}\right\},\end{aligned} \tag{4.3.13}$$

and all other λ_i are zero.

Both examples above correspond to inflection point inflation, rather than to inflation near a maximum or saddle point. This is unfortunate, as for inflection point inflation the spectral index is bounded to be $n_s \simeq 0.92$, which is ruled out. We review this argument in appendix C. However, the spectral index can

[9] $\lambda_3 = 0$ only vanishes for $\phi_0 = 1$, but is non-zero for other positions of the minima.

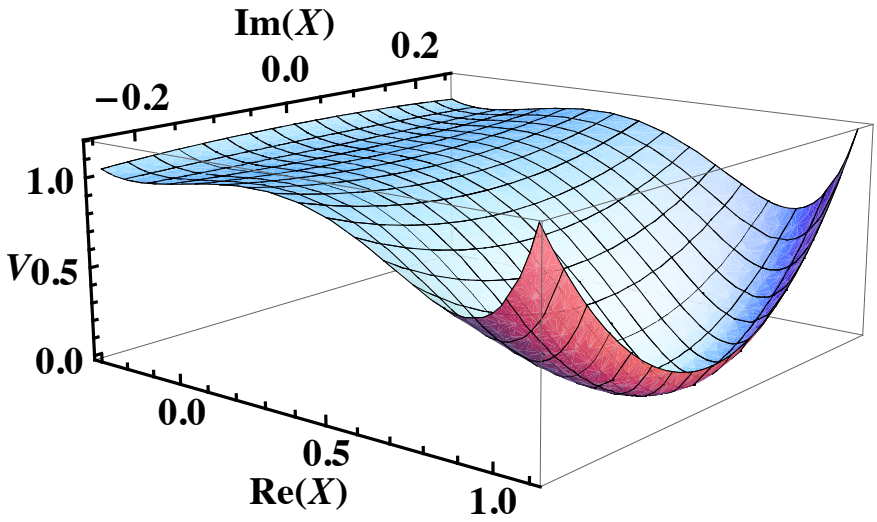

Figure 4.2 *– Scalar potential for small field inflation corresponding to the first solution (4.3.12).*

be larger if the cubic term is absent or unnaturally small, as is the case for inflation at a maximum rather than an inflection point. Then the correction to the spectral index (B.0.4) is set by the quartic term in the Taylor expansion around the extremum, rather than by cubic term, with an upper bound $n_s \lesssim 0.95$. In our set-up this would require an extra tuning condition $V_{\phi\phi\phi} \approx 0$; without it we always find a saddle point.

The first solution above (4.3.12) has a supersymmetric Minkowksi minimum. In this scenario the supersymmetry breaking observed today is not related to the supersymmetry breaking during inflation. The second solution (4.3.13), however, does end in a supersymmetry breaking minimum, and the gravitino mass today can be related to the inflationary scale. The gravitino mass is $m_{3/2} \sim 10^{-7}$ in Planck units, see appendix C.

There is a huge difference between the two solutions when combined with other spectator fields. The first solution has a supersymmetry preserving vacuum in which $W \to 0$. Although at this exact point our description in terms of a Kähler function G breaks down, we can nevertheless describe the behavior of

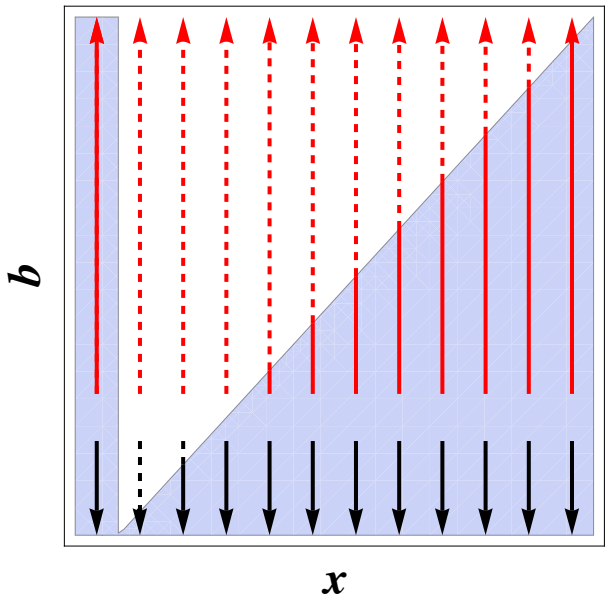

Figure 4.3 *– Stability plot of the spectator z-fields for a separable Kähler function $G = g(X, \bar{X}) + \tilde{g}(z, \bar{z})$. The trajectories for small field inflation are vertical lines, going upward (red) to infinity for solution (4.3.12) which has a supersymmetry preserving vacuum, and downward (black) to zero for (4.3.13) which has a supersymmetry breaking vacuum. Dashed lines indicate unstable trajectories. The position on the horizontal axis depends on the specifics of the spectator sector. Solution (4.3.12) always leads to an instability for $|x| > 1$.*

the potential as we approach this singular limit. We find that $b \propto V_0/W_0 \to \infty$, which implies that if we draw the stability diagram for the simplified case of separable Kähler functions (4.2.20), see Fig. 4.3, this inflationary model corresponds to vertical trajectories going upwards to infinity. The position on the horizontal axis given by $|x|$ depends on the specifics of the spectator sector, but it is clear that for all $|x| > 1$ one of the fields becomes tachyonic as the inflaton approaches its minimum, and the potential is unstable. Hence, solution (4.3.12) with a supersymmetry vacuum can only be combined with different fields if this extra sector has $|x| < 1$ (for several fields the eigenvalues of the $|x|^2$ matrix should all be less than unity, and in fact in chapter 5 we will consider the statistical properties of a truncated sector with a large number of fields). This puts enormous limitations on the spectator sector. For $|x| < 1$ the masses of the spectator fields vanish in the vacuum, as discussed at the end of section (4.2.4). However, in a subsequent supersymmetry breaking phase transition they may pick up a soft mass term. This disastrous conclusion may be avoided by taking more generic Kähler functions.

In contrast, solution (4.3.13) has a supersymmetry breaking vacuum, and the parameter $b = V_0/W = 0$ vanishes in the minimum. The inflaton trajectory again corresponds to a vertical trajectory in the stability diagram, but now going downwards. Except for a small region near $|x| = 1$ there are no instabilities in the potential, and at least for the separable Kähler function (4.2.20) sgoldstino inflation can straightforwardly be combined with a spectator sector. In the region $|x| > 1$ the spectator fields are heavy in the vacuum and can be integrated out to get a low energy EFT. In the other limit $|x| < 1$ the spectator fields are of the same order as the gravitino mass (see the discussion at the end of section 4.2.4), and are relatively light.

Other proposals for small field sgoldstino inflation

In the recent literature there have been claims for small field sgoldstino inflation, with no or very little fine-tuning of the parameters in the potential. As argued in this paper, unless some symmetry principle is invoked, this is not possible as the slow roll parameters generically blow up in the small field limit. Indeed we find that these proposals do not work, although the devil is sometimes in the details. I will describe one of the setups, which illustrates how to not deal with multi-field dynamics, and refer to our original paper [3] for further details.

Refs. [182, 183] propose a model of sgoldstino inflation in a single field set-up without tuning of parameters. To address the η problem they add a logarithmic term to the Kähler potential

$$\begin{aligned} K &= X\bar{X} + aX\bar{X}(X+\bar{X}) + b(X\bar{X})^2 + ... - 2\ln(1+X+\bar{X}), \\ W &= fX + f_n M. \end{aligned} \tag{4.3.14}$$

However, in the small field regime the logarithm can simply be expanded and does not alter the qualitative structure of the potential. It also does not enhance the symmetry.

Taking arbitrary parameters, except for the constraint that the minimum at the origin is stable and has zero cosmological constant, both the epsilon and eta-parameter exceed unity throughout the whole field space $|X| < 1$. Slow roll inflation cannot happen. In [182] it is actually claimed that $\epsilon < 1$, but what they calculate is $\epsilon_\theta = g^{\theta\theta}(V_\theta/V)^2$, where we again decomposed the field $X = (\phi + i\theta)/\sqrt{2}$ and g_{ij} is the metric in field space. However, in a situation where the potential falls much steeper in the ϕ-direction than in the θ-direction, this is not the relevant slow roll parameter. Instead, one should use the more general multi-field generalization $\epsilon = g^{ij}V_iV_j/V^2$.

Ref. [183] shows inflationary trajectories with a large number of efolds $N > 60$. However, their trajectories are calculated in the – non-applicable – slow roll approximation. For all initial points in field space proposed in [182, 183] we have solved the full two-dimensional field equations and the slow-roll approximations to them. In all cases the slow roll solutions wildly diverge from the full solutions, which can only give inflation for less than an e-fold, confirming once more that this setup does not provide a slow roll regime. The only way to get inflation in the set-up of [182, 183], in any case, is to tune parameters near an extremum, along the lines of our example (4.3.11).

4.4 Conclusions

Inflationary models in supergravity, where the inflaton sits in a complex scalar superfield, necessarily involve a multi-field analysis. Any extra fields present during inflation must be integrated out to give an effective single-field slow-roll dynamics that is consistent with the CMB. However, even very heavy fields can leave a detectable imprint in the spectrum of primordial perturbations, in particular through a reduction in the speed of sound of the adiabatic perturbations, as deeply explained along the previous chapters of this thesis. The correct effective field theory for the adiabatic mode has a variable speed of sound that depends on the background trajectory. A necessary condition to recover the standard single-field slow roll description is that the trajectory should have no turns into the heavy directions. In this case, the speed of sound is unity, equal to the speed of light, and integrating out the extra fields gives the same effective action as truncating the heavy fields at their adiabatic minima.

In supersymmetric models there is an extra complication. One has to integrate out whole supermultiplets in order to obtain an effective supergravity description for the remaining superfields. This is only possible if the superfields that are being integrated out are in configurations that do not contribute to supersymmetry breaking.

Sgoldstino inflation naturally implements these two conditions. The full inflationary dynamics is confined to the sgoldstino plane. Putting the scalar components of all other superfields at their minima is a consistent truncation of the parent theory. This makes sgoldstino inflationary models extremely attractive, because of their simplicity and robustness.

We have analysed sgoldstino inflation scenarios exploiting the fact that the Kähler function $G = K + \log|W|^2$ has a relatively simple separable form which allows some aspects to be analysed in a model-independent way. We derived a necessary and sufficient condition on the Kähler function for the stability of the supersymmetry-preserving sector, the spectator fields that are integrated out.

Figure 4.1 shows the constraint for a separable Kähler function, in particular for hybrid F-term inflation (which is a well studied case of sgoldstino inflation) and small field inflation.

In the case of small field sgoldstino inflation we were able to provide some viable fine-tuned examples around inflection points. The spectral index is rather low, but a higher spectral index would be possible with additional fine-tuning. Rather surprisingly, the inflationary model can only be straightforwardly combined with a spectator sector if the minimum after inflation breaks supersymmetry. In our inflation example with a supersymmetry preserving Minkowski vacuum the spectator sector is very constrained by the condition that there should be no tachyonic modes in the system. This is illustrated in figure 4.3.

Summarising, in this work we provide proof of principle for the viability of inflationary models where the supersymmetry breaking field is the inflaton. More importantly, the presence of an additional sector that preserves supersymmetry can be incorporated in the description if the decoupling and stability constraints are satisfied.

Here we restricted the analysis to inflationary dynamics and a separable Kähler function, but in the next chapter we extend the analysis to more general Kähler functions, and we derive constraints using the supersymmetric and non-supersymmetric directions, not only for the inflationary dynamics but also for a stationary vacuum. Moreover, we will give an example in which the quasi-separable (non-generic) structure of the Kähler function is naturally realised. In order to study systems with a large number is fields in the supersymmetric sector, we also use random matrix theory techniques to describe their statistics. This completes the picture of constraints on inflation in supergravity due to the presence of additional fields.

5

Perturbative stability along the supersymmetric directions of the landscape

In this chapter we generalise the study of the perturbative stability of non-supersymmetric configurations in $\mathcal{N} = 1$ supergravity models with a spectator sector not involved in supersymmetry breaking. Motivated by the supergravity description of complex structure moduli in Large Volume Compactifications of type IIB-superstrings, we concentrate on models where the interactions are consistent with the supersymmetric truncation of the spectator fields, and we describe their couplings by a random ensemble of generic supergravity theories. We characterise the mass spectrum of the spectator fields in terms of the statistical parameters of the ensemble and the geometry of the scalar manifold. Our results show that the non-generic couplings between the spectator and the supersymmetry breaking sectors can stabilise all the tachyons which typically appear in the spectator sector before including the supersymmetry breaking effects, and we find large regions of the parameter space where the supersymmetric sector remains stable with probability close to one. We discuss these results about the stability of the supersymmetric sector in two physically relevant situations: non-supersymmetric Minkowski vacua, and slow-roll inflation driven by the supersymmetry breaking sector. For the class of models we consider, we have reproduced the regimes in which the KKLT and Large Volume Scenarios stabilise all supersymmetric moduli. We have also identified a new regime in which the supersymmetric sector is stabilised at a very robust type of dS minimum without invoking a large mass hierarchy.

5.1 Introduction

In the last decade, many promising cosmological models have been derived in the framework of string theory and supergravity in order to understand the mechanisms responsible for the present acceleration of the universe, and for inflation. The construction of those models is far from trivial, in particular due to the fact that the supergravity description typically involves hundreds of scalar fields, *the moduli*. Any cosmological model requires a good understanding of the effective scalar potential along all directions in field space, since any tachyonic instability can easily spoil their predictions. Instead of performing an exhaustive analysis involving all the fields, one can characterise the properties of the effective potential following a statistical treatment [207–216].

One particular method to characterise the properties of the landscape is to study random ensembles of generic four dimensional $\mathcal{N} = 1$ supergravity theories with a large number of fields, $\mathrm{N} \gg 1$, where the couplings are treated as random variables [210–212, 217, 218]. This framework is known as *random supergravity*. Although a generic supergravity theory cannot capture the specific properties of the supergravity Lagrangians, these ensembles are expected to describe correctly the generic features of the landscape. In this framework it has been shown that the construction of viable cosmological models is very constrained. In particular, this method has been used to determine the probability of occurrence of dS minima of the scalar potential which could describe the present day accelerated expansion. It was proven in [211, 212] that, in the case of generic supergravity theories, only an exponentially small fraction of the total number of critical points are non-tachyonic, $P_{\min} \sim \mathrm{e}^{-\mathrm{N}^p}$, with p being a number of order one, and N the number of scalar fields of the supergravity theory. Similarly, the possibility of constructing viable models of inflation in the string landscape has also been considered in several works [217, 218], where it was argued that prolonged periods of inflation are very rare due to the large probability of encountering instabilities along the inflationary trajectory, and this favours small field inflationary models. The random supergravity approach is a powerful tool in those situations where there is very little information available about the effective low energy Lagrangian under study.

Interestingly enough, in the so-called *Large Volume Scenario* (LVS), numerical analyses of specific compactifications show that the probability that a de Sitter critical point of the potential is tachyon-free is rather close to unity [213–216]. This is already true when the number of fields is small, $\mathrm{N} \sim 5$, and the probability *increases* as the number of fields becomes larger [215]. This is in contrast with the results of the random supergravity approach.

The underlying reason for this apparent contradiction between the random supergravity approach and the analysis of the effective potential in LVS, is

the fact that the random supergravity approach does not take into account the structure of the effective supergravity Lagrangian, or in other words, the non-generic structure of the Kähler potential for this case. The main objective of the present work is to study a random supergravity theory which captures the essential features of the couplings in these theories. We will prove that taking into account very general properties of this type of Lagrangians, it is possible to reconcile the results of these two approaches regarding the existence of stable dS vacua, and indeed we find that for non-generic couplings that resemble LVS the probability of finding stable dS vacua is exponentially close to one. In addition, we will explore the predictions of this random supergravity theory regarding the stability of the supersymmetric sector during inflation.

The intuition that the different sectors of the theory — namely complex structure moduli/dilaton (supersymmetric) sector and the Kähler moduli (non-supersymmetric) sector — are decoupled from each other is a misconception of the standard two-step approach to moduli stabilisation and the construction of stable dS vacua [219–221]. The consistency of using a low energy effective action for the Kähler moduli obtained by the approximate supersymmetric truncation of the complex structure and dilaton fields has been extensively checked in the literature [184–187, 189, 222, 223]. However this does not imply that the two sectors are decoupled. As we have seen in the previous chapter, the masses of the truncated sector depend on the dynamical sector.

This point becomes very important when considering the stability of the supersymmetric sector. It is often assumed that, in order for these fields to remain non-tachyonic in the full model, it is necessary to stabilise them at a supersymmetric AdS minimum of the scalar potential before including the couplings to the non-supersymmetric sector and the supersymmetry breaking effects. In the present work we will prove that this is not necessarily the case. In particular, we will study the stability of non-supersymmetric configurations on generic supergravity theories including only chiral multiplets. For the proof it will be sufficient to consider the stability along the supersymmetry-preserving directions of field space. We will show that the condition that the supersymmetric sector must be stabilised at a minimum of the scalar potential before including supersymmetry breaking, is not sufficient in general to ensure the stability in of the full non-supersymmetric configuration, and moreover, we will argue that there are physically relevant situations, as in LVS, where this condition is not even necessary. As a consequence, stable non-supersymmetric configurations will correspond in general to saddle points, or even AdS maxima of the scalar potential in the supersymmetric limit, that is, before the spontaneous breaking of supersymmetry is included. This claim has been already confirmed by numerical analyses elsewhere [216].

Here we will analyse the stability of supersymmetric sectors in $\mathcal{N} = 1$

supergravity theories using the random supergravity techniques developed in [210–212]. Since it is not consistent to study a supersymmetric sector in isolation, that is, neglecting the remaining fields and the effects of supersymmetry breaking, we need to choose an appropriate framework to be able to implement the random supergravity approach. In particular, we will concentrate on supergravity models with couplings compatible with freezing one sector of the theory at a supersymmetric critical point of the potential, and in particular we will study models where the couplings are consistent with the *exact supersymmetric truncation* of a sector of the fields [177], as we did in the previous chapter. In a consistent supersymmetric truncation, the solutions to the equations of motion obtained after truncating the supersymmetric sector are also exact solutions to the equations of the full model, and moreover, supersymmetry is exactly preserved in the reduced theory.

We perform the stability analysis of the supersymmetric sector and derive a set of necessary conditions for the stability of non-supersymmetric configurations in $\mathcal{N}=1$ supergravity models with no gauge interactions. This set of constraints is complementary to the ones studied in [194, 195, 224–227], which ensure the stability of the scalar potential along the sGoldstino direction, that is, along the direction of supersymmetry breaking. In these works the necessary condition was translated into a constraint on the geometry of the Kähler manifold, which was expressed in terms of the *holomorphic sectional curvature* at the extremum, $S[X] \equiv -R_{X\bar{X}X\bar{X}}$, and of the square of the Hubble parameter measured in units of the gravitino mass[1], $\gamma = V/3m_{3/2}^2 \simeq H^2/m_{3/2}^2$:

$$S[X] \geq -\frac{2}{3}\frac{1}{1+\gamma}.$$

Here we will derive an analogous set of conditions which ensure the stability along the remaining directions orthogonal to the sGoldstino, or in other words, the supersymmetry-preserving directions. This set of constraints depends not only on the parameter γ and on the geometry of the Kähler manifold, but also on the spectrum of masses of the chiral fermions m_λ and on their derivatives along the sGoldstino direction $\partial m_\lambda/\partial X$. These constraints can be expressed as a bound on the curvature of the Kähler manifold at the extremum through the quantity $B[X,\lambda] = -R_{X\bar{X}\lambda\bar{\lambda}}$, known as the *holomorphic bisectional curvature*, along the directions defined by the sGoldstino ξ^X and the supersymmetric directions ξ^λ:

$$3(\gamma+1)\,B[X,\lambda] \geq -(m_\lambda \pm 1)\big(m_\lambda \pm (3\gamma+1)\big) \mp \sqrt{3(\gamma+1)}\,\frac{\partial m_\lambda}{\partial X}.$$

In addition, we shall discuss examples where this set of constraints is not only necessary, but also sufficient to ensure the stability along the supersymmetric directions at the critical point, and prove that the type of couplings which allow this

[1] The correspondence between γ and b in the previous chapter is given by $b = 3\gamma$.

situation arise naturally when the model is consistent with the supersymmetric truncation of one sector of the moduli space. Moreover, we will show that field configurations minimising the gravitino mass along the supersymmetric directions are the best candidates to remain stabilised for arbitrary values of the uplifting γ. This could already be seen from the stability diagram presented in the previous chapter.

However, without some knowledge about the spectrum of fermion masses of the supersymmetric sector, these conditions are still not very informative. Following [209–212], we will adopt a statistical approach under the assumption that the supersymmetric sector contains a large number of fields. In particular, we will consider models where the couplings are consistent with the supersymmetric truncation of one sector of the theory, and we will describe the supersymmetric sector by a random ensemble of supergravity theories. Proceeding in this way, we find the mass spectrum of the fermions using random matrix theory techniques, and we shall derive constraints on the geometry of the Kähler manifold, expressed as bounds on the bisectional curvature $B[X, \lambda]$. These bounds will depend in general on the statistical parameters defining the random ensemble of supergravity theories, such as the standard deviation of the fermion masses, which sets the typical ratio of the mass of the heaviest fermion to the gravitino mass.

In the following, for the sake of simplicity and given the limitations of space, I present the main ingredients and key arguments that we used in order to get our results, and further details can be found in the original work [4].

5.2 Aspects of $\mathcal{N} = 1$ supergravity

Already in section 1.4.1 and in chapter 4 we reviewed the basic properties of the scalar potential and its critical points. The class of supergravity actions we study in the present work only involve complex scalar fields ξ^I and their superpartners, the Weyl fermions χ^I (chiral multiplets with no gauge interactions). The fields are labeled with the index I running in $I = 1, \ldots, \mathrm{N}$ for N chiral multiplets.

At critical points ξ_0 where supersymmetry is spontaneously broken, the gradient of the Kähler function $G_I|_{\xi_0}$ defines a direction in field space known as the *sGoldstino direction*. The sGoldstino corresponds to the supersymmetric partner of the would-be Goldstone fermion associated to broken supersymmetry. We will also describe this direction in terms of the unit vector z_X with coordinates

$$z_{X,I} = \frac{G_I}{\sqrt{G_K G^K}}. \tag{5.2.1}$$

From the supersymmetry transformations (1.4.6) it follows that a homogeneous bosonic field configuration ξ_0 where supersymmetry is unbroken must necessarily

satisfy the set of necessary conditions

$$G_I|_{\xi_0} = 0, \qquad \text{for all} \qquad I = 1, \ldots, \text{N}. \tag{5.2.2}$$

Actually, it is easy to check that supersymmetric configurations are also critical points of the scalar potential, see Eqs. (1.4.12) and (1.4.13) in section 1.4.2, and thus they are called *supersymmetric critical points*. Due to the form of the scalar potential (1.4.5), supersymmetric critical points are always AdS:

$$V|_{\xi_0} = -3\mathrm{e}^G < 0, \tag{5.2.3}$$

except in those cases where the superpotential vanishes, for which they are Minkowski vacua, $V|_{\xi_0} = 0$.

5.2.1 The structure of the Hessian

For completeness and in order to establish our notation, let us review some aspects of the mass matrix already explained in section 4.2.1. In order to determine the stability properties of an extremum of the scalar potential, we need to study the eigenvalue spectrum of the corresponding Hessian,

$$\mathcal{H} = \begin{pmatrix} \nabla_I V_{\bar{J}} & \nabla_I V_J \\ \nabla_{\bar{I}} V_{\bar{J}} & \nabla_{\bar{I}} V_J \end{pmatrix}, \tag{5.2.4}$$

which determines the squared-masses of the scalar fields at Minkowski and de Sitter critical points. In this subsection we will describe the different contributions of the Hessian and will relate them to the masses of the fermions and to the geometry of the Kähler manifold.

After using the stationarity conditions (1.4.12), the second covariant derivatives of the scalar potential at the extremum ξ_0 of V read[2]

$$\begin{aligned} \nabla_I V_{\bar{J}} &= (G_{I\bar{J}} - G_I G_{\bar{J}})\, V + \mathrm{e}^G \left[G^{K\bar{L}} (\nabla_K G_I)(\nabla_{\bar{L}} G_{\bar{J}}) + G_{I\bar{J}} - R_{I\bar{J}K\bar{L}} G^K G^{\bar{L}} \right] , \\ \nabla_I V_J &= (\nabla_I G_J - G_I G_J)\, V + \mathrm{e}^G \left[2\nabla_I G_J + G^K \nabla_K \nabla_I G_J \right] . \end{aligned} \tag{5.2.5}$$

In these expressions it is straightforward to identify the mass of the gravitino $m_{3/2}$ and the mass matrix of the chiral fermions M_{IJ}:

$$m_{3/2} \equiv \mathrm{e}^{G/2}, \qquad M_{IJ} \equiv \mathrm{e}^{G/2} \nabla_I G_J. \tag{5.2.6}$$

To simplify the notation, in what follows we will measure all the masses and energies in units of the gravitino mass, thus we perform the rescaling

$$\mathcal{H} \to m_{3/2}^2\, \mathcal{H}, \qquad \text{and} \qquad M_{IJ} \to m_{3/2}\, M_{IJ}. \tag{5.2.7}$$

[2] To make contact to the notation of [83, 84], note that at any supersymmetric critical point ξ_0 the covariant derivatives and the regular derivatives of $G(\xi, \bar{\xi})$ coincide.

Similarly, we will parameterise the expectation value of the scalar potential at an extremum ξ_0 by the quantity:[3]

$$\gamma \equiv \frac{V}{3\, m_{3/2}^2} \simeq \frac{H^2}{m_{3/2}^2}, \tag{5.2.8}$$

which is essentially the square of the Hubble parameter H in units of the gravitino mass. The structure of the Hessian becomes particularly clear when we choose the fields ξ^I so that they have canonical kinetic terms at the critical point, i.e. $G_{I\bar{J}}|_{\xi_0} = \delta_{I\bar{J}}$. Moreover, we will require that one of the axis of the local frame points along the sGoldstino direction, i.e. $G_I \equiv G_X\, \delta_{IX}$, this is the so-called *sGoldstino basis*. In these coordinates it is straightforward to show that the Hessian reads[4]

$$\mathcal{H} = (\mathcal{M}+\mathbb{1})\big(\mathcal{M}+(3\gamma+1)\mathbb{1}\big) + \sqrt{3(\gamma+1)}\,\nabla_X\mathcal{M} - 3(\gamma+1)\mathcal{R} - 9\gamma(\gamma+1)\mathcal{P}_X. \tag{5.2.9}$$

Here $\mathcal{M}$ and $\nabla_X\mathcal{M}$ are the (rescaled) fermion mass matrix and its derivative along the sGoldstino direction written in the 2N−vector notation, $\mathcal{R}$ is a matrix built from the components of the Riemann tensor, and $\mathcal{P}_X$ is the projector along the sGoldstino direction:

$$\mathcal{M} = \begin{pmatrix} 0 & \nabla_I G_J \\ \nabla_{\bar{I}} G_{\bar{J}} & 0 \end{pmatrix},\ \mathcal{R} = \begin{pmatrix} R_{X\bar{X}I\bar{J}} & 0 \\ 0 & R_{\bar{X}X\bar{I}J} \end{pmatrix},\ \mathcal{P}_X = \begin{pmatrix} \delta_{IX}\delta_{\bar{J}\bar{X}} & \delta_{IX}\delta_{JX} \\ \delta_{\bar{I}\bar{X}}\delta_{\bar{J}\bar{X}} & \delta_{\bar{I}\bar{X}}\delta_{JX} \end{pmatrix}. \tag{5.2.10}$$

For convenience, we will define the following shorthand to refer to the first term of the Hessian in (5.2.9):

$$\mathcal{H}_\gamma \equiv (\mathcal{M}+\mathbb{1})\big(\mathcal{M}+(3\gamma+1)\mathbb{1}\big). \tag{5.2.11}$$

5.3 Necessary conditions for metastability

In this section we will present our approach to characterise the perturbative stability of a consistently decoupled supersymmetric sector. We will derive a set of necessary conditions that should be satisfied by any homogeneous field configuration free of tachyons, and we will discuss some of their implications. As we shall show, our results can be applied both to the study of the perturbative stability of critical points of the scalar potential, or to analyse the viability of inflationary models which include a set of spectator fields not directly involved in the inflationary dynamics or supersymmetry breaking.

[3] Recall that b in chapter 4 equals 3γ.

[4] We also have the freedom to choose the sGoldstino vector to be real, which results into $G_X = \sqrt{3(\gamma+1)}$.

For a Minkowski or de Sitter field configuration to be metastable, all the eigenvalues of the Hessian matrix (5.2.9) have to be positive. Since a generic expression of the eigenvalues in terms of G and its derivatives is too involved, we follow a different strategy. In the series of papers [194, 195, 224–227] they made use of the following observation: if the Hessian is positive definite, so it is its projection along any vector $Z = (z, \bar{z})^T$:

$$\langle Z, \mathcal{H}\, Z\rangle \geq 0. \tag{5.3.1}$$

In particular, the authors of [194, 195, 224–227] studied the condition obtained from imposing this requirement along the (complex) sGoldstino directions

$$Z_{+X} = \frac{1}{\sqrt{2}}\begin{pmatrix} z_X \\ z_{\bar{X}} \end{pmatrix} \qquad \text{and} \qquad Z_{-X} = \frac{\mathrm{i}}{\sqrt{2}}\begin{pmatrix} z_X \\ -\bar{z}_X \end{pmatrix}. \tag{5.3.2}$$

As was discussed in detail in [194, 195], the corresponding constraint (5.3.1) is particularly restrictive due to the stationarity conditions, which imply that the vectors $Z_{\pm X}$ are eigenvectors of the fermion mass matrix $\mathcal{M}$:

$$\mathcal{M}\, Z_{\pm X} = \mp(3\gamma + 1)\, Z_{\pm X}. \tag{5.3.3}$$

Combining the necessary conditions associated to the vectors $Z_{\pm X}$, it is possible to find a restriction on the geometry of the Kähler manifold which, when expressed in terms of the *sectional curvature* $S[X] \equiv -R_{X\bar{X}X\bar{X}}$, reads:

$$S[X] \geq -\frac{2}{3}\frac{1}{1+\gamma}. \tag{5.3.4}$$

In the present section we will derive a set of complementary conditions obtained when considering the other $2\mathrm{N} - 2$ real directions orthogonal to the sGoldstino, that is, those preserving supersymmetry. Thus, in the rest of our analysis the term $\mathcal{P}_X$ in (5.2.9) will always be absent.

5.3.1 Metastability conditions

To characterise the eigenvalue spectrum of the Hessian it is convenient to work in a local frame where the fermion mass matrix $\mathcal{M}$ is diagonal, since in this basis the term $\mathcal{H}_\gamma$ of the Hessian (5.2.9) is also diagonal. Due to the special structure of $\mathcal{M}$, it is possible to show that it has $2\mathrm{N}$ real eigenvalues arranged in pairs of the form[5,6]

$$\mathcal{M}\, Z_{\pm\lambda} = \pm m_\lambda\, Z_{\pm\lambda}, \qquad \text{with} \qquad \lambda = 1, \ldots, \mathrm{N}. \tag{5.3.5}$$

[5] The details of the diagonalisation can be found in Appendix C.

[6] Note the change of notation with respect to [3, 83, 84], where the masses of the fermions were denoted by $|x_\lambda| \equiv m_\lambda$.

The corresponding normalised eigenvectors are given by $Z_{+\lambda} = \frac{1}{\sqrt{2}}(z_\lambda, \bar{z}_\lambda)^T$ and $Z_{-\lambda} = \frac{1}{\sqrt{2}}(\mathrm{i}z_\lambda, -\mathrm{i}\bar{z}_\lambda)^T$, where z_λ solves

$$M\,\bar{z}_\lambda = m_\lambda z_\lambda, \tag{5.3.6}$$

and we choose $m_\lambda \geq 0$. Since M is symmetric, we can always find a set of orthonormal vectors z_λ which satisfy the previous equation. Indeed, after requiring the fields to have canonical kinetic terms, it is still possible to redefine them using a unitary transformation of the form $\tilde{\xi} = \xi\, U$. Performing these transformations we can bring the matrix M to a diagonal form $M = UDU^T$, where U is unitary and $D = \mathrm{diag}(m_\lambda)$, with $m_\lambda \in \mathbb{R}^+$. This result, known as Takagi's factorisation, applies to any complex symmetric matrix, and the eigenvectors z_λ can be read from the columns of the unitary matrix $U_{I\lambda} = z_{\lambda,I}$. Note that this diagonalisation is also consistent with the choice of the sGoldstino basis since the vectors $Z_{\pm X}$ associated to the sGoldstino direction are also eigenvectors of the matrix $\mathcal{M}$, (5.3.3). The particular eigenvalue m_X is related to the unphysical Goldstone fermion of broken supersymmetry, and thus it does not have the interpretation of a mass. The rest of the parameters m_λ, with $\lambda = 1, \ldots, \mathrm{N}-1$, determine the mass spectrum of the chiral fermions χ^I.

In general, the contributions to the Hessian proportional to $\nabla_X \mathcal{M}$ and $\mathcal{R}$ will not be diagonal in the basis formed by $Z_{\pm\lambda}$, but their diagonal elements in this frame

$$\langle Z_{\pm\lambda}, \nabla_X \mathcal{M}\, Z_{\pm\lambda}\rangle = \pm\frac{\partial m_\lambda}{\partial X}, \qquad\qquad \langle Z_{\pm\lambda}\, \mathcal{R}\, Z_{\pm\lambda}\rangle = -B[X,\lambda], \tag{5.3.7}$$

have a simple physical interpretation. First, it can be shown that the parameters $\partial m_\lambda/\partial X$ are the derivatives of the fermion masses along the sGoldstino direction (see appendix C). Second, the set of $\mathrm{N}-1$ quantities $B[X,\lambda] \equiv -R_{X\bar{X}\lambda\bar{\lambda}}$ are the so-called *bisectional curvatures* along the planes formed by the sGoldstino direction z_X and each of the eigenvectors z_λ, which has also been used to characterise the stability of the inflationary trajectory [86]. The viability of the studied models translates into constraints on the geometry of the Kähler manifold through the bisectional curvature.

In order to derive a set of simple necessary constraints, we will use the projection of the Hessian along all the $2\mathrm{N}-2$ supersymmetric $Z_{\pm\lambda}$ directions, $\mu^2_{\pm\lambda} \equiv \langle Z_{\pm\lambda}, \mathcal{H}\, Z_{\pm\lambda}\rangle$. Collecting the results above we find the following conditions for Minkowski and dS vacua:

$$\mu^2_{\pm\lambda} = (m_\lambda \pm 1)\big(m_\lambda \pm (3\gamma+1)\big) \pm \sqrt{3(\gamma+1)}\,\frac{\partial m_\lambda}{\partial X} + 3(\gamma+1)\,B[X,\lambda] \geq 0, \tag{5.3.8}$$

for all $\lambda = 1, \ldots, \mathrm{N}-1$. Similarly to [194, 195, 224–227], one can find a necessary condition which does not depend on the derivatives of the fermion masses by

adding together the quantities $\mu^2_{+\lambda}$ and $\mu^2_{-\lambda}$, which for $\gamma \geq 0$ reads

$$\mu^2_{+\lambda} + \mu^2_{-\lambda} \geq 0 \qquad \Longrightarrow \qquad B[X,\lambda] \geq -\frac{m^2_\lambda + 3\gamma + 1}{3(\gamma+1)}. \tag{5.3.9}$$

In the case of AdS critical points, the requirement of stability implies that all the squared-masses of the scalar fields have to satisfy the Breitenlohner-Freedman bound [228], and therefore all the previous conditions have to be modified accordingly. For instance, taking into account that we work in units of the gravitino mass, the set of conditions (5.3.8) become

$$\mu^2_{\pm\lambda} \geq \frac{3}{4}\,\frac{V(\xi_0)}{m^2_{3/2}} = \frac{9}{4}\gamma. \tag{5.3.10}$$

To understand the implications of the set of constraints (5.3.8) and their dependence on the different parameters of the theory, (the spectrum of fermion masses and their derivatives, the geometry of the Kähler manifold, and the supersymmetry breaking scale), we will now discuss them in two different contexts:

- First, we will analyse the metastability of supersymmetric critical points, where we recover known results. In that situation the parameters $\mu^2_{\pm\lambda}$ are the exact eigenvalues of the Hessian, and therefore the corresponding constraints (5.3.10) are both necessary and sufficient to guarantee the perturbative stability of the configuration.

- Second, we will discuss non-supersymmetric configurations, focusing on the perturbative stability of the fields preserving supersymmetry. This analysis is both applicable to the case when the field configuration represents a non-supersymmetric vacuum or when it is responsible for driving an inflationary phase. In the latter case, the perturbative stability of all the fields not related to the inflaton or the sGoldstino is a requirement for the viability of the model, since the presence of any large tachyonic instability would spoil the slow-roll conditions. Additionally, the masses of the non-inflating fields must remain larger than the Hubble parameter in order to avoid large isocurvature fluctuations, which are ruled out by the observations. Even if they remain sufficiently massive, if these fields deviate from geodesics, they might leave imprints in the CMB temperature spectra [1, 103].

Let us emphasise that in general the conditions (5.3.8,5.3.9) are necessary but cannot guarantee the perturbative stability along the supersymmetric directions of a non-supersymmetric configuration. However, as we shall discuss in later sections, there are interesting situations where these conditions become both necessary and sufficient. For instance, whenever the term $\mathcal{H}_\gamma$ dominates over the rest of contributions to the Hessian, since then the quantities $\mu^2_{\pm\lambda}$ can be identified as the eigenvalues of the Hessian to first order in perturbation theory.

We shall leave the discussion of these cases for section 5.4.

For simplicity, in the following analyses we will assume that all the parameters involved in the constraints (5.3.8) are independent from each other and can be varied freely. More complicated situations are possible, for example when two or more of the parameters have a functional dependence on each other, but we will not consider them here.

5.3.2 Supersymmetric vacua and uplifting to dS

As we discussed above, supersymmetric critical points are AdS as long as the superpotential is non-zero, $W \neq 0$, and in particular they satisfy $\gamma = -1$. Therefore, the Hessian (5.2.9) is simply given by:

$$\mathcal{H} = (\mathcal{M}+\mathbb{1})(\mathcal{M}-2\,\mathbb{1}) \quad \Longrightarrow \quad \mu^2_{\pm\lambda} = (m_\lambda \pm 1)(m_\lambda \mp 2) = \left(m_\lambda \mp \tfrac{1}{2}\right)^2 - \tfrac{9}{4} \geq -\frac{9}{4}\,. \tag{5.3.11}$$

This implies that the Hessian is also diagonal in the basis that diagonalises $\mathcal{M}$, and therefore the parameters $\mu^2_{\pm\lambda}$ can be identified with the complete set of eigenvalues of $\mathcal{H}$. Then the set of conditions (5.3.10) are *necessary and sufficient*, and in addition they can be applied to all directions $Z_{\pm\lambda}$, with $\lambda = 1, \ldots, \text{N}$, since there is no sGoldstino at supersymmetric critical points. From the eigenvalues (5.3.11) one can see what type of extremum the supersymmetric critical point ξ_0 is, namely:

$$\begin{aligned} &m_\lambda > 2 \quad \text{for all } \lambda \quad \Rightarrow \quad \text{local AdS minimum,} \\ &m_\lambda < 1 \quad \text{for all } \lambda \quad \Rightarrow \quad \text{local AdS maximum,} \end{aligned} \tag{5.3.12}$$

and any other combination corresponds to AdS saddle points ($m_\lambda = 1, 2$ give flat directions). However, supersymmetric critical points are always perturbatively stable regardless of the possible negative curvature of the potential, since they are AdS and the Breitenlohner-Freedman bound (5.3.10) is always satisfied, as can be seen from eq. (5.3.11).

As discussed in the introduction, supersymmetric vacua play an important role in the construction of de Sitter vacua in cosmological models. It is possible to engineer a dS vacuum by the *uplifting* of a supersymmetric AdS vacuum ξ_0 to dS, which consists in introducing a physical mechanism to break supersymmetry. Ideally, these mechanisms add a positive definite correction to the scalar potential δV_{uplift}, possibly field-dependent, so that the vacuum expectation value of V becomes positive at ξ_0^I,

$$V = V_{\text{susy}}|_{\xi_0} + \delta V_{\text{uplift}}|_{\xi_0} \geq 0, \tag{5.3.13}$$

while the supersymmetric configuration is still a metastable critical point of the potential. In general, the supersymmetric field configuration ξ_0 is not a

critical point of the uplifting term δV_{uplift}, and thus the critical points of the final potential typically shift away from ξ_0, or disappear completely. That is why in general one should ensure that the original supersymmetric critical point ξ_0 is a minimum, demanding all chiral fermions to have masses larger than twice the gravitino mass, cf. (5.3.12).

One of the aims of this work is to study the metastability of a supersymmetric sector embedded in a larger model where supersymmetry is already broken. As we shall see in section 5.6, in that case the constraint we just discussed is no longer necessary. In particular we will prove that a stable configuration of the embedded supersymmetric sector may correspond to any type of AdS critical point (even a saddle point or maximum) in the supersymmetric limit $\gamma \to -1$. In other words, the embedding of the supersymmetric sector in a larger model may turn an AdS maximum or a saddle point in the supersymmetric limit to a metastable configuration after supersymmetry breaking by other sector. The coupling between the embedded supersymmetric sector and the fields breaking supersymmetry can be seen as a non-generic type of F-term uplifting mechanism, like those studied in [83, 84].

5.3.3 Non-supersymmetric configurations

In the present subsection we will analyse the set of constraints (5.3.8) in the case when the field configuration is non-supersymmetric. As we mention above, we shall consider both the case where the configuration is an extremum of the scalar potential, and where the vacuum energy of the fields is driving an inflationary phase. In order to proceed we analyse the different contributions to the Hessian separately: first we will discuss the term depending on the fermion mass matrix $\mathcal{H}_\gamma$, and then we will characterise the effect of including the contributions associated to the derivatives of the fermions masses $\nabla_X \mathcal{M}$, and the curvature of the Kähler manifold, $\mathcal{R}$.

Dependence on the fermion masses, $\mathcal{H} = \mathcal{H}_\gamma$

We begin with the simplest case where $\mathcal{H}_\gamma$ is the only non-zero contribution to the Hessian:

$$\nabla_X \mathcal{M} = \mathcal{R} = 0 \qquad \Longrightarrow \qquad \mathcal{H} = \mathcal{H}_\gamma = (\mathcal{M} + \mathbb{1})\big(\mathcal{M} + (3\gamma + 1)\mathbb{1}\big). \quad (5.3.14)$$

Then, as in the case of supersymmetric critical points, the Hessian is diagonal in the basis of eigenvectors $Z_{\pm\lambda}$ of the fermion mass matrix, and the quantities $\mu^2_{\pm\lambda}$ can be identified with the eigenvalues of $\mathcal{H}$, which read:

$$\mu^2_{\pm\lambda} = (m_\lambda \pm 1)\big(m_\lambda \pm (3\gamma + 1)\big) = \big(m_\lambda \pm \tfrac{1}{2}(3\gamma + 2)\big)^2 - \tfrac{9}{4}\gamma^2. \quad (5.3.15)$$

Therefore, the stability of the configurations along the supersymmetric directions is entirely determined by the fermion mass spectrum m_λ and the parameter γ.

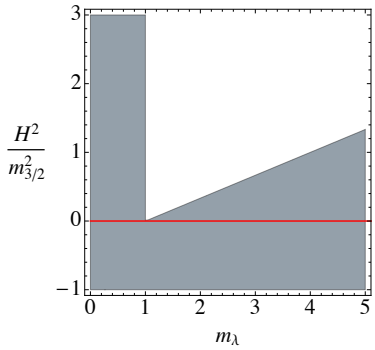

Figure 5.1 *– Stability diagram for a Hessian of the form* (5.3.14)*, with* $\partial_X \mathcal{M} = \mathcal{R} = 0$*. In this case the conditions* (5.3.8) *are both necessary and sufficient, and the shaded area represents the region of parameter space where they are satisfied. Configurations which minimise the gravitino mass* $m_{3/2}^2 = \mathrm{e}^G$ *(*$m_\lambda < 1$*) remain stable for arbitrary large values of the parameter* $\gamma \gg 1$*.*

Since all the eigenvalues of the Hessian are bounded below by $-\frac{9}{4}\gamma^2$ it follows that, when the configuration is an AdS critical point, $\gamma \in [-1, 0)$, these eigenvalues always satisfy the Breitenlohner-Freedman bound (5.3.10), and thus it is always stable. However, if the configuration is either Minkowski or de Sitter ($\gamma \geq 0$), stability demands

$$\mu_{\pm\lambda}^2 \geq 0 \qquad \Longrightarrow \qquad m_\lambda < 1 \quad \text{or} \quad m_\lambda > 3\gamma + 1 \quad \text{for all } \lambda. \tag{5.3.16}$$

Thus, in Minkowski vacua ($\gamma = 0$) the supersymmetric sector is always metastable, possibly with flat directions if one or more of the fermion masses equals the gravitino mass, $m_\lambda = 1$. An interesting consequence for de Sitter configurations (either a vacuum or at a point of the inflationary trajectory) is that, if all fermion masses are smaller than the gravitino mass, i.e. $m_\lambda < 1$, the supersymmetric sector remains tachyon-free for arbitrary large values of the cosmological constant. Conversely, if the fermion spectrum contains any mass larger than $m_{3/2}$, the critical point will always become unstable for sufficiently large values of the Hubble parameter. These results are illustrated in Fig. 5.1, which shows the stability diagram of a non-supersymmetric configuration along a direction orthogonal to the sGoldstino. The horizontal axis is related to the mass of the corresponding fermionic partner m_λ, and the quantity on the vertical axis is the parameter γ. In the diagram, the perturbatively stable configurations are represented by the grey shaded area.

This simple example already illustrates the claim made in the previous subsection: in general, the condition $m_\lambda > 2$ necessary for a supersymmetric critical point to be a minimum, is neither necessary or sufficient when the supersymmetric sector is embedded in a larger model. The special structure of the Hessian

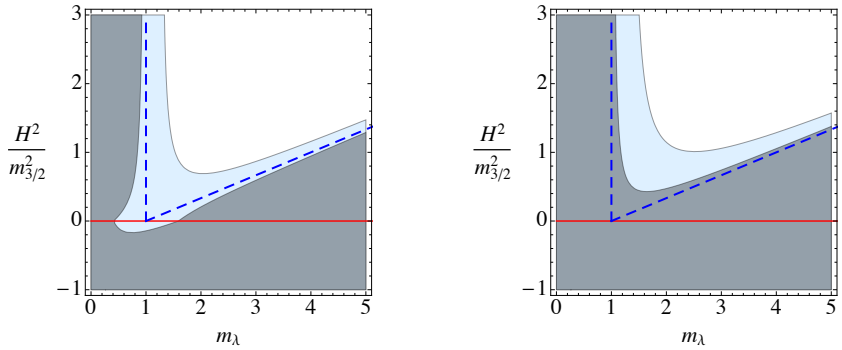

Figure 5.2 *– Stability diagram associated to the spectrum given by equation (5.3.8). Coloured areas show, for different choices of parameters, the regions where the stability conditions are satisfied, while in the white area we would have tachyons. LEFT: $\partial m_\lambda/\partial X = 0.2$, with $B[X,\lambda] = 0$ (grey area) and $B[X,\lambda] = 0.3$ (light blue area). RIGHT: $\partial m_\lambda/\partial X = -0.2$, with $B[X,\lambda] = 0$ (grey area), and $B[X,\lambda] = 0.3$ (light blue area). The dashed line represents the constraints in the case $B[X,\lambda] = \partial m_\lambda/\partial X = 0$, showed in figure 5.1.*

discussed in this example arises naturally in models of F-term uplifting where some heavy moduli are truncated while preserving supersymmetry [83, 84]. In the context of inflation this type of couplings have also been considered in [3], see chapter 4. We discuss more about this class of models in sections 5.4 and 5.6.

Dependence on the fermion mass derivatives and the curvature

In general, when the terms $\partial_X \mathcal{M}$ and $\mathcal{R}$ are taken into account, the Hessian will not be diagonal in the basis formed by the vectors $Z_{\pm\lambda}$, and the set of necessary conditions (5.3.8) will not be sufficient to ensure the stability of the critical point.

Let us first focus on the contribution coming from the term in the Hessian proportional to the derivative of the fermions mass matrix $\nabla_X \mathcal{M}$, while keeping the curvature term set to zero $\mathcal{R} = 0$. In Fig. 5.2, focusing on the grey regions, we have represented the region of parameter space satisfying the stability conditions (5.3.8) for a particular direction in field space z_λ (shaded grey area) setting two different constant values of the fermion mass derivatives, $\partial m_\lambda/\partial X = 0.2$ (left plot) and $\partial m_\lambda/\partial X = -0.2$ (right plot), and with a zero bisectional curvature $B[X,\lambda] = 0$. Since these conditions are in general necessary but not sufficient, a field configuration located in the grey shaded region is not necessarily stable, but those out of the shaded area will definitely contain one or more tachyonic directions in the spectrum. Note that when the derivatives of the fermion masses

satisfy

$$\frac{\partial m_\lambda}{\partial X}\Big|_{\rm opt} = -\frac{3\gamma+2}{\sqrt{3(\gamma+1)}} m_\lambda, \tag{5.3.17}$$

the two parameters $\mu^2_{\pm\lambda}$ become equal, and both constraints (5.3.8) reduce to the less restrictive condition (5.3.9). Therefore, in the case of dS and Minkowski configurations ($\gamma \geq 0$), as the derivatives of the fermion masses approach this optimum value, the stability constraints on the fermion masses m_λ and the parameter γ become milder, as observed in the diagrams.

The effect of having a non-zero $\mathcal{R}$ is simpler to analyse. The set of necessary conditions (5.3.8) clearly favour positive values for the bisectional curvature $B[X,\lambda] > 0$. We can check that this is indeed the case in the plots of Fig. 5.2, where we have displayed the region of parameter space satisfying the stability conditions (5.3.8) for two different constant values of the bisectional curvature, $B[X,\lambda] = 0$ (grey area), and $B[X,\lambda] = 0.3$ (light blue area).

When the Hubble scale is large compared to any of the fermion masses, $H \gg m_{3/2}$ and $H \gg m_\lambda\, m_{3/2}$[7], the bisectional curvatures play a fundamental role determining the stability of the inflationary trajectory. In that limit (keeping $\partial m_\lambda/\partial X$ fixed) the range of fermionic masses where the field configuration is free of tachyons is

$$0 \leq m_\lambda \lesssim 1 + B[X,\lambda]. \tag{5.3.18}$$

Then, when the bisectional curvature is zero, we recover the limit discussed above and only configurations where the largest mass of the chiral fermions satisfies $m_\lambda|_{\rm max} < 1$, remain stable for arbitrarily large values of γ. However, positive values improve the stability, as shown by the light blue regions of Fig. 5.2, and negative values of the bisectional curvature shrink the range of fermion masses compatible with stable dS configurations. Actually, when $B[X,\lambda] < -1$, the field associated to the direction z_λ always becomes tachyonic for sufficiently large values of the Hubble parameter, $\gamma \gg 1$, and therefore the corresponding field configuration is necessarily unstable.

These constraints are of interest both for the construction of de Sitter vacua with small cosmological constant $\gamma \approx 0$ (as in the present vacuum), and for models of inflation, to study the stability of the supersymmetric sector along the inflationary trajectory. The study of the viability of inflationary models using the presented constraints deserves further consideration and we will report on it in a future publication. We will now start with the stability analysis of consistently decoupled sectors, focusing on those models were they only act as spectators both in supersymmetry breaking and inflation.

[7]Recall that we measure the chiral fermion masses m_λ in units of the gravitino mass, $m_{3/2}$.

5.4 Modeling the supersymmetric sector

Having presented the main tool for our analysis, that is, the set of constraints (5.3.8), we now turn to the problem at hand: the study of the perturbative stability of a decoupled supersymmetric sector, such as the complex structure moduli in the KKLT constructions, and Large Volume Scenarios of Type IIB flux compactifications [219–221]. Motivated by these scenarios, where stabilisation of the complex structure moduli can be studied using a statistical treatment [209–212], we will focus on theories where the supersymmetric sector contains a large number of fields, and we will characterise the couplings using a statistical description. On the one hand, we will require the interactions of the model to be consistent with the *exact supersymmetric truncation* of the decoupled sector (section 5.4.1), and on the other hand we will assume that the couplings of the supersymmetric sector are generic and can be treated as random variables. In particular we will characterise the spectrum of fermion masses of the supersymmetric sector m_λ, and their derivatives, $\partial m_\lambda / \partial X$, using standard techniques from random matrix theory (section 5.4.2).

5.4.1 Supersymmetric decoupling

As discussed previously and extensively in this thesis, integrating out a heavy sector in a consistent way is only possible in certain situations. The type of couplings between the integrated and surviving sectors which allow for the reduced theory to be approximately supersymmetric have been discussed extensively in the literature [82, 186, 187, 189].

The simplest way of satisfying these conditions is to require the couplings to be consistent with the *supersymmetric truncation* of the heavy sector [177]. In a consistent truncation of a given theory, the solutions of the reduced theory are *exact* solutions of the full theory. This type of constructions are interesting for our purposes because they enable us to study the perturbative stability of the truncated sector on its own. In addition, the truncated fields will remain on geodesic trajectories. In this sense we can say that the truncated sector is *supersymmetrically decoupled* from the fields in the reduced theory. Interestingly, it has been shown [188, 229] that the large volume limit of type IIB flux compactifications are a particular realisation of this class of models, and moreover, in that case the conditions (5.3.8) are not only necessary, but also sufficient to ensure the stability of the supersymmetric sector.

Let us consider a heavy supersymmetric sector with fields H^α and a light supersymmetry-breaking sector with fields L^i. We have seen that in order for the truncated fields to preserve supersymmetry regardless of the configuration of the surviving sector L^i, the Kähler function has to satisfy the following set of

constraints:

$$G_\alpha(H_0, \bar{H}_0, L, \bar{L}) = 0 \qquad \text{for all} \qquad L^i \qquad \text{and} \qquad \alpha = 1 \dots \mathrm{N}_h. \tag{5.4.1}$$

Since the equations (5.4.1) must hold for any value of the light fields L^i, the couplings between the two sectors are very constrained. Taking derivatives with respect to the coordinates L^i and $L^{\bar{i}}$ we find the following implications:

$$G_{i\alpha}(H_0, \bar{H}_0, L, \bar{L}) = 0, \qquad R_{i\bar{j}k\bar{\alpha}} = 0, \tag{5.4.2}$$

$$M_{i\alpha}|_{H_0} = 0, \qquad \nabla_X M_{i\alpha}|_{H_0} = 0. \tag{5.4.3}$$

The previous conditions imply that the Hessian itself must be block diagonal in the two sectors:

$$\mathcal{H} = \mathcal{H}_h \oplus \mathcal{H}_l. \tag{5.4.4}$$

Therefore, as we anticipated at the beginning of the section, if the couplings are compatible with the consistent truncation the supersymmetric sector, it is consistent to study the perturbative stability of the supersymmetric sector independently of the sector surviving the truncation, i.e. it is sufficient to consider the block of the Hessian $\mathcal{H}_h$:

$$\mathcal{H}_h = (\mathcal{M}_h + \mathbb{1})\big(\mathcal{M}_h + (3\gamma+1)\mathbb{1}\big) + \sqrt{3(\gamma+1)}\,\nabla_X \mathcal{M}_h - 3(\gamma+1)\mathcal{R}_h. \tag{5.4.5}$$

In the following, we consider models with a supersymmetrically decoupled sector in the sense described above, focusing on the stability of the configuration defining the truncation, H_0^α, along the supersymmetric directions H^α.

5.4.2 Statistical description

Since the fine details of this subsection are not essential for the understanding of our results, we will review the main facts and concepts, and refer to the reader to the original work [4] for further details. In order to study the perturbative stability of the supersymmetrically decoupled sector, we need to characterise the eigenvalue spectrum of the fermion mass matrix $\mathcal{M}_h$ and the properties of its derivative $\nabla_X \mathcal{M}_h$. At a generic point of the reduced theory, where $H^\alpha = H_0^\alpha$, these matrices read

$$\mathcal{M}_h = \begin{pmatrix} 0 & M_{\alpha\beta} \\ \bar{M}_{\bar{\alpha}\bar{\beta}} & 0, \end{pmatrix}, \qquad \nabla_X \mathcal{M}_h = \begin{pmatrix} 0 & \nabla_X M_{\alpha\beta} \\ \nabla_{\bar{X}} \bar{M}_{\bar{\alpha}\bar{\beta}} & 0 \end{pmatrix}, \tag{5.4.6}$$

where the tensors $M_{\alpha\beta} = \nabla_\alpha G_\beta$ and $\nabla_X M_{\alpha\beta} = \nabla_X(\nabla_\alpha G_\beta)$ will depend in general on the configuration H_0^α and on the light fields L^i. In realistic scenarios with a large number of fields, it is more practical to follow the methods proposed by Denef and Douglas [209, 210] and later developed in [211, 212], who use a statistical approach. Indeed, treating the components of the tensors $M_{\alpha\beta}$ and $\nabla_X M_{\alpha\beta}$ as random variables, makes possible to characterise the properties of the matrices (5.4.6) using random matrix theory techniques (see [230]).

Probability distribution of the couplings

Following [211, 212], we assume that the random variables $M_{\alpha\beta} = M_{\beta\alpha}$ are characterised by a unique probability distribution Ω, with zero mean and standard deviation σ for $\alpha \neq \beta$ and $\sqrt{2}\sigma$ for $\alpha = \beta$:

$$M_{\alpha\beta} \in \Omega(0,\sigma) \quad \text{if} \quad \alpha < \beta, \quad \text{and} \qquad M_{\alpha\alpha} \in \Omega(0,\sqrt{2}\sigma). \tag{5.4.7}$$

Note that the corresponding joint probability distribution is invariant under supersymmetry and Kähler transformations, and diffeomorphisms on the Kähler manifold. In the limit where the size of the matrices is very large, i.e. large number of H^α fields, the results we will now present do not depend on any higher moments of the distribution Ω.

The quantities in the Hessian (5.4.5) associated to the supersymmetry breaking sector, i.e. γ and the gravitino mass $m_{3/2}$, will be regarded as parameters and studied in a case by case basis. Moreover, following the works in [207–210] we also assume that the geometry of the Kähler manifold is also determined by the parent theory. Note that these quantities depend on the configuration H_0^α and on the light fields L^i, and therefore our predictions about the stability of the supersymmetric sector will depend on the distribution of the couplings, the geometry of the moduli space, and the supersymmetry breaking scale.

In the following, we bring a few results of random matrix theory to characterise the spectrum of masses of the fermions m_λ and their derivatives along the sGoldstino direction $\partial m_\lambda/\partial X$. We then incorporate them to the analysis of the perturbative stability of the supersymmetric sector through the constraints (5.3.8).

The Altland-Zimbauer CI-ensemble

The set of hermitian matrices with the same structure as (5.4.6), and random complex entries drawn from a probability distribution with the properties given in (5.4.7), form the so-called *Altland-Zimbauer* or *CI-ensemble*. Taking the distribution Ω to be gaussian, the joint probability density for the fermion masses m_λ is given by

$$f(m_1,\ldots,m_{\mathrm{N}_h}) = \mathcal{C}\ \exp\left(-\frac{1}{2\sigma^2}\sum_{\lambda=1}^{\mathrm{N}_h} m_\lambda\ + \sum_{\lambda<\nu}^{\mathrm{N}_h} \ln|m_\nu - m_\lambda| + \sum_{\lambda=1}^{\mathrm{N}_h} \ln m_\lambda\right). \tag{5.4.8}$$

The spectrum of eigenvalues is characterised by the spectral density $\rho(m)\,dm$, which gives the average number of fermions with mass in the interval $[m, m+dm)$. When $\mathrm{N}_h \to \infty$ the spectral density is closely related to the Wigner's semicircle

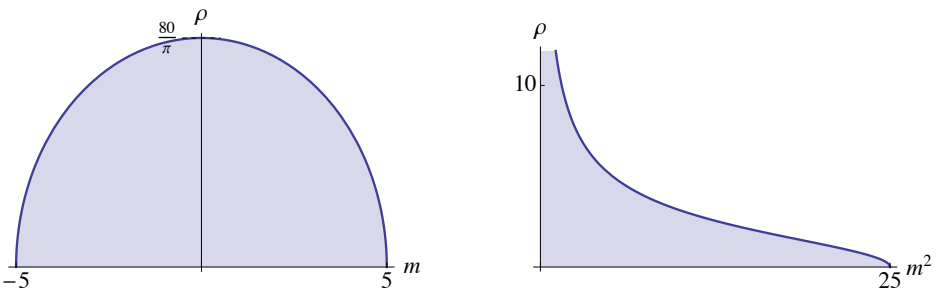

Figure 5.3 – *Typical spectrum of fermion masses for* $m_h = 5$ *and* $\mathrm{N}_h = 100$. *LEFT: The spectral density of the fermion mass matrix* $\mathcal{M}$ *resembles Wigner's semicircle law to leading order in* $1/\mathrm{N}$. *RIGHT: The Marčenko-Pastur law gives the typical distribution for the square of the fermion masses* m^2.

law (SC) and reads:[8]

$$\rho_{\mathrm{SC}}(m) = \frac{4\,\mathrm{N}_h}{\pi m_h^2}\sqrt{m_h^2 - m^2}, \qquad \rho_{\mathrm{MP}}(m^2) = \frac{2\,\mathrm{N}_h}{\pi m_h^2\, m}\sqrt{m_h^2 - m^2}, \quad (5.4.9)$$

for $m \leq m_h$, and zero otherwise; where $m_h^2 = 4\mathrm{N}_h\sigma^2$. For later convenience we have also written the distribution of the square of the fermion masses $\rho_{\mathrm{MP}}(m^2)\,dm^2$, which is a particular case of the so-called Marčenko-Pastur law (MP) [231]. The fact that the spectral density (5.4.9) has a compact support in the large N_h limit does not imply that the probability of finding eigenvalues out from the specified range is zero. The previous expression only gives the *typical* spectrum of a large matrix from the CI-ensemble, but other *atypical* spectra are possible, with the cost of a suppressed probability (see appendix D). In fact, the chance of finding a mass fluctuation outside the boundaries $(0, m_h)$ is determined by the Tracy-Widom distribution [232], which predicts an exponential suppression of the form $\mathrm{e}^{-a\mathrm{N}_h^2}$.

The matrix $\nabla_X\mathcal{M}$ has similar symmetries and structure as $\mathcal{M}$, so we will assume that it can also be identified as an element from the CI-ensemble, but with a standard deviation σ_{D}. In the following, we analyse in detail the perturbative stability of the supersymmetrically truncated sector combining the constraints (5.3.8) with the statistical characterisation of the fermion mass spectrum just discussed.

[8] Actually the spectral density of the CI-ensemble presents a characteristic cleft of width $1/\mathrm{N}_h$ near $m = 0$, where it behaves as $\rho_\chi(m) \sim m$, but we will neglect it as it becomes a subleading effects in the large N_h limit.

5.5 Statistics of supersymmetric vacua

Our starting point in this section are the results of section 5.3.2 regarding the character of AdS supersymmetric critical points. We now incorporate the statistical properties of the fermionic mass spectrum given by random matrix theory as discussed in the previous section, and we will review the results obtained in [212], stating that the probability of obtaining a tachyon-free vacuum after uplifting a supersymmetric AdS minimum to a stable dS is exponentially suppressed. In section 5.6 we will explore more general settings where the dS vacuum is constructed without requiring one sector of the fields to be stabilised at an AdS minimum, and show that the probability of the vacuum being tachyon-free can still be made of order one for certain values of the parameters which determine the distribution of the couplings and the geometry of the moduli space.

5.5.1 Eigenvalue spectrum of the Hessian

Supersymmetric AdS critical points are extrema of the Kähler function, and thus also of the gravitino mass (5.2.6). Moreover, at an AdS supersymmetric critical point, the Hessian of the scalar potential is closely related to the Hessian of the gravitino mass squared $m_{3/2}^2 = \mathrm{e}^G$, which we shall denote by $\mathcal{G}$. After rescaling $\mathcal{G}$ as in (5.2.7), and taking into account that the fields are canonically normalised, it can be shown that

$$\mathcal{G} = \mathbb{1} + \mathcal{M} \qquad \Longrightarrow \qquad \mathcal{H} = \mathcal{G}\big(\mathcal{G} - 3\,\mathbb{1}\big). \tag{5.5.1}$$

As was pointed out in [83, 84], this relation implies a one-to-one correspondence between the supersymmetric AdS maxima and the minima of the gravitino mass, which holds in full generality when gauge interactions are included [84]. To see this point, note that $\mathcal{G}$ is also diagonal in the basis of $Z_{\pm\lambda}$ and the eigenvalues are given by

$$g_{\pm\lambda} = 1 \pm m_\lambda \ . \tag{5.5.2}$$

Thus, the gravitino mass is minimised in field configurations where all the fermion masses satisfy $m_\lambda < 1$, which corresponds precisely to supersymmetric AdS maxima (5.3.12).

Given the relation between $\mathcal{H}$ and the Hessian of the gravitino mass, $\mathcal{G}$, let us start characterising the dependence of the spectral density of $\mathcal{G}$ on the parameter m_h which determines the distribution of the fermion masses. It is easy to see that for $m_h < 1$, the fermion mass distribution is bounded to values smaller than the gravitino mass, and the eigenvalues of $\mathcal{G}$ in (5.5.2) are positive, so those critical points correspond to minima of the gravitino mass. For $m_h > 1$ we have saddle points, and in the limit of very large standard deviations only half of the eigenvalues of $\mathcal{G}$ are positive.

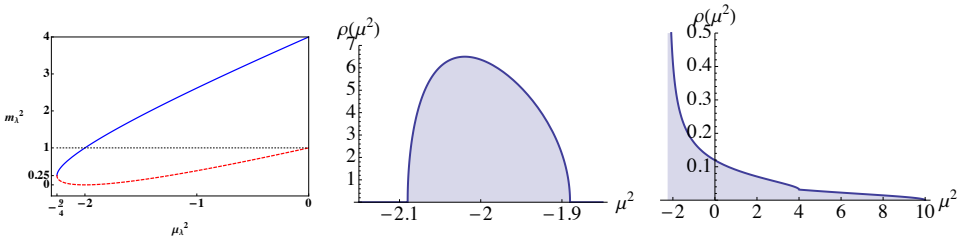

Figure 5.4 *– LEFT: the two branches when inverting eq.* (5.3.11)*. Note that for $m_\lambda < 1$, that is, fermion masses smaller than the gravitino mass, we are in a supersymmetric AdS maximum. CENTER: probability distribution function in* (5.5.4) *for $m_h = 0.1$, where all modes are BF-allowed tachyons. RIGHT: probability distribution function in* (5.5.4) *for $m_h = 3$. In the plots the spectral densities are normalised to unity.*

One can perform a similar analysis of the Hessian, which is given in terms of $\mathcal{G}$ in (5.5.1). Then one can realise that for $m_h < 1$ the typical supersymmetric critical point is an AdS maximum, and as m_h becomes larger, the number of negative eigenvalues approaches zero asymptotically. It is interesting to note that saddle points are the dominant type of critical point for most values of m_h, and moreover, there is no finite value of the standard deviation of the fermions where the typical critical point is a supersymmetric minimum.

Let us now calculate the scalar mass spectrum for a typical supersymmetric critical point. The expression (5.3.11) relating the eigenvalues of the Hessian $\mathcal{H}$ to the fermion masses can be used in combination with the Marčenko-Pastur law (5.4.9) to determine the typical spectral density of $\mathcal{H}$. First, expressing the square of the fermion masses in terms of the eigenvalues of the Hessian μ^2, cf. eq. (5.3.11), we find a multiple-valued function with two branches, which we denote by $m_\pm^2(\mu^2)$, and are displayed in Fig. 5.4. Then, the contribution from each of the branches to the spectral density of $\mathcal{H}$ reads simply:

$$\rho_{\text{MP}}\left(m_\pm^2\right)\left|\frac{dm_\pm^2}{d\mu^2}\right| = \Theta(m_h^2 - m_\pm^2)\,\frac{2}{\pi m_h^2}\sqrt{\frac{m_h^2 - m_\pm^2}{\mu^2 + \frac{9}{4}}}\ , \tag{5.5.3}$$

where $m_\pm^2$ should be understood as functions of μ^2, and the Heaviside theta functions Θ are a reflection of the support of the Marčenko-Pastur distribution for each of the branches. The total eigenvalue density function, given the spectrum of the Hessian, can then be written as [212]:

$$\rho(\mu^2)d\mu^2 = \left[\rho_{\text{MP}}\left(m_+^2\right)\left|\frac{dm_+^2}{d\mu^2}\right| + \rho_{\text{MP}}\left(m_-^2\right)\left|\frac{dm_-^2}{d\mu^2}\right|\right]d\mu^2\ . \tag{5.5.4}$$

Illustrative examples of the distribution (5.5.4) are given in figure 5.4. In those plots we see that this spectrum interpolates between a shifted Wigner semicircle law for $m_h \to 0$, corresponding to AdS maxima, and a shifted version of the Marčenko-Pastur distribution for spectrum for $m_h \gg 1$, corresponding to supersymmetric critical points which are *typically* AdS saddle points.

5.5.2 Uplifting a supersymmetric sector

As we discussed in section 5.3.2, generic uplifting mechanisms require the existence of a supersymmetric minimum for the uplifted critical point to be stable. The fact that there is no region of parameter space where supersymmetric AdS minima are the typical critical point does not imply that they do not exist. Supersymmetric minima require an atypical fluctuation of the smallest fermion mass, $m_1 \geq 2$, cf. eq. (5.3.12). Although in [209] it is argued that metastability is a relatively mild constraint, the probability of such fluctuation is exponentially suppressed [212, 233]:

$$\mathbb{P}(m_1 > 2) \sim \mathrm{e}^{-\frac{8\mathrm{N}^2}{m_h^2}}. \tag{5.5.5}$$

This result implies that when $m_h \lesssim \mathrm{N}$, the vacua obtained using standard uplifting mechanisms will typically lead to tachyonic instabilities. For instance, if the number of fields of the supersymmetric sector is of the order of hundreds $\mathrm{N} \sim 100$, this regime corresponds to configurations where all the chiral fermions are lighter than about a hundred times the mass of the gravitino, $m_\lambda \lesssim 100$ in our units. Nevertheless, as argued in [212], when the masses of the fermions are typically much larger that the gravitino, $m_h \gg \mathrm{N}$, the AdS vacua are typically tachyon-free and thus they are good candidates to construct stable dS vacua using an uplifting mechanism.

As we will now discuss in detail, the results of studying the stability of a supersymmetric sector in isolation no longer hold when it is embedded in a larger model where supersymmetry is already broken. Indeed, the couplings between supersymmetric and non-supersymmetric sectors can stabilise the tachyons which appear when the supersymmetric sector is considered alone. The possibility of such an effect was discussed in detail in the context of $F-$term uplifting mechanisms consistent with the supersymmetric truncation of the supersymmetric sector, [83, 84].

5.6 Stability of non-supersymmetric configurations

As explained in section 5.3.3, moving away from the supersymmetric limit $\gamma = -1$ introduces a rich phenomenology, but more importantly, it is essential to describe inflation and the present vacuum, both needing a stable dS configuration. In this

section we study the probability that uplifting AdS critical points results into stable dS critical points by making use of random matrix theory techniques explained in section 5.4.2. We will argue that the presence of a supersymmetric sector imposes restrictions on the type of couplings that can give rise to these stable configurations. These restrictions appear as bounds on the geometry of the field target manifold. Furthermore, we will derive the supersymmetric mass spectrum for well motivated scenarios in which the heavy sector of the theory is consistently truncated in a supersymmetric way, as described in detail in section 5.4.1.

Already in section 5.3.3 we found necessary conditions for the metastability of non-supersymmetric configurations, and we have seen that not only the projection of the Hessian along the sGoldstino direction imposes constraints [194, 224–226], but also the presence of a supersymmetric sector might help or not in the stability of uplifted dS configurations, as shown in Figs. 5.2 and 5.6. We shall also see that these constraints can be applied not only to dS vacua, but also to inflation, where additional conditions must be satisfied [3, 195, 234].

5.6.1 Separable Kähler function

The simplest class of theories consistent with the supersymmetric truncation of the heavy sector at a configuration H_0^α are characterised by separable Kähler functions of the form [82–85]

$$G(H,\bar{H},L,\bar{L}) = G_h(H,\bar{H}) + G_l(L,\bar{L}), \qquad \text{with} \qquad \partial_\alpha G_h|_{H_0} = 0. \tag{5.6.1}$$

In these theories the Kähler manifold has a cross-product structure $\mathcal{K} = \mathcal{K}_h \otimes \mathcal{K}_l$, and the reduced manifold, $\mathcal{K}_l$, is clearly a totally geodesic submanifold. When the Kähler manifold has this cross-product structure, the stability analysis is particularly simple, since all the bisectional curvatures of the heavy sector are zero $B[X,\lambda] = -R_{X\bar{X}\alpha\bar{\alpha}} = 0$, as well as the matrix $\nabla_X \mathcal{M}_h$, and thus the Hessian matrix has the structure discussed in section 5.3.3. Written in terms of the Hessian of the gravitino mass $\mathcal{G}$, it reads:

$$\mathcal{H}_h = \mathcal{G}\big(\mathcal{G} + 3\gamma\,\mathbb{1}\big). \tag{5.6.2}$$

The scalar mass eigenvalues are given by (5.3.15). Proceeding as in the previous section, we can also calculate the eigenvalue density function for the scalar masses after the uplifting. First, by inverting (5.3.15) we can find an expression for the fermion masses m^2 in terms of the eigenvalues of the Hessian μ^2. The two branches read:

$$m^2_\pm(\mu) = \left[\tfrac{1}{2}(3\gamma+2) \pm \sqrt{\mu^2 + \tfrac{9}{4}\gamma^2}\right]^2 , \qquad \left|\frac{d\,m^2_\pm}{d\,\mu^2}\right| = \frac{|m_\pm|}{\sqrt{\mu^2+\frac{9}{4}\gamma^2}} . \tag{5.6.3}$$

As in the previous section, we use the Marčenko-Pastur law (5.4.9) and substitute it in (5.5.4) to find the eigenvalue density function of the scalar masses. Illustrative examples of the mass distribution are given in Fig. 5.5.

Stability of non-supersymmetric Minkowski vacua

For de Sitter vacua with a small cosmological constant $\gamma \approx 0$, the Hessian of the supersymmetric sector has a very simple expression

$$\mathcal{H}_h = \mathcal{G}^2 \qquad \Longrightarrow \qquad \mu^2_{\pm\lambda} = (m_\lambda \pm 1)^2, \tag{5.6.4}$$

from which is clear that the supersymmetric sector is always stable, with possible zero-modes whenever the function G has a flat direction, i.e. for each fermionic mass satisfying, $m_\lambda = 1$. In the case $m_h < 1$, the spectral density of the scalar masses resembles the Wigner's semicircle law, and the maximum fermion mass is always smaller than the gravitino mass $m_\lambda|_{\max} < 1$. Therefore, typical critical points do not present zero-modes and, moreover, the spectrum of masses of the scalar fields presents a gap, that is, the masses are bounded below by a positive value

$$\mu^2|_{\min} = (m_h - 1)^2 < 1. \tag{5.6.5}$$

Note that in this type of models the lightest scalar field of the supersymmetric sector is lighter than the gravitino. When $m_h > 1$ the spectral density has a closer shape to the Marčenko-Pastur law, and the spectrum typically contains zero-modes.

This case is particularly interesting since it corresponds to Type IIB flux compactifications at tree level, before including loop and non-perturbative corrections. In that case we can identify the (supersymmetric) $H-$sector with the set of complex structure and dilaton fields, while the (non-supersymmetric) $L-$sector would correspond to the set of Kähler moduli. In particular, due to the no-scale structure of the Kähler sector one has $G^{(L)|i\bar{j}} G^{(L)}_i G^{(L)}_{\bar{j}} = 3$, and therefore, when the complex structure and dilaton fields are fixed at a supersymmetric critical point of the potential, we have $\gamma = 0$, that is, a non-supersymmetric Minkowski vacuum, which is precisely the case at hand.

Stability of the supersymmetric sector during inflation

During inflation we have $\gamma > 0$, the size depending on the particular inflationary model under consideration. For instance, for inflationary models based on the standard KKLT construction, the stability of the volume modulus requires the Hubble parameter to be at most of order of the gravitino mass, $\gamma \lesssim 1$ [235], however there are modifications of this framework which allow for values of the Hubble parameter much larger than the gravitino mass $\gamma \gg 1$ [236].

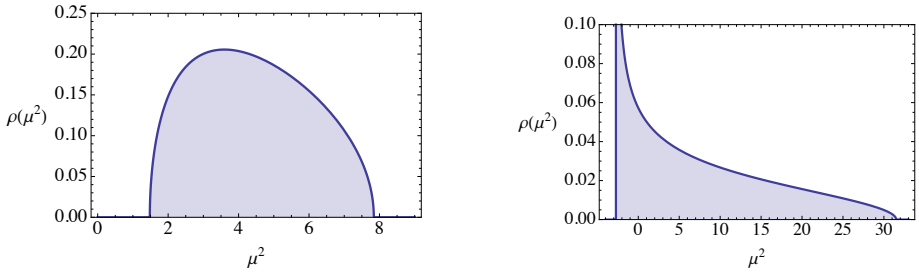

Figure 5.5 – *Probability density function $\rho(\mu^2)$ for the mass spectrum after an uplifting consistent with the supersymmetric truncation of the moduli sector. The masses are measured in units of the gravitino mass. LEFT: When the standard deviation of fermionic masses is small, i.e. $m_h \leq m_{3/2}$, the typical configuration of the truncated sector contains no tachyons (in the plot $m_h = 0.6$, $\gamma = 1.1$). RIGHT: When the standard deviation of fermionic masses satisfies $m_h \geq m_{3/2}$, the typical mass spectrum of truncated fields H_0^α contains tachyons, and it is thus unstable (in the plot $m_h = 3.2$, $\gamma = 1.1$).*

It can be seen from (5.3.16) that only for configurations with all the fermion masses smaller than the gravitino mass, the scalar spectrum is free of tachyons. If the standard deviation of fermion masses is larger than the gravitino mass, the spectrum will necessarily contain tachyons (except for exponentially suppressed configurations that we describe below). Recall that those configurations correspond to AdS maxima in the supersymmetric limit $\gamma \to -1$. The typical mass spectrum for $m_h < 1$ is displayed in the left plot of fig. 5.5. It can be seen that the mass of the lightest scalar field in those configurations is bounded below by

$$\mu_\lambda|^2_{\text{min}} = (m_h - 1)\big(m_h - (3\gamma + 1)\big). \tag{5.6.6}$$

This is quite interesting, since it implies that the corresponding mass gap becomes wider the higher the value of the Hubble parameter, implying that for $\gamma \gg 1$ it becomes very unlikely that one of these configurations becomes tachyonic during inflation. Nevertheless, in this limit the typical mass of the lightest scalar field is still of order of the Hubble parameter H (that is, $\mu^2 \sim \gamma$), implying that there might be situations where is not possible to neglect fluctuations of the fields of the truncated sector during inflation.

In those cases when $m_h > 1$, the fermion with the largest mass is typically heavier than the gravitino and the configuration of the supersymmetric sector H_0^α is unstable, see right plot in fig. 5.5. Let us point out the difference with respect to the results in AdS of the previous section: here the Wigner-type spectra correspond to minima, while the Marčenko-Pastur type always contain tachyonic directions, as opposed to the behaviour for supersymmetric vacua. When $m_h > 1$, there might still be an exponentially suppressed fraction of configurations H_0

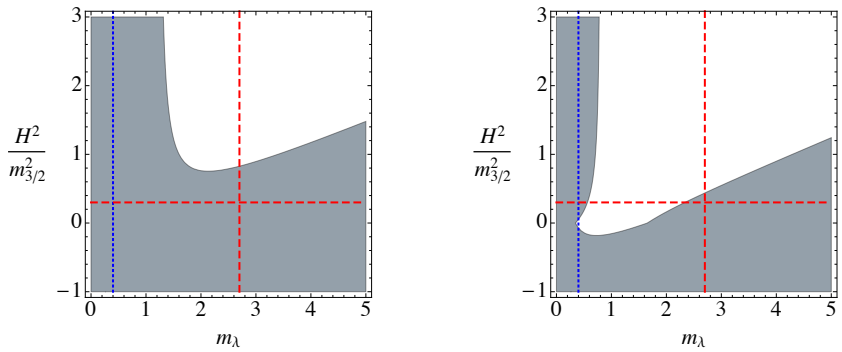

Figure 5.6 *– Stability diagram of a field configuration H_0^α of the supersymmetric sector for a general Kähler function satisfying* (5.4.1)*. The grey area is the region where the necessary conditions for stability* (5.3.8) *are satisfied. The vertical lines correspond to two different values of the mass scale of the truncated sector with $m_h = 0.4$ (blue dotted), $m_h = 2.7$ (red dashed), and the horizontal line to $\gamma = 0.3$. In both diagrams $\partial m_\lambda / \partial X = 0.1$, while the maximum value of the bisectional curvatures is set to $B = 0.2$ (left plot) and $B = -0.2$ (right plot).*

where the $H-$sector remains stable. Indeed, it follows from (5.3.16) that atypical configurations where either the heaviest fermion is lighter than the the gravitino $m_\lambda|_{\rm max} < 1$, or the mass of the lightest fermion satisfies $m_\lambda|_{\rm min} > 3\gamma + 1$, remain tachyon-free. The probability of those fluctuated spectra can be estimated to leading order in $1/\mathrm{N}_h$ and they read (see appendix D):

$$\mathbb{P}\big(m_\lambda|_{\rm min} > 3\gamma + 1\big) \sim \mathrm{e}^{-\frac{2(3\gamma+1)^2}{m_h^2}\mathrm{N}_h^2} \quad , \quad \mathbb{P}\big(m_\lambda|_{\rm max} < 1\big) \sim \mathrm{e}^{-\frac{1}{6}|x|^3\mathrm{N}_h^2} \ , \quad (5.6.7)$$

where $x \equiv -1 + m_h^{-2}$. Note that, in general, the Hubble parameter (and thus γ) will vary during inflation, especially at the end of the slow-roll stage. Therefore, in simple models with a separable Kähler function (5.6.1), a point representing the configuration H_0^α on the stability diagram of fig. 5.1 will move vertically as a reflection of the inflationary trajectory, as we have seen in chapter 4. The different possibilities in the simplest case where the supersymmetric sector contains a single field were studied in [3].

Let us emphasise that in a broad region of the parameter space, the most stable configurations during inflation are those where the fermionic mass spectrum is fully contained within smaller values than the gravitino mass, that is, those that correspond to minima of the gravitino mass.

5.6.2 Quasi-separable Kähler function

There are certain situations in which the terms of the Hessian (5.4.5) spoiling the separable structure, $\nabla_X \mathcal{M}$ and $\mathcal{R}$, become subdominant, and one can write

$$G(H,\bar{H},L,\bar{L}) = G^{(h)}(H,\bar{H}) + G^{(l)}(L,\bar{L}) + \epsilon\, G_{int}(H,\bar{H},L,\bar{L}) \ , \qquad (5.6.8)$$

with $\epsilon \ll 1$. Therefore the mass spectrum can be calculated to leading order in perturbation theory (see appendix C for details), and the necessary conditions for stability (5.3.8) become sufficient. As we will see, this class of couplings have a remarkable property: in a large region of parameter space all vacua remain stable after the uplifting to dS, including those coming from supersymmetric vacua with BF-allowed tachyons. In Fig. 5.2 we have plotted the stability diagram for a particular eigenspace h_λ with four different choices of the parameters. The grey and light blue areas represent, for different choices of $\partial m_\lambda/\partial X$ and $B[X,\lambda] = -R_{X\bar{X}\lambda\bar{\lambda}}$, the region of parameter space where the necessary conditions (5.3.8) are satisfied. Note that, as in the separable case, the minima of the gravitino mass, i.e. when $m_\lambda \leq 1$, still have better stability properties than any other field configuration when $H \gg m_{3/2}$, i.e. for $\gamma \gg 1$, which is relevant for inflation.

The stability diagrams signal the regions of the parameter space where the stability conditions are met. Now, since the horizontal axis describes *one* of the masses of the supersymmetric sector, it is important to take into account that when we describe *distributions*, with $m_h = m_\lambda|_{\max}$, all the masses of the supersymmetric sector are distributed according to the Marčenko-Pastur law along the interval $[0, m_h]$. Therefore, if there is a white region between 0 and m_h for a given γ, our scalar spectrum will contain tachyons, even if a configuration (m_h,γ) falls within the grey region. This is illustrated by the red vertical dashed line in the right plot of Fig. 5.6. A possible loophole to this argument is that of atypical fluctuated fermionic spectra such that all the fermionic masses are contained within a region that remains stable, but as we argued before, in this setup those configurations are exponentially suppressed.

As we discussed in previous sections, the bisectional curvature is zero in KKLT constructions since the moduli space has a direct product structure for the complex structure and Kähler sectors, and is naturally suppressed in Large Volume Scenarios. For the latter type of models, the deviations of the Hessian from the separable case, which are given by the derivative of the fermion mass matrix and the curvature term, are suppressed by powers of volume.

5.6.3 Non-separable Kähler function

In this section we will consider the stability analysis of the truncated sector for a general Kähler function satisfying the condition (5.4.1) for the supersymmetric

truncation of the heavy sector. In this situation the Hessian of the scalar potential along the supersymmetric sector reads

$$\mathcal{H}_h = \mathcal{G}\big(\mathcal{G} + 3\gamma\,\mathbb{1}\big) + \sqrt{3(\gamma+1)}\,\nabla_X\mathcal{G} - 3(\gamma+1)\mathcal{R}. \tag{5.6.9}$$

The parameters $\mu^2_{\pm\lambda}$ can no longer be identified with the squared-masses of the scalar fields of the supersymmetric sector. Therefore, the conditions (5.3.8) are necessary but not sufficient to guarantee the stability of the supersymmetric sector.

In generic situations the bisectional curvatures will take any value, but if the Kähler manifold is regular at H_0, the bisectional curvatures will normally be bounded, $B[X,\lambda] \in [B_{\min}, B_{\max}]$, for all $\lambda = 1,\ldots,\mathrm{N}_h$. The bound on the bisectional curvature (5.3.9) depends on the fermion mass, which in principle can take values between 0 and m_h. Since it must be satisfied for all the fermion masses in the distribution, let us impose it for the most restrictive one, which is $m_\lambda = 0$. In that case the bisectional curvature is constrained by the following bound:

$$B_{\max} \geq -\frac{3\gamma+1}{3(\gamma+1)}\ . \tag{5.6.10}$$

Let us consider this bound in physically relevant situations: almost Minkowski vacua and during inflation. A summary of the bounds can be seen in Tab. 5.1.

Non-supersymmetric Minkowski vacua

For $\gamma \simeq 0$ the Hessian reads

$$\mathcal{H}_{susy} = \mathcal{G}^2 + \sqrt{3}\nabla_X\mathcal{G} - 3\mathcal{R} \ \Rightarrow\ \mu^2_{\pm\lambda} = (m_\lambda \pm 1)^2 + \sqrt{3}\frac{\partial m_\lambda}{\partial X} + 3B[X,\lambda] \geq 0. \tag{5.6.11}$$

First, we know that the present vacuum is described by a small and positive cosmological constant, $\gamma \simeq 0$, so from (5.6.10):

$$B_{\max} \geq -\tfrac{1}{3} \quad \text{(dS vacuum)} \tag{5.6.12}$$

Regarding stable dS vacua, we have seen that small perturbations in the bisectional curvature or derivatives of the masses can cause instabilities or, on the contrary, can improve the stability. In particular, if the parameters satisfy

$$\frac{1}{\sqrt{3}}\sigma_{\mathrm{D}} \leq B_{\min}\ , \tag{5.6.13}$$

the necessary stability conditions (5.3.8) are satisfied by typical vacua, but any other case requires a case by case analysis. For example when $\partial m_\lambda/\partial X > 0$ and $B[X,\lambda] < 0$, uplifting to stable dS vacua strongly constrains m_h to small values, to the point that for $B[X,\lambda] < -1/3$ the only (exponentially suppressed) hope is to have an atypical fluctuated fermionic spectrum such that all the masses fall on the stable region.

$H \ll m_{3/2}$ (Dark energy)	$H \approx m_{3/2}$ (Inflation)	$H \gg m_{3/2}$ (Inflation)
$B_{\max} \geq -\frac{1}{3}$	$B_{\max} \gtrsim -\frac{2}{3}$	$B_{\max} \gtrsim -1$

Table 5.1 – *Necessary conditions for the stability of a typical configuration of the supersymmetric sector. B_{max} is the maximum value that can be attained by the bisectional curvature at (H_0^α, L_0^i) varying the sGoldstino direction z_X, and the direction of the fermion mass eigenstate z_λ.*

Stability of the supersymmetric sector during inflation

Another interesting limit is $H \gg m_{3/2}$, or in other words $\gamma \gg 1$, which is relevant for inflation. In those cases we have the following necessary conditions:

$$H \approx m_{3/2}: \quad B_{\max} \geq -\tfrac{2}{3}\ , \qquad\qquad H \gg m_{3/2}: \quad B_{\max} \geq -1 \tag{5.6.14}$$

When the parameters satisfy

$$m_h \leq 1 + B_{\min} \tag{5.6.15}$$

all the stability constraints (5.3.8) are satisfied by the supersymmetric sector, and thus with probability $P \sim \mathcal{O}(1)$ the supersymmetric sector will remain tachyon-free along the inflationary trajectory. Other situations have to be studied in a case by case basis.

In order for the fluctuations of the supersymmetric sector to be suppressed during inflation with $\gamma \approx 1$ we would have the slightly tighter constraint $B_{\max} \geq -1/2$.

5.7 Conclusions

In this chapter we have extended the analysis of chapter 4 in several aspects. Our results illustrate, in a different context that chapters 2 and 3, the importance of considering the coupling between different sectors of the theory. In this chapter we have studied the type of coupling that is necessary for the stability of a supersymmetric sector which is embedded in a theory with broken supersymmetry. This case falls outside the scope of previous analyses. In particular we have considered $\mathcal{N} = 1$ supergravity models involving only chiral multiplets, and which are consistent with the supersymmetric truncation of the fields preserving supersymmetry. This class of theories is characterised by a Kähler function G satisfying:

$$\partial_\alpha G(H, \bar{H}, L, \bar{L})|_{H_0} = 0 \quad \text{for all} \quad L^i\ ,$$

where L^i are the fields in the supersymmetry breaking sector, and H^α are the fields in the supersymmetric sector which are frozen at a configuration H_0^α. In addition, following [211, 212], we have treated the couplings in the decoupled (supersymmetric) sector as random variables, and we studied the Hessian of the scalar potential using tools from random matrix theory. This analysis is motivated by the supergravity description of the dilaton and complex structure moduli in KKLT constructions and Large Volume Scenarios of type-IIB flux compactifications, where the complex structure and dilaton fields are truncated from the theory before considering the stability of the Kähler moduli, and the truncation is done in a way that leaves supersymmetry approximately unbroken. The stability of the truncated sector is crucial to ensure the viability of cosmological models based on supergravity theories with this structure, both when they describe the present vacuum with a small cosmological constant (dark energy), as well as for scenarios of slow-roll inflation. The main conclusion of our analysis is that, in a broad range of parameters, the configuration of a decoupled supersymmetric sector H_0^α remains free of tachyons with order one probability, $\mathbb{P}_{\text{stable}} \sim \mathcal{O}(1)$.

In order to perform the analysis we have derived the set of necessary conditions (5.3.8) for the stability of the supersymmetric sector. These conditions, which can be seen as constraints on the Kähler potential K and the superpotential W, are expressed in terms of the ratio of the Hubble parameter to the gravitino mass ($\gamma = H^2/m_{3/2}^2$), the masses the chiral fermions and their derivatives along the sGoldstino direction (m_λ and $\partial m_\lambda/\partial X$, respectively), and the bisectional curvatures of the Kähler manifold

$$B[X,\lambda] \equiv -R_{I\bar{J}K\bar{L}}\, z_X^{\ I}\, \bar{z}_X^{\ \bar{J}}\, z_\lambda^{\ K}\, \bar{z}_\lambda^{\ \bar{L}}.$$

Here $R_{I\bar{J}K\bar{L}}$ are the components of the Riemann tensor, z_X is a unit vector along the sGoldstino direction, and the z_λ form an orthonormal basis on the supersymmetric sector. In general, the conditions (5.3.8) are necessary but can not guarantee the stability of the truncated supersymmetric sector. Still, assuming that the number of H^α fields is large, $\mathrm{N}_h \gg 1$, and that there is no large hierarchy between the masses in the truncated sector and the supersymmetry breaking scale (as in LVS), we were able to derive generic constraints on the geometry of the moduli space. In particular, we have shown that positive values of the bisectional curvatures $B[X,\lambda]$ considerably improve the stability of the supersymmetric sector, as is summarised in Table 5.1.

We have analysed in detail a class of models which includes physically relevant scenarios, and for which the conditions (5.3.8) are *necessary and sufficient* for the stability of the supersymmetric sector. This also allows us to perform a detailed study of the scalar mass spectrum and establish specific criteria to achieve tachyon-free spectra. This class of models is characterised by an almost separable Kähler function:

$$G(H,\bar{H},L^i,\bar{L}) = G_h(H,\bar{H}) + G_l(L,\bar{L}) + \epsilon\, G_{mix}(H,\bar{H},L,\bar{L}),$$
$$\text{with} \quad \partial_\alpha G_h|_{H_0} = \partial_\alpha G_{mix}|_{H_0} = 0 \quad \text{and} \quad \epsilon \ll 1.$$

When the parameter ϵ is set to zero, this type of Kähler function describes a large class of no-scale models, and in particular it includes the effective supergravity description of type-IIB compactifications to zero-order in α' and non-perturbative corrections. In the latter case the fields H^α are identified with the dilaton and complex structure moduli, and L^i with the Kähler sector. When ϵ is small but non-zero, this type of theories include models with a similar structure to the effective description of LVS, where the magnitude of ϵ is suppressed by the volume of the compact space, $\epsilon \sim 1/\mathcal{V}$. We have then studied case by case the typical scalar mass distribution of the supersymmetric sector and its dependence on the parameters appearing in (5.3.8). A fundamental quantity that determines the stability of field configurations is the mass scale of the supersymmetric sector in units of the gravitino mass, denoted by m_h. This parameter is defined in such a way that typically the fermion masses are distributed in the interval $m_\lambda \in [0, m_h]$. When the mass scale of the supersymmetric sector is larger than the gravitino mass, $m_h > 1$, the typical spectrum has the following general features:

- At Minkowski vacua the spectrum has no tachyons in the fully separable case ($\epsilon = 0$). However, depending on the parameters, the scalar mass spectrum may contain a significant fraction of fields with can be much lighter than the gravitino.

- Minkowski configurations are very susceptible to become tachyonic when the Kähler function has a small non-separable term, for instance with $\epsilon \sim \mathcal{O}(10^{-1} - 10^{-2})$. However, in LVS the parameter $\epsilon \sim 1/\mathcal{V}$ is exponentially small, and in practice we recover the fully separable case, for which Minkowski vacua are metastable.

- In the regime $m_h \sim \mathcal{O}(1 - 10^2)$, typical field configurations always become tachyonic for sufficiently large values of the ratio $\gamma = H^2/m_{3/2}^2$.

- When the mass scale m_h is much larger than the gravitino mass, $m_h \gg \text{N}_h \gg 1$, the supersymmetric sector is always stable. This is precisely the hierarchy needed in KKLT type of stabilisation mechanisms.

Conversely, when the mass scale of the supersymmetric sector is smaller than the gravitino mass, $m_h < 1$, the spectrum displays a mass gap which protects the stability of the truncated sector. Therefore, provided the non-separable corrections to the Kähler function are small, *the truncated sector is typically stable in the regime $m_h < 1$, regardless of the ratio $H/m_{3/2}$*. Interestingly, in this regime, the configuration of the supersymmetric sector always corresponds to minima of the Kähler function G. The presence of the mass gap in the spectrum suggests that the robust stability properties of the minima of G will survive

in more realistic models where the truncation of the supersymmetric sector is only approximate. Therefore, the minima of the Kähler function can be of interest in exploring new stabilisation mechanisms, for example in cases where the supersymmetric sector is not protected by a large mass hierarchy, as in KKLT constructions, or where the non-separable corrections in the Kähler function are small but not exponentially suppressed as in Large Volume Scenarios.

From our analysis it follows that, in general, *supersymmetric AdS minima are more difficult to realise than the stabilisation of a supersymmetric sector*, when this sector is embedded in a theory where supersymmetry is spontaneously broken. In other words, a decoupled supersymmetric sector can be stabilised at configurations which do not correspond to supersymmetric minima in the absence of supersymmetry breaking. This discussion already allows us to understand the situation in LVS in relation to the random supergravity analysis that we have performed here and the one in [212]. Recall that in LVS all moduli can be stabilised in a very model-independent way, while the fraction of configurations of the complex structure moduli which correspond to supersymmetric minima of the potential induced by fluxes is exponentially small $\mathbb{P}_{\rm susy} \sim \exp(-8{\rm N}_h^2/m_h^2)$ [212]. Conversely, our results indicate that there can be a large fraction of stable configurations for the supersymmetric moduli when the supersymmetry breaking effects are included, $\mathbb{P}_{\rm stable} \sim \mathcal{O}(1)$. This can be easily understood from the discussion in the previous paragraph: by considering only supersymmetric AdS minima of the scalar potential induced by the fluxes, we are discarding most configurations where the supersymmetric sector is stable. Actually, *the non-generic couplings between the supersymmetric sector and the remaining moduli can turn all the Breitenlohner-Freedman allowed tachyons of supersymmetric critical points into stable modes.* In Large Volume Scenarios the no-scale structure of the Kähler sector is fundamental in order to achieve the stabilisation of the supersymmetric moduli.

Many interesting questions regarding the implications for inflation in supergravity arise from our analysis. In particular, it is important to understand which situations lead to a supersymmetric sector with a scalar mass distribution where all the scalar field masses remain much larger than the Hubble scale, since this would describe a stable supersymmetric sector with suppressed isocurvature fluctuations. It would also be useful to study the inflationary constraints in particular models where inflation is driven by a field orthogonal to the sGoldstino direction, or in other words, a field contained in the supersymmetric sector, as in [86]. Last, it is interesting to understand why there is an optimum negative value for $\partial m_\lambda/\partial X$ that optimises the stability, as well as the effect of this term in the scalar spectral density and its physical interpretation.

6

Conclusions

The research performed in the last four years during my PhD has been focused on several aspects of the early universe, but they all have one aspect in common: the effect of additional heavy sectors on the inflationary dynamics. Together with my collaborators, we have explored theoretical and phenomenological aspects of the embedding of inflation in more complete theories, where the presence of heavy degrees of freedom may leave detectable traces in the data. Besides, it is reasonable to contemplate the possibility of having the inflaton coupled to another sector, such as the Standard Model, or a heavy supersymmetric sector, which might be modifying the basic predictions and leaving hints of its presence.

It is common in the literature to assume that very heavy degrees of freedom can be integrated out without further consequences. Fortunately, the effect of these heavy fields is often negligible and the naive effective theory is justified. However, this is not always the case, and it is important to provide a robust theoretical framework which accounts for this effect. Moreover, in some cases a graceful realisation of inflation can be completely ruined by the presence of instabilities in the additional sector that we might just have forgotten about.

In chapter 2 we have computed the change in the CMB power spectrum and primordial bispectrum due to a transient reduction in the speed of sound, and we have seen that even reductions in the speed of sound as mild as a few percent are potentially detectable by current experiments. If the hints of anomalies seen in the CMB were confirmed by future data releases, it is important to understand if they have a primordial origin, and we have taken a step towards this goal. An essential point of the analysis performed in chapter 2 is that the fits to the data are consistently interpreted by an underlying theory. That is, rather than a blind search, we have searched in the region of parameters where the theory and

its predictions are reliable. This was analysed in full detail in chapter 3 from different points of view: we checked several methods and approximations, we double-checked with different Boltzmann codes, and in this process we provided simpler methods to calculate the observational signatures given by effective theories of single-field inflation. This makes a difference with respect to other searches where more significant fits were found, however the underlying physical description breaks down in that regime, and then is practically equivalent to a blind search. On top of that, our predictions go beyond the power spectrum, and have a clearly correlated signal in the bispectrum. This means that if this physical mechanism is able to predict both signatures in good agreement with data, the significance of those predictions increases considerably.

In chapter 4 we considered the effects of an additional supersymmetric sector on supergravity realisations of inflation. We know that if supergravity is to provide an accurate framework for inflation, supersymmetry must be broken by some sector. We analysed the possibility that the inflaton itself is responsible for the breaking of supersymmetry. Naturally, for inflation to be realised, all the other fields must remain stable, and the experimental bounds on isocurvature modes and non-gaussianity constrain their masses and couplings. Since the masses of the supersymmetry preserving fields change during inflation, this imposes constraints on the inflationary regimes and on the parent supergravity. Once these constraints are satisfied, in addition we must face the usual problems of inflation with two fields, which have been explained in the previous chapters. Even more, in supergravity we need to deal with the η problem, and we have showed that in the context of sGoldstino inflation the only option is to fine-tune small field trajectories.

A generalisation from many different perspectives has been given in chapter 5. First of all, we considered the effect of an additional supersymmetric sector with an arbitrarily large number of fields, which allows us to describe it with statistical techniques. We also extended the analysis to more general Kähler functions and found physical scenarios in which those types of couplings naturally arise. More importantly, in previous studies the projection of the mass matrix along the sGoldstino direction was used to derive bounds that constrain inflation. Here we derived complementary bounds by projecting the mass matrix along the supersymmetric directions and imposing stability on the supersymmetric sector. These bounds not only contain the geometry of the field manifold, but also involve the statistical properties of the fermion mass spectrum.

On the other hand, we also stepped aside from the inflationary dynamics in chapter 5 and looked for the existence of stable de Sitter vacua, which supposedly describe the current vacuum in which we live, or alternatively, a hypothetical pre-inflationary stage. We have provided an explanation for an apparent contradiction regarding the stability of uplifted de Sitter vacua in Large

Volume Scenarios. While the uplifting of supersymmetric anti-de Sitter minima to stable de Sitter vacua happens with an exponentially suppressed probability (unless a large mass hierarchy is imposed), uplifting supersymmetric anti-de Sitter maxima results into stable de Sitter vacua with probability exponentially close to one. Moreover, the latter field configurations correspond to minima of the gravitino mass and are stable for arbitrarily large values of the uplifting. In this way, we have seen again that the presence of an additional supersymmetric sector has important consequences in the supergravity description, and we have derived complementary constraints for inflation and the existence of stable de Sitter vacua to those presented in chapter 4 and elsewhere in the literature.

I hope that the results presented in this thesis clarify the role of heavy fields in inflationary cosmology, and that they emphasise the importance of considering their presence in order to provide more consistent, accurate, and complete descriptions and predictions derived from our inflationary models. Future experiments will indeed be sensitive to the interactions of the inflaton with other sectors, and I will keep doing my best to develop new techniques and insights that might help in their detection.

A

Conventions and useful formulae for Kähler manifolds

In this thesis we work in units of $c = \hbar = 1$. Thus, the Plank mass m_{pl} is simply given by

$$m_{pl}^{-2} \equiv \frac{G}{\hbar c} = G, \tag{A.0.1}$$

where G is the Newtons' constant. In general, we will also set the reduced Plank mass M_p to one:

$$M_p^{-2} = 8\pi G = 1, \tag{A.0.2}$$

except in the cases where it is more convenient to keep it explicitly for the sake of clarity. Unless specified, the following notation holds throughout the manuscript: the dot ($\dot{}$) denotes derivative with respect to cosmic time t. The prime ($'$) denotes derivative with respect to the argument. **Boldface** denotes a three-dimensional vector. The meaning of the main indices and symbols used along this thesis is summarised in the table A.1.

Here we compute some useful formulae related to the geometry of Kähler manifolds. First we give the expressions of the Christoffel symbols, Riemann tensor, and other useful quantities in terms of the Kähler function G and its derivatives. In A.1 we also give the explicit expressions in the case where there is a supersymmetric sector and a supersymmetry breaking sector, so we differentiate between the supersymmetric and the sGoldstino directions. In A.2 we focus on the case where the Kähler manifold is a direct product of these two sectors, so that $G_{\rm total} = G_{\rm SUSY} + G_{\cancel{\rm SUSY}}$. In A.3 we rewrite these formulas in terms of the Kähler potential K and the superpotential W, which is especially useful in the case of a vanishing superpotential, since in that case the Kähler function G is ill defined. In

Symbol	Meaning	Chapters
$\mu = 0, 1, 2, 3$	Space-time indices, x^0 being the time coordinate	All
$i = 1, 2, 3$	Spatial indices	All
τ	Conformal time	1-3
ℓ	Multipole, angular scale	1-3
c_s	Speed of sound of the adiabatic mode	1-3
$s = \dot{c}_s/c_s H$	Rate of change of the speed of sound	1-3
X^i	Supersymmetry breaking fields, usually only X	4-5
z^i	Supersymmetry preserving fields	4
$A = (X, i)$	Index running over all scalar fields	4
$b = G^A G_A - 3$	Amount of supersymmetry breaking	4
$3\gamma = G^A G_A - 3$	Amount of supersymmetry breaking	5
$\lambda = 1, \ldots, \mathrm{N}$	Supersymmetric directions	5
m	Chiral fermion mass	5
μ	Eigenvalue of the Hessian of the potential (scalar mass)	5
m_h	Standard deviation of chiral fermion masses (largest mass in the typical spectrum)	5

Table A.1 *– Summary of indices and symbols.*

A.4 we focus on relevant quantities for inflation such as the scalar potential and its derivatives, and in A.5 we take the limit of vanishing superpotential, where we will see that the physical quantities are well defined in the limit $W \to 0$, as it should be. The generic expressions for the Christoffel symbols, the Riemann tensor, and other useful geometrical quantities derived from the Kähler function G are the following:

$$\Gamma^a_{bc} = G^{a\bar{d}}(\partial_b G_{c\bar{d}}) \ , \tag{A.0.3}$$

$$\partial_a G^{b\bar{c}} = -G^{b\bar{d}} G^{e\bar{c}} (\partial_a G_{e\bar{d}}) = -G^{e\bar{c}} \Gamma^b_{ae} \ , \tag{A.0.4}$$

$$\partial_a \Gamma^d_{bc} = G^{d\bar{e}} (\partial_a \partial_b G_{c\bar{e}}) - \Gamma^d_{ae} \Gamma^e_{bc} \ , \tag{A.0.5}$$

$$\nabla_{\bar{a}} \Gamma^d_{bc} = \partial_{\bar{a}} \Gamma^d_{bc} = G^{d\bar{e}} (\partial_{\bar{a}} \partial_b G_{c\bar{e}}) - \Gamma^e_{bc} G^{d\bar{f}} (\partial_{\bar{a}} G_{e\bar{f}}) \ , \tag{A.0.6}$$

$$R_{a\bar{b}c\bar{d}} = R_{c\bar{b}a\bar{d}} = R_{a\bar{d}c\bar{b}} = G_{e\bar{d}} (\partial_{\bar{b}} \Gamma^e_{ac}) = \partial_a \partial_{\bar{b}} G_{c\bar{d}} - \Gamma^e_{ac} (\partial_{\bar{b}} G_{e\bar{d}}) \ , \tag{A.0.7}$$

$$\begin{aligned} \nabla_a \nabla_b G_c = {} & \partial_a \partial_b G_c - G^{\bar{d}} (\partial_a \partial_b G_{c\bar{d}}) - \Gamma^d_{ab} (\partial_c G_d) - \Gamma^d_{bc} (\partial_a G_d) - \Gamma^d_{ac} (\partial_b G_d) \\ & + G_d (\Gamma^e_{ab} \Gamma^d_{ce} + \Gamma^e_{bc} \Gamma^d_{ae} + \Gamma^e_{ac} \Gamma^d_{be}) \ . \end{aligned} \tag{A.0.8}$$

A.1 Supersymmetric and sGoldstino directions

Here we specialise to situations where there is a supersymmetric sector embedded in a theory with supersymmetry breaking, which applies to chapters 4 and 5. Let us assume that the supersymmetry breaking direction is aligned in the X-field (sGoldstino) direction, as in sGoldstino inflation, while all the other fields (z_i) preserve supersymmetry. This translates into the conditions:

$$G_i(X,\bar{X},z_i^{(0)},\bar{z}_{\bar{i}}^{(0)})=0 \quad , \quad G_X(X,\bar{X},z_i^{(0)},\bar{z}_{\bar{i}}^{(0)})\neq 0 \tag{A.1.1}$$

where $(z_i^{(0)},\bar{z}_{\bar{i}}^{(0)})$ is the so-called supersymmetric critical point. This means that any term containing one single derivative of G with respect to the z_i fields will vanish. We introduce the index notation (A,i), where A runs over all fields (X,z_i) and i runs only over the z_i fields. As in chapters 4 and 5, we will consider the case where supersymmetric sector is truncated. In this section we compute all the possible elements of the second and third covariant derivatives, Christoffel symbols and Riemann tensor for the particular case described above. The reader should keep in mind that all expressions are evaluated in the supersymmetric critical point.

- Second covariant derivatives:

$$\begin{aligned}\nabla_X G_X &= \partial_X G_X - \Gamma^X_{XX} G_X \\ \nabla_X G_i &= \nabla_i G_X = 0 \\ \nabla_i G_j &= \partial_i G_j - \Gamma^X_{ij} G_X\end{aligned} \tag{A.1.2}$$

- Christoffel symbols:

$$\begin{aligned}\Gamma^X_{XX} &= G^{X\bar{A}}(\partial_X G_{X\bar{A}}) = G^{X\bar{X}}(\partial_X G_{X\bar{X}}) \\ \Gamma^i_{XX} &= G^{i\bar{A}}(\partial_X G_{X\bar{A}}) = 0 \\ \Gamma^X_{Xi} &= G^{X\bar{A}}(\partial_X G_{i\bar{A}}) = 0 \\ \Gamma^i_{Xj} &= G^{i\bar{A}}(\partial_X G_{j\bar{A}}) = G^{i\bar{k}}(\partial_X G_{j\bar{k}}) \\ \Gamma^X_{ij} &= G^{X\bar{A}}(\partial_i G_{j\bar{A}}) = G^{X\bar{X}}(\partial_i G_{j\bar{X}}) \\ \Gamma^k_{ij} &= G^{k\bar{A}}(\partial_i G_{j\bar{A}}) = G^{k\bar{l}}(\partial_i G_{j\bar{l}})\end{aligned} \tag{A.1.3}$$

Note that the Christoffel symbols with a single spectator index vanish.

- Third covariant derivatives:

$$\begin{aligned}
\nabla_X\nabla_X G_X &= \partial_X\partial_X G_X - G^{\bar{X}}(\partial_X\partial_X G_{X\bar{X}}) - 3\Gamma^X_{XX}(\partial_X G_X) + 3G_X(\Gamma^X_{XX})^2 \\
\nabla_X\nabla_X G_i &= \nabla_X\nabla_i G_X = \nabla_i\nabla_X G_X = 0 \\
\nabla_X\nabla_i G_j &= \partial_X\partial_i G_j - G^{\bar{X}}(\partial_X\partial_i G_{j\bar{X}}) - \Gamma^k_{Xi}(\partial_j G_k) - \Gamma^X_{ij}(\partial_X G_X) - \Gamma^k_{Xj}(\partial_i G_k) \\
&\quad + G_X(\Gamma^k_{Xi}\Gamma^X_{jk} + \Gamma^X_{ij}\Gamma^X_{XX} + \Gamma^k_{Xj}\Gamma^X_{ik}) \\
\nabla_i\nabla_j G_k &= \partial_i\partial_j G_k - G^{\bar{X}}(\partial_i\partial_j G_{k\bar{X}}) - \Gamma^l_{ij}(\partial_k G_l) - \Gamma^l_{jk}(\partial_i G_l) - \Gamma^l_{ik}(\partial_j G_l) \\
&\quad + G_X(\Gamma^l_{ij}\Gamma^X_{kl} + \Gamma^l_{jk}\Gamma^X_{il} + \Gamma^l_{ik}\Gamma^X_{jl})
\end{aligned} \tag{A.1.4}$$

- Riemann tensor:

$$\begin{aligned}
R_{X\bar{X}X\bar{X}} &= \partial_X\partial_{\bar{X}}G_{X\bar{X}} - \Gamma^X_{XX}(\partial_{\bar{X}}G_{X\bar{X}}) \\
R_{X\bar{X}X\bar{\imath}} &= R_{X\bar{X}i\bar{X}} = R_{X\bar{\imath}X\bar{X}} = R_{i\bar{X}X\bar{X}} = 0 \\
R_{X\bar{X}i\bar{\jmath}} &= R_{X\bar{\jmath}i\bar{X}} = R_{i\bar{X}X\bar{\jmath}} = R_{i\bar{\jmath}X\bar{X}} = \partial_X\partial_{\bar{X}}G_{i\bar{\jmath}} - \Gamma^k_{Xi}(\partial_{\bar{X}}G_{k\bar{\jmath}}) \\
R_{X\bar{\imath}j\bar{k}} &= R_{j\bar{\imath}X\bar{k}} = R_{X\bar{k}j\bar{\imath}} = R_{j\bar{k}X\bar{\imath}} = \partial_X\partial_{\bar{\imath}}G_{j\bar{k}} - \Gamma^l_{Xj}(\partial_{\bar{\imath}}G_{l\bar{k}}) \\
R_{i\bar{X}j\bar{k}} &= R_{j\bar{X}i\bar{k}} = R_{i\bar{k}j\bar{X}} = R_{j\bar{k}i\bar{X}} = \partial_i\partial_{\bar{X}}G_{j\bar{k}} - \Gamma^l_{ij}(\partial_{\bar{X}}G_{l\bar{k}}) \\
R_{i\bar{\jmath}k\bar{l}} &= R_{k\bar{\jmath}i\bar{l}} = R_{i\bar{l}k\bar{\jmath}} = R_{k\bar{l}i\bar{\jmath}} = \partial_i\partial_{\bar{\jmath}}G_{k\bar{l}} - \Gamma^m_{ik}(\partial_{\bar{\jmath}}G_{m\bar{l}}) - \Gamma^X_{ik}(\partial_{\bar{\jmath}}G_{X\bar{l}})
\end{aligned} \tag{A.1.5}$$

A.2 Separable Kähler function $G_{\mathbf{total}} = G_{\mathbf{SUSY}} + G_{\mathbf{\cancel{SUSY}}}$

When the Kähler function is of the separable form

$$G(X,\bar{X},z_i,\bar{z}_{\bar{\imath}}) = g(X,\bar{X}) + \tilde{g}(z_i,\bar{z}_{\bar{\imath}})\ , \tag{A.2.1}$$

is clear that all mixed derivatives vanish in every point. Furthermore, we impose the condition (A.1.1) at the supersymmetric critical point. This leads to a enormous simplification of our equations. We rewrite (A.1.2)-(A.1.5) for this simple case:

- Second covariant derivatives:

$$\begin{aligned}
\nabla_X G_X &= \partial_X G_X - \Gamma^X_{XX}G_X \\
\nabla_X G_i &= \nabla_i G_X = 0 \\
\nabla_i G_j &= \partial_i G_j
\end{aligned} \tag{A.2.2}$$

- Christoffel symbols:

$$\begin{aligned}\Gamma^X_{XX} &= G^{X\bar{X}}(\partial_X G_{X\bar{X}})\\ \Gamma^i_{XX} &= \Gamma^X_{Xi} = \Gamma^i_{Xj} = \Gamma^X_{ij} = 0\\ \Gamma^k_{ij} &= G^{k\bar{l}}(\partial_i G_{j\bar{l}})\end{aligned} \tag{A.2.3}$$

- Third covariant derivatives:

$$\begin{aligned}\nabla_X\nabla_X G_X &= \partial_X\partial_X G_X - G^{\bar{X}}(\partial_X\partial_X G_{X\bar{X}}) - 3\Gamma^X_{XX}(\partial_X G_X) + 3G_X(\Gamma^X_{XX})^2\\ \nabla_X\nabla_X G_i &= \nabla_X\nabla_i G_j = 0\\ \nabla_i\nabla_j G_k &= \partial_i\partial_j G_k - \Gamma^l_{ij}(\partial_k G_l) - \Gamma^l_{jk}(\partial_i G_l) - \Gamma^l_{ik}(\partial_j G_l)\end{aligned} \tag{A.2.4}$$

- Riemann tensor:

$$\begin{aligned}R_{X\bar{X}X\bar{X}} &= \partial_X\partial_{\bar{X}}G_{X\bar{X}} - \Gamma^X_{XX}(\partial_{\bar{X}}G_{X\bar{X}})\\ R_{X\bar{X}X\bar{i}} &= R_{X\bar{X}i\bar{X}} = R_{X\bar{i}X\bar{X}} = R_{i\bar{X}X\bar{X}} = 0\\ R_{X\bar{X}i\bar{j}} &= R_{X\bar{j}i\bar{X}} = R_{i\bar{X}X\bar{j}} = R_{i\bar{j}X\bar{X}} = 0\\ R_{X\bar{i}j\bar{k}} &= R_{j\bar{i}X\bar{k}} = R_{X\bar{k}j\bar{i}} = R_{j\bar{k}X\bar{i}} = 0\\ R_{i\bar{X}j\bar{k}} &= R_{j\bar{X}i\bar{k}} = R_{i\bar{k}j\bar{X}} = R_{j\bar{k}i\bar{X}} = 0\\ R_{i\bar{j}k\bar{l}} &= R_{k\bar{j}i\bar{l}} = R_{i\bar{l}k\bar{j}} = R_{k\bar{l}i\bar{j}} = \partial_i\partial_{\bar{j}}G_{k\bar{l}} - \Gamma^m_{ik}(\partial_{\bar{j}}G_{m\bar{l}})\end{aligned} \tag{A.2.5}$$

A.3 Geometric quantities in terms of K and W

It can be useful to have the expressions obtained along this thesis in terms of the Kähler potential K and the superpotential W, especially if we want to analyse the case where $W = 0$. Is a critical case in the sense that many quantities diverge, but not the physical ones, as we will see. Moreover, some models only work in this case (see [86]), so it convenient to have the expressions displayed above in terms of K and W, since the Kähler function G is not well defined in that case.

We introduce the Kähler covariant derivative $D_aW \equiv W_a + K_aW$. Notice that we are not specifying any sectors, so lower case letters run over all possible values. When we distinguish between supersymmetric and non-supersymmetric sectors, as in section A.1, we will reintroduce the notation with capital letters $A = (X, i)$. The Kähler function, first derivatives, and metric are given by:

$$G = K + \ln|W|^2 \ , \ e^G = e^K|W|^2 \tag{A.3.1}$$

$$G_a = K_a + \frac{1}{W}W_a = \frac{1}{W}D_aW \ , \ G_{\bar{b}} = K_{\bar{b}} + \frac{1}{\bar{W}}\bar{W}_{\bar{b}} = \frac{1}{\bar{W}}D_{\bar{b}}\bar{W} \tag{A.3.2}$$

$$G_{a\bar{b}} = K_{a\bar{b}} \ , \ G^{a\bar{b}} = K^{a\bar{b}} \tag{A.3.3}$$

$$G^{\bar{b}} = G^{a\bar{b}}G_a = K^{a\bar{b}}\left(K_a + \frac{1}{W}W_a\right) \tag{A.3.4}$$

Using the previous equations, we can already rewrite the scalar potential:

$$\begin{aligned} V &= e^K\left(K^{a\bar{b}}D_aWD_{\bar{b}}\bar{W} - 3|W|^2\right) \\ &= e^K\left(K^{a\bar{b}}\left(W_a + K_aW\right)\left(\bar{W}_{\bar{b}} + K_{\bar{b}}\bar{W}\right) - 3|W|^2\right) \end{aligned} \tag{A.3.5}$$

The Christoffel symbols and higher derivatives of the Kähler function read:

$$\Gamma^a_{bc} = K^{a\bar{d}}K_{bc\bar{d}} \tag{A.3.6}$$

$$\partial_aG_b = G_{ab} = K_{ab} + \frac{1}{W}W_{ab} - \frac{1}{W^2}W_aW_b \tag{A.3.7}$$

$$\begin{aligned} G_{abc} &= K_{abc} + \frac{1}{W}W_{abc} - \frac{1}{W^2}(W_{ab}W_c + W_{ac}W_b + W_{bc}W_a) \\ &\quad + \frac{2}{W^3}W_aW_bW_c \end{aligned} \tag{A.3.8}$$

Using the above expressions we can compute the second and third covariant derivatives, given by:

$$\nabla_aG_b = K_{ab} + \frac{1}{W}W_{ab} - \frac{1}{W^2}W_aW_b - K^{c\bar{d}}K_{ab\bar{d}}\left(K_c + \frac{1}{W}W_c\right) \tag{A.3.9}$$

$$\begin{aligned} \nabla_a\nabla_bG_c &= K_{abc} + \frac{1}{W}W_{abc} - \frac{1}{W^2}(W_{ab}W_c + W_{ac}W_b + W_{bc}W_a) + \frac{2}{W^3}W_aW_bW_c \\ &\quad - K^{e\bar{d}}K_{abc\bar{d}}\left(K_e + \frac{1}{W}W_e\right) - K^{d\bar{e}}K_{ab\bar{e}}\left(K_{cd} + \frac{1}{W}W_{cd} - \frac{1}{W^2}W_cW_d\right) \\ &\quad - K^{d\bar{e}}K_{bc\bar{e}}\left(K_{ad} + \frac{1}{W}W_{ad} - \frac{1}{W^2}W_aW_d\right) \\ &\quad - K^{d\bar{e}}K_{ca\bar{e}}\left(K_{bd} + \frac{1}{W}W_{bd} - \frac{1}{W^2}W_bW_d\right) \\ &\quad + \left(K_d + \frac{1}{W}W_d\right)K^{e\bar{f}}K^{d\bar{g}}\left(K_{ab\bar{f}}K_{ce\bar{g}} + K_{bc\bar{f}}K_{ae\bar{g}} + K_{ca\bar{f}}K_{be\bar{g}}\right) \end{aligned} \tag{A.3.10}$$

Last, the Riemann tensor is simply written as:

$$R_{a\bar{b}c\bar{d}} = K_{a\bar{b}c\bar{d}} - K^{e\bar{f}}K_{ac\bar{f}}K_{\bar{b}\bar{d}e} \ . \tag{A.3.11}$$

A.4 Physical quantities relevant for inflation

In this section we compute several quantities that are relevant for the inflationary dynamics, such as the scalar potential and the elements of the mass matrix. In this section we will use the index notation $A = (X, i)$, where X represents the sGoldstino and i runs over the spectator fields z_i. First we will write explicitly the scalar potential and its first and second derivatives, and then we evaluate the scalar potential and its first derivative at the supersymmetric critical point, where the spectator sector satisfies $G_i(X, z_0^i) = 0$. These expressions can be used to calculate, for instance, the 'potential' slow-roll parameters, and get an estimate of the viability and amount of inflation for a given model. One can also study the stability of a given model as we did in chapters 4 and 5 by using the elements of the mass matrix. In any case, it is convenient to have the explicit expressions for cases where the superpotential vanishes at one or more points of the inflationary trajectory. The generic lengthy expressions for the scalar potential and its derivatives are the following:

$$V = e^K \left(K^{A\bar{B}} \left(W_A + K_A W \right) \left(\bar{W}_{\bar{B}} + K_{\bar{B}} \bar{W} \right) - 3|W|^2 \right) , \tag{A.4.1}$$

$$\begin{aligned} V_A = {} & e^K \left(K_A + \frac{1}{W} W_A \right) \left(K^{B\bar{C}} \left(W_B + K_B W \right) \left(\bar{W}_{\bar{C}} + K_{\bar{C}} \bar{W} \right) - 2|W|^2 \right) \\ & + e^K K^{B\bar{C}} \left(K_{\bar{C}} \bar{W} + \bar{W}_{\bar{C}} \right) \Big(W K_{AB} + W_{AB} \\ & - \frac{1}{W} W_A W_B - K^{D\bar{E}} K_{AB\bar{E}} \left(K_D W + W_D \right) \Big) , \end{aligned} \tag{A.4.2}$$

$$\begin{aligned} \nabla_A \nabla_{\bar{B}} V = {} & \left[K_{A\bar{B}} - \left(K_A + \frac{1}{W} W_A \right) \left(K_{\bar{B}} + \frac{1}{\bar{W}} \bar{W}_{\bar{B}} \right) \right] V \\ & + \left(K_A + \frac{1}{W} W_A \right) V_{\bar{B}} + \left(K_{\bar{B}} + \frac{1}{\bar{W}} \bar{W}_{\bar{B}} \right) V_A + e^K |W|^2 K^{C\bar{D}} \\ & \times \left[K_{AC} + \frac{1}{W} W_{AC} - \frac{1}{W^2} W_A W_C - K^{E\bar{F}} K_{AC\bar{F}} \left(K_E + \frac{1}{W} W_E \right) \right] \\ & \times \left[K_{\bar{B}\bar{D}} + \frac{1}{\bar{W}} \bar{W}_{\bar{B}\bar{D}} - \frac{1}{\bar{W}^2} \bar{W}_{\bar{B}} \bar{W}_{\bar{D}} - K^{E\bar{F}} K_{\bar{B}\bar{D}E} \left(K_{\bar{F}} + \frac{1}{\bar{W}} \bar{W}_{\bar{F}} \right) \right] \\ & + e^K |W|^2 \Bigg[\left(-K_{A\bar{B}C\bar{D}} + K^{E\bar{F}} K_{AC\bar{F}} K_{\bar{B}\bar{D}E} \right) K^{C\bar{H}} K^{I\bar{D}} \\ & \times \left(K_{\bar{H}} + \frac{1}{\bar{W}} \bar{W}_{\bar{H}} \right) \left(K_I + \frac{1}{W} W_I \right) + K_{A\bar{B}} \Bigg] , \end{aligned}$$

$$
\begin{aligned}
\nabla_A\nabla_B V = &\left[K_{AB} + \frac{1}{W}W_{AB} - \frac{1}{W^2}W_A W_B - K^{E\bar{F}}K_{AB\bar{F}}\left(K_E + \frac{1}{W}W_E\right)\right.\\
&\left.-\left(K_A + \frac{1}{W}W_A\right)\left(K_B + \frac{1}{W}W_B\right)\right]V\\
&+\left(K_A + \frac{1}{W}W_A\right)V_B + \left(K_B + \frac{1}{W}W_B\right)V_A + 2e^K|W|^2\\
&\times\left[K_{AB} + \frac{1}{W}W_{AB} - \frac{1}{W^2}W_A W_B - K^{E\bar{F}}K_{AB\bar{F}}\left(K_E + \frac{1}{W}W_E\right)\right]\\
&+ e^K|W|^2K^{C\bar{D}}\left(K_{\bar{D}} + \frac{1}{\bar{W}}\bar{W}_{\bar{D}}\right)\\
&\times\left[K_{ABC} + \frac{1}{W}W_{ABC} - \frac{1}{W^2}(W_{AB}W_C + W_{AC}W_B + W_{BC}W_A)\right.\\
&+\frac{2}{W^3}W_A W_B W_C - K^{E\bar{D}}K_{ABC\bar{D}}\left(K_E + \frac{1}{W}W_E\right)\\
&-K^{D\bar{E}}K_{AB\bar{E}}\left(K_{CD} + \frac{1}{W}W_{CD} - \frac{1}{W^2}W_C W_D\right)\\
&-K^{D\bar{E}}K_{BC\bar{E}}\left(K_{AD} + \frac{1}{W}W_{AD} - \frac{1}{W^2}W_A W_D\right)\\
&-K^{D\bar{E}}K_{CA\bar{E}}\left(K_{BD} + \frac{1}{W}W_{BD} - \frac{1}{W^2}W_B W_D\right) + \left(K_D + \frac{1}{W}W_D\right)\\
&\left.\times K^{E\bar{F}}K^{D\bar{G}}\left(K_{AB\bar{F}}K_{CE\bar{G}} + K_{BC\bar{F}}K_{AE\bar{G}} + K_{CA\bar{F}}K_{BE\bar{G}}\right)\right]
\end{aligned}
$$

When there is a spectator sector sitting on a supersymmetric critical point $z_i^{(0)}$, this configuration is also a critical point of the scalar potential, $V_i\big|_0 = 0$, as it has been extensively reviewed along this thesis. However, this is not the case for the supersymmetry breaking sector. As we have done previously, considering the supersymmetry breaking aligned with the sGoldstino direction X, the scalar potential and its first derivative in the sGoldstino direction will be:

$$
V\big|_0 = e^K\left(K^{X\bar{X}}\left(W_X + K_X W\right)\left(\bar{W}_{\bar{X}} + K_{\bar{X}}\bar{W}\right) - 3|W|^2\right) \tag{A.4.3}
$$

$$
\begin{aligned}
V_X\big|_0 = &\, e^K\left(K_X + \frac{1}{W}W_X\right)\left(K^{X\bar{X}}\left(W_X + K_X W\right)\left(\bar{W}_{\bar{X}} + K_{\bar{X}}\bar{W}\right) - 2|W|^2\right),\\
&+ e^K K^{X\bar{X}}\left(K_{\bar{X}}\bar{W} + \bar{W}_{\bar{X}}\right)\left(WK_{XX} + W_{XX} - \frac{1}{W}W_X W_X\right.\\
&\left.- K^{X\bar{X}}K_{XX\bar{X}}\left(K_X W + W_X\right)\right).
\end{aligned} \tag{A.4.4}
$$

A.5 Vanishing superpotential

Now we will take the limit $W \to 0$. This does not make sense in sGoldstino inflation, since in that limit we would also have $W_X = 0$, which implies that the field X preserves supersymmetry. Hence, we cannot have sGoldstino inflation when $W = 0$. But this limit might be very interesting to analyse models for which the superpotential vanishes during inflation. Notice that once we fix the superpotential, we are fixing (some of) the fields. If the superpotentials of different sectors are combined by multiplication, the dynamical sector can be used to stabilise the inflationary trajectory, and this is precisely the functional freedom claimed in [86]. We assume that supersymmetry is broken in at least one of the sectors, which is necessary in order to achieve inflation or stable dS vacua.

Then, in the special case of $W \to 0$ the divergent terms of the expressions in section A.4 cancel with each other. The expressions for the scalar potential and its first derivative in this case read:

$$V \xrightarrow{W\to 0} e^K K^{A\bar{B}} W_A \bar{W}_{\bar{B}} \ , \tag{A.5.1}$$

$$V_A \xrightarrow{W\to 0} e^K K^{B\bar{C}} \bar{W}_{\bar{C}} \left[W_A K_B + K_A W_B + W_{AB} - K^{D\bar{E}} K_{AB\bar{E}} W_D \right] \ . \tag{A.5.2}$$

B

Small spectral index for inflection point inflation

In this appendix we derive the spectral index and power spectrum for inflection point inflation, following the work of Refs. [197, 198]. To a very good approximation the inflationary observables only depend on the η-parameter at the extremum and on the number of efolds.

Expanding the potential around the inflection point gives:

$$V = V_0(1 + 1/2\eta_0\phi^2 + C_3\phi^3 + C_4\phi^4 + ...), \tag{B.0.1}$$

with $\eta, C_3 < 0$ so that the field rolls towards the minimum at positive ϕ values. Inflation ends when the C_3 term becomes important, and $\epsilon \approx 1$, which occurs for field values $\phi_f^2 \sim \sqrt{2}/(3|C_3|)$. We can calculate the number of efolds

$$N \approx \int_{\phi_f}^{\phi_N} \frac{V}{V'} = \frac{1}{\eta} \log \left[\frac{\phi}{3C_3\phi + \eta} \right]_{\phi_f}^{\phi_N}, \tag{B.0.2}$$

where we used $V \approx V_0$ above. The above expression can be inverted to obtain the value of the inflaton field N efolds before the end of inflation ϕ_N:

$$\phi_N = \frac{\mathrm{e}^{N\eta_0}\eta_0/C3}{-3(\mathrm{e}^{N\eta_0} - 1) - \eta_0/(\phi_f C_3)} \approx \frac{\mathrm{e}^{N\eta_0}\eta_0}{-3C_3(\mathrm{e}^{N\eta_0} - 1)}, \tag{B.0.3}$$

where in the second step we used $\eta_0/(\phi_f|C_3|) \ll 1$. This is a good approximation as $\eta_0 \ll 1$ is fine-tuned, whereas C_3, and thus ϕ_f, is naturally of order one[1]. Note

[1] To be precise, $C_3 = \mathcal{O}(1)$ for $\phi_0 \sim 1$. For minima at smaller field values generically C_3 increases, as a sharper turnover of the potential is needed. We do not find valid solutions for minima for $\phi_0 \gg 1$ much larger, as then other local minima at smaller field values appear.

that in this limit, the number of efolds is independent of the end of inflation, as ϕ_f has dropped out of the equation. As a result the inflationary observables are insensitive to the precise coefficients of the higher order terms in (B.0.1). The spectral index is

$$n_s \approx 1 + 2\eta \approx 1 + 2\eta_0 + 12C_3\phi_N \approx 1 - 2\eta_0 \frac{(\mathrm{e}^{\eta_0 N} + 1)}{(\mathrm{e}^{\eta_0 N} - 1)}, \tag{B.0.4}$$

where we used that $\epsilon \ll \eta$. For $N < 50 - 60$ one finds $n_s < 0.92 - 0.93$ for the whole range of $|\eta_0| \lesssim 10^{-2}$. The power spectrum is

$$P_\zeta = \frac{V}{150\pi^2\epsilon} = \frac{3C_3^2 \mathrm{e}^{-4N\eta_0}(\mathrm{e}^{N\eta_0} - 1)^4 V_0}{25\pi^2\eta_0^4} \tag{B.0.5}$$

with $P_\zeta = 4 \times 10^{-10}$ measured by WMAP.

For the first example (4.3.12) in the text $\eta_0 = 0$ and $C_3 = -2.39$. For $\eta_0 = 0$, the expressions simplify to

$$n_s - 1 = -\frac{4}{N}, \quad P_\zeta = \frac{3C_3^2 N^4 V_0}{25\pi^2}, \quad (\text{for } \eta_0 = 0). \tag{B.0.6}$$

Choosing $N = 50$ this gives $n_s = 0.92$ and $V_0 = 9 \times 10^{-16}$. The second example (4.3.13) has $C_3 = -3.69$, and gives the same spectral index and similar $V_0 = 4 \times 10^{-16}$. The gravitino mass today is related to the inflationary scale via $m_{3/2} = \mathrm{e}^{K/2} W|_{\min} \sim 10^2 \sqrt{V_0} \sim 10^{-7}$, far above the electroweak scale.

C

Mass spectrum for quasi-separable Kähler functions

In this appendix we derive in full detail the result in (5.3.8), which refers to the eigenvalues of the mass matrix for Kähler functions with small coupling between the heavy and light sectors. On our way, we will also derive the result (5.3.15) for separable Kähler functions. We will briefly review eigenvalue perturbation theory and afterwards we will use this to calculate the perturbed eigenvalues for a Kähler function with a small mixing between sectors.

Perturbation theory

Consider a $n \times n$ square matrix $\mathcal{H} = \mathcal{H}_0 + \delta\mathcal{H}$, where the elements of $\delta\mathcal{H}$ are much smaller than those of $\mathcal{H}_0$. Let us denote by $\lambda_{0,i}$ the eigenvalues of $\mathcal{H}_0$, where $i = 1, \ldots, n$. The eigenvectors corresponding to those eigenvalues form a orthonormal basis with which one can build the matrix A that diagonalises $\mathcal{H}_0$, that is, $A^\dagger \mathcal{H}_0 A = \mathrm{diag}(\lambda_{0,1}, \ldots, \lambda_{0,n})$.

Then, to first order in perturbation theory, the eigenvalues of the full matrix $\mathcal{H}$ will be given by

$$\lambda_i = \left(A^\dagger \mathcal{H} A\right)_{ii} = \lambda_{0,i} + \left(A^\dagger \delta\mathcal{H} A\right)_{ii} \ , \quad i = 1, \ldots, n \ . \tag{C.0.1}$$

In other words, the perturbation over the 'bare' eigenvalues is given by the diagonal elements of the matrix perturbation in the basis that diagonalises the 'bare' matrix.

Perturbed eigenvalues

Let us consider a Kähler function with a small interaction term:

$$G(H, \bar{H}, L, \bar{L}) = A(H, \bar{H}) + B(L, \bar{L}) + \epsilon\, G_{\mathrm{int}}(H, \bar{H}, L, \bar{L}) \ , \tag{C.0.2}$$

where the heavy fields H^α are consistently truncated at the supersymmetric critical point such that[1]

$$A_\alpha|_{H_0} = G_{\mathrm{int},\alpha}|_{H_0} = 0 \ . \tag{C.0.3}$$

We take the Hessian matrix in section 5.6.3, given by

$$\mathcal{H} = \begin{pmatrix} \nabla_\alpha \nabla_{\bar\beta} V & \nabla_{\bar\alpha}\nabla_{\bar\beta} V \\ \nabla_\alpha \nabla_\beta V & \nabla_{\bar\alpha}\nabla_\beta V \end{pmatrix} \ , \tag{C.0.4}$$

where the elements are

$$\nabla_\alpha \nabla_\beta V|_{H_0,L_0} = \mathrm{e}^G \left[(3\gamma+2)\nabla_\alpha G_\beta + G^i\, \nabla_i(\nabla_\alpha G_\beta)\right] \ , \tag{C.0.5}$$
$$\nabla_\alpha \nabla_{\bar\beta} V|_{H_0,L_0} = \mathrm{e}^G \left[\delta_{\alpha\bar\beta}\,(3\gamma+1) + \delta^{\gamma\bar\sigma}\,(\nabla_\gamma G_\alpha)\left(\nabla_{\bar\sigma} G_{\bar\beta}\right) - R_{i\bar j\alpha\bar\beta}\, G^i G^{\bar j}\right] \ .$$

We define the following quantities

$$M_{\alpha\beta} \equiv \nabla_\alpha G_\beta = M_{\beta\alpha} \ , \tag{C.0.6}$$
$$Y_{\alpha\beta} \equiv G^i\, \nabla_i\,(\nabla_\alpha G_\beta) = Y_{\beta\alpha} \ , \tag{C.0.7}$$
$$\Omega_{\alpha\beta} \equiv -R_{i\bar j\alpha\bar\beta}\, G^i G^{\bar j} = \Omega^*_{\bar\beta\alpha} \ . \tag{C.0.8}$$

One can recast the mass matrix $\mathcal{H}$ in terms of the quantities above as follows:

$$\mathcal{H} = \mathcal{H}_0 + \delta\mathcal{H} \tag{C.0.9}$$

$$= \begin{pmatrix} \mathrm{e}^G[(3\gamma+1)\mathbb{I}+MM^*] & \mathrm{e}^G(3\gamma+2)M^* \\ \mathrm{e}^G(3\gamma+2)M & \mathrm{e}^G[(3\gamma+1)\mathbb{I}+M^*M] \end{pmatrix} + \begin{pmatrix} \mathrm{e}^G\Omega & \mathrm{e}^G Y^* \\ \mathrm{e}^G Y & \mathrm{e}^G\Omega^T \end{pmatrix} \ ,$$

where the terms in $\delta\mathcal{H}$ are at least $\mathcal{O}(\epsilon)$. It is possible to perform a transformation of the fields such that

$$M \to \tilde M = UMU^t \ , \tag{C.0.10}$$

where U is a unitary matrix. Thanks to the symmetry properties of M, we can easily see that MM^* is hermitian and hence it can be diagonalised by a unitary transformation. In fact, given the transformation of M, it follows that

$$\tilde M\tilde M^* = U(MM^*)U^\dagger = \mathrm{diag}\left(|\lambda_1|^2\,\mathbb{I}_{n_1},\ldots,|\lambda_p|^2\,\mathbb{I}_{n_p}\right) = \tilde M^*\tilde M \ , \tag{C.0.11}$$

where n_p is the degeneracy of the p^{th} eigenvalue. A direct consequence of the above is that $[\tilde M, \tilde M\tilde M^*] = 0$, which means that $\tilde M$ is block diagonal in the subspaces of dimension n_p. We will denote each of those matrices by $\tilde M_p$, satisfying

$$\tilde M_p \tilde M_p^* = |\lambda_p|^2\,\mathbb{I}_{n_p} \ . \tag{C.0.12}$$

[1] Since we want to impose this condition for any value of ϵ, both functions A and G_{int} must satisfy this requirement.

Now, since $\tilde{M}_p$ is complex and symmetric, we can always rewrite it using Takagi's factorisation, i.e. $\tilde{M}_p = V_p D_p V_p^t$, where V_p is unitary and D_p is diagonal and contains the non-negative square roots of the eigenvalues of $\tilde{M}_p \tilde{M}_p^\dagger$. Therefore, we may write $\tilde{M}_p = V_p V_p^t |\lambda_p|$.

Given this, let us transform the fields once more, in such a way that the resulting transformation of $\tilde{M}_p$ is the following:

$$\tilde{M}_p \to M'_p = V_p^\dagger \tilde{M}_p V_p^* = |\lambda_p|\, \mathbb{I}_{n_p} \ . \tag{C.0.13}$$

After this, the unperturbed mass matrix $\mathcal{H}_0$ has been rewritten in a new basis as $\mathcal{H}'_0$ and it has four blocks of size $n_1 + \cdots + n_p$ each, which are diagonal:

$$\mathcal{H}'_0 = \mathrm{e}^G \left(\begin{array}{ccc|ccc} \left[(3\gamma{+}1){+}|\lambda_1|^2\right]\mathbb{I}_{n_1} & & \mathbf{0} & (3\gamma{+}2)|\lambda_1|\mathbb{I}_{n_1} & & \mathbf{0} \\ & \ddots & & & \ddots & \\ \mathbf{0} & & \left[(3\gamma{+}1){+}|\lambda_p|^2\right]\mathbb{I}_{n_p} & \mathbf{0} & & (3\gamma{+}2)|\lambda_p|\mathbb{I}_{n_p} \\ \hline (3\gamma{+}2)|\lambda_1|\mathbb{I}_{n_1} & & \mathbf{0} & \left[(3\gamma{+}1){+}|\lambda_1|^2\right]\mathbb{I}_{n_1} & & \mathbf{0} \\ & \ddots & & & \ddots & \\ \mathbf{0} & & (3\gamma{+}2)|\lambda_p|\mathbb{I}_{n_p} & \mathbf{0} & & \left[(3\gamma{+}1){+}|\lambda_p|^2\right]\mathbb{I}_{n_p} \end{array}\right) . \tag{C.0.14}$$

We can always solve the eigenvalue problem by rearranging rows and columns to make the mass matrix block diagonal, with blocks of dimension $2n_1, \ldots, 2n_p$ given by the matrices

$$\mathcal{H}'^{(p)}_0 = \mathrm{e}^G \begin{pmatrix} \left(|\lambda_p|^2{+}3\gamma{+}1\right)\mathbb{I}_{n_p} & (3\gamma{+}2)|\lambda_p|\,\mathbb{I}_{n_p} \\ (3\gamma{+}2)|\lambda_p|\,\mathbb{I}_{n_p} & \left(|\lambda_p|^2{+}3\gamma{+}1\right)\mathbb{I}_{n_p} \end{pmatrix} \ ; \ \mathcal{H}'_0 = \begin{pmatrix} \mathcal{H}'^{(1)}_0 & & \mathbf{0} \\ & \ddots & \\ \mathbf{0} & & \mathcal{H}'^{(p)}_0 \end{pmatrix} . \tag{C.0.15}$$

Although the previous step is not strictly necessary, it makes the eigenvalue problem more visual to solve it for each subspace. We easily find the eigenvalues, which have degeneracy n_p each, and are given by:

$$m^2_{p\pm} = \mathrm{e}^G \left[|\lambda_p|^2 + (3\gamma+1) \pm |\lambda_p|(3\gamma+2)\right] = \mathrm{e}^G \left[\left(|\lambda_p| \pm \tfrac{1}{2}(3\gamma+2)\right)^2 - \tfrac{9}{4}\gamma^2\right] . \tag{C.0.16}$$

This is the result displayed in (5.3.15). The eigenvectors are easily found through the equation:

$$\begin{pmatrix} \mp(3\gamma{+}2)|\lambda_p|\,\mathbb{I}_{n_p} & (3\gamma{+}2)|\lambda_p|\,\mathbb{I}_{n_p} \\ (3\gamma{+}2)|\lambda_p|\,\mathbb{I}_{n_p} & \mp(3\gamma{+}2)|\lambda_p|\,\mathbb{I}_{n_p} \end{pmatrix} \begin{pmatrix} \vec{a} \\ \vec{b} \end{pmatrix} = \begin{pmatrix} 0 \\ 0 \end{pmatrix} \Rightarrow \vec{u}_\pm = \frac{1}{\sqrt{2}|\vec{a}|} \begin{pmatrix} \vec{a} \\ \pm\vec{a} \end{pmatrix} . \tag{C.0.17}$$

Since they are n_p times degenerate, we can choose n_p linearly independent vectors with a 1 in the p^{th} position and 0 in all the others. The matrix of change of basis is then:

$$A_p = \frac{1}{\sqrt{2}} \begin{pmatrix} \mathbb{I}_{n_p} & \mathbb{I}_{n_p} \\ \mathbb{I}_{n_p} & -\mathbb{I}_{n_p} \end{pmatrix} \Rightarrow A_p^\dagger \mathcal{H}'^{(p)}_0 A_p = \mathrm{diag}\left(m^2_{p+}\mathbb{I}_{n_p}, m^2_{p-}\mathbb{I}_{n_p}\right) \ . \tag{C.0.18}$$

We can repeat the process for every block, which leads to our final result for the unperturbed mass matrix:

$$A = \begin{pmatrix} A_1 & & \mathbf{0} \\ & \ddots & \\ \mathbf{0} & & A_p \end{pmatrix} \quad \Rightarrow \quad A^\dagger {\mathcal{H}'}_0 A = \begin{pmatrix} m_{1+}^2 \mathbb{I}_{n_1} & & & & \mathbf{0} \\ & m_{1-}^2 \mathbb{I}_{n_1} & & & \\ & & \ddots & & \\ & & & m_{p+}^2 \mathbb{I}_{n_p} & \\ \mathbf{0} & & & & m_{p-}^2 \mathbb{I}_{n_p} \end{pmatrix} . \tag{C.0.19}$$

We retrieve the results of [3, 83, 84]. Now we just have to express the perturbed matrix $\delta\mathcal{H}'$ in the basis that diagonalises $\mathcal{H}'_0$. In order to do that, we first have to undo the rearranging of rows and columns we did to get to (C.0.15) (which was only done to facilitate the discussion). Instead of rearranging, it is easy to realise that the matrix that diagonalises $\mathcal{H}'_0$ (C.0.14) is

$$A = \frac{1}{\sqrt{2}} \begin{pmatrix} \mathbb{I}_{n_1+\cdots+n_p} & \mathbb{I}_{n_1+\cdots+n_p} \\ \mathbb{I}_{n_1+\cdots+n_p} & -\mathbb{I}_{n_1+\cdots+n_p} \end{pmatrix} \Rightarrow \tag{C.0.20}$$

$$\Rightarrow A^\dagger {\mathcal{H}'}_0 A = \operatorname{diag}\left(m_{1+}^2 \mathbb{I}_{n_1}, \ldots, m_{p+}^2 \mathbb{I}_{n_p}, m_{1-}^2 \mathbb{I}_{n_1}, \ldots, m_{p-}^2 \mathbb{I}_{n_p}\right) \tag{C.0.21}$$

Therefore, the leading order correction to the eigenvalues (C.0.16) due to $\delta\mathcal{H}$ in (C.0.9) is given by the diagonal elements of the matrix

$$A^\dagger \delta\mathcal{H}\, A = \frac{1}{2} \begin{pmatrix} \mathrm{e}^G \left[\left(\Omega + \Omega^T\right) + \left(Y + Y^*\right)\right] & \mathrm{e}^G \left[\left(\Omega - \Omega^T\right) + \left(Y - Y^*\right)\right] \\ \mathrm{e}^G \left[\left(\Omega - \Omega^T\right) - \left(Y - Y^*\right)\right] & \mathrm{e}^G \left[\left(\Omega + \Omega^T\right) - \left(Y + Y^*\right)\right] \end{pmatrix} , \tag{C.0.22}$$

where Ω and Y have been already transformed according to (C.0.10) and (C.0.13). To first order in perturbation theory, the eigenvalues then read

$$m_{p\pm}^2 + \delta m_{p\pm}^2 = \mathrm{e}^G \left\{ |\lambda_p|^2 + (3\gamma + 1) + \omega_p \pm \left[|\lambda_p| (3\gamma + 2) + y_p \right] \right\} , \tag{C.0.23}$$

where $\omega_p \equiv \Omega_{pp} = -R_{i\bar{j}p\bar{p}} G^i G^{\bar{j}}$ and $y_p \equiv \mathrm{Re}(Y_{pp}) = \mathrm{Re}(G^i \nabla_i \left(\nabla_p G_p\right))$. This result was derived in [3] for the simplest case of one light field and one heavy field[2]. We emphasise that the quantities y_p and ω_p are $\mathcal{O}(\epsilon)$ plus subleading corrections.

The matrix Y is proportional to the derivative of the fermion mass matrix along the sGoldstino direction. Thus, in the basis that diagonalises M, it is possible to show that $\tilde{Y} \equiv V^\dagger Y V^*$ has the following form:

$$\tilde{Y} = V(G^i \partial_i X) V^t = G^i \partial_i D + G^i \left(V^\dagger \partial_i V D - D\, V^t \partial_i V^* \right) , \tag{C.0.24}$$

where the unitary matrix V and the diagonal matrix D are the ones appearing in the Takagi's factorisation of $M = V D V^t$. Due to the unitarity of V the

[2] The notation in [3] is slightly different, it corresponds to $\gamma \to b/3$.

matrix $V^\dagger \partial_i V$ is anti-hermitian, and therefore its diagonal elements have to be purely imaginary $(V^\dagger \partial_i V)_{pp} = \mathrm{i}\theta_p$, with $\theta_p \in \mathbb{R}$. Then, in this basis, the diagonal elements of Y read

$$\tilde{Y}_{pp} = G^i \left(\partial_i |\lambda_p| + \mathrm{i}2|\lambda_p|\theta_p\right), \qquad \Longrightarrow \qquad y_p = G^i \partial_i |\lambda_p|, \tag{C.0.25}$$

implying that the perturbation y_p is just proportional to the derivative of the eigenvalues of the matrix M along the sGoldstino direction. In order to reduce the dependence on $|\lambda_p|$ of the perturbation parameters appearing in the Hessian, it is convenient to write it in terms of $\tilde{y}_p \equiv y_p/|\lambda_p|$, which gives

$$\tilde{y}_p = G^i \partial_i \log(|\lambda_p|). \tag{C.0.26}$$

D

Random matrix theory: atypical minima and fluctuated spectra

In this appendix we review the expressions for the probability of occurrence of atypical fluctuations of the fermionic mass spectra, and in particular we will discuss the probability distribution of the lightest and largest fermion masses. As we have discussed in the main text, the CI-ensemble describes the statistical properties of the fermion mass matrix $\mathcal{M}_h$ for a generic supersymmetric sector. The CI-ensemble is closely related to the set of Wishart ensemble [212] for which there are many results in the literature regarding fluctuated spectra. For this reason we will first discuss known results for the Wishart ensemble, and then we will translate them into properties of the fermion mass spectrum in a generic supersymmetric sector.

D.1 Typical spectral density in the Wishart and CI-ensembles

The Wishart ensemble is composed of matrices of the form $\mathcal{W} = AA^\dagger$, where A is an $\mathrm{N} \times \mathrm{M}$ real or complex matrix, (with $\mathrm{M} \geq \mathrm{N}$), whose entries are independent and identically distributed (i.i.d.) random variables drawn from a statistical distribution with zero mean and variance σ^2: $A_{IJ} \in \Omega(0, \sigma)$. When $\Omega = N(0, \sigma)$ is a normal distribution, the joint probability distribution for the ordered eigenvalues $\lambda_1 \leq \lambda_2, \ldots, \leq \lambda_{\mathrm{N}}$ is [237]:

$$f(\lambda_1, \ldots, \lambda_{\mathrm{N}}) = \mathcal{C} \ \exp\left(-\frac{\beta}{2}\left(\frac{1}{\sigma^2}\sum_{a=1}^{\mathrm{N}}\lambda_a \ - 2\sum_{a<b}^{\mathrm{N}}\ln|\lambda_b - \lambda_a| - \xi\sum_{a=1}^{\mathrm{N}}\ln\lambda_a\right)\right), \tag{D.1.1}$$

where $\xi = \mathrm{M} - \mathrm{N} + 1 - 2/\beta$, and $\beta = 1, 2$ for real and complex matrices, respectively. The eigenvalue density function for the eigenvalues of $\mathcal{W}$ is given by the Marčenko-Pastur law [231],

$$\rho_{\mathrm{MP}}(\lambda)\, d\lambda = \frac{1}{2\pi\sigma^2\lambda}\sqrt{(\lambda_+ - \lambda)(\lambda - \lambda_-)}\, d\lambda\,, \tag{D.1.2}$$

with support $\lambda \in [\lambda_-, \lambda_+]$, where

$$\lambda_\pm = \mathrm{N}\sigma^2(1 \pm \sqrt{\eta})^2\,, \qquad \text{and} \qquad \eta = \mathrm{M}/\mathrm{N} \geq 1. \tag{D.1.3}$$

The joint probability distribution for the eigenvalues of a matrix from the CI-ensemble was given in eq. (5.4.8). As was pointed out in [212], the p.d.f. of the eigenvalues of a Wishart matrix (D.1.1) reduces to (5.4.8) for $\beta = 1$ and $\mathrm{M} = \mathrm{N} + 1$ after doing the identification $\lambda_a \leftrightarrow m_\lambda^2$. Moreover, as we are interested in results to leading leading order in $1/\mathrm{N}$, it will be sufficient to discuss square Wishart matrices $\mathrm{N} \approx \mathrm{M}$. Thus, since the fermion mass matrix of a generic supergravity theory can be identified with an element of the CI ensemble, the typical spectral density of the fermion masses m_λ is also given by the Marčenko-Pastur law (D.1.2) with $\lambda = m^2$. Defining $m_h \equiv 2\sqrt{\mathrm{N}}\sigma$, we have that to leading order in $1/\mathrm{N}$ the fermion mass density function reads:

$$\rho_{\mathrm{MP}}(m^2)dm^2 = \frac{2\mathrm{N}}{\pi m_h^2 m}\sqrt{m_h^2 - m^2}\; dm^2, \tag{D.1.4}$$

which has support in $m^2 \in \left[0, m_h^2\right]$. In the limit $\mathrm{N} \to \infty$ the bounds of the support coincide with the expectation value of the smallest and largest fermionic masses squared, m_1^2 and m_{N}^2 respectively [238]:

$$\mathbb{E}[m_1^2] = 0, \qquad\qquad \mathbb{E}[m_{\mathrm{N}}^2] \approx m_h^2. \tag{D.1.5}$$

D.2 Probability distributions of the limiting eigenvalues

Let us first discuss the probability distribution of the largest eigenvalue λ_{N} of a real, almost square Wishart matrix, $\beta = 1$, $\mathrm{M} \approx \mathrm{N}$. The probability distribution of large $\mathcal{O}(\sigma^2\mathrm{N})$ fluctuations of λ_{N} far to the right and left of its mean value λ_+ was calculated in [239] and [240], respectively, and are given by:

$$\begin{aligned} t > \lambda_+ : \quad \lim_{\mathrm{N}\to\infty} \mathbb{P}(\lambda_{\mathrm{N}} \leq t) \quad &\approx \quad 1 - \left(\sqrt{x+1} + \sqrt{x}\right)^{2\mathrm{N}} \mathrm{e}^{-2\mathrm{N}\sqrt{x(x+1)}}, \\ t < \lambda_+ : \quad \lim_{\mathrm{N}\to\infty} \mathbb{P}(\lambda_{\mathrm{N}} \leq t) \quad &\approx \quad \left(\frac{x+1}{\sqrt{\mathrm{e}}}\right)^{\frac{\mathrm{N}^2}{2}} \mathrm{e}^{-\frac{\mathrm{N}^2}{4}(1-x)^2}\,, \end{aligned} \tag{D.2.1}$$

where $x \equiv (t - \lambda_+)/\lambda_+$. For large but finite values of N, the maximum value of a Wishart matrix, λ_{N}, *typically* fluctuates over a region of size $\mathcal{O}(\sigma^2\,\mathrm{N}^{-1/3})$,

and the corresponding probability distribution for these small fluctuations can be approximated by the Tracy-Widom distribution $F_1(x)$ [232, 238, 239]:

$$\mathbb{P}(\lambda_{\rm N} \leq t) \approx F_1\left(\frac{\eta^{\frac{1}{12}}{\rm N}^{\frac{1}{3}}\,(t-\lambda_+)}{\sigma^{\frac{2}{3}}\lambda_+^{\frac{2}{3}}}\right) \approx F_1\left(2^{\frac{2}{3}}{\rm N}^{\frac{2}{3}}\,\frac{(t-\lambda_+)}{\lambda_+}\right)\,, \tag{D.2.2}$$

where we have used the leading order approximation $\eta = 1$ and $\lambda_+ \approx 4{\rm N}\sigma^2$ for large N in the last step. For the asymptotic values of the probability (D.2.2), see [241] and references therein. In particular, to leading order in $1/{\rm N}$, the cumulative probability distribution for the largest eigenvalue $\lambda_{\rm N}$ is:

$$\begin{aligned} t > \lambda_+ : \quad \lim_{{\rm N}\to\infty} \mathbb{P}_{\rm N}(\lambda_{\rm N} \leq t) &\approx 1 - \frac{{\rm e}^{-\frac{4}{3}{\rm N}\,x^{\frac{3}{2}}}}{8\sqrt{\pi}\,{\rm N}\,x^{\frac{3}{2}}} - \frac{{\rm e}^{-\frac{8}{3}{\rm N}\,x^{\frac{3}{2}}}}{64\pi{\rm N}\,x^{\frac{3}{2}}}\,, \\ t < \lambda_+ : \quad \lim_{{\rm N}\to\infty} \mathbb{P}_{\rm N}(\lambda_{\rm N} \leq t) &\approx \tau_1\,\frac{{\rm e}^{-\frac{1}{6}|x|^3{\rm N}^2}}{2^{\frac{1}{24}}{\rm N}^{\frac{1}{24}}|x|^{\frac{1}{16}}}\,, \end{aligned} \tag{D.2.3}$$

where $\tau_1 \equiv 2^{-11/48}\,{\rm e}^{\frac{1}{2}\zeta'(-1)}$, and $\zeta'(-1) = -0.16542\ldots$ is the derivative of the Riemann zeta function evaluated at -1. It is easy to check that, to leading order in $\mathcal{O}(1/{\rm N})$, the probability distributions in (D.2.1) match the tail behaviour of the Tracy-Widom distributions in the limit $t \to \lambda_+$, which describes small fluctuations.

The probability distribution of the smallest eigenvalue λ_1 of a real square Wishart matrix was derived in [233]. To leading order in $1/{\rm N}$ it is given by:

$$\lim_{{\rm N}\to\infty} \mathbb{P}(\lambda_1 \geq t) \approx \frac{\lambda_+}{4{\rm N}^2}\,{\rm e}^{-\frac{2{\rm N}^2}{\lambda_+}t}. \tag{D.2.4}$$

D.3 Probability of atypical field configurations

In chapter 5, where we study the stability of a consistently truncated supersymmetric sector in models with a separable Kähler function, we estimated the probability of occurrence of critical points with light scalar fields, i.e. with a mass $\mu^2|_{min} \leq \alpha^2$, in the regime $m_h < 1-\alpha$. We argued that, due to the relation between scalar and fermion masses, this would require the largest fermion mass fermion to be above its expectation value $m_{\rm N} \geq 1-\alpha > m_h$. Using the first equation in (D.2.1), and taking into account the relation between the Wishart and CI-ensembles, we find

$$1-\alpha > m_h : \quad \lim_{{\rm N}\to\infty} \mathbb{P}(m_{\rm N} \geq 1-\alpha) \approx \left(\sqrt{x+1}+\sqrt{x}\right)^{2{\rm N}}\,{\rm e}^{-2{\rm N}\sqrt{x(x+1)}}, \tag{D.3.1}$$

with $x = (1-\alpha)^2/m_h^2 - 1$. The Tracy-Widom distribution gives an accurate description in the limit $m_h \to (1-\alpha)^-$, where the deviations of $m_{\rm N}$ from its

expectation value are small.

Now we turn to the stability of the truncated sector, when the sector surviving the truncation is driving a period of inflation, and the Kähler function is also separable in the two sectors. In general, in the regime where the mass scale m_h is larger than the gravitino mass ($m_h > 1$), the typical spectrum contains tachyons (see right plot in Fig. 5.5). However, as illustrated by (5.6.7), there is an exponentially suppressed probability that the fermionic spectrum fluctuates in such a way that the scalar spectrum is free of tachyons. There are two possible types of configurations which are non-tachyonic: when the fermion masses are confined to $m_\lambda < 1$, or to $m_\lambda > 3\gamma + 1$, for all λ. It is interesting to check, for a configuration with a Hubble parameter given in terms of γ, in what regime of parameters one of these types of critical points becomes more abundant than the other. The probability that the fermion masses are bounded below as $m_\lambda \geq 3\gamma+1$, can be calculated from (D.2.4):

$$\lim_{\mathrm{N}\to\infty} \mathbb{P}\Big(m_1 \geq 3\gamma + 1\Big) \approx \frac{m_h^2}{4\mathrm{N}^2}\, \mathrm{e}^{-\frac{2\mathrm{N}^2}{m_h^2}(3\gamma+1)^2} \ . \tag{D.3.2}$$

On the other hand, the probability that the fermion masses are bounded above by $m_{\mathrm{N}} = 1$, also to leading order in $1/\mathrm{N}$, can be derived from the second equation in (D.2.1):

$$\lim_{\mathrm{N}\to\infty} \mathbb{P}\Big(m_{\mathrm{N}} \leq 1\Big) \approx \frac{\mathrm{e}^{-\mathrm{N}^2/4}}{m_h^{\mathrm{N}^2}}\, \mathrm{e}^{-\frac{\mathrm{N}^2}{4}\left(2-\frac{1}{m_h^2}\right)^2} \ . \tag{D.3.3}$$

From the above expressions it can be seen that a fluctuation to a minimum of the Kähler function, where all $m_\lambda < 1$ (D.3.2), becomes more likely than a fluctuation to large fermionic masses (D.3.3) when the following condition is satisfied:

$$(2+\mathrm{N}^2)\log m_h - 2\log(2\mathrm{N}) - \frac{2\mathrm{N}^2}{m_h^2}(1+3\gamma)^2 + \frac{\mathrm{N}^2}{4} + \frac{\mathrm{N}^2}{4}\left(2-\frac{1}{m_h^2}\right)^2 < 0 \ . \tag{D.3.4}$$

In the regime $\mathrm{N} \gg m_h \gg 1$ and with γ comparable to m_h the expression above simplifies to

$$\gamma^2 \geq \frac{m_h^2}{18}\left(\log m_h + \tfrac{5}{4}\right) \ , \tag{D.3.5}$$

which can be rewritten in terms of the Hubble parameter as follows:

$$H^2 \gtrsim \frac{m_h m_{3/2}}{3\sqrt{2}}\sqrt{\log m_h + \frac{5}{4}} \ . \tag{D.3.6}$$

We can see that regardless of the value of the mass scale of the supersymmetric sector m_h, there is always a value of the Hubble parameter (D.3.6) above which the largest fraction of stable critical points corresponds to a minimum of the Kähler function. This is particularly important for cosmological models which

involve a large inflationary scale H and a low supersymmetry breaking scale. This result depends strongly on the value of the mass scale of the supersymmetric sector m_h which, as we discussed in section 5.4.2, should also be regarded as a random variable depending on the value of the gravitino mass $m_{3/2}$, and its statistical properties should be derived from a realistic characterisation of the String Theory Landscape.

Bibliography

[1] A. Achucarro, V. Atal, P. Ortiz, and J. Torrado, *Localized correlated features in the CMB power spectrum and primordial bispectrum from a transient reduction in the speed of sound*, *Phys.Rev.* **D89** (2014) 103006, [arXiv:1311.2552].

[2] A. Achucarro, V. Atal, B. Hu, P. Ortiz, and J. Torrado, *Inflation with moderately sharp features in the speed of sound: GSR and in-in formalism for power spectrum and bispectrum*, *Phys.Rev.* **D90** (2014) 023511, [arXiv:1404.7522].

[3] A. Achucarro, S. Mooij, P. Ortiz, and M. Postma, *Sgoldstino inflation*, *JCAP* **1208** (2012) 013, [arXiv:1203.1907].

[4] K. Sousa and P. Ortiz, *Perturbative Stability along the Supersymmetric Directions of the Landscape*, arXiv:1408.6521.

[5] A. H. Guth, *The Inflationary Universe: A Possible Solution to the Horizon and Flatness Problems*, *Phys.Rev.* **D23** (1981) 347–356.

[6] A. A. Starobinsky, *Relict Gravitation Radiation Spectrum and Initial State of the Universe. (In Russian)*, *JETP Lett.* **30** (1979) 682–685.

[7] A. A. Starobinsky, *Dynamics of Phase Transition in the New Inflationary Universe Scenario and Generation of Perturbations*, *Phys.Lett.* **B117** (1982) 175–178.

[8] K. Sato, *First Order Phase Transition of a Vacuum and Expansion of the Universe*, *Mon.Not.Roy.Astron.Soc.* **195** (1981) 467–479.

[9] A. D. Linde, *A New Inflationary Universe Scenario: A Possible Solution of the Horizon, Flatness, Homogeneity, Isotropy and Primordial Monopole Problems*, *Phys.Lett.* **B108** (1982) 389–393.

[10] A. Albrecht and P. J. Steinhardt, *Cosmology for Grand Unified Theories with Radiatively Induced Symmetry Breaking*, *Phys.Rev.Lett.* **48** (1982) 1220–1223.

[11] A. A. Penzias and R. W. Wilson, *A Measurement of excess antenna temperature at 4080-Mc/s*, *Astrophys.J.* **142** (1965) 419–421.

[12] W. H. Kinney, *TASI Lectures on Inflation*, `arXiv:0902.1529`.

[13] D. Baumann, *TASI Lectures on Inflation*, `arXiv:0907.5424`.

[14] D. Langlois, *Lectures on inflation and cosmological perturbations*, *Lect.Notes Phys.* **800** (2010) 1–57, [`arXiv:1001.5259`].

[15] V. Mukhanov, *Physical foundations of cosmology*. Cambridge Univ. Pr., Cambridge, UK, 2005.

[16] D. H. Lyth and A. R. Liddle, *The primordial density perturbation: Cosmology, inflation and the origin of structure*. Cambridge Univ. Pr., Cambridge, UK, 2009.

[17] A. Friedmann, *On the Possibility of a world with constant negative curvature of space*, *Z.Phys.* **21** (1924) 326–332.

[18] G. Lemaître, *Un Univers homogène de masse constante et de rayon croissant rendant compte de la vitesse radiale des nébuleuses extra-galactiques*, *Annales de la Societe Scietifique de Bruxelles* **47** (1927) 49–59.

[19] H. P. Robertson, *Kinematics and World-Structure*, *Ap. J.* **82** (Nov., 1935) 284.

[20] H. P. Robertson, *Kinematics and World-Structure II.*, *Ap. J.* **83** (Apr., 1936) 187.

[21] H. P. Robertson, *Kinematics and World-Structure III.*, *Ap. J.* **83** (May, 1936) 257.

[22] A. G. Walker, *On milne's theory of world-structure*, *Proceedings of the London Mathematical Society* **s2-42** (1937), no. 1 90–127, [`http://plms.oxfordjournals.org/content/s2-42/1/90.full.pdf+html`].

[23] J. M. Bardeen, P. J. Steinhardt, and M. S. Turner, *Spontaneous Creation of Almost Scale - Free Density Perturbations in an Inflationary Universe*, *Phys.Rev.* **D28** (1983) 679.

[24] V. F. Mukhanov, *Gravitational Instability of the Universe Filled with a Scalar Field*, *JETP Lett.* **41** (1985) 493–496.

[25] M. Sasaki, *Large Scale Quantum Fluctuations in the Inflationary Universe*, *Prog.Theor.Phys.* **76** (1986) 1036.

[26] T. Bunch and P. Davies, *Quantum Field Theory in de Sitter Space: Renormalization by Point Splitting*, *Proc.Roy.Soc.Lond.* **A360** (1978) 117–134.

[27] U. H. Danielsson, *A Note on inflation and transPlanckian physics*, *Phys.Rev.* **D66** (2002) 023511, [hep-th/0203198].

[28] B. R. Greene, K. Schalm, G. Shiu, and J. P. van der Schaar, *Decoupling in an expanding universe: Backreaction barely constrains short distance effects in the CMB*, *JCAP* **0502** (2005) 001, [hep-th/0411217].

[29] P. D. Meerburg, J. P. van der Schaar, and P. S. Corasaniti, *Signatures of Initial State Modifications on Bispectrum Statistics*, *JCAP* **0905** (2009) 018, [arXiv:0901.4044].

[30] M. G. Jackson and K. Schalm, *Model Independent Signatures of New Physics in the Inflationary Power Spectrum*, *Phys.Rev.Lett.* **108** (2012) 111301, [arXiv:1007.0185].

[31] **WMAP** Collaboration, C. Bennett *et. al.*, *Nine-Year Wilkinson Microwave Anisotropy Probe (WMAP) Observations: Final Maps and Results*, *Astrophys.J.Suppl.* **208** (2013) 20, [arXiv:1212.5225].

[32] **Planck Collaboration** Collaboration, P. Ade *et. al.*, *Planck 2013 results. I. Overview of products and scientific results*, arXiv:1303.5062.

[33] V. F. Mukhanov and G. V. Chibisov, *Quantum Fluctuation and Nonsingular Universe. (In Russian)*, *JETP Lett.* **33** (1981) 532–535.

[34] **Planck collaboration** Collaboration, P. Ade *et. al.*, *Planck 2013 results. XV. CMB power spectra and likelihood*, arXiv:1303.5075.

[35] T. Allen, B. Grinstein, and M. B. Wise, *Nongaussian Density Perturbations in Inflationary Cosmologies*, *Phys.Lett.* **B197** (1987) 66.

[36] T. Falk, R. Rangarajan, and M. Srednicki, *The Angular dependence of the three point correlation function of the cosmic microwave background radiation as predicted by inflationary cosmologies*, *Astrophys.J.* **403** (1993) L1, [astro-ph/9208001].

[37] A. Gangui, F. Lucchin, S. Matarrese, and S. Mollerach, *The Three point correlation function of the cosmic microwave background in inflationary models*, *Astrophys.J.* **430** (1994) 447–457, [astro-ph/9312033].

[38] V. Acquaviva, N. Bartolo, S. Matarrese, and A. Riotto, *Second order cosmological perturbations from inflation*, *Nucl.Phys.* **B667** (2003) 119–148, [astro-ph/0209156].

[39] J. M. Maldacena, *Non-Gaussian features of primordial fluctuations in single field inflationary models*, *JHEP* **0305** (2003) 013, [astro-ph/0210603].

[40] L. Keldysh, *Diagram technique for nonequilibrium processes*, *Zh.Eksp.Teor.Fiz.* **47** (1964) 1515–1527.

[41] S. Weinberg, *Quantum contributions to cosmological correlations*, *Phys.Rev.* **D72** (2005) 043514, [hep-th/0506236].

[42] V. F. Mukhanov, *CMB-slow, or how to estimate cosmological parameters by hand*, *Int.J.Theor.Phys.* **43** (2004) 623–668, [astro-ph/0303072].

[43] U. Seljak and M. Zaldarriaga, *A Line of sight integration approach to cosmic microwave background anisotropies*, *Astrophys.J.* **469** (1996) 437–444, [astro-ph/9603033].

[44] A. Lewis, A. Challinor, and A. Lasenby, *Efficient computation of CMB anisotropies in closed FRW models*, *Astrophys.J.* **538** (2000) 473–476, [astro-ph/9911177].

[45] J. Lesgourgues, *The Cosmic Linear Anisotropy Solving System (CLASS) I: Overview*, arXiv:1104.2932.

[46] D. Blas, J. Lesgourgues, and T. Tram, *The Cosmic Linear Anisotropy Solving System (CLASS) II: Approximation schemes*, *JCAP* **1107** (2011) 034, [arXiv:1104.2933].

[47] **Planck Collaboration** Collaboration, P. Ade *et. al.*, *Planck 2013 results. XVI. Cosmological parameters*, arXiv:1303.5076.

[48] **Planck Collaboration** Collaboration, P. Ade *et. al.*, *Planck 2013 Results. XXIV. Constraints on primordial non-Gaussianity*, arXiv:1303.5084.

[49] D. Spergel, R. Flauger, and R. Hlozek, *Planck Data Reconsidered*, arXiv:1312.3313.

[50] E. Komatsu, D. N. Spergel, and B. D. Wandelt, *Measuring primordial non-Gaussianity in the cosmic microwave background*, *Astrophys.J.* **634** (2005) 14–19, [astro-ph/0305189].

[51] M. Bucher, B. Van Tent, and C. S. Carvalho, *Detecting Bispectral Acoustic Oscillations from Inflation Using a New Flexible Estimator*, arXiv:0911.1642.

[52] J. Fergusson, M. Liguori, and E. Shellard, *The CMB Bispectrum*, *JCAP* **1212** (2012) 032, [arXiv:1006.1642].

[53] D. Babich, P. Creminelli, and M. Zaldarriaga, *The Shape of non-Gaussianities*, *JCAP* **0408** (2004) 009, [astro-ph/0405356].

[54] L. Senatore, K. M. Smith, and M. Zaldarriaga, *Non-Gaussianities in Single Field Inflation and their Optimal Limits from the WMAP 5-year Data*, *JCAP* **1001** (2010) 028, [arXiv:0905.3746].

[55] **BICEP2 Collaboration** Collaboration, P. Ade *et. al.*, *BICEP2 I: Detection Of B-mode Polarization at Degree Angular Scales*, arXiv:1403.3985.

[56] D. H. Lyth, *What would we learn by detecting a gravitational wave signal in the cosmic microwave background anisotropy?*, *Phys.Rev.Lett.* **78** (1997) 1861–1863, [hep-ph/9606387].

[57] M. J. Mortonson and U. Seljak, *A joint analysis of Planck and BICEP2 B modes including dust polarization uncertainty*, arXiv:1405.5857.

[58] R. Flauger, J. C. Hill, and D. N. Spergel, *Toward an Understanding of Foreground Emission in the BICEP2 Region*, arXiv:1405.7351.

[59] A. Zee, *A Broken Symmetric Theory of Gravity*, *Phys.Rev.Lett.* **42** (1979) 417.

[60] L. Smolin, *Towards a Theory of Space-Time Structure at Very Short Distances*, *Nucl.Phys.* **B160** (1979) 253.

[61] B. Spokoiny, *Inflation and generation of perturbations in broken symmetric theory of gravity*, *Phys.Lett.* **B147** (1984) 39–43.

[62] D. Salopek, J. Bond, and J. M. Bardeen, *Designing Density Fluctuation Spectra in Inflation*, *Phys.Rev.* **D40** (1989) 1753.

[63] F. L. Bezrukov and M. Shaposhnikov, *The Standard Model Higgs boson as the inflaton*, *Phys.Lett.* **B659** (2008) 703–706, [arXiv:0710.3755].

[64] J. Garcia-Bellido, D. G. Figueroa, and J. Rubio, *Preheating in the Standard Model with the Higgs-Inflaton coupled to gravity*, *Phys.Rev.* **D79** (2009) 063531, [arXiv:0812.4624].

[65] F. Bezrukov, D. Gorbunov, and M. Shaposhnikov, *On initial conditions for the Hot Big Bang*, *JCAP* **0906** (2009) 029, [arXiv:0812.3622].

[66] J. Barbon and J. Espinosa, *On the Naturalness of Higgs Inflation*, *Phys.Rev.* **D79** (2009) 081302, [arXiv:0903.0355].

[67] D. P. George, S. Mooij, and M. Postma, *Quantum corrections in Higgs inflation: the real scalar case*, *JCAP* **1402** (2014) 024, [arXiv:1310.2157].

[68] F. Quevedo, *Lectures on string/brane cosmology*, *Class.Quant.Grav.* **19** (2002) 5721–5779, [hep-th/0210292].

[69] R. Kallosh, *On inflation in string theory*, *Lect.Notes Phys.* **738** (2008) 119–156, [hep-th/0702059].

[70] L. McAllister and E. Silverstein, *String Cosmology: A Review*, *Gen.Rel.Grav.* **40** (2008) 565–605, [arXiv:0710.2951].

[71] D. Baumann and L. McAllister, *Advances in Inflation in String Theory*, *Ann.Rev.Nucl.Part.Sci.* **59** (2009) 67–94, [arXiv:0901.0265].

[72] D. Baumann and L. McAllister, *Inflation and String Theory*, arXiv:1404.2601.

[73] K. A. Olive, *Inflation*, *Phys.Rept.* **190** (1990) 307–403.

[74] D. H. Lyth and A. Riotto, *Particle physics models of inflation and the cosmological density perturbation*, *Phys.Rept.* **314** (1999) 1–146, [hep-ph/9807278].

[75] M. Yamaguchi, *Supergravity based inflation models: a review*, *Class.Quant.Grav.* **28** (2011) 103001, [arXiv:1101.2488].

[76] M. Nakahara, *Geometry, topology and physics*. Taylor & Francis, New York, USA, 1990.

[77] D. Freedman and A. Van Proeyen, *Supergravity*. Cambridge University Press, 2012.

[78] E. D. Stewart, *Inflation, supergravity and superstrings*, *Phys.Rev.* **D51** (1995) 6847–6853, [hep-ph/9405389].

[79] M. K. Gaillard, H. Murayama, and K. A. Olive, *Preserving flat directions during inflation*, *Phys.Lett.* **B355** (1995) 71–77, [hep-ph/9504307].

[80] M. Kawasaki, M. Yamaguchi, and T. Yanagida, *Natural chaotic inflation in supergravity*, *Phys.Rev.Lett.* **85** (2000) 3572–3575, [hep-ph/0004243].

[81] S. Antusch, M. Bastero-Gil, K. Dutta, S. F. King, and P. M. Kostka, *Chaotic Inflation in Supergravity with Heisenberg Symmetry*, *Phys.Lett.* **B679** (2009) 428–432, [arXiv:0905.0905].

[82] P. Binetruy, G. Dvali, R. Kallosh, and A. Van Proeyen, *Fayet-Iliopoulos terms in supergravity and cosmology*, *Class.Quant.Grav.* **21** (2004) 3137–3170, [hep-th/0402046].

[83] A. Achucarro and K. Sousa, *F-term uplifting and moduli stabilization consistent with Kahler invariance*, *JHEP* **0803** (2008) 002, [arXiv:0712.3460].

[84] A. Achucarro, S. Hardeman, and K. Sousa, *F-term uplifting and the supersymmetric integration of heavy moduli*, *JHEP* **0811** (2008) 003, [arXiv:0809.1441].

[85] A. Achucarro, S. Hardeman, and K. Sousa, *Consistent Decoupling of Heavy Scalars and Moduli in N=1 Supergravity*, *Phys.Rev.* **D78** (2008) 101901, [arXiv:0806.4364].

[86] R. Kallosh, A. Linde, and T. Rube, *General inflaton potentials in supergravity*, *Phys.Rev.* **D83** (2011) 043507, [arXiv:1011.5945].

[87] J. Garcia-Bellido and D. Wands, *Metric perturbations in two field inflation*, *Phys.Rev.* **D53** (1996) 5437–5445, [astro-ph/9511029].

[88] C. Gordon, D. Wands, B. A. Bassett, and R. Maartens, *Adiabatic and entropy perturbations from inflation*, *Phys.Rev.* **D63** (2001) 023506, [astro-ph/0009131].

[89] S. Groot Nibbelink and B. van Tent, *Density perturbations arising from multiple field slow roll inflation*, hep-ph/0011325.

[90] S. Groot Nibbelink and B. van Tent, *Scalar perturbations during multiple field slow-roll inflation*, *Class.Quant.Grav.* **19** (2002) 613–640, [hep-ph/0107272].

[91] D. Wands, N. Bartolo, S. Matarrese, and A. Riotto, *An Observational test of two-field inflation*, *Phys.Rev.* **D66** (2002) 043520, [astro-ph/0205253].

[92] C. M. Peterson and M. Tegmark, *Testing Two-Field Inflation*, *Phys.Rev.* **D83** (2011) 023522, [arXiv:1005.4056].

[93] S. Cremonini, Z. Lalak, and K. Turzynski, *Strongly Coupled Perturbations in Two-Field Inflationary Models*, *JCAP* **1103** (2011) 016, [arXiv:1010.3021].

[94] C. M. Peterson and M. Tegmark, *Testing multifield inflation: A geometric approach*, *Phys.Rev.* **D87** (2013), no. 10 103507, [arXiv:1111.0927].

[95] A. Avgoustidis, S. Cremonini, A.-C. Davis, R. H. Ribeiro, K. Turzynski, *et. al.*, *The Importance of Slow-roll Corrections During Multi-field Inflation*, *JCAP* **1202** (2012) 038, [arXiv:1110.4081].

[96] K. A. Malik and D. Wands, *Cosmological perturbations*, *Phys.Rept.* **475** (2009) 1–51, [arXiv:0809.4944].

[97] D. Wands, K. A. Malik, D. H. Lyth, and A. R. Liddle, *A New approach to the evolution of cosmological perturbations on large scales*, *Phys.Rev.* **D62** (2000) 043527, [astro-ph/0003278].

[98] C. Cheung, P. Creminelli, A. L. Fitzpatrick, J. Kaplan, and L. Senatore, *The Effective Field Theory of Inflation*, *JHEP* **0803** (2008) 014, [arXiv:0709.0293].

[99] C. Burgess, J. M. Cline, and R. Holman, *Effective field theories and inflation*, *JCAP* **0310** (2003) 004, [hep-th/0306079].

[100] S. Weinberg, *Effective Field Theory for Inflation*, *Phys.Rev.* **D77** (2008) 123541, [arXiv:0804.4291].

[101] A. J. Tolley and M. Wyman, *The Gelaton Scenario: Equilateral non-Gaussianity from multi-field dynamics*, *Phys.Rev.* **D81** (2010) 043502, [arXiv:0910.1853].

[102] A. Achucarro, J.-O. Gong, S. Hardeman, G. A. Palma, and S. P. Patil, *Mass hierarchies and non-decoupling in multi-scalar field dynamics*, *Phys.Rev.* **D84** (2011) 043502, [arXiv:1005.3848].

[103] A. Achucarro, J.-O. Gong, S. Hardeman, G. A. Palma, and S. P. Patil, *Features of heavy physics in the CMB power spectrum*, *JCAP* **1101** (2011) 030, [arXiv:1010.3693].

[104] G. Shiu and J. Xu, *Effective Field Theory and Decoupling in Multi-field Inflation: An Illustrative Case Study*, *Phys.Rev.* **D84** (2011) 103509, [arXiv:1108.0981].

[105] S. R. Behbahani, A. Dymarsky, M. Mirbabayi, and L. Senatore, *(Small) Resonant non-Gaussianities: Signatures of a Discrete Shift Symmetry in the Effective Field Theory of Inflation*, *JCAP* **1212** (2012) 036, [arXiv:1111.3373].

[106] S. Cespedes, V. Atal, and G. A. Palma, *On the importance of heavy fields during inflation*, *JCAP* **1205** (2012) 008, [arXiv:1201.4848].

[107] A. Achucarro, J.-O. Gong, S. Hardeman, G. A. Palma, and S. P. Patil, *Effective theories of single field inflation when heavy fields matter*, arXiv:1201.6342.

[108] X. Gao, D. Langlois, and S. Mizuno, *Influence of heavy modes on perturbations in multiple field inflation*, *JCAP* **1210** (2012) 040, [arXiv:1205.5275].

[109] A. Achucarro, V. Atal, S. Cespedes, J.-O. Gong, G. A. Palma, *et. al.*, *Heavy fields, reduced speeds of sound and decoupling during inflation*, *Phys.Rev.* **D86** (2012) 121301, [arXiv:1205.0710].

[110] E. Castillo, B. Koch, and G. Palma, *On the integration of fields and quanta in time dependent backgrounds*, arXiv:1312.3338.

[111] A. Achucarro, J.-O. Gong, G. A. Palma, and S. P. Patil, *Correlating features in the primordial spectra*, *Phys.Rev.* **D87** (2013) 121301, [arXiv:1211.5619].

[112] J.-O. Gong, K. Schalm, and G. Shiu, *Correlating correlation functions of primordial perturbations*, arXiv:1401.4402.

[113] **Planck Collaboration** Collaboration, P. Ade *et. al.*, *Planck 2013 results. XXII. Constraints on inflation*, arXiv:1303.5082.

[114] A. A. Starobinsky, *Spectrum of adiabatic perturbations in the universe when there are singularities in the inflation potential*, *JETP Lett.* **55** (1992) 489–494.

[115] L.-M. Wang and M. Kamionkowski, *The Cosmic microwave background bispectrum and inflation*, *Phys.Rev.* **D61** (2000) 063504, [astro-ph/9907431].

[116] J. A. Adams, B. Cresswell, and R. Easther, *Inflationary perturbations from a potential with a step*, *Phys.Rev.* **D64** (2001) 123514, [astro-ph/0102236].

[117] J.-O. Gong, *Breaking scale invariance from a singular inflaton potential*, *JCAP* **0507** (2005) 015, [astro-ph/0504383].

[118] X. Chen, R. Easther, and E. A. Lim, *Generation and Characterization of Large Non-Gaussianities in Single Field Inflation*, *JCAP* **0804** (2008) 010, [arXiv:0801.3295].

[119] F. Arroja, A. E. Romano, and M. Sasaki, *Large and strong scale dependent bispectrum in single field inflation from a sharp feature in the mass*, *Phys.Rev.* **D84** (2011) 123503, [arXiv:1106.5384].

[120] J. Martin and L. Sriramkumar, *The scalar bi-spectrum in the Starobinsky model: The equilateral case*, *JCAP* **1201** (2012) 008, [arXiv:1109.5838].

[121] P. Adshead, C. Dvorkin, W. Hu, and E. A. Lim, *Non-Gaussianity from Step Features in the Inflationary Potential*, *Phys.Rev.* **D85** (2012) 023531, [arXiv:1110.3050].

[122] F. Arroja and M. Sasaki, *Strong scale dependent bispectrum in the Starobinsky model of inflation*, *JCAP* **1208** (2012) 012, [arXiv:1204.6489].

[123] Y.-i. Takamizu, S. Mukohyama, M. Sasaki, and Y. Tanaka, *Non-Gaussianity of superhorizon curvature perturbations beyond δ N formalism*, *JCAP* **1006** (2010) 019, [arXiv:1004.1870].

[124] N. Bartolo, D. Cannone, and S. Matarrese, *The Effective Field Theory of Inflation Models with Sharp Features*, *JCAP* **1310** (2013) 038, [arXiv:1307.3483].

[125] E. D. Stewart, *The Spectrum of density perturbations produced during inflation to leading order in a general slow roll approximation*, *Phys.Rev.* **D65** (2002) 103508, [astro-ph/0110322].

[126] J. Choe, J.-O. Gong, and E. D. Stewart, *Second order general slow-roll power spectrum*, *JCAP* **0407** (2004) 012, [hep-ph/0405155].

[127] C. Dvorkin and W. Hu, *Generalized Slow Roll for Large Power Spectrum Features*, *Phys.Rev.* **D81** (2010) 023518, [arXiv:0910.2237].

[128] P. Adshead, W. Hu, C. Dvorkin, and H. V. Peiris, *Fast Computation of Bispectrum Features with Generalized Slow Roll*, *Phys.Rev.* **D84** (2011) 043519, [arXiv:1102.3435].

[129] V. Miranda, W. Hu, and P. Adshead, *Warp Features in DBI Inflation*, *Phys.Rev.* **D86** (2012) 063529, [arXiv:1207.2186].

[130] P. Adshead, W. Hu, and V. Miranda, *Bispectrum in Single-Field Inflation Beyond Slow-Roll*, *Phys.Rev.* **D88** (2013) 023507, [arXiv:1303.7004].

[131] W. Hu, *Generalized Slow Roll for Non-Canonical Kinetic Terms*, *Phys.Rev.* **D84** (2011) 027303, [arXiv:1104.4500].

[132] M. Park and L. Sorbo, *Sudden variations in the speed of sound during inflation: features in the power spectrum and bispectrum*, *Phys.Rev.* **D85** (2012) 083520, [arXiv:1201.2903].

[133] M. Nakashima, R. Saito, Y.-i. Takamizu, and J. Yokoyama, *The effect of varying sound velocity on primordial curvature perturbations*, *Prog.Theor.Phys.* **125** (2011) 1035–1052, [arXiv:1009.4394].

[134] R. Bean, X. Chen, G. Hailu, S.-H. H. Tye, and J. Xu, *Duality Cascade in Brane Inflation*, *JCAP* **0803** (2008) 026, [arXiv:0802.0491].

[135] R. H. Ribeiro, *Inflationary signatures of single-field models beyond slow-roll*, *JCAP* **1205** (2012) 037, [arXiv:1202.4453].

[136] X. Gao, D. Langlois, and S. Mizuno, *Oscillatory features in the curvature power spectrum after a sudden turn of the inflationary trajectory*, *JCAP* **10** (2013) 23, [arXiv:1306.5680].

[137] R. Saito and Y.-i. Takamizu, *Localized Features in Non-Gaussianity from Heavy Physics*, *JCAP* **1306** (2013) 031, [arXiv:1303.3839].

[138] T. Noumi and M. Yamaguchi, *Primordial spectra from sudden turning trajectory*, arXiv:1307.7110.

[139] L. Covi, J. Hamann, A. Melchiorri, A. Slosar, and I. Sorbera, *Inflation and WMAP three year data: Features have a Future!*, *Phys.Rev.* **D74** (2006) 083509, [astro-ph/0606452].

[140] M. Benetti, M. Lattanzi, E. Calabrese, and A. Melchiorri, *Features in the primordial spectrum: new constraints from WMAP7+ACT data and prospects for Planck*, *Phys.Rev.* **D84** (2011) 063509, [arXiv:1107.4992].

[141] P. Adshead and W. Hu, *Fast Computation of First-Order Feature-Bispectrum Corrections*, *Phys.Rev.* **D85** (2012) 103531, [arXiv:1203.0012].

[142] M. Benetti, *Updating constraints on inflationary features in the primordial power spectrum with the Planck data*, *Phys.Rev.* **D88** (Oct., 2013) 087302, [arXiv:1308.6406].

[143] J. Hamann, L. Covi, A. Melchiorri, and A. Slosar, *New Constraints on Oscillations in the Primordial Spectrum of Inflationary Perturbations*, *Phys.Rev.* **D76** (2007) 023503, [astro-ph/0701380].

[144] M. Benetti, S. Pandolfi, M. Lattanzi, M. Martinelli, and A. Melchiorri, *Featuring the primordial power spectrum: new constraints on interrupted slow-roll from CMB and LRG data*, *Phys.Rev.* **D87** (2013) 023519, [arXiv:1210.3562].

[145] J. Martin and C. Ringeval, *Superimposed oscillations in the WMAP data?*, *Phys.Rev.* **D69** (2004) 083515, [astro-ph/0310382].

[146] R. Flauger, L. McAllister, E. Pajer, A. Westphal, and G. Xu, *Oscillations in the CMB from Axion Monodromy Inflation*, *JCAP* **1006** (2010) 009, [arXiv:0907.2916].

[147] M. Aich, D. K. Hazra, L. Sriramkumar, and T. Souradeep, *Oscillations in the inflaton potential: Complete numerical treatment and comparison with the recent and forthcoming CMB datasets*, *Phys.Rev.* **D87** (2013) 083526, [arXiv:1106.2798].

[148] P. D. Meerburg, R. A. M. J. Wijers, and J. P. van der Schaar, *WMAP7 constraints on oscillations in the primordial power spectrum*, *MNRS* **421** (Mar., 2012) 369–380, [arXiv:1109.5264].

[149] H. Peiris, R. Easther, and R. Flauger, *Constraining Monodromy Inflation*, *JCAP* **1309** (2013) 018, [arXiv:1303.2616].

[150] P. D. Meerburg, D. N. Spergel, and B. D. Wandelt, *Searching for Oscillations in the Primordial Power Spectrum: Perturbative Approach (Paper I)*, arXiv:1308.3704.

[151] P. D. Meerburg and D. N. Spergel, *Searching for Oscillations in the Primordial Power Spectrum: Constraints from Planck (Paper II)*, arXiv:1308.3705.

[152] B. Audren, J. Lesgourgues, K. Benabed, and S. Prunet, *Conservative Constraints on Early Cosmology: an illustration of the Monte Python cosmological parameter inference code*, *JCAP* **1302** (2013) 001, [arXiv:1210.7183].

[153] L. Verde, *Statistical methods in cosmology*, *Lect.Notes Phys.* **800** (2010) 147–177, [arXiv:0911.3105].

[154] X. Chen, R. Easther, and E. A. Lim, *Large Non-Gaussianities in Single Field Inflation*, *JCAP* **0706** (2007) 023, [astro-ph/0611645].

[155] K. M. Smith, C. Dvorkin, L. Boyle, N. Turok, M. Halpern, *et. al.*, *On quantifying and resolving the BICEP2/Planck tension over gravitational waves*, arXiv:1404.0373.

[156] V. Miranda, W. Hu, and P. Adshead, *Steps to Reconcile Inflationary Tensor and Scalar Spectra*, arXiv:1403.5231.

[157] R. Bousso, D. Harlow, and L. Senatore, *Inflation After False Vacuum Decay: New Evidence from BICEP2*, arXiv:1404.2278.

[158] D. K. Hazra, A. Shafieloo, G. F. Smoot, and A. A. Starobinsky, *Ruling out the power-law form of the scalar primordial spectrum*, arXiv:1403.7786.

[159] A. Ashoorioon, K. Dimopoulos, M. Sheikh-Jabbari, and G. Shiu, *Non-Bunch-Davis Initial State Reconciles Chaotic Models with BICEP and Planck*, arXiv:1403.6099.

[160] J.-Q. Xia, Y.-F. Cai, H. Li, and X. Zhang, *Evidence for bouncing evolution before inflation after BICEP2*, arXiv:1403.7623.

[161] C. Burgess, M. Horbatsch, and S. Patil, *Inflating in a Trough: Single-Field Effective Theory from Multiple-Field Curved Valleys*, *JHEP* **1301** (2013) 133, [arXiv:1209.5701].

[162] D. Baumann and D. Green, *Equilateral Non-Gaussianity and New Physics on the Horizon*, *JCAP* **1109** (2011) 014, [arXiv:1102.5343].

[163] S. Pi and M. Sasaki, *Curvature Perturbation Spectrum in Two-field Inflation with a Turning Trajectory*, *JCAP* **1210** (2012) 051, [arXiv:1205.0161].

[164] X. Chen and Y. Wang, *Quasi-Single Field Inflation with Large Mass*, *JCAP* **1209** (2012) 021, [arXiv:1205.0160].

[165] Y.-F. Cai, W. Zhao, and Y. Zhang, *CMB Power Asymmetry from Primordial Sound Speed Parameter*, *Phys.Rev.* **D89** (2014) 023005, [arXiv:1307.4090].

[166] M. Konieczka, R. H. Ribeiro, and K. Turzynski, *The effects of a fast-turning trajectory in multiple-field inflation*, arXiv:1401.6163.

[167] V. Miranda and W. Hu, *Inflationary Steps in the Planck Data*, arXiv:1312.0946.

[168] P. Adshead and W. Hu, *Bounds on non-adiabatic evolution in single-field inflation*, arXiv:1402.1677.

[169] D. Cannone, N. Bartolo, and S. Matarrese, *Perturbative Unitarity of Inflationary Models with Features*, arXiv:1402.2258.

[170] J.-O. Gong and E. D. Stewart, *The Density perturbation power spectrum to second order corrections in the slow roll expansion*, *Phys.Lett.* **B510** (2001) 1–9, [astro-ph/0101225].

[171] P. Creminelli and M. Zaldarriaga, *Single field consistency relation for the 3-point function*, *JCAP* **0410** (2004) 006, [astro-ph/0407059].

[172] N. Kaloper and A. Lawrence, *Natural Chaotic Inflation and UV Sensitivity*, arXiv:1404.2912.

[173] X. Chen and M. H. Namjoo, *Standard Clock in Primordial Density Perturbations and Cosmic Microwave Background*, arXiv:1404.1536.

[174] A. Lewis and S. Bridle, *Cosmological parameters from CMB and other data: a Monte- Carlo approach*, *Phys. Rev.* **D66** (2002) 103511, [astro-ph/0205436].

[175] A. Achucarro, V. Atal, B. Hu, P. Ortiz, and J. Torrado , in preparation.

[176] J. Garriga and V. F. Mukhanov, *Perturbations in k-inflation*, *Phys.Lett.* **B458** (1999) 219–225, [hep-th/9904176].

[177] K. Sousa, *Consistent supersymmetric decoupling in cosmology*, *PhD Thesis (2012), ISBN 978-90-8593-127-0*.

[178] X. Chen and Y. Wang, *Quasi-Single Field Inflation and Non-Gaussianities*, *JCAP* **1004** (2010) 027, [arXiv:0911.3380].

[179] M. Dine, L. Randall, and S. D. Thomas, *Baryogenesis from flat directions of the supersymmetric standard model*, *Nucl.Phys.* **B458** (1996) 291–326, [hep-ph/9507453].

[180] M. Dine, L. Randall, and S. D. Thomas, *Supersymmetry breaking in the early universe*, *Phys.Rev.Lett.* **75** (1995) 398–401, [hep-ph/9503303].

[181] L. Alvarez-Gaume, C. Gomez, and R. Jimenez, *Minimal Inflation*, *Phys.Lett.* **B690** (2010) 68–72, [arXiv:1001.0010].

[182] L. Alvarez-Gaume, C. Gomez, and R. Jimenez, *A Minimal Inflation Scenario*, *JCAP* **1103** (2011) 027, [arXiv:1101.4948].

[183] L. Alvarez-Gaume, C. Gomez, and R. Jimenez, *Phenomenology of the minimal inflation scenario: inflationary trajectories and particle production*, *JCAP* **1203** (2012) 017, [arXiv:1110.3984].

[184] S. de Alwis, *Effective potentials for light moduli*, *Phys.Lett.* **B626** (2005) 223–229, [hep-th/0506266].

[185] S. de Alwis, *On integrating out heavy fields in SUSY theories*, *Phys.Lett.* **B628** (2005) 183–187, [hep-th/0506267].

[186] D. Gallego and M. Serone, *An Effective Description of the Landscape. I.*, *JHEP* **0901** (2009) 056, [arXiv:0812.0369].

[187] D. Gallego and M. Serone, *An Effective Description of the Landscape - II*, *JHEP* **0906** (2009) 057, [arXiv:0904.2537].

[188] D. Gallego, *On the Effective Description of Large Volume Compactifications*, *JHEP* **1106** (2011) 087, [arXiv:1103.5469].

[189] L. Brizi, M. Gomez-Reino, and C. A. Scrucca, *Globally and locally supersymmetric effective theories for light fields*, *Nucl.Phys.* **B820** (2009) 193–212, [arXiv:0904.0370].

[190] S. Hardeman, J. M. Oberreuter, G. A. Palma, K. Schalm, and T. van der Aalst, *The everpresent eta-problem: knowledge of all hidden sectors required*, *JHEP* **1104** (2011) 009, [arXiv:1012.5966].

[191] A. Achucarro, S. Hardeman, J. M. Oberreuter, K. Schalm, and T. van der Aalst, *Decoupling limits in multi-sector supergravities*, *JCAP* **1303** (2013) 038, [arXiv:1108.2278].

[192] P. Binetruy and M. K. Gaillard, *Temperature Corrections, Supersymmetric Effective Potentials and Inflation*, *Nucl.Phys.* **B254** (1985) 388.

[193] S. C. Davis and M. Postma, *Successfully combining SUGRA hybrid inflation and moduli stabilisation*, *JCAP* **0804** (2008) 022, [arXiv:0801.2116].

[194] L. Covi, M. Gomez-Reino, C. Gross, J. Louis, G. A. Palma, *et. al.*, *de Sitter vacua in no-scale supergravities and Calabi-Yau string models*, *JHEP* **0806** (2008) 057, [arXiv:0804.1073].

[195] L. Covi, M. Gomez-Reino, C. Gross, J. Louis, G. A. Palma, *et. al.*, *Constraints on modular inflation in supergravity and string theory*, *JHEP* **0808** (2008) 055, [arXiv:0805.3290].

[196] I. Ben-Dayan, R. Brustein, and S. P. de Alwis, *Models of Modular Inflation and Their Phenomenological Consequences*, *JCAP* **0807** (2008) 011, [arXiv:0802.3160].

[197] P. Brax, S. C. Davis, and M. Postma, *The Robustness of n(s) 0.95 in racetrack inflation*, *JCAP* **0802** (2008) 020, [arXiv:0712.0535].

[198] A. D. Linde and A. Westphal, *Accidental Inflation in String Theory*, *JCAP* **0803** (2008) 005, [arXiv:0712.1610].

[199] M. Dine and L. Pack, *Studies in Small Field Inflation*, *JCAP* **1206** (2012) 033, [arXiv:1109.2079].

[200] R. Barbieri, E. Cremmer, and S. Ferrara, *Flat and Positive Potentials in $N = 1$ Supergravity*, *Phys.Lett.* **B163** (1985) 143.

[201] D. H. Lyth and T. Moroi, *The Masses of weakly coupled scalar fields in the early universe*, *JHEP* **0405** (2004) 004, [hep-ph/0402174].

[202] E. J. Copeland, A. R. Liddle, D. H. Lyth, E. D. Stewart, and D. Wands, *False vacuum inflation with Einstein gravity*, *Phys.Rev.* **D49** (1994) 6410–6433, [astro-ph/9401011].

[203] A. D. Linde, *Chaotic Inflation*, *Phys.Lett.* **B129** (1983) 177–181.

[204] A. D. Linde, *Hybrid inflation*, *Phys.Rev.* **D49** (1994) 748–754, [astro-ph/9307002].

[205] G. Dvali, Q. Shafi, and R. K. Schaefer, *Large scale structure and supersymmetric inflation without fine tuning*, *Phys.Rev.Lett.* **73** (1994) 1886–1889, [hep-ph/9406319].

[206] A. D. Linde and A. Riotto, *Hybrid inflation in supergravity*, *Phys.Rev.* **D56** (1997) 1841–1844, [hep-ph/9703209].

[207] S. Ashok and M. R. Douglas, *Counting flux vacua*, *JHEP* **0401** (2004) 060, [hep-th/0307049].

[208] M. R. Douglas, *Statistics of string vacua*, hep-ph/0401004.

[209] F. Denef and M. R. Douglas, *Distributions of nonsupersymmetric flux vacua*, *JHEP* **0503** (2005) 061, [hep-th/0411183].

[210] F. Denef and M. R. Douglas, *Distributions of flux vacua*, *JHEP* **0405** (2004) 072, [hep-th/0404116].

[211] D. Marsh, L. McAllister, and T. Wrase, *The Wasteland of Random Supergravities*, *JHEP* **1203** (2012) 102, [arXiv:1112.3034].

[212] T. C. Bachlechner, D. Marsh, L. McAllister, and T. Wrase, *Supersymmetric Vacua in Random Supergravity*, *JHEP* **1301** (2013) 136, [arXiv:1207.2763].

[213] Y. Sumitomo and S.-H. H. Tye, *A Stringy Mechanism for A Small Cosmological Constant*, *JCAP* **1208** (2012) 032, [arXiv:1204.5177].

[214] Y. Sumitomo and S. H. Tye, *A Stringy Mechanism for A Small Cosmological Constant - Multi-Moduli Cases -*, *JCAP* **1302** (2013) 006, [arXiv:1209.5086].

[215] Y. Sumitomo and S.-H. H. Tye, *Preference for a Vanishingly Small Cosmological Constant in Supersymmetric Vacua in a Type IIB String Theory Model*, *Phys.Lett.* **B723** (2013) 406–410, [arXiv:1211.6858].

[216] K. Metallinos, *Numerical exploration of the string theory landscape*, *ProQuest Dissertations and Theses* (2013) 114.

[217] M. D. Marsh, L. McAllister, E. Pajer, and T. Wrase, *Charting an Inflationary Landscape with Random Matrix Theory*, *JCAP* **1311** (2013) 040, [arXiv:1307.3559].

[218] F. G. Pedro and A. Westphal, *The Scale of Inflation in the Landscape*, arXiv:1303.3224.

[219] S. B. Giddings, S. Kachru, and J. Polchinski, *Hierarchies from fluxes in string compactifications*, *Phys.Rev.* **D66** (2002) 106006, [hep-th/0105097].

[220] S. Kachru, R. Kallosh, A. D. Linde, and S. P. Trivedi, *De Sitter vacua in string theory*, *Phys.Rev.* **D68** (2003) 046005, [hep-th/0301240].

[221] V. Balasubramanian, P. Berglund, J. P. Conlon, and F. Quevedo, *Systematics of moduli stabilisation in Calabi-Yau flux compactifications*, *JHEP* **0503** (2005) 007, [hep-th/0502058].

[222] K. Choi, A. Falkowski, H. P. Nilles, M. Olechowski, and S. Pokorski, *Stability of flux compactifications and the pattern of supersymmetry breaking*, *JHEP* **0411** (2004) 076, [hep-th/0411066].

[223] M. Rummel and A. Westphal, *A sufficient condition for de Sitter vacua in type IIB string theory*, *JHEP* **1201** (2012) 020, [arXiv:1107.2115].

[224] M. Gomez-Reino and C. A. Scrucca, *Locally stable non-supersymmetric Minkowski vacua in supergravity*, *JHEP* **0605** (2006) 015, [hep-th/0602246].

[225] M. Gomez-Reino and C. A. Scrucca, *Constraints for the existence of flat and stable non-supersymmetric vacua in supergravity*, *JHEP* **0609** (2006) 008, [hep-th/0606273].

[226] M. Gomez-Reino and C. A. Scrucca, *Metastable supergravity vacua with F and D supersymmetry breaking*, *JHEP* **0708** (2007) 091, [arXiv:0706.2785].

[227] L. Covi, M. Gomez-Reino, C. Gross, G. A. Palma, and C. A. Scrucca, *Constructing de Sitter vacua in no-scale string models without uplifting*, *JHEP* **0903** (2009) 146, [arXiv:0812.3864].

[228] P. Breitenlohner and D. Z. Freedman, *Positive Energy in anti-De Sitter Backgrounds and Gauged Extended Supergravity*, *Phys.Lett.* **B115** (1982) 197.

[229] D. Gallego, *Light field integration in SUGRA theories*, arXiv:1301.6177.

[230] L. Mehta, *Random Matrices*. Academic Press, 1991.

[231] V. A. Marčenko and L. Pastur, *Distribution of the eigenvalues in certain sets of random matrices*, *Math USSR-Sb* **1** (1967) 457–483.

[232] C. A. Tracy and H. Widom, *Level spacing distributions and the Airy kernel*, *Commun.Math.Phys.* **159** (1994) 151–174, [hep-th/9211141].

[233] A. Edelman, *Eigenvalues and condition numbers of random matrices*, *SIAM Journal on Matrix Anal. and Applic.* **9** (1988) 543–560.

[234] A. Borghese, D. Roest, and I. Zavala, *A Geometric bound on F-term inflation*, *JHEP* **1209** (2012) 021, [arXiv:1203.2909].

[235] R. Kallosh and A. D. Linde, *Landscape, the scale of SUSY breaking, and inflation*, *JHEP* **0412** (2004) 004, [hep-th/0411011].

[236] J. J. Blanco-Pillado, R. Kallosh, and A. D. Linde, *Supersymmetry and stability of flux vacua*, *JHEP* **0605** (2006) 053, [hep-th/0511042].

[237] J. Wishart, *The generalised product moment distribution in samples from a normal multivariate population*, *Biometrika* **20A** (1928) no. 1, 32–52.

[238] M. Johnstone, *On the distribution of the largest eigenvalue in principal components analysis*, *Ann. Statist* **29** (2001) 295–327.

[239] K. Johansson, *Shape Fluctuations and Random Matrices*, *Communications in Mathematical Physics* **209** (2000) 437–476, [`math/9903134`].

[240] P. Vivo, S. N. Majumdar, and O. Bohigas, *Large deviations of the maximum eigenvalue in Wishart random matrices*, *Journal of Physics A Mathematical General* **40** (2007) 4317–4337, [`cond-mat/0701371`].

[241] C. Tracy and H. Widom, *The distributions of random matrix theory and their applications*, in *New Trends in Mathematical Physics* (V. Sidoravi?ius, ed.), pp. 753–765. Springer Netherlands, 2009.

Summary

> *"The ancient teachers of this science," said he, "promised impossibilities, and performed nothing. The modern masters promise very little; they know that metals cannot be transmuted, and that the elixir of life is a chimera. But these philosophers, whose hands seem only made to dabble in dirt, and their eyes to pour over the microscope or crucible, have indeed performed miracles. They penetrate into the recesses of nature, and show how she works in her hiding-places. They ascend into the heavens: they have discovered how the blood circulates, and the nature of the air we breathe. They have acquired new and almost unlimited powers; they can command the thunders of heaven, mimic the earthquake, and even mock the invisible world with its own shadows." Such were the professor's words – rather let me say such the words of the fate – enounced to destroy me. As he went on I felt as if my soul were grappling with a palpable enemy; one by one the various keys were touched which formed the mechanism of my being: chord after chord was sounded, and soon my mind was filled with one thought, one conception, one purpose.*
>
> Mary Shelley, *Frankenstein*, 1818

One of the most fascinating enigmas of mankind is the origin of the universe. Throughout the time, philosophers, astronomers, mathematicians, physicists, chemists, biologists,... have been chasing the answer to this conundrum, which is still a mystery. However, scientists have tried really hard and they have been able to follow the universe evolution backwards in time until its very first second. It is no wonder that I also wanted to participate in this hunt, although my goal is to answer slightly more modest questions.

The universe is made of particles and energy, but we only understand 5% of its content, the so-called baryonic matter, like protons and neutrons. As for the rest, we know there must exist about 27% of something we call dark matter (because we cannot see it), which so far has not been directly detected. However, the existence of a non-visible matter component is required to explain certain observations of galaxies and clusters of galaxies. And the big mystery of dark energy fills the rest of the cake, accounting for approximately 68% of the universe content. We also do not know what it is, but we know it drives the present expansion of the universe and that somehow this energy is stored in the vacuum. In view of this, ignorance might be a curse rather than a blessing.

On the bright side, we understand very well most of the processes that the universe underwent until now: from the formation of the first atoms to the gigantic clusters of galaxies. Because we understand the physics behind it, we have been able to play backwards the movie of the universe until the time of the Big Bang. But in between there was a very special moment: the first burst of light, that is called the cosmic microwave background radiation, or CMB for short. This light was emitted when the universe was approximately 380000 years old, and it travelled all the way towards us during 13000 million years! This is the oldest photograph of the universe.

The same way that the light of the Sun takes eight minutes to reach us, so we see the Sun as it was eight minutes ago, when we look at the CMB we see the universe as it was 13000 millions years ago. This light is visible with special telescopes and there is a beautiful picture of it in the first chapter of this thesis. Although we can still rewind the movie of the universe until the very first instant (because we know how the physical laws work up to the electroweak scale), we have no experiment able to measure directly any background before the CMB. Before that time, the universe was so hot that everything inside the cosmic fluid was colliding. The multiple collisions taking place did not let the light particles move freely, so not even the light could escape the cosmic fluid and travel towards us. The universe was opaque.

When the CMB was observed for the first time in 1965, there was finally solid proof that the early universe was extremely homogeneous, so extraordinarily homogeneous that the Big Bang theory was not able to explain it. This is because the standard Big Bang theory predicts a stage of decelerated expansion. Essentially, in a universe where gravity is attractive, matter tends to cluster and form regions with more density than others. In other words, gravitational attraction produces decelerated expansion and inhomogeneities, which were not in agreement with the CMB observations.

It was not until the 1980's that a solution was proposed, which could explain the homogeneity of the early universe: before the Big Bang there must exist a

period of accelerated expansion! This would explain why the universe is the way it is. That period of accelerated expansion was called inflation, and it is tremendously successful. Its predictions are in remarkable agreement with the CMB experiments, and it provides an easy way to explain the peculiarities of the early universe. Indeed, what happened during the very early epoch of accelerated expansion left fingerprints in the CMB, and we are looking with a magnifying glass searching for signatures of inflation.

Now comes the role of the theoretician, who has to propose mechanisms that explain how gravity was acting as if it was repulsive. In the last thirty years, physicists have been trying to unveil the mysteries of inflation, looking for descriptions that would explain naturally the accelerated expansion. At the same time, it has been possible to test those theories to some degree with the help of the CMB data. The simplest explanation is the very presence of a single particle, such as the Higgs boson, that drove the early and brutal accelerated expansion of the universe.

At this point, the simplest models are very successful, but the experiments are becoming so accurate that we are starting to see hints of anomalies that we are not quite sure how to explain with these simplest models. These anomalies might be there or not, but we want to be ready.

In addition, the knowledge of physics during the first second of the universe is not so robust. When gravity becomes as important as electromagnetic or nuclear forces and the quantum and gravitational effects are comparable, our standard theories simply do not work. Enormous efforts have been made in this respect by elaborating theories such as superstrings and supergravity. Describing inflation in the context of these theories is an indirect way to test them.

In this spirit, in this thesis I have started a search, together with my collaborators, for the presence of additional particles during inflation. These particles are expected to be there if inflation is to be described by new physics, participating in the expansion of the early universe. We have investigated how to incorporate these additional particles in our theories, in a way that the theory is still well understood and consistent. More importantly, we have also calculated the effect of these additional particles in the observations of the CMB, so that we make predictions in agreement with the experiments. After four years, we do not have a conclusive evidence for these additional particles yet. But the current experiments are already potentially sensitive to the presence of these particles, and it might be that in the very near future they detect new features. Perhaps these features can be explained by the presence of additional particles, all together playing to inflate the very early universe. They might be already giving us subtle hints through the picture of a very young universe...

Samenvatting

Eén van de meest fascinerende raadsels waar de mens zich voor gesteld ziet gaat over de oorsprong van het universum. Door de eeuwen heen zijn filosofen, sterrenkundigen, wiskundigen, natuurkundigen, scheikundigen, biologen,... op zoek geweest naar een antwoord, dat nog steeds een mysterie blijft. Echter, wetenschappers zijn er met een enorme inspanning in geslaagd om het universum te volgen terug in de tijd tot in de allereerste seconde. Geen wonder dat ik ook mee wilde doen aan deze zoektocht, ook al is mijn doel om ietwat meer bescheiden vragen te beantwoorden.

Het universum bestaat uit deeltjes en energie, maar we begrijpen slechts 5% van haar inhoud, de zogenaamde baryonische materie, zoals protonen en neutronen. Wat de rest betreft, we weten dat er ongeveer 27% moet bestaan van iets dat we donkere materie noemen (omdat we het niet kunnen zien), dat tot nu toe nog niet direct waargenomen is. Echter, het bestaan van een onzichtbare materiecomponent is vereist om huidige observaties van melkwegstelsels en clusters van melkwegstelsels te verklaren. Tenslotte is er het grote mysterie van donkere energie die de resterende 68% van de inhoud van het universum voor haar rekening neemt. Ook in dit geval weten we niet wat het is, maar wel dat het zorgt voor de huidige expansie van ons heelal en dat deze energie op één of andere manier in het vacuüm is opgeslagen. Zo bezien is er weinig zaligs aan onze onwetendheid.

Aan de andere kant begrijpen we de meeste processen die het universum tot op heden ondergaan is wel heel goed: van de formatie van de eerste atomen tot aan de enorme clusters van melkwegstelsels. Omdat we de fysica hierachter begrijpen, hebben we de film kunnen terugdraaien tot het moment van de oerknal. Onderweg passeren we echter een heel speciaal moment: het eerste

uitgezonden licht, dat de kosmische achtergrondstraling genoemd wordt (of CMB straling, voor Cosmic Microwave Background). Dit licht werd uitgezonden toen het universum ongeveer 380.000 jaar oud was, en het is 13 miljard jaar onderweg geweest, de hele weg naar ons toe! Dit is de oudste foto van het universum.

Net zoals het licht van de zon acht minuten onderweg is om ons te bereiken, wat betekent dat als we naar de zon kijken, we haar zien zoals ze er acht minuten geleden uitzag, zo zien we als we naar de CMB kijken het universum zoals het er 13 miljard jaar geleden uitzag. Dit licht is zichtbaar met speciale telescopen en er staat een prachtige afbeelding van in het eerste hoofdstuk van dit proefschrift. Ook al kunnen we de film van het universum terugdraaien tot het allereerste moment (omdat we weten hoe de natuurwetten tot op dat moment werken), hebben we geen experiment dat in staat is om direct iets van voor de CMB te meten. Voor die tijd was het universum zo heet dat alles in de kosmische vloeistof extreem reactief was. De vele botsingen die plaats vonden beletten de lichtdeeltjes om vrij te bewegen, waardoor zelfs licht de vloeistof niet kon ontsnappen om naar ons toe te reizen. Het universum was dof – ondoordringbaar voor licht.

Toen de CMB in 1965 voor het eerst geobserveerd werd, hadden natuurkundigen eindelijk een stevig bewijs dat het vroege universum extreem homogeen is, zo buitengewoon homogeen dat de oerknaltheorie het niet kon verklaren. Dit komt doordat de standaard-oerknaltheorie een periode van vertraagde expansie voorspelt. Het komt erop neer dat in een universum waarin zwaartekracht een aantrekkende kracht is, materie de neiging heeft om te klonteren en daardoor gebiedjes te vormen met een hogere dichtheid dan het gemiddelde. Met andere woorden, het aantrekkende karakter van de zwaartekracht produceert een vertraagde expansie en ook inhomogeniteiten, die niet waargenomen werden in de CMB.

Het duurde tot aan de jaren ‘80 voordat meerdere fysici een oplossing voorstelden die de homogeniteit van het vroege universum kon verklaren: voor de oerknal moet er een periode zijn geweest van versnelde expansie! Dit zou verklaren waarom het universum is zoals het is. Die periode van versnelde expansie werd *inflatie* genoemd en is enorm succesvol. Haar voorspellingen komen opmerkelijk goed overeen met de CMB experimenten, en zij verschaft een makkelijke manier om de bijzonderheden van het vroege universum te verklaren. Wat er gebeurde tijdens deze zeer vroege fase van afstotende zwaartekracht heeft inderdaad vingerafdrukken achtergelaten in de CMB, en wij zijn met een vergrootglas op zoek naar deze sporen van inflatie.

Nu verschijnt de theoreticus ten tonele, om mechanismen voor te stellen die uitleggen hoe zwaartekracht afstotend kon lijkt te zijn. In de laatste dertig jaar hebben fysici geprobeerd om de mysteries van inflatie bloot te leggen, door naar beschrijvingen te zoeken die de versnelde expansie op een natuurlijke

manier uit konden leggen. Tegelijkertijd hebben we deze theorieën tot op zekere schaal kunnen testen met behulp van de gegevens uit de CMB. De eenvoudigste oplossing is de aanwezigheid van een enkel deeltje, zoals het Higgs boson, dat de vroege agressieve expansie van het heelal verklaart.

Op dit moment zijn de simpelste modellen het meest succesvol, maar de experimenten beginnen zo nauwkeurig te worden dat we mogelijke sporen van anomalieën in beeld krijgen, waarvan we niet echt weten hoe we die met de simpelste modellen kunnen verklaren. En als deze anomalieën echt blijken te zijn, willen we klaar zijn om ze te kunnen verklaren.

Daarbij is onze kennis van de fysica tijdens de eerste seconde van het universum niet zo robuust. Wanneer zwaartekracht even belangrijk wordt als elektromagnetische of kernkrachten en quantum- en zwaartekrachtseffecten vergelijkbaar worden, werken onze standaardtheorieën domweg niet meer. Enorme inspanningen zijn getroost in dit opzicht in het opstellen van theorieën zoals supersnaren en superzwaartekracht. De beschrijving van inflatie in de context van deze theorieën is een indirecte manier om ze te testen.

In deze geest ben ik in dit proefschrift een zoektocht begonnen, samen met mijn collega's, naar de aanwezigheid van extra deeltjes tijdens inflatie. Deze deeltjes worden verwacht aanwezig te zijn in het geval inflatie beschreven moet worden met nieuwe fysica, en nemen deel aan de expansie van het vroege universum. We hebben onderzocht hoe we zulke deeltjes in onze theorieën moeten inbouwen, op een manier die de theorie goed interpreteerbaar en consistent laat. Belangrijker is dat we ook de invloed van deze extra deeltjes op de CMB-observaties berekend hebben, zodanig dat we voorspellingen doen die overeenkomen met de experimenten. Na vier jaar hebben we nog geen definitief bewijs voor de aanwezigheid van deze extra deeltjes. Echter, huidige experimenten zijn in potentie al gevoelig voor de aanwezigheid van deze deeltjes, en het zou kunnen dat in de zeer nabije toekomst ze deze nieuwe kenmerken waar gaan nemen. Misschien kunnen ze verklaard worden door de aanwezigheid van extra deeltjes, in een samenspel om het vroege universum te laten expanderen. Ze zouden ons nu al subtiele hints kunnen geven via het beeld van het zeer jonge universum...

Publications

- '*Sgoldstino Inflation.*' Ana Achúcarro, Sander Mooij, Pablo Ortiz and Marieke Postma. *JCAP* **1208** (2012) 013, arXiv:1203.1907[hep-th].
- '*Localized correlated features in the CMB power spectrum and primordial bispectrum from a transient reduction in the speed of sound.*' Ana Achúcarro, Vicente Atal, Pablo Ortiz and Jesús Torrado. *Phys.Rev.* **D89** (2014) 103006, arXiv:1311.2552[astro-ph.CO].
- '*Inflation with moderately sharp features in the speed of sound: GSR and in-in formalism for power spectrum and bispectrum.*' Ana Achúcarro, Vicente Atal, Bin Hu, Pablo Ortiz and Jesús Torrado. *Phys.Rev.* **D90** (2014) 023511, arXiv:1404.7522[astro-ph.CO].
- '*Perturbative stability along the supersymmetric directions of the landscape.*' Kepa Sousa and Pablo Ortiz. arXiv:1408.6521[hep-th].

Curriculum Vitæ

I was born in Madrid, Spain, on 6 December 1985. I attended primary and high school at 'Padre Manyanet' until 2003. Later in September of the same year I started my bachelor in Physics in Universidad Autónoma de Madrid (UAM). During my last and fifth year I received a grant to collaborate in the Theoretical Physics department with Dr. Luis M. Robledo on a project related to modelling nuclear fission. I graduated in 2008 and a few months later I started the Master program on Theoretical Physics in Universidad Autónoma de Madrid. During my master studies I benefited two consecutive years from an MSc scholarship given by the same university. From 2009 to 2010, on the second year of the master program, I wrote a master thesis on "Phenomenology of massive neutrinos in particle physics and astrophysics", supervised by Dr. Michele Maltoni. I graduated in 2010 and rapidly moved to Leiden, The Netherlands, where I started my PhD under the supervision of Prof. dr. Ana Achúcarro and co-supervision of Prof. dr. Jan-Willem van Holten. I was affiliated to two institutions: the Instituut-Lorentz for Theoretical Physics at Leiden University, and the National Institute for Subatomic Physics (Nikhef) in Amsterdam. I was financially supported by the Dutch Foundation for Fundamental Research on Matter (FOM). During my PhD I was teaching assistant for the courses on Elementary Particle Physics (two years), and Theory of General Relativity (two years). In 2014 I was awarded the "Teaching assistant of the year" prize. During the last year, I have enjoyed several stays at the Theoretical Physics department of the University of the Basque Country (UPV/EHU).

Acknowledgements

My biggest thanks go to my supervisor Ana Achúcarro, who has inspired me along the four years of my PhD. I have enjoyed uncountable discussions with her, and also being a teaching assistant next to her, she has pushed even further my motivation to teach. At the personal level, she has had a tremendous stamina in managing situations, supporting me in the best and worst moments. Last, she has given me the opportunity to present our work in a very large number of meetings, the chance to take the leadership, and trusted me to do so. For those reasons and everything else I thank you.

Secondly, I want to thank my co-supervisor Jan-Willem van Holten, who shared his expertise in Supersymmetry and Supergravity with me. He has been always willing to discuss and help me with the most technical aspects of the work. He has always shown himself understanding, flexible, and professional. I thank you for offering your valuable help all these years.

I also want to thank the collaborators that have worked together with me in the articles presented in this thesis: Ana Achúcarro, Vicente Atal, Bin Hu, Sander Mooij, Marieke Postma, Kepa Sousa and Jesús Torrado. I have tremendously enjoyed working with them, and I really hope we keep collaborating in the future. It has been a great pleasure to learn so much from them, not only in offices with blackboards, but also in bars (or borrels) with food and drinks. 'Giving birth' to articles is a hard but joyful task when you are surrounded by the right people. Thank you for making of this such a pleasant journey.

I am grateful to the members of the Theoretical Physics department at the University of the Basque Country for their hospitality and for the stimulating and kind atmosphere during my visits, especially to José Juan Blanco-Pillado, Jonathan Frazer and Jon Urrestilla. I also want to acknowledge plenty of discussions with Andrea Borghese, Diederik Roest, Marco Scalisi and Ivonne Zavala, and the hospitality of the University of Groningen.

There is a multitude of physicists that have been by my side during these four years, with whom I have talked about Physics and life in every lunch, meeting, or gathering we have held together in the Netherlands. In addition to those aforementioned, an incomplete list of these people is the following: Ted van der Aalst, Giuseppe d'Ambrosi, Dražen Glavan, Marija Kovacevic, Ivano Lodato, Wout Merbis, Valentin Reys, Wessel Valkenburg, Jan Weenink, Yvette Welling, and all the other cosmologists in Leiden. Special thanks to the organizers and participants of the Theoretical Cosmology meetings and Theory meetings, I personally enjoyed the big family that we have formed over the years. In these meetings, I have not only benefited from a large network of theoretical physicists, but also made many good friends. I thank you for all the good moments we have shared together.

But I would have never arrived to the Netherlands without my previous formation as a theoretical physicist in Madrid, where I studied seven years. My physicist friends have made of me the physicist that I am today, and without them I would not be the same. I cannot count the hours we have spent working together among coffees, teas, beers and 'palmeras', and how much I learnt from all of you, not to mention the great days and nights we spent together in Madrid and elsewhere in the world. Alba, Clara, Edu, Emilio, Drino, Ernesto, Fito, Luis, Manuela, Miguel, Paco, Paloma, Paula, Pepe and Yago, thanks for everything.

Outside the physics world, I have counted on many friends who have been my family in the Netherlands. They have supported and helped me, put up with my stubbornness, but most of all, we have shared all kind of great experiences. They have made these years much more enjoyable and easier to me. I sincerely thank Ander, Arachne, Bego, César, Fani, Guillem, Manu and Mónica... a thousand thanks for being there. Here I also want to thank those persons who first helped me to settle down in Leiden: Brian, Fran, Leanne, Marianne and Saskia, thanks for receiving me with open arms.

To my family, that during their lives have been working very hard so that I could write this little book; I will always be grateful to them. They have always been at my side, especially during the last four years, and I could have never gotten here without them. A million thanks for you unconditional love and support.

To my dear Helena, who has been a source of endless support, standing by my side, taking all in, listening to my incomprehensible speeches, making every day more unique than the previous one, taking care of me, and sharing joy with me. This journey has been so much more rewarding with you at my side. You have encouraged me and helped me when I needed it most. For all this, I love you and I thank you.